Polyproline and Collagen Peptides Derived from 4(*R*/*S*)-OH/NH$_2$-L/D-Proline: Synthesis, Conformational and Morphological Studies

A thesis

Submitted in partial fulfillment of the requirements

Of the degree of

Doctor of Philosophy

By

Shahaji H. More

ID: 20123192

Research Supervisor

Prof. Krishna N. Ganesh

IISER PUNE

INDIAN INSTITUTE OF SCIENCE EDUCATION AND RESEARCH, PUNE

2018

This work is dedicated to...

My family

and

Teacher

CERTIFICATE

I certify that the work incorporated in the thesis entitled **"Polyproline and Collagen Peptides Derived from 4(*R*/*S*)-OH/NH$_2$-L/D-Proline: Synthesis, Conformational and Morphological Studies***"*** submitted by **Mr. Shahaji H. More** was carried out by the candidate, under my supervision. The work presented here or any part of it has not been included in any other thesis submitted previously for the award of any degree or diploma from any other university or institution.

Date: 14th Dec, 2018 Pune   **Prof. Krishna N. Ganesh**

                                                                                              (Research Supervisor)

DECLARATION

I declare that, this written submission represents my ideas in my own words and where others' ideas have been included, I have adequately cited and referenced the original sources. I also declare that I have adhered to all principles of academic honesty and integrity and have not misrepresented or fabricated or falsified any idea / data / fact/ source in my submission. I understand that violation of the above will be cause for disciplinary action by the Institute and can also evoke penal action from the sources which have thus not been properly cited or from whom proper permission has not been taken when needed.

Date: 14th Dec, 2018 Pune   **Mr. Shahaji H. More**

                                                            ID: 20123192

Acknowledgements

It gives me pleasure to express my deep sense of gratitude towards my research supervisor Prof. Krishna N. Ganesh for his support and guidance. He has been the constant source of inspiration throughout my doctoral research. He has always taken efforts to improve my presentation skills, writing skills and independent thinking.

I sincerely thank to IISER Pune for providing fantastic facilities to carry out doctoral research. I am very grateful to my research advisory committee members Dr. H. N Gopi and Dr. G. J. Sanjayan for their suggestions, comments through various RAC meetings. I would like to acknowledge CSIR-India for providing research fellowship during the last five years.

I am very thankful to have co-operative environment in lab from my senior and junior colleagues. I thank my seniors Dr. Mahesh, Dr. Nitin, Dr. Satish, Dr. Vijay, Mr. Madhan and Mr. Prabhakar. I thank my juniors, Mr. Pramod, Mr. Manoj, Mr. Iranna, Mr. Abdul, Mr. Omshankar, Mr. Rajat and Mr. Gourav. I had a wonderful company with my friends Dr. Trimbak, Mr. Vijay, Mr. Navanath, Mr. Shekhar, and all IISER, NCl friends.

I shall always remain indebted to my parents, and my entire family, for their unconditional support, blessings and patience. My father Mr. Hanumantrao and brother Mr. Naresh with sister in law Mrs. Chhaya, always insisted me to do better, I express my thanks towards them for believing in me. I would like to thank an adorable person in my life, Mayura for her continuous support and believing in me, a sweet nephew Niraj and sweet nieces Tejshree. They always made me forget all the tension & frustration.

Finally, I would like to thank my mother Shindhu (Akka). I hope with my ability and dedication, I would be able to translate her dreams into reality.

Shahaji.

Contents

Chapter 1

Introduction to D-amino acids, Polyproline and Collagen Peptides

Chapter 2

Self-assembly of 4(*R/S*)-D-Aminopolyproline

Chapter 3

Alternate and Block Heterochiral Plypeptides from 4(*R*/*S*)-Hydroxy-L/D Proline

Chapter 4

Self-assembly of 4(*R/S*)-Hydroxy/Amino Collagen Peptide Spiegelmers

Section A: Self-assembly of 4(*R/S*)-Hydroxy Collagen Peptide Spiegelmers

Section B: Self-assembly of 4(*R/S*)-Amino Collagen Peptide Spiegelmers

Abbreviations & Symbols

Ac	Acetyl
Ac$_2$O	Acetic anhydride
Aib	α-Aminoisobutyric acid
Ala	Alanine
L-*Amp*	(2*S*,4*R*)-Aminoproline
L-*amp*	(2*S*,4*S*)-aminoproline
L-*Hyp*	(2*S*,4*R*)-Hydroxyproline (*trans*-4-hydroxy-L-proline)
L-*hyp*	(2*S*,4*S*)-hydroxyproline (*cis*-4-hydroxy-L-proline)
Arg	Arginine
Asn	Asparagine
Azp	(2*S*,4*R*)-Azidoproline
azp	(2*S*,4*S*)-azidoproline
(Boc)$_2$O	Boc anhydride
^{o}C	Degree Celsius
Cbz	Benzyloxycarbonyl
CD	Circular Dichroism
CMPs	Collagen mimetic peptides
CRPs	Collagen Related Peptides
D-	Dextro-
D-*Amp*	(2*R*,4*R*)-Aminoproline
D-*amp*	(2*R*,4*S*)-aminoproline
D-*Hyp*	(2*R*,4*R*)-Hydroxyproline (*cis*-4-hydroxy-D-proline)
D-*hyp*	(2*R*,4*S*)-hydroxyproline (*trans*-4-hydroxy-D-proline)
DCM	Dichloromethane
DIAD	Diisopropyl azodicarboxylate
DIPEA	*N,N*- Diisopropylethylamine
DMF	*N,N*-Dimethylformamide
DMS	Dimethyl sulfide
DNA	Deoxyribonucleic acid
ECM	Extracellular matrix
eq.	equivalents
ESI-MS	Electron Spray Ionization Mass Spectrometry
Et	Ethyl
Flp	(2*S*,4*R*)-Fluoroproline
flp	(2*S*,4*S*)-fluoroproline
Fmoc	9-Fluorenylmethoxycaronyl
g	Gram
Glu	Glutamine
Gly	Glycine
h	Hours
HBTU	(2-(1H-Benzotriazole-1-yl)-1,1,3,3-tetramethyl-uronium-hexafluorophosphate)
HOBt	N- Hydroxybenzotriazole
HPLC	High Performance Liquid Chromatography
Hz	Hertz

in situ	In the reaction mixture
in vivo	Within the living organism
in vitro	outside the living organism
IR	Infra-Red
kJ	kilojoules
$K_{trans/cis}$	Ratio of *trans/cis*
L-	Levo-
Leu	Leucine
Lys	Lysine
M	Molar
MALDI-TOF	Matrix Assisted Laser Desorption Ionization-Time of Flight
MeCN	Acetonitrile
MeOH	Methanol
Mep	(2*S*,4*R*)-Methylproline
mep	(2*S*,4*S*)-methylproline
Mg	milligram
mL	millilitre
MHz	megahertz
min	minutes
μ	Micron
μl	Microliter
μM	Micromolar
mL	Microliter
mmol	millimolar
MsCl	methanesulfonylchloride
ν	nu (frequency)
NaN_3	Sodium azide
Nm	Nanometer
NMP	N-Methyl-2-pyrrolidone
NMR	Nuclear Magnetic Resonance
Pd-C	Palladium on carbon
Phe_L	L-Phenylalanine
Phe_D	D-Phenylalanine
Pro_L	L-Proline
Pro_D	D-Proline
ppm	parts per million
PP-II	Polyproline-II
PP-I	Polyproline-I
R	Rectus
$R_{p/n}$	Ratio of positive to negative band intensities
RNA	Ribonucleic acid
S	Sinister
SPPS	Solid Phase Peptide Synthesis
t-Boc	*tert*-butyloxycarbonyl
t-Butyl	*tert*-butyl
TFA	Trifluoroacetic acid
TFE	2,2,2-Trifluoroethanol
THF	Tetrahedrofuran

TIS	Triisopropylsilane
TMS	Tetramethylsilane
T_m	Melting temperature
α	Alpha
β	Beta

Abstract

The thesis entitled "**Polyproline and Collagen Peptides Derived from 4(R/S)-OH/NH$_2$-L/D-Proline: Synthesis, Conformational and Morphological Studies**" is comprised of studies towards the design and synthesis of peptides based on 4(R/S)-hydroxy/amino L/D prolines in homochiral, heterochiral polyproline and collagen. Their conformational preferences under various physical environments are also explored. These peptides exhibited interesting morphological properties, which may have importance in various biomedical applications and in protein engineering.

The work is an attempt to understand the behaviour of 4(R/S)-hydroxy/ amino substitution on proline with an emphasis on the stereochemistry at C2 and C4 in both homo and heterochiral polyproline peptides under different solvents. The investigating of D-β-structure in heterochiral prolyl polypeptide may give new directions to guide future research work in peptide engineering.

The substitution of 4(R/S)-hydroxy/ amino L/D proline in collagen sequences showed mirror image conformations with similar thermal stability, and resulted into different nano-structures depending upon whether they are present as the chirally pure state or as a mixture of the spiegelmers.

Chapter 1: Introduction to D-amino acids, polyproline and collagen peptides

Chapter 2: Self-assembly of 4(R/S)-D-aminopolyproline

Chapter 3: Alternate and block heterochiral polypeptides from 4(R/S)-hydroxy-L/D proline

Chapter 4: Self-assembly of 4(R/S) hydroxyl/ amino collagen peptide spiegelmers

Chapter 1: Introduction to D-amino acids, polyproline and collagen peptides

This chapter gives the literature overview on the use of D-amino acids in designing, and engineering proteins for biomedical applications. It also explains the rationale for undertaking the research work, while emphasizing the recent advancements in the field of polyproline and collagen peptides and their applications.

Chapter 2: Self-assembly of 4(R/S)-D-aminopolyproline

This chapter deals with the comparative study of peptides **P1-P10** (Scheme 1) to understand the effect of chirality originating from C2 position of proline in polyproline peptides. H-bonding substitution and *cis* disposition of stereochemistry at C2 and C4 are prerequisites to show conformational change between PP-II and β-structure when solvent changes from water to TFE.

Fully N-terminus protected peptides **P1-P10** were synthesized by solid phase peptide synthesis using Fmoc chemistry and cleaved from solid support. Finally purified by HPLC and characterized by MALDI-TOF analysis.

Scheme 1
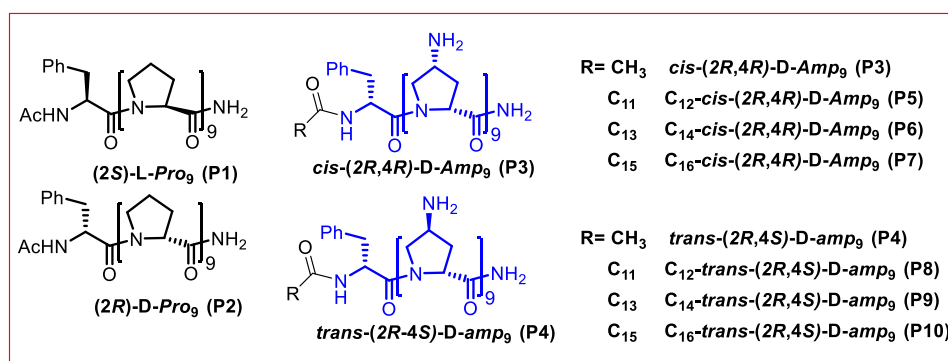
The peptide conformation is dependent on the nature of solvent.[1] Trifluoroethanol is known to break the helix by removing hydration sphere around the peptide back bone.[2] Solvent dependent conformational change between PP-II and *β*-structure has been reported.[3-5] Since the earlier reported peptides are L-peptides, we thought to examine whether similar effect is present in enantiomer D-peptides as well.

The conformational studies of peptides **P1-P10** were carried out by CD spectroscopic technique in both the solvents, water and TFE. The unsubstituted polyproline peptides **P1** (L-*Pro₉*) and **P2** (D-*Pro₉*) showed mirror image conformation both in water and TFE due to opposite stereochemistry at C2 position. The peptides **P2-P4** adopts right-handed PP-II conformation in water and only peptide **P3** [*cis*-(2R,4R)-D-*Amp₉*] showed conformational change from PP-II to D-*β*-structure (*β*-structure originating from D-proline) in solvent TFE (Figure 1).

Abstract
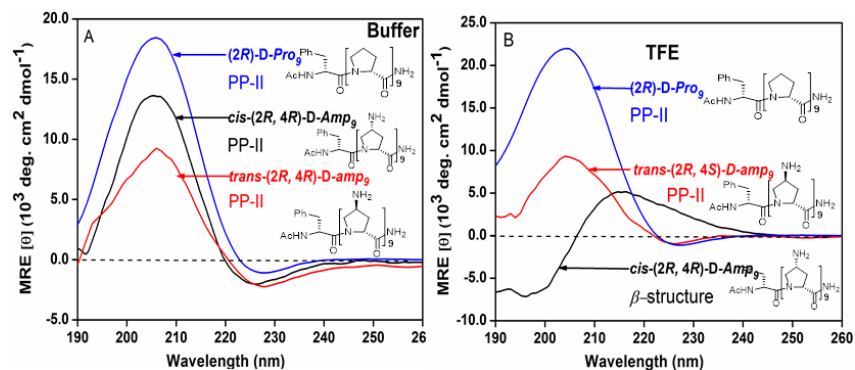
Figure 1 CD Spectra of peptides **A) P2-P4** in buffer and **B) P2-P4** in TFE at concentration 300 μM.

Superimposed CD spectra of the peptide **P3** [*cis*-(2*R*,4*R*)-D-*Amp9*] and **P11** [*cis*-(2*S*,4*S*)-L-*amp9*] in water, where they appear as mirror image right-handed and left-handed PP-II (Figure 2A). In solvent TFE, peptides **P3** and **P11** exhibit mirror image *β*-structure of each other with very small changes in intensity (Figure 2B).
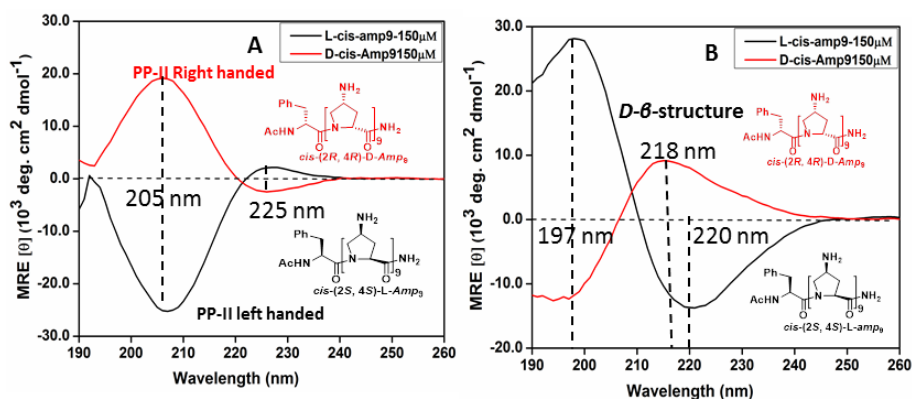
Figure 2. CD spectra of **P3** [*cis*-(2*R*,4*R*)-D-*Amp9*], **P11** [*cis*-(2*S*,4*S*)-L-*amp9*][3] **A**) Buffer and **B**) TFE.

Literature report suggests that the peptide **P13** [*cis*-(2*S*,4*S*)-L-*hmp9*] shows *β*-structure in TFE and self-assemble to form nanowires.[5] To examine the morphologies of self-assembled structure of D-peptides **P1-P10** FE-SEM and AFM techniques are used. It has been observed that peptides **P1**-**P4** self-assembled to form needle or nano spherical particles in water (Figure 3A-D).
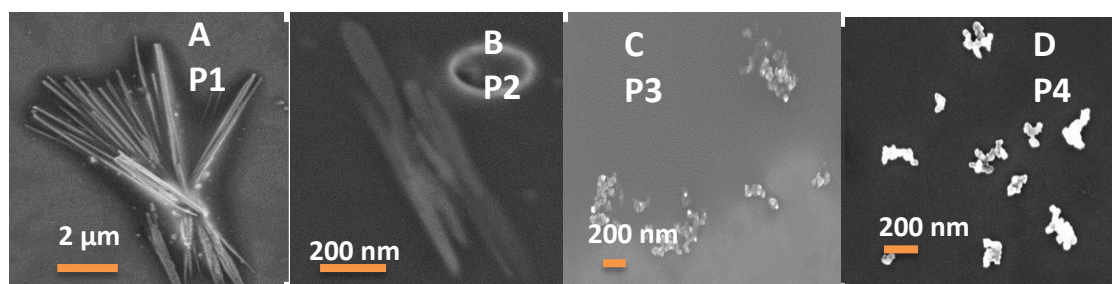
Figure 3. FE-SEM images of peptides **P1**-**P4** in water

Among peptides **P1**-**P10**, only the peptide **P3** formd D-β-structure as seen by the CD spectra in TFE. In solvent TFE, β-structure forming peptide **P3**, self-assembled to long lengthy, twisted nano fibers with 20 nm width, around 80 nm helical pitch and 1-1.5 µm in length (Figure 4 C).
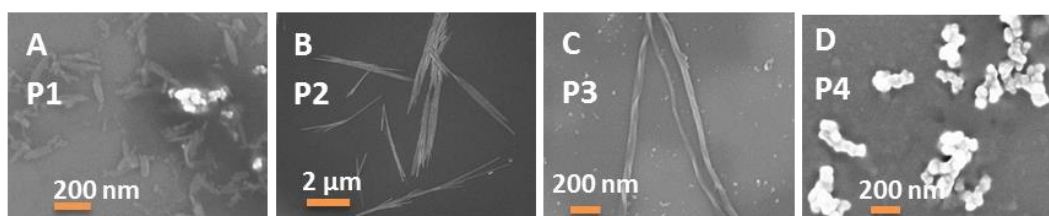
Figure 4. FE-SEM images of peptides **P1**-**P4** in TFE

In isolation both peptides exhibit similar forms of left-handed twisted fibers with similar dimensions (Figure 5A, C). To find out the chirality effect on handedness of self-assembled nano structure, mixing experiment was carried out. On mixing the two enantiomeric peptides **P3** and **P11** in identical concentrations, increased number of fibers were seen with more twists and less helical pitch. Figure 5 C is the mixed β-structure co-assembled into left-handed fibrils with large aggregates as compared to that of each pure enantiomer.
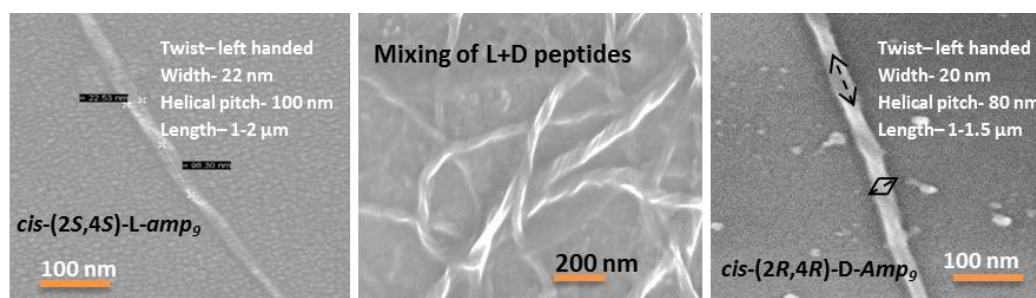
Figure 5. FE-SEM images of **P11** *cis*-(2*S*,4*S*)-L-*amp$_9$*[3] and **P3** *cis*-(*2R*,4*R*)-D-*Amp$_9$* in TFE.

The possible molecular inter-chain hydrogen bonds arrangement involved in 4-NH$_2$ in D-β-structure are shown (Figure 6). Thus, on one hand, the stereochemistry at C2 dictates the handedness of the helix, and at C4 on the other hand, the results illustrate a fine balance between stereoelectronic, H-bonding effects in orchestrating the novel structural conversion discussed in this chapter.
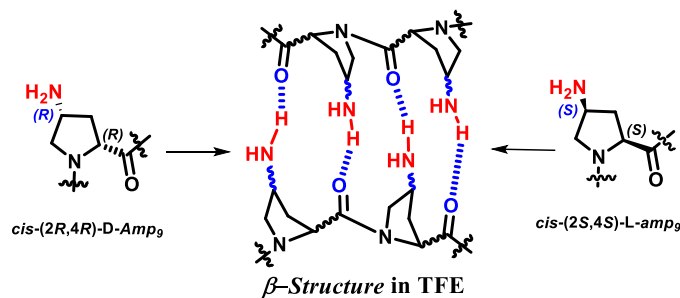
Figure 5. Molecular β-structure arrangement of *cis-(2R,4R)-D-Amp$_9$* and *cis-(2S,4S)-L-amp$_9$* in TFE

Chapter 3: Alternate and block heterochiral polypeptides from 4(R/S)-hydroxy-L/D-proline

Linus Pauling proposed model for polypeptides such as α-helix and β-sheets. In β-sheets he explained two types i.e. pleated and rippled sheet structure with parallel and antiparallel orientation.[6] The structure described are applicable for polypeptides constructed entirely from L-amino acids or of D-amino acid residues (homochiral peptides). He proposed that similar rippled sheet structures could be constructed with polypeptide chains having alternate D and L amino acid residues (heterochiral). Helices for alternate L, D peptides are explained theoretically and experimentally by several authors. Such structures are composed with torsional angles of the enantiomers located in respective *β* regions of Ramachandran plot.

This chapter is directed towards the study of heterochiral alternate and block prolyl polypeptides **P1-P12** (Scheme 2).

Scheme 2

Alternate peptides **P1**-**P8** & **P12**

P1 Phe_L-L[DL]$_4$ **P2** Phe_L-L$_t$[L$_c$L$_t$]$_4$ **P3** Phe_L-L$_t$[D$_t$L$_t$]$_4$ **P4** Phe_D-D$_t$[L$_t$D$_t$]$_4$ **P5** Phe_L-L$_c$[D$_c$L$_c$]$_4$

P6 Phe_D-L$_t$[D$_t$L$_t$]$_4$ **P7** Phe_L-D$_t$[L$_t$D$_t$]$_4$ **P8** PA-[L$_t$D$_t$]$_4$ **P12** C$_{14}$-Phe_LL$_t$[D$_t$L$_t$]$_4$

Block peptides **P9**-**P11**

P9 Phe_L-[L$_c$]$_4$[L$_t$]$_5$ **P10** Phe_D-[D$_t$]$_4$[L$_t$]$_5$ **P11** Phe_D-[D$_c$]$_4$[L$_c$]$_5$
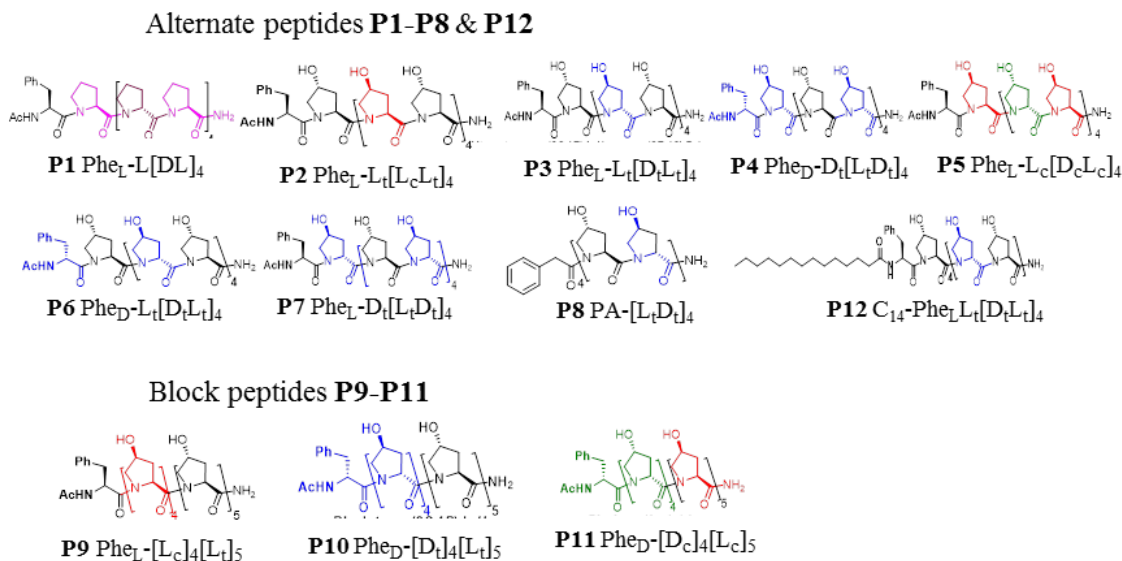
The conformational studies of the synthesized peptides **P1**-**P12** were carried out by CD spectroscopy in the solvents, water and TFE. Among all heterochiral alternate and block prolyl polypeptides, only peptide **P3** Phe_L-L$_t$[D$_t$L$_t$]$_4$ showed conformational change. In water, the peptide **P3** adopts left-handed PP-II form whereas, in a hydrophobic solvent like TFE it exhibits D-β-structure (Figure 6). The peptide **P4** Phe_D-D$_t$[L$_t$D$_t$]$_4$ has exact opposite residues from initial C-terminus to final N-terminus but failed to show an inversion of β-structure.
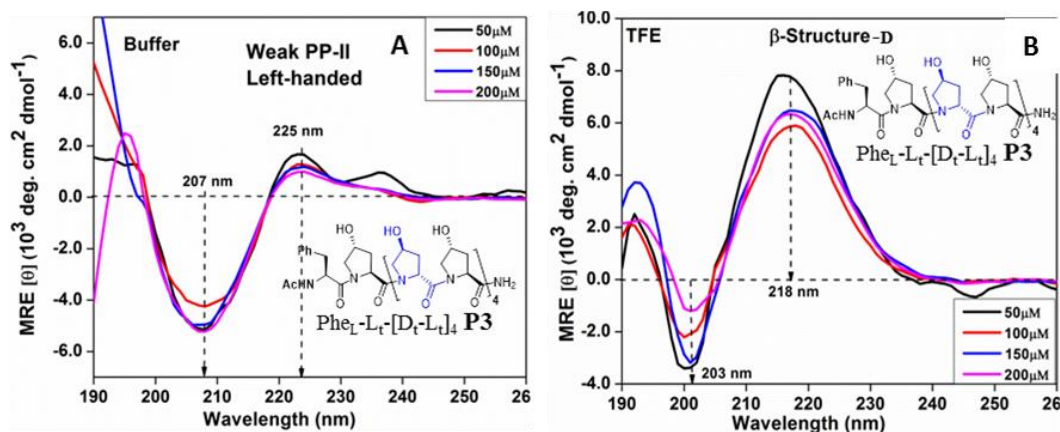
Figure 6. CD spectra of peptide **P3** Phe_L-L$_t$[D$_t$L$_t$]$_4$ in buffer **A)** and in TFE **B)**

The chirality of N-terminus phenylalanine may have an effect on the helical handedness. To probe the effect of chiral L-phenylalanine, we have substituted D-phenylalanine in the peptide **P6** Phe_D-L$_t$[D$_t$L$_t$]$_4$ and maintained the alternate chirality

throughout the sequence. We observed D-*β*-structure in both solvent water and TFE (Figure 7).
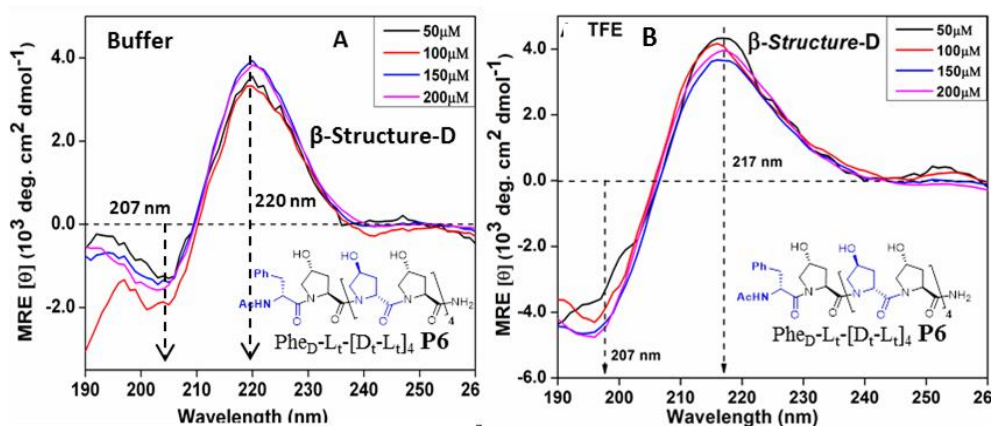
Figure 7. CD spectra of peptide **P6** Phe$_D$-L$_t$[D$_t$L$_t$]$_4$ **A)** in buffer and **B)** in TFE.

In order to examine if the chirlaity of N-terminus phenylalanine induces the peptide conformation, peptide **P8** PA-[L$_t$D$_t$]$_4$ having N-terminus achiral phenylacyl moiety was synthesized. The peptide **P8** adopts D-*β*-structure at low as well as at high concentration in both the solvents, water and TFE. This experiment suggested that, when equal number residues of opposite chirality are present, then synthesized peptide is likely to form *β*-structure.

In order to find out the morphology of synthesized peptides **P1-P12,** their FE-SEM and AFM images were recorded. The peptide **P3** showed self-assembled nanospheres of around 200 nm diameter in water. In TFE, peptide **P3** self-assembled into nanorods of dimensions 200 nm length, 20-30 nm width. This observation correlates with CD study and suggests that the peptide **P3** is capable of self-assembling into nanowires on increasing molecular interactions.
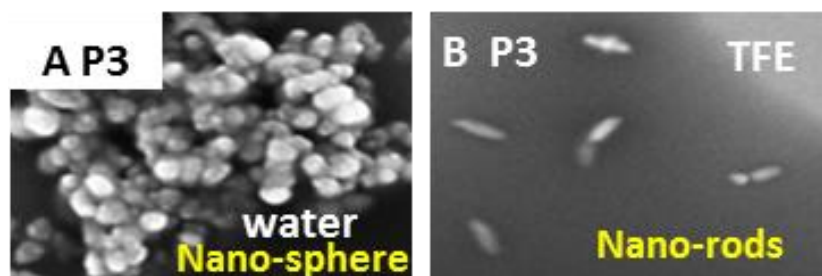
Figure 8. FE-SEM images of peptide **P3 A)** in water **B)** in TFE

To increase the molecular interactions (hydrophobic and hydrophilic), the peptide **P3** was conjugated with fatty acid to have peptide **P12** C_{14}-Phe$_L$L$_t$[D$_t$L$_t$]$_4$. It is observed in the CD spectra that conjugation did not alter the conformation in the respective solvents. In water, the peptide **P12** self-assembled to nanospheres of around 1μm as in diameter, seen in AFM and in FE-SEM images (Figure 9A-C).
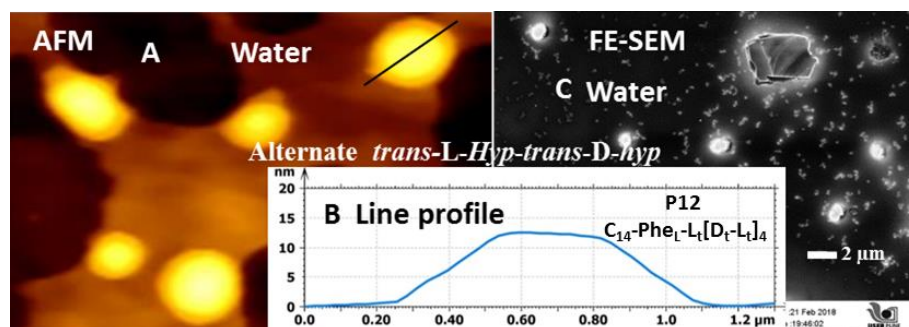
Figure 9: A) AFM, **B)** Line profile and **C)** FE-SEM of peptide **P12** C_{14}-Phe$_L$L$_t$[D$_t$L$_t$]$_4$ in water

In solvent TFE, the peptide **P12** self-assembled to long nanofibers of around 2-3 μm in length. The height of the fiber is around 20 nm. Moreover these wires had left-handed twist with shallow grooves. The depth of groove varied between 4-6 nm on the surface of the nanofibers (Figure 10).
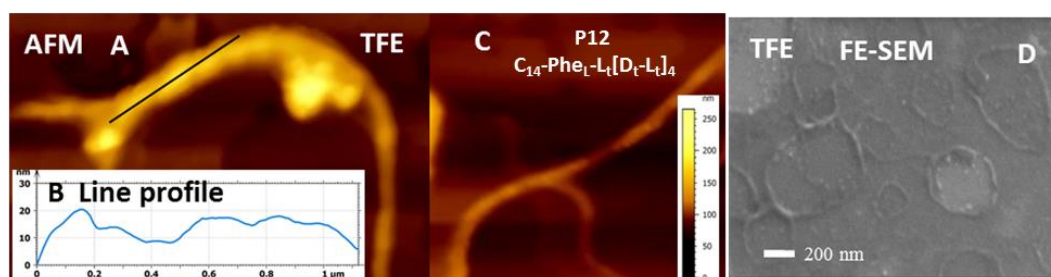
Figure 10: A,C) AFM, **B)** Line profile and **D)** FE-SEM of peptide **P12** C_{14}-Phe$_L$L$_t$[D$_t$L$_t$]$_4$ in TFE

Chapter 4: Self-assembly of 4(R/S) hydroxy/ amino collagen peptide spiegelmers

Collagen is an abundant structural protein found in mammals.[7] The primary structure of collagen is composed of X-Y-Gly repeat. The amino acids in the X and Y positions are predominantly (2*S*)-L-proline (Pro, 28%) and (2*S*,4*R*)-L-4-hydroxyproline (Hyp 38%) respectively. Hydroxyl group in hydroxyproline (Hyp) provides exceptional mechanical strength, broad resistance to the proteolytic enzyme and thermal stability to the triple-helical structure of collagen.

Abstract

Crystal structure of collagen shows that hydroxyl groups are pointing in one direction on the periphery of the circle (Figure 11A). By this logic in the enantiomeric peptide chain, the 4-OH groups must point in the opposite direction as in (Figure 11B) 4(*R* Vs *S*). On this basis, upon mixing, these enantiomeric peptides may come together through complementary association of hydrogen bonds generated by the hydroxyl groups.
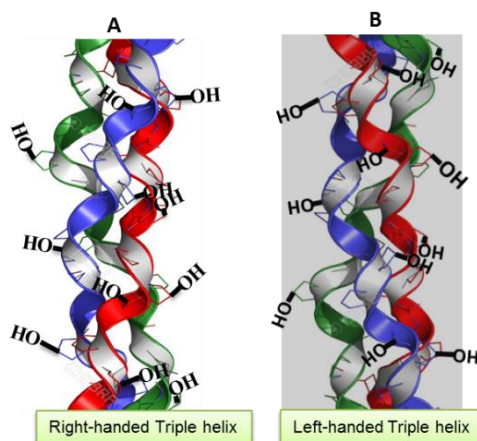
Figure 11. A) L-collagen right-handed[8] **B)** proposed D-collagen left-handed[9]

It was previously reported in literature that having 4(*R*)-aminoproline (*Amp*) instead of *Hyp* in collagen triple-helix at Y site enhances the triplex thermal stability. At all pH conditions, *Amp* incorporated collagen sequences formed stronger triple helices as compared to *Hyp*.[10,11] Amino group has an increased the H-bond potential (with 2 hydrogens), and it is a better hydrogen bond donor. Since the amino group is ionisable, it gets protonated to NH_3^+ (even at pH 7.0).

Based on the above mentioned facts, packing of opposite handed enantiomeric collagen peptides into ordered self-assembled structure is explored in this chapter. This chapter is further divided into two sections.

Section A: Self-assembly of 4(R/S) hydroxy collagen peptide spiegelmer

The present work is a comparative study of collagen peptides **P1** & **P2** (Scheme 1). Peptide **P1** & **P2** are synthesized successfully, cleaved from solid support, purified by HPLC and characterized by MALDI-TOF analysis.

Scheme 3: Collagen peptides **P1-P2**
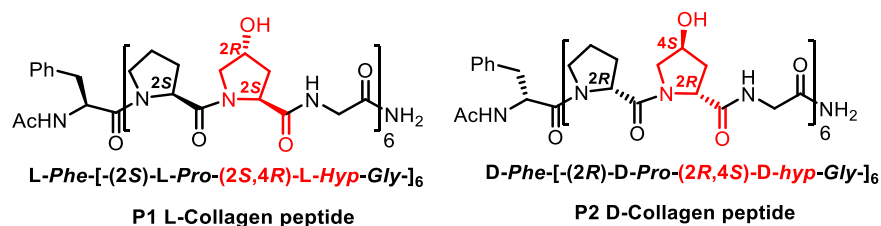
Abstract

In this chapter CD spectroscopy is used to determine the secondary structure of peptides **P1** and **P2,** and the effect of temperature on characteristic CD spectral bands to measure the thermal stability of the peptides. In the CD spectra, a weak positive CD band at 225 nm and a large negative CD band at 205 nm, which are the characteristic peaks of left-handed polyproline-II (PP-II) helix in solution, are observed for L-collagen peptide **P1**. The enantiomeric D-collagen peptide **P2** showed CD spectra that is a mirror image of the L-collagen peptides **P1**. Figure 12A, shows the exact mirror image, inversion of CD bands for these oppositely handed collagen triple helix peptides.

The thermal melting T_m values for peptides **P1** and **P2** are almost identical. The values obtained from minima of the graph are 30 ^{o}C & 29 ^{o}C respectively (Figure 12B).
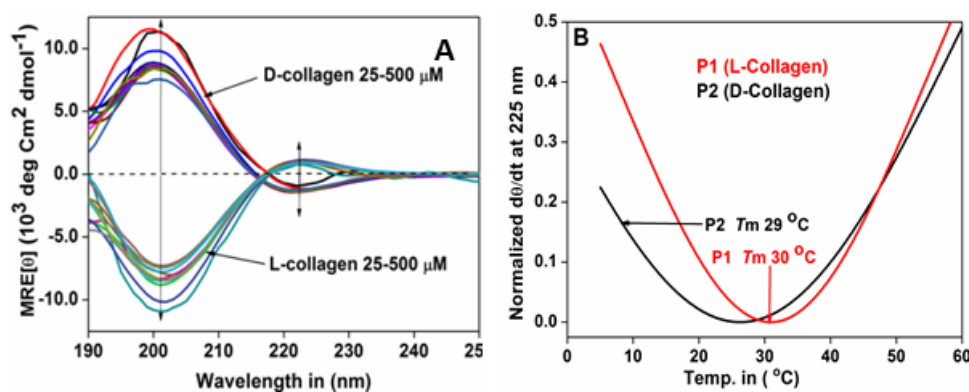
Figure 12. Opposite handed CD spectra **A)** and thermal melting graphs **B)** for peptide **P1** and **P2**

The collagen peptide has an innate tendancy to self-assemble to form higher order fibrous stuctures. To examine the morphology of the synthesized collagen peptides **P1** & **P2**, FE-SEM and AFM images were recorded. It is observed that the individual peptides **P1** and **P2** self-assembled to regular rice grain shaped nanoparticles of size 300 nm as seen in FE-SEM.

Abstract
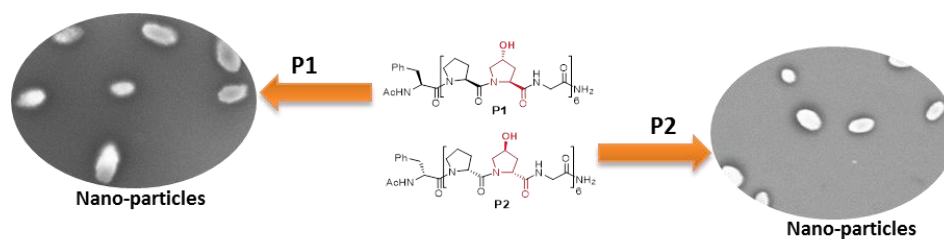
Figure 13. FE-SEM images of collagen peptide **P1** and **P2** in water

The enantiomeric peptides **P1** and **P2** were mixed in stoichiometric amounts at concentrations 250 μM, and annealed at 80 °C, cooled and FE-SEM images were recorded (Figure 14B). The image showed a network-like structures, sticky form suggesting no defined self-assembled pattern. The regular shapes of nanoparticles seen in individual peptides were lost upon mixed annealing.

In another experiment, the enantiomeric peptides were mixed stoichiometrically in their triple helix form at room temperature and FE-SEM & AFM images of the mixtures were recorded. Unlike in the previous annealed experiments, at 250 μM, the triple helix forms inter self-assembly (Figure 14A). The enantiomeric peptides exhibited fusion leading to hollow spherical vesicle type of particles.
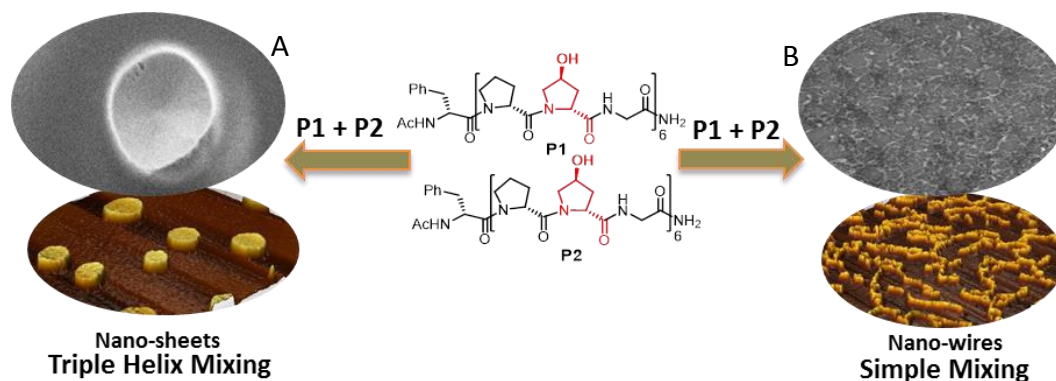
Figure 14. FE-SEM & AFM images of mixed collagen peptide **P1** and **P2**, **A)** Triple helix mixing, **B)** Simple mixing.

Section B: Self-assembly of 4(R/S) amino collagen peptide spiegelmer

In this section two enantiomeric peptides **P3** (L-amino collagen) and **P4** (D-amino collagen) are synthesized and cleaved from solid support, purified by HPLC and characterized by MALDI-TOF analysis (Scheme 4).

XX

Scheme 4: Amino collagen peptides **P3** & **P4**

L-*Phe*-[-(2S)-L-*Pro*-(2S,4R)-L-*Amp*-*Gly*-]$_6$

P3 L-Amino collagen peptide

D-*Phe*-[-(2R)-D-*Pro*-(2R,4S)-D-*amp*-*Gly*-]$_6$

P4 D-Amino collagen peptide
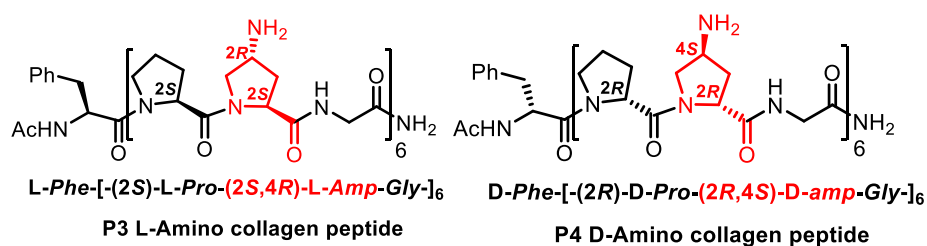
The secondary structures and thermal stability of these enantiomeric amino collagen peptides **P3** & **P4** are examined using CD. The positve CD band at 225 nm, and negative CD band at 200 nm in L-amino collagen **P3** suggest that the synthesized peptide adopts left handed PP-II helix. In case of **P4** D-amino collagen peptide (Figure 23B), weak negative CD band at 225 nm and strong positive CD band at 200 nm with cross over at 215 nm suggest that the peptides in which D-amino prolines are incorporated are showing mirror image conformation of L-amino collagen.
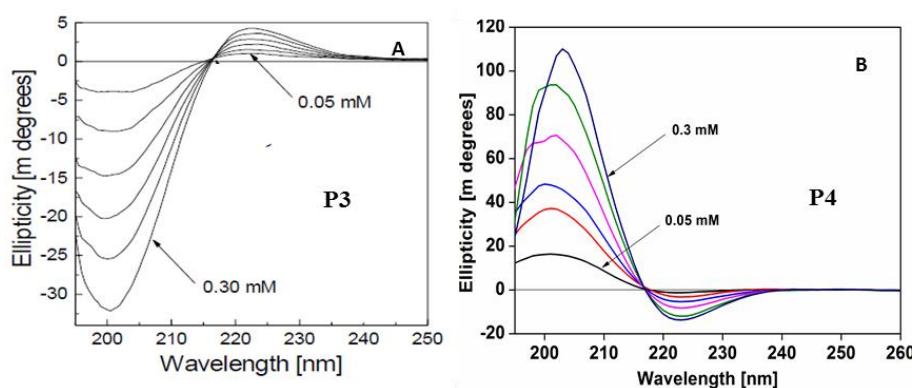
Figure 15(**A-B**). CD spectra of peptide **A)** Peptide **P3*** **B)** Peptide **P4** at 25^0 C, concentration

      range 0.05-0.3 mM in 10 mM sodium phosphate buffer at pH 7.2

      *Graph taken from reference 10

Figure 26 shows comparative T_ms of L-amino collagen peptide **P3** and D-amino collagen peptide **P4** in pH range, from 3.0 to 12.0. Thus there are no stability differences seen between the two enantiomeric peptides at acidic, neutral and basic conditions. However 4(R) Amino L-proline substitution in L-collagen as well as 4(S) amino D-proline in D-collagen sequence enhance the triplex stability at all pH range, from 3.0 to 12.0, compared to corresponding hydroxyl collagen peptides. The triplex stability of both enantiomeric peptides were the least at pH 9.0 and increased at both acidic and basic pH
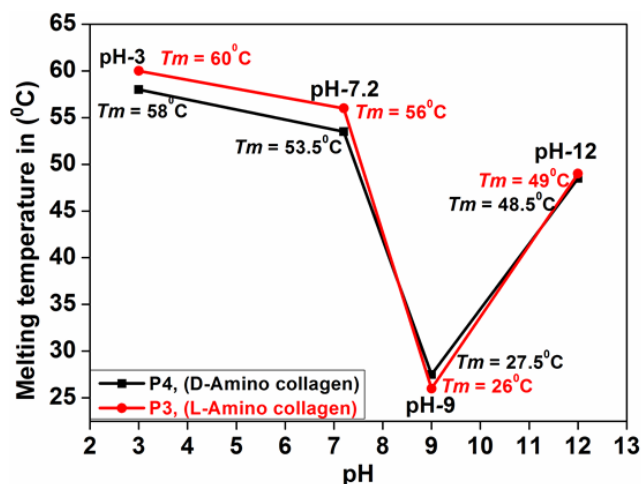
Figure 16. Melting temperatures of (red) **P3**[10] and (black) **P4** at pH range, from 3.0 to 12.0.

Amino collagen peptides **P3** & **P4** self-assembled into nanospheres of size around 500 nm in diameter at physiological condition (pH 7.0) (Figure 17).
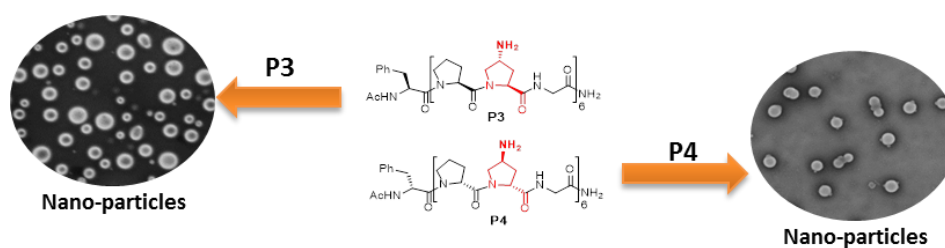
Figure 17. FE-SEM images of amino collagen peptide **P3** and **P4** at pH 7.2

The peptide **P3** and **P4** when mixed stoichiometrically, triple-helix forms inter self-assembled to form nanosheets with sharp edges (Figure 33F). Even when the peptides **P3** & **P4** mixed together and then annealed, they resulted into the same morphological nano structures i.e. nanosheets of around 1-2 um size (Figure 18).
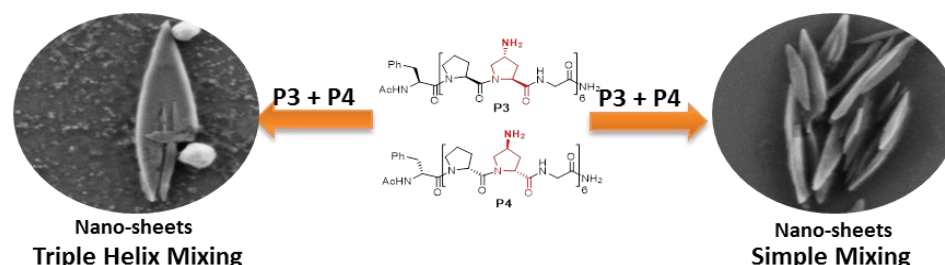
Figure 18. FE-SEM & AFM images of mixed amino collagen peptide **P3** and **P4**, **A)** Triple helix mixing, **B)** Simple mixing at pH 7.2

Abstract

References:

(1) Ninad, P.; Kim, S., Solvent-Protein interactions. *Chem Rev.* **2006,** *106*, 1616–1623.

(2) Sonnichsen, F. D.; Van Eky, J. C.; Hodges, R. S.; Sykes, B. D., Effect of Trifluoroethanol on Proteins Secondary Structure: An NMR and CD Study Using a Synthetic Actin Peptides. *Biochemistry*. **1992,** *31*, 8790-8798.

(3) Mahesh, V. S.; Krishna, N. G., Water Induced Switching of Beta-structure to Polyproline II Conformation in the 4S-Amino proline Polypeptide Via H-bond Rearrengment. *Org. Lett*, **2010**, *12*, 5390-5393.

(4) Nitin, D. B.; Madhanagopal, B.; Mahesh, V. S.; Krishna, N. G., Stereo dependent and solvent-specific formation of unusual β-structure through side chain-backbone H-bonding in C4(*S*)-(NH$_2$/OH/NHCHO)-L-prolyl polypeptides. *Peptide. Science,* **2017**, *108*, 22981-22992.

(5) Nitin, D. B.; Mahesh, V. S.; Krishna, N. G., A nanofiber assembly directed by the non-classical antiparallel beta-structure from 4S(OH) proline polypeptides. *chem. Commun.,* **2016**, 52, 4884-4887.

(6) Linus, Pauling and Robert B. Corey, Two rippled-sheet configuration of polypeptide chains, and a note about the pleated sheets. *PNAS,* **1953**, *39,* 253-255.

(7) Prockop, Kivirikko, K. I., *Annu. Rev. Biochem.* **1995**, *64*, 403-434.

(8) Image taken from internet source link given below and modified to show hydroxyl groups pointing outside of the helix
https://www.google.co.in/search?q=collagen+images&source=lnms.

(9) Image in ref no 8 was vertically rotated twice to get mirror image using Microsoft program.

(10) Babu, R. I.; Ganesh, K. N., *J. Am. Chem. Soc.* **2001,** *123,* 2079.

(11) (a) Umashankar, M.; Babu, R. I.; Ganesh, K. N., *Chem.Commun*. **2003**, 2606; (b) Umashankar, M.; Sonar, M. V.; Bansode, N. D.; Ganesh, K. N*., J. Org. Chem.***2015,** *80*,8552.

Chapter 1

Introduction to D-Amino acids, Polyproline and Collagen Peptides

Chapter 1: Introduction

1.0 Introduction to chirality in biomolecules

The biosphere is inherently chiral. Biopolymers like proteins and nucleic acids are made up of monomers which have uniform chirality. While the amino acids in proteins have L-configuration, the sugars, ribose, and deoxyribose, in nucleic acids have D-configuration.

Even though proteins usually comprise of L-amino acids exclusively, D-amino acids do occur in nature. D-amino acids are also found in natural peptides synthesized by microorganisms. For example, tyrocidine and gramicidine are synthesized by bacteria *Bacillus brevis*. D-amino acids such as D-glutamic acid, D-alanine are found in the cell wall of bacteria where it plays an important role of protection to the bacteria.[1] D-amino acids are also found in higher organisms. D-aspartic acid and D-serine regulate neurotransmission in the brain.[2] Enzymes uses post-translational epimerization to produce the D-amino acids from L-amino acids. Different peptides such as opioid, dermorphins and deltorplims containing D-amino acids are found in the skin of various frog species belonging to the phyllomedusinae[3] and cone snails produces contryphans peptides.[4]

D-amino acids are always degraded slower than their L-counterparts, but there are some examples of enzymes that can degrade L-amino acid and D-amino acids with the same rate.[5] The reason behind this selection, and the prebiotic processes that led to this chiral preferences are still under intense debate and many speculations and theories have been put forth.[6] It is apparent, however, that for the macromolecules to be structurally well-defined and function, they need to be homochiral. With a random mixture of L and D enantiomers of amino acids in a sequence, it would be impossible for the biopolymers to attain regular structures. Even a single change of amino acid configuration from L to D amino acid in proteins, or from D-sugar to L-sugar in nucleic acids would result in the collapse of the structure and loss of function. On the contrary, in some cases, it has been shown that the judicious incorporation of D amino acids into proteins expands their structural motif and provides enhanced stability to the proteins.[7] Such studies put many theories on homochirality in biomolecules in question. Construction of an entire protein by inverting all the L-amino acids into D-amino acids on the other hand, has shown that a total inversion of the structure including chirality at the monomer level, is reflected in the handedness of helix associated

with the secondary structures in the proteins and eventually results in structure of the protein turning into its mirror image of L-enantiomer.[8]

Because the biomolecules are chiral, the biochemical interactions among them must be inherently chiral.[6] Chirality plays a key role in various molecular recognition processes. Molecular recognition happens through different ways. In DNA for example, the nucleobases recognize each other by H bonding. Similarly, recognition also happens through chirality, based on which a biomolecule recognize its correct partner.[8] Recognition properties and functions associated with chirality vary from point to point. There are peptides and proteins in which recognition happens through homochirality,[9] whereas in some peptide molecules such as poly-L-lysine, poly-D-lysine and ambidextrous peptides recognition happens between heterochiral species.[10,11] There are a few examples present in the literature where there is no specificity in recognition between homochiral and heterochiral species.[12]

One of the ways of expression of homochirality and heterochirality is in terms of gel formation ability of the synthetic peptides. There are instances where homochirality and heterochirality are individually responsible for better gelling ability.[13-18] In one of the examples, homochirality confers superior mechanical strength, while heterochirality provides kinetics of gel formation.[16] However, there are cases where gel formation is independent of chirality. It is also possible to tune the mechanical strength and kinetics of such supramolecular aggregates by taking advantage of several factors including chirality, side chains, temperature, etc. It is reported that chirality of supramolecular aggregates can be fine-tuned by alternating the alky side chains,[19] changing the solvent,[20] modulating the pH values,[21] ultra-sonication, and temperature.[22]

1.1 Conformational analysis of polypeptides

Proteins are hetero biopolymers of homochirality and are linear chains of different combinations of amino acids that fold into three-dimensional shapes which are crucial to perform a wide range of the functions in cell, the amino acids in the sequence directing the three-dimensional folding of proteins.[23] Polypeptide conformations can be described in terms of three main chain torsion angles: (a) ϕ (*phi*) the torsion angle about C_α-N σ-bond (R-C_α-N-H), (b) ψ (*psi*), the angle about the σ-bond between carbonyl group and C_α (R-C_α-C-O) and (c) ω the angle about the amide bond (O-C-N-H) (Figure 1). The σ-bonds (except in proline) are relatively flexible and the preferred values for ϕ and ψ angles depend upon the nature of

the α-substituent. Allowed values for φ and ψ are graphically shown by Ramachandran through φ *versus* ψ plot.[24] The torsional angles of each residue in a peptide define the geometry of its attachment to its two adjacent residues by positioning its planar peptide bond relative to the two adjacent planar peptide bonds. Thus torsion angles are among the most important local structural parameters that control protein folding.
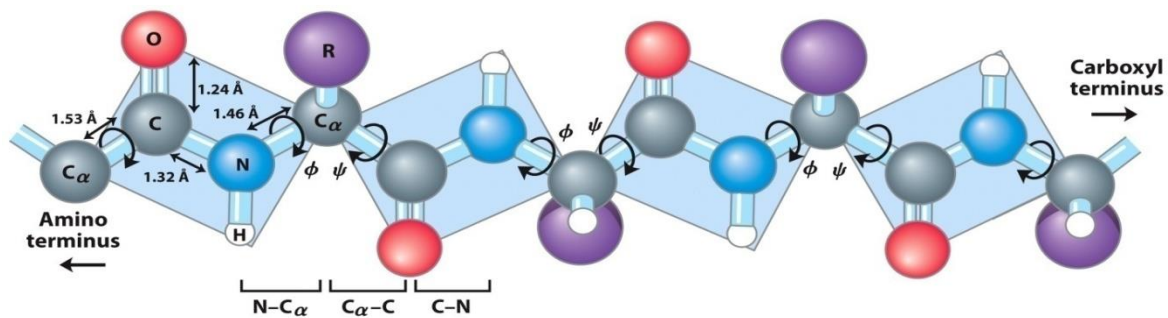
Figure 1. Illustration of peptide plane and the torsion angles.

1.1.1 Ramachandran plot

The sterically allowed values of φ and ψ can be determined by calculating the distances between the atoms of a tri-peptide at all values of φ and ψ for the central peptide unit. Such calculations lead to Ramachandran plot[24] (Figure 2), which defines the energetically allowed secondary structures for all sets of combinations of φ and ψ angles. The contours indicate the extent of allowed (light blue) and most favored (dark blue) combinations of (φ, ψ). The black circles show the locations of the ideal phi, psi values for the most putative regular secondary structural features, *β*-strands (in antiparallel and parallel sheets) and α-helices. Outside the contours, the corresponding conformations are disfavored.

It is understood from the plot, that all L-residues correspond to negative values of φ and positive values of ψ. There are few conformations such as α-helix left-handed in which φ and ψ corresponds to positive values.
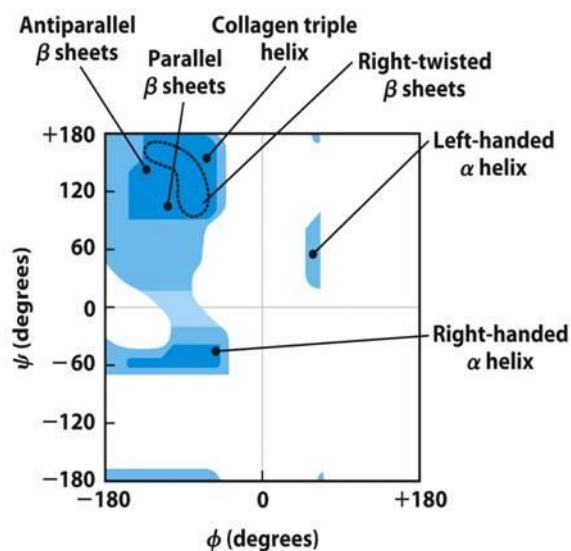
Figure 2. Ramachandran plot for a variety of peptide structures.[24]

1.1.2 Achiral amino acids Glycine and α-aminoisobutyric acid are alternative for D-amino acids

Glycine is achiral and less sterically hindered amino acid. It therefore imposes less constraint into the polypeptide chains. Due to its high flexibility, it is often found in loop regions, where the polypeptide chain takes a sharp turn. This is the reason for the high conservation of glycine residues in protein families such as collagen. Due to the absence of a substituent at Cα, glycine can adopt conformation on either side of the φ-ψ in the Ramachandran plot occupying the largest area in the map (Figure 3).
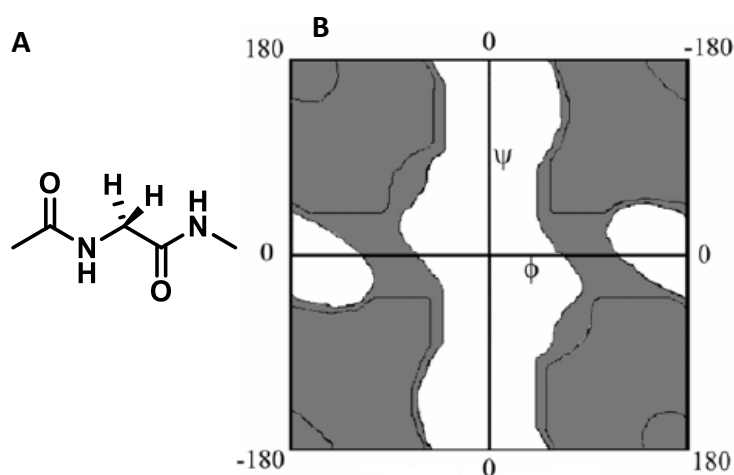
Figure 3. A) N-acetyl-glycine **B)** Allowed regions of Gly in Ramachandran plot.[25]

Achiral amino acids such as glycine (Gly) and α-aminoisobutyric acid (Aib) can be used as an alternative for D-amino acids in the peptide design because they support both conformations with positive and negative values of ϕ.[25] Stereochemically allowed regions for L-amino acids correspond to negative values of ϕ, and hence handedness of the conformations formed by L-polypeptides are mostly in right-handed form. Similarly for D-amino acids, ϕ values are positive, and the corresponding D-polypeptides form helices of left-handed conformation.

1.1.3 ϕ-ψ values of L-Pro and D-Pro are mirror image

L-Proline is the most constrained amino acid present in proteins. Due to cyclisation of side chain, it forms pyrrolidine ring and the rotation around C_α-N σ-bond (ϕ) is restricted to the value -60° (± 20); the allowed values of ϕ for D-proline are +60° (± 20) (Figure 4).
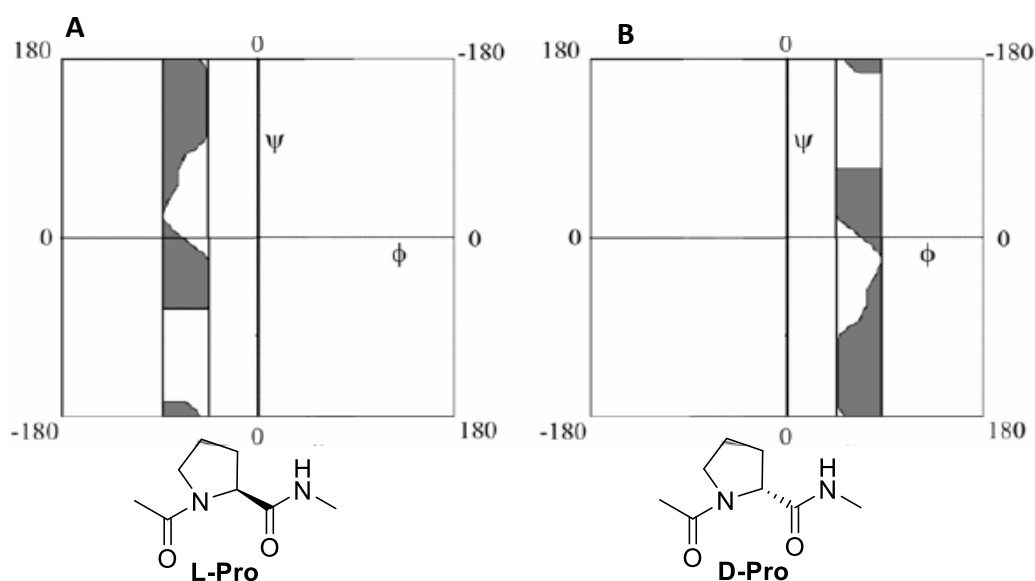
Figure 4. Ramachandran plots **A)** N-acetyl-L-proline **B)** N-acetyl-D-proline[25]

1.1.3a Use of L-Pro and D-Pro for turns and β-hairpin

Depending upon the number of intervening atoms in a turn before the first H-bond is formed, different types of turns are identified. In an α-turn, the end residues are separated by four peptide bonds ($i \rightarrow i\pm4$) (Figure 5A); in a *β*-turn (the most common form) by three bonds ($i \rightarrow i\pm3$) (Figure 5B); in a γ-turn by two bonds ($i \rightarrow i\pm2$) (Figure 5C) and in a π-turn by five bonds ($i \rightarrow i\pm5$) (Figure 5D).
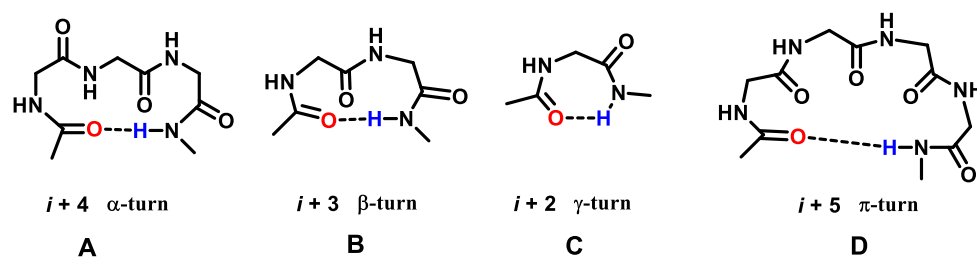
Figure 5. Representation of (A) α-turn, (B) β- turn, (C) γ-turn and (D) π turn.

β-Hairpins are widely present in globular proteins with an antiparallel β-sheet formation which are facilitated by introducing the reverse turn.[26] β-Hairpin motifs adopt specific conformations, depending upon the number of residues in the turn and the number of *inter*-strand hydrogen bonds formed between two oppositely oriented β-sheets.

Proline is often present at the end of helices and functions as a helix disruptor. L-Pro-Gly dipeptide sequence in peptide introduces γ-turn and acts as a nucleation site for β-hairpins. Two residue β-turns belong to the type II' and I' turns. In II' (prime) turn, the amino acid at positions i+1 holds the conformation containing ϕ values $\sim +60^0$ and ψ values at -120^0. Type I' (prime) turn at residue i+1 adopts ϕ, $\psi \sim +60^0$, and $+30^0$ respectively.[25,27]
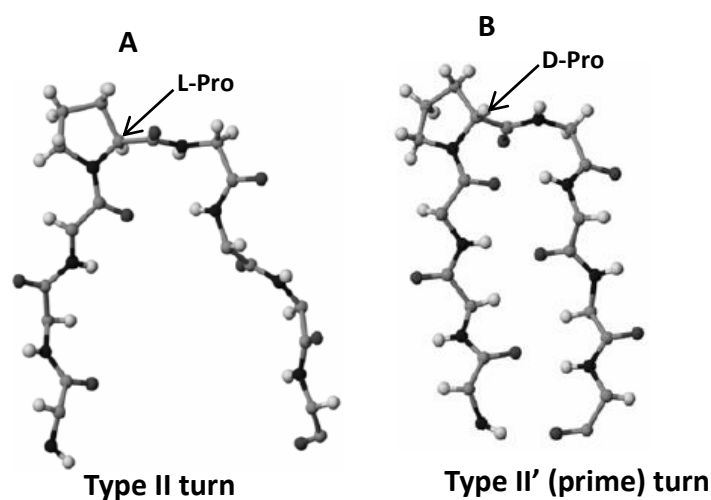
Figure 6. Turns in β-hairpin **A)** Type II turn, **B)** Type II'(prime) turn.

Crystallographic studies of octapeptide (Boc-LVVLPGLV-OMe) shows that L-Pro-Gly gives type II turn but the two strands remains away from each other (Figure 6A) whereas, in the previous peptide, L-Pro on replacing with D-Pro produces type II' (type II prime) turn, which holds two strands in close proximity, suggesting D-Pro to be better than L-Pro to introduce tight β-turns (Figure 6B).[25,28]

The stabilizing effect of D-Pro in type II' turn was a crucial finding which suggested the key structural importance of D-amino acid in the design of *β*-hairpin.[29] D-Proline residue provides strong conformational outcomes when inserted in the L-amino acid sequences. Middle incorporation of D-Pro-Gly sequences are used to generate the multi-stranded antiparallel β-sheet structures (Figure 7).[30,31]

Three stranded β-sheet   **Four stranded β-sheet**
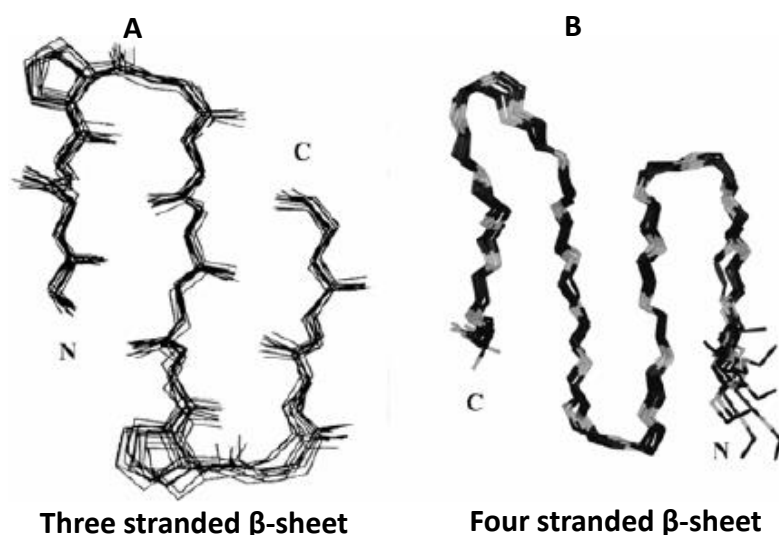
Figure 7. D-Pro-Gly segments in β-hairpin to produce turn in **A)** Three stranded β-sheet[30] and **B)** four stranded β-sheet.[31]

The dipeptide D-Pro-AA that is used to introduce turns was explored in a 20 mer β-hairpin motif, which self-assembled to form macroscopic hydrogel useful for various purposes.[32]

1.1.4 Effect of D-amino acids on *β*-sheet

A *β*-sheet (Figure 8) is made up of individual strands of peptide chains which are held together by hydrogen bonds between the neighboring chains (*inter*-strand). The side chains project above or below the sheet, and well placed to interact with side chains of an adjacent sheet. *β*-sheets are stabilized by (1) hydrogen bonds, (2) their side chains interactions, (3) favorable (ϕ, ψ) angles (in *β*-region of the Ramachandran plot), and (4) Van der Waals attractions.

A Parallel
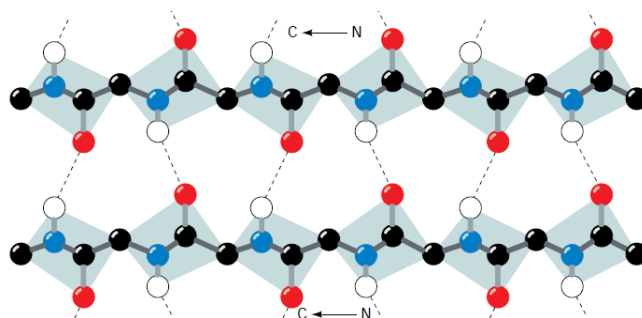
B Antiparallel
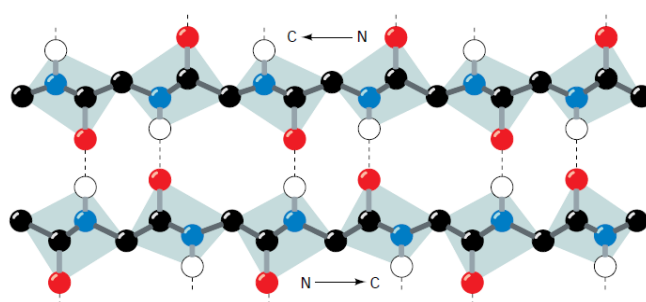
Figure 8. The β-sheets with dashed lines indicating hydrogen bonding between the polypeptide strands (A) parallel (B) an antiparallel β-sheet.[24]

Depending upon relative orientations of adjacent chains, which can run in either same or opposite directions, β-sheets are categorized into two types

➢ In parallel β-sheet, both the hydrogen-bonded chains pointing in the same direction (Figure 8A). (N→C; N→C).

➢ In antiparallel β-sheet, the neighboring hydrogen-bonded polypeptide chains run in opposite directions (Figure 8B). (N→C; C→N)

The incorporation of D-amino acids in the β-sheet forming sequence reduces the intermolecular interactions among the peptide chains and thereby hampers their propensity of secondary conformation.[33] Similarly, another report suggests that there is a complete disruption of β-sheet conformation on incorporation of D-amino acids.[34] Shortest tri-peptide (Phe-Phe-Val) is known to self-assemble to gel at neutral pH. In particular, the central residue alone is able to dictate the chirality of supramolecular arrangements of the peptide.[35] In contrast, one of the studies indicates that the peptide made from D-amino acids acquires β-structure in dilute conditions while its L-analogue peptide does not fold into β-sheet

suggesting the structural role of D-amino acids.[36] Another example suggests that D-enantiomer shows temperature dependent transition in conformation from β-sheet to α-helix while L-enantiomer fails to show such conformational transition. At room temperature, D-peptide folds into β-sheet whereas, at high temperature (110 ^{0}C), the peptide forms an α-helix.[37]

1.1.5 Effect of D-amino acids on α helix

α-Helix is a common secondary structural element of protein and consists of right-handed spiral conformation (Figure 9). An ideal α-helix has 3.6 residue per turn, with helical pitch 0.54 nm and rise of 0.15 nm (Figure 9). However, α-helices are slightly distorted in proteins with 3.5 to 3.7 amino acids per turn. In an α-helix, carbonyl oxygen of ith residue of the peptide chain is hydrogen bonded to amide NH of the $i+4^{th}$ residue toward the C-terminus. Each hydrogen bond consists of total 13 atoms (the carbonyl oxygen, 11 backbone atoms and the amide hydrogen). The α-helix is also termed as 3.6_{13} helix. The hydrogen bonds stabilizing the helix are parallel to the axis of the helix.[24]
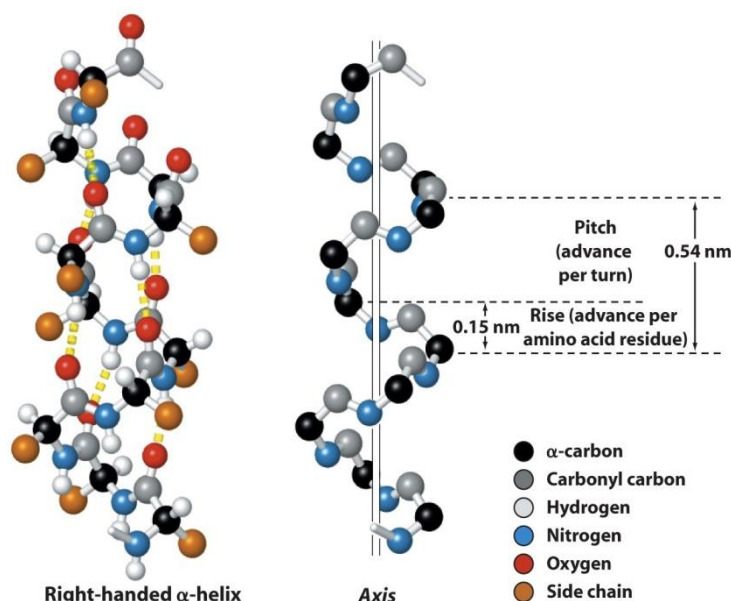
Figure 9. The α helix, dotted lines show hydrogen bonds.[24]

In contrast to β-sheet, introduction of one D-residue in a 14-mer polypeptide showed complete disruption of gel formation, suggesting that the supramolecular structures formed from L-amino acids (homochiral) sequences are better preserved as compared to D-residue inserted (heterochiral) sequences.[38] A coiled-coil forming 7-mer with repeating unit, EWEALEKKLAALE-$_L$AKLQALEKKLEALEHG forms α helical dimers at high

concentration. However, replacing an alanine in the above coiled-coil peptide to D-Ala (EWEALEKKLAALE-DAKLQALEKKLEALEHG) showed destabilizing effect on α helical dimer formation.[39]

A 10-mer peptide (Boc-Leu-Aib-Val-Ala-Leu-Aib-Val-LAla-LLeu-Aib-OMe) forms perfect α-helix (Figure 10A). On introduction of two D-residues near the C-terminus, (Boc-Leu-Aib-Val-Ala-Leu-Aib-Val-DAla-DLeu-Aib-OMe), resulted in the disruption of the α-helix (Figure 10B).[40,41]
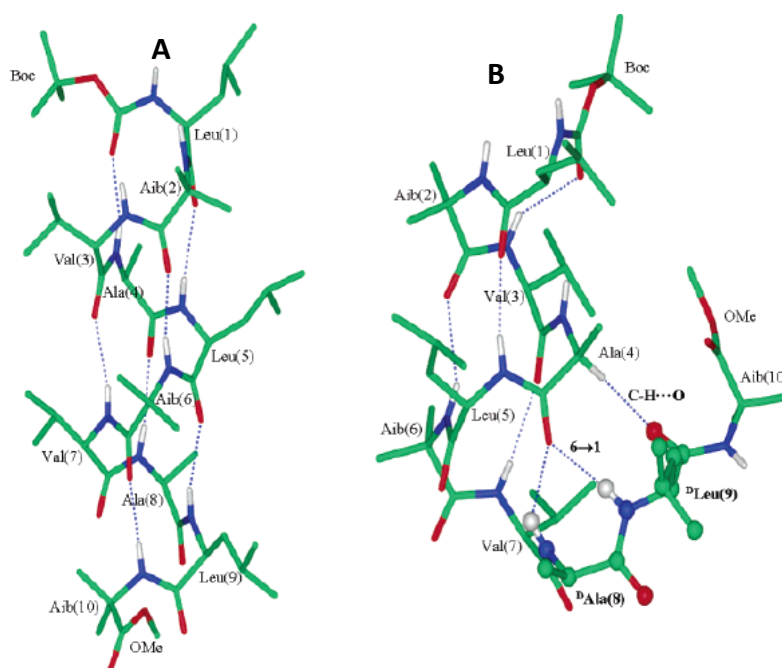
Figure 10. A) Perfect α helix, B) Disruption of α helix by D-amino acids.

1.1.6 D-amino acid as the helix termination

Literature suggest that Gly or Asn residues are responsible for the helix termination.[42] In the design of synthetic peptides, this mode of helix termination can be achieved by incorporating achiral amino acids such as Gly, Aib or D-amino acids towards the end of C-terminus. The helix termination ability of D-amino acid residues can be used to construct ambidextrous structures, in which right and left-handed helical components are present in the same polypeptide chain.[43]

1.1.7 Effect of alternating LD sequence on conformation

Alternating LD residues in the peptide sequence results in a change of conformation as compared to that of homochiral peptides. Regular alternation of configuration was observed in

natural peptides synthesized by microorganisms. Antibiotics tyrocidine and gramicidin D contain a mixture of peptides synthesized by bacteria *Bacillus brevis*. They are composed of different peptide segments with different combinations of L & D amino acids. Theoretical and experimental studies on alternation LD sequences suggest that peptides adopt helical structures, the two amino acids containing peptide forms β-sheet conformation and their respective φ-ψ values lie on opposite sides in the Ramachandran plot (figure 11).[44]
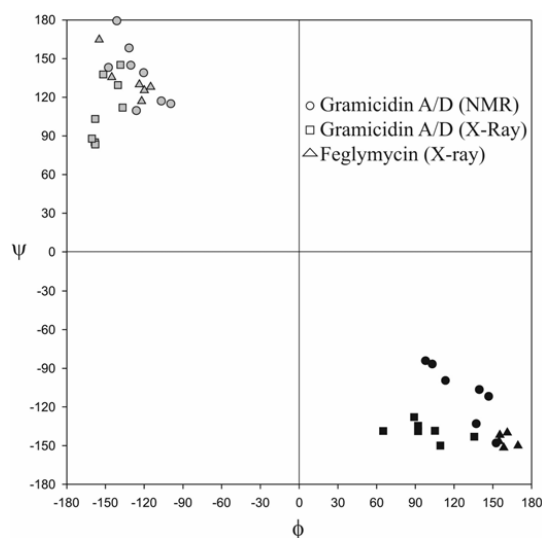
Figure 11. Ramachandran plot of observed φ-ψ values for gramicidin A/D and antibiotic feglymycin.

In the mid 20 century, Linus Pauling proposed structural models for polypeptides in the form of α-helix, *β*-sheet. He proposed two types of *β*-sheets pleated and rippled sheet with parallel and antiparallel orientation.[45] The *β*-sheets structure described is suited for polypeptide chains constructed entirely from L-amino acids or of D-amino acid residues. He had observed similar rippled sheet structures could be constructed with polypeptide chains having alternate D and L amino acid residues.

Helices from alternate LD peptides have been described by several authors.[44] These regular structures have basic DL-dipeptide repeating units form either single or double stranded helices. These structures observed experimentally and supported theoretical calculations compose of the torsional angles of the enantiomers located in respective *β* regions in the Ramachandran plot.

1.1.8 The effect of D-amino acids on self-assembled structure and gelation.

It is not easy to predict the effects of D-amino acids on the self-assembly and on gelation. Generally, it is known that random incorporation of D-amino acids into peptide

sequences result in the collapse of the structure. For retaining the conformational features, one needs to carefully choose the site of D-amino acid incorporation, so that it minimizes the possibility of major conformational changes. It has been seen that introduction of a single D-residue into the peptide can alter the supramolecular structure, but it depends upon the number of residues, and the sites of incorporation.

One study highlights the importance of incorporation of D-amino acid at the N-terminus.[35] Homochiral peptides of sequences (L-Leu-L-Phe-L-Phe, L-Val-L-Phe-L-Phe, and L-Phe-L-Phe-L-Val) do not self-assemble to form a gel, whereas its heterochiral peptides with the incorporation of corresponding D-residue to the N-terminus (D-Leu-L-Phe-L-Phe, D-Val-L-Phe-L-Phe and D-Phe-L-Phe-L-Val) rapidly self-assemble to form hydrogels based on antiparallel β sheets.

In contrast, another interesting study by Yang *et. al.*[46] highlights the importance of D-amino acid at the C-terminus. They synthesized homochiral and heterochiral amphiphilic dipeptides containing phenylalanine, alanine (Phe-Ala) and conjugated a lipid chain at the end. It showed that the chirality of the C-terminus decides the chiral orientation of the supramolecular structure. They also observed that the homochiral lipopeptides self-assemble into parallel β sheets whereas heterochiral lipopeptides self-assemble into antiparallel β sheet (Figure 12).
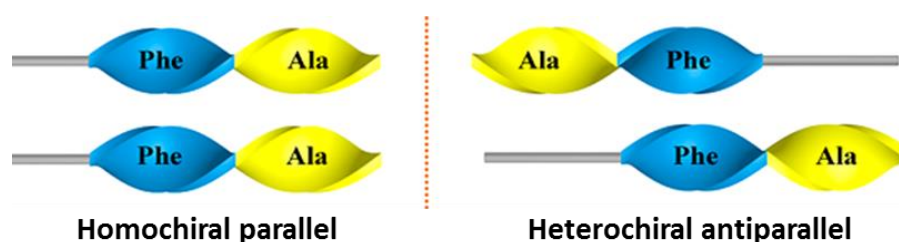
Figure 12: Packing of homochiral and heterochiral lipodipeptides.[46]

1.1.9 Self-assembly of enantiomeric peptides

In 1962, it was shown that the methyl ester of helical homo-polypeptides of L-glutamate and its enantiomer D-glutamate when mixed at room temperature form rigid gel in organic solvents like chloroform:dioxane while and precipitation occurred in solvents like DMF.[47] Fuhrhop *et al.*[48] showed that poly (L-Lysine) forms right-handed α-helix whereas poly (D-Lysine) forms a left-handed α-helix. Interestingly upon mixing these together in equimolar amounts, they precipitate into β-pleated sheet structure arranged in an anti-parallel

orientation (figure 13A). This study was extended by other authors and suggested that self-assembled amyloid like nano-fibrillar structures are originating from β-sheets of polylysine racemate at room temperature and undergo a transition from α-helix to β-sheet.[49]
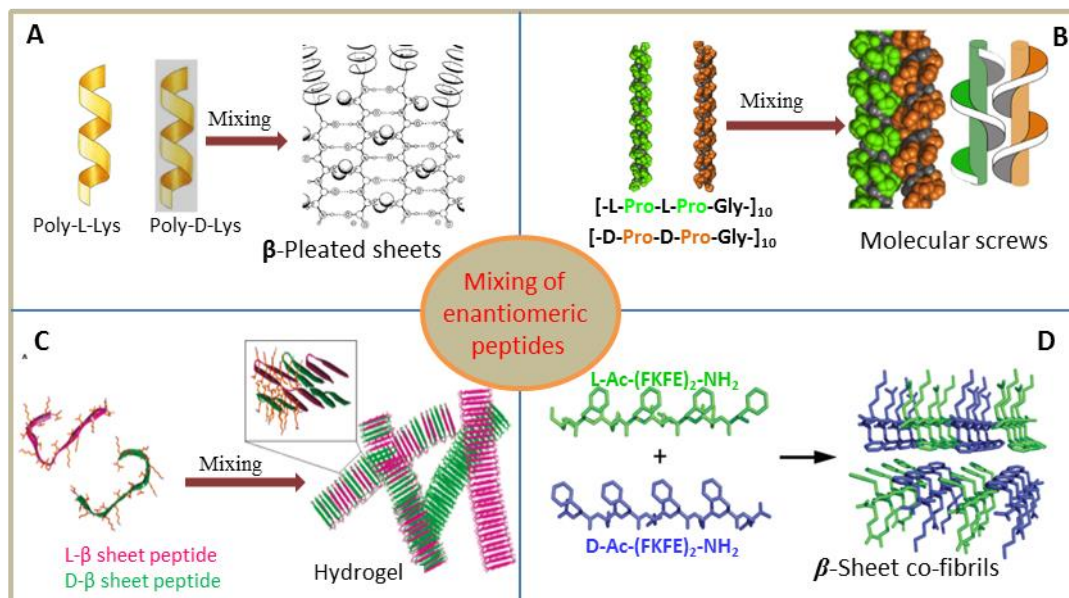
Figure 13. Self-assembly of various enantiomeric peptide.[48,50-52]

Incorporation of D-proline in the collagen triads X-Y-Gly (at bith X & Y) leads to a left-handed triple helix. On mixing the left and right-handed triple helix solution,[50] nano-sheet formations were observed based on hydrophobic groove interactions (Figure 13B). Schneider *et al.*[51] synthesized a 20-mer β-hairpin forming peptide which self-assembles into hydrogel constituting of a network of peptide fibrils (Figure 13C). When peptides of L-amino acids and D-amino acids were mixed in equimolar concentrations, mechanical rigidity of the hydrogel could be controlled. The hydrogel formed by an equimolar concentration of enantiomeric peptides showed four-fold enhancement in rigidity compared to the hydrogel made from individual peptides of the same overall concentration. Nilson *et al.*[52] synthesized two octamer amphipathic peptides L-peptide [Ac-(FKFE)$_2$-NH$_2$] and D-peptide [Ac-(FKFE)$_2$-NH$_2$] derived from L and D amino acids respectively and found that mixing of these enantiomeric peptides resulted in alternate co-assembly of β-sheet fibrils (Figure 13D).

1.1.10 Effect of D-amino acid containing peptide in therapeutics

It has been shown that prudent incorporation of D-amino acids into the sequence of L-amino acid in an appropriate position provides resistance to proteolytic activity which results

in greater *in vivo* stability.[53] Incorporation of D-amino acids in the L-peptide sequence, enhances the activity and selectivity towards bacteria.[54]

Schneider *et.al.*[51] synthesized a 20-mer peptide sequence (VKVKVKVK-$_D$PPTKVKVKVKV-NH$_2$). An interesting property of this peptide is that it folds into *β*-hairpin under cellular conditions, which further self-assembles into a hydrogel made up of a network of peptide fibrils (Figure 14). It has been shown that these peptide hydrogels showed strong antibacterial activity and exhibit low cytotoxicity.[32]
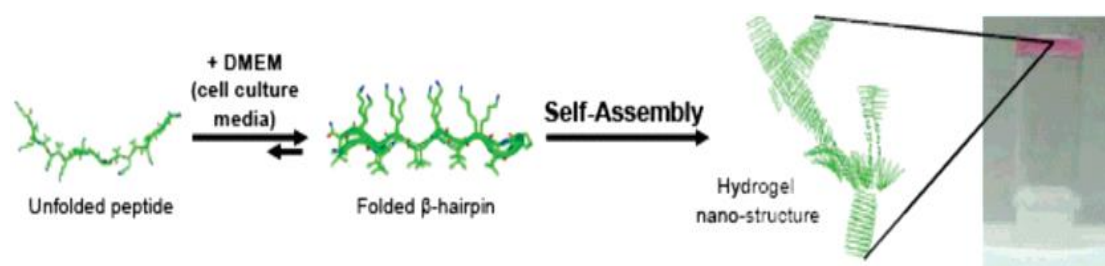
Figure 14. Hydrogel formation from *β*-hairpin peptide[51]

The side chains of amino acids are very important for exhibiting antibacterial activity. Marchesan *et. al.*[35] synthesized a set of heterochiral peptides $_D$L$_L$F$_L$F, $_D$V$_L$F$_L$F, and $_L$F$_D$L$_L$F which self-assemble to form a gel. Among these peptides, only peptide $_D$L$_L$F$_L$F showed little activity towards the Gram-negative strains *E.coli* and *K. pneumonia* but its analog did not show such activity, suggesting the role of leucine side chain which was differs from valine by only one methylene unit.[35,55]

1.1.11 Effect of D-amino acids containing peptides in amyloidosis therapy

Amyloid beta (Aβ) is hydrophobic and intrinsically disordered aggregation-prone protein which is believed to play a pivotal role in Alzheimer's diseases. Aβ42 is the cleavage product of the transmembrane protein. It is more neurotoxic and exists as fibrils. It has been shown that the aggregation of amyloid Aβ(1-42) leads to oligomeric fibrils and is the key process responsible for the progression of Alzheimer diseases.[56] A small fragment from the Aβ(1-42) peptide, i.e. pentamer L peptide KLVFF has been intensely studied which showed independent self-assembling and gelling properties.[57]

The conjugation of D-amino acids containing D peptide (KLVFF) to the γ-dipeptide at N-terminus is promising candidate to treat amyloidosis. The resulting 7-mer peptide was capable to bind to Aβ(1-42) peptide showing a dose-responsive reduction in cytotoxicity.[58]

Raskatov *et al.*[59] synthesized L-Aβ42 peptide and its mirror image peptide D-Aβ42. Interestingly, they found that the racemic L/D-Aβ42 forms fibrils more rapidly than any of its pure enantiomer. On equimolar mixture of the natural L-enantiomer and its mirror image Aβ42 shows a remarkable suppression in oligomer formation, producing a racemic mixture, which results in non-toxic fibrils.

1.1.12 Use of D-amino acids containing peptides for drug delivery and selectivity.

Delivery of drugs to the appropriate target site with enhanced selectivity has been a very challenging task. Peptide hydrogel based drug delivery is an emerging field where the drug can be covalently or non-covalently attached to the peptide. Covalent conjugation of the drug to gel-forming peptide provides interesting properties by which one can fine-tune the drug activity such as delivery and selectivity.

Many drug molecules carry carboxylic acid as the functional group which can be used to covalently conjugate with the peptide by either N-terminal amine or side chain amine of amino acid. There are several examples of covalent conjugation of drug to the peptide; but in respect to D amino acid containing peptides, very few examples exist. In one of the studies, anti-inflammatory drug naproxen was covalently conjugated to the D-peptides of sequence PhePheLys, PhePheTyr, PhePheLysTyr. It formed hydrogel at neutral pH and provided an enhancement in selectivity as well.[60]

In non-covalent approach, the drugs are usually encapsulated into the hydrogel. The percentage of encapsulation of drug into the gel matrix depends upon the interactions between them. The advantage with the non-covalent approach is that we can vary the amount of drug added into the peptide gelator thereby providing dose responsive drug release. Similarly, it is also used to deliver those drugs which suffer from the solubility in water such as curcumin which is hydrophobic in nature which properties of antioxidant, anti-inflammation and anti-tumorigenic. Schneider *et.al.*[61] encapsulated curcumin on to a gel matrix which was made from the peptide and demonstrated that peptide gel is acting as an effective vehicle for delivery of curcumin without affecting the supramolecular structure of hydrogels. In another example, 10-hydroxycamptothecine was formulated with D-amino acid containing self-assembling peptides which also does not alter the fiber morphology and delivers the hydrophobic drug to the target site with increased aqueous stability, suggesting the superiority of D-amino acid containing peptides over the L-homochiral peptides.[62]

1.2 Polyprolyl peptides

Apart from the above mentioned regular secondary structures (α-helix, *β*-sheets and turns) another important secondary structure is the polyproline-II helix (PP-II). Polyproline-II helix is present in both folded proteins as well as in unfolded proteins. Proline is the only naturally occurring imino acid in proteins and plays a unique structural role in guiding protein folding, fiber formation and in various molecular interactions such as protein-protein, protein-nucleic acid interactions.[63]

1.2.1 Polyproline conformations

Polyproline helix in proteins comprises repeating proline residues displaying a specific type of protein secondary structure. The poly-L-proline-II (PP-II) helix is important, not only in fibrillar proteins like collagen, but it is important also in folded and unfolded states of most proteins. Apart from the structure, PP-II conformation plays crucial role in a wide variety of biologically important molecular recognitions processes. Moreover, it plays a major role in signal transduction and in protein complex assembly. The PP-II helices are frequently encountered in numerous binding sites, specifically those of SH3 domains. PP-II helices are also found in various functional proteins involved in transcription, self-assembly, cell motility, elasticity and pathogenesis of bacterial and viral origin.

There are two types of polyproline helices known, termed as polyproline-I (PP-I) and polyproline-II (PP-II). The most interesting aspect of PP-I and PP-II conformation is that being tertiary amides, thus lack N-H bond to form any *inter*-chain or *intra*-chain H-bonds to stabilize helical structures. PP-I helix has all backbone tertiary amide bonds in the *cis* ($\omega_0 = 0°$) conformation, while in PP-II, amide bonds are all *trans* ($\omega_0 = 180°$). The right-handed PP-I helix has all amide bonds in the *cis* form, while the PP-II helix is extended left-handed helix with all of its amide bonds in the *trans* form.

PPII (*trans*)   **PPI (*cis*)**
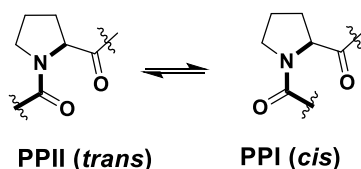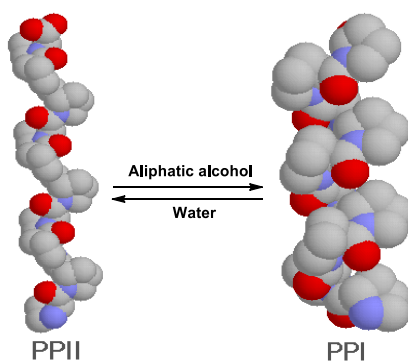
Figure 15. Solvent-induced switching between PP-II↔PP-I conformations.

Polyprolines adopt classical PP-II conformation in water, and in hydrophobic solvents it adopt PP-I conformation (Figure 15).

Table 1. Comparison between PP-II and PP-I conformations.

Parameter	PP-II conformation	PP-I conformation
Direction of helix	Left-handed	Right-handed
Amide bond conformation	*Trans*	*Cis*
Nature of helix	Fully extended	More compact
Dihedral angles	$\omega=180°$, $\phi = -75°$, $\psi = +145°$	$\omega=0°$, $\phi = -75°$, $\psi = +160°$
Helical pitch	9.4 Å per turn, 3.3 proline residues per turn	5.6 Å per turn, 3.3 proline residues per turn
Orientation of amide bond in the peptide backbone	Nearly perpendicular to the helix axis	Nearly parallel to the helix axis
Preferred solvent	Water	Aliphatic alcohols
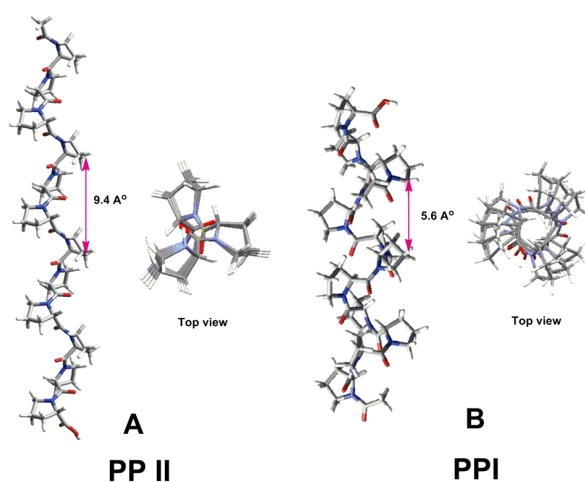
Figure 16. A) Model structure of polyproline-II (PP-II) conformation along with top view. **B)** Model structure of polyproline-I (PP-I) conformation along with top view.

1.2.2 Crystal structure of an oligoproline PP-II helix

Wennemers et $al.$[64] reported the crystal structure of hexaproline (Figure 17). Analysis of crystal structure showed a correlation between ϕ and ψ angles and the $exo/endo$ ring pucker. When ϕ and ψ are close to $-65°$ and $+140°$, then the C^{γ}-exo ring pucker was observed. Conversely, ϕ and ψ angles around $-73°$ and $+155°$, respectively, then the C^{γ}-$endo$ ring puckering was observed.
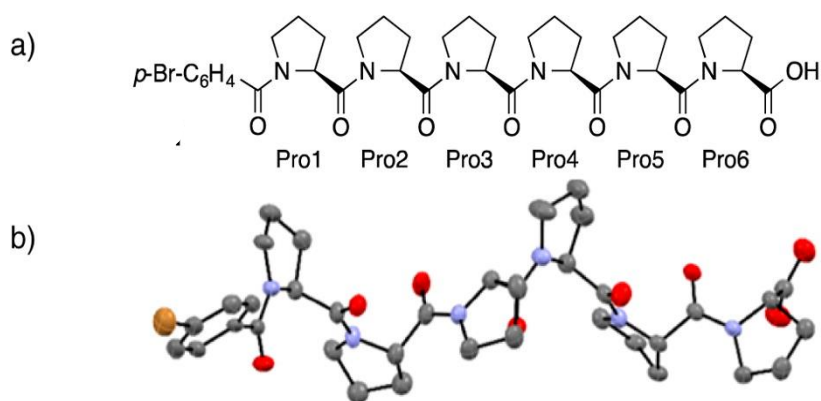
Figure 17. **a)** Hexaproline p-Br-C_6H_4-Pro_6-OH **b)** Crystal structure of hexaproline.[64]

Crystal structure suggested the role of coordinating water molecules around the PP-II helix, but hydration is not a prerequisite for PP-II helicity. Crystallographic data showed that the amide bonds within the oligoproline helix interact with each other through $n{\rightarrow}\pi^*$ type of interaction. This $n{\rightarrow}\pi^*$ interaction is found to be the largest when the pucker of proline ring is C^{γ}-exo.

1.2.3 Stability of polyproline conformation

The absence of hydrogen bond donor is one of the distinctive structural properties of PP-II helices, compared to the other common secondary structures found in proteins. This structural feature leaves several unsatisfied hydrogen bond acceptors free to establish $intra$ or $inter$-molecular interactions. Due to the absence of specific hydrogen bonding patterns, the formation of PP-II helices in globular proteins is in fact quite unusual.[65]

The $n{\rightarrow}\pi^*$ electronic interaction between non-bonded electron pair of one carbonyl (O_i) and the empty π^* orbital of another carbonyl (C_{i+1}) provides stabilization to PP-II helix.[66] Different studies also suggested the importance of coordinating water molecules for the

stability of the PP-II helix.[67] In the absence of coordinating water molecules, a PP-I helix with all *cis*-amide bonds predicted to be most stable.[68]

1.2.4 Factors Affecting on Polyproline Conformation

1.2.4a *Cis/trans* peptide bond

Peptide bonds mostly exist in *trans* conformation, due to the side chain present at C^α (steric clash) *cis/trans* energy barrier is high. In amino acid proline where side chain is cyclized the energy barrier between *cis/trans* isomerization is less. Hence proline always exist in two conformational equilibria i.e. *endo* versus *exo* ring pucker and *trans* versus *cis* amide bond conformation (Figure 18). The literature reports suggest that there is a correlation between proline puckering and the *cis/trans* peptide bond conformation. The C^γ-*exo* ring pucker in proline stabilizes the *trans* conformation and adopts stable PP-II helix, whereas C^γ-*endo* ring pucker favors *cis* amide bond and takes PP-I conformation.[69]
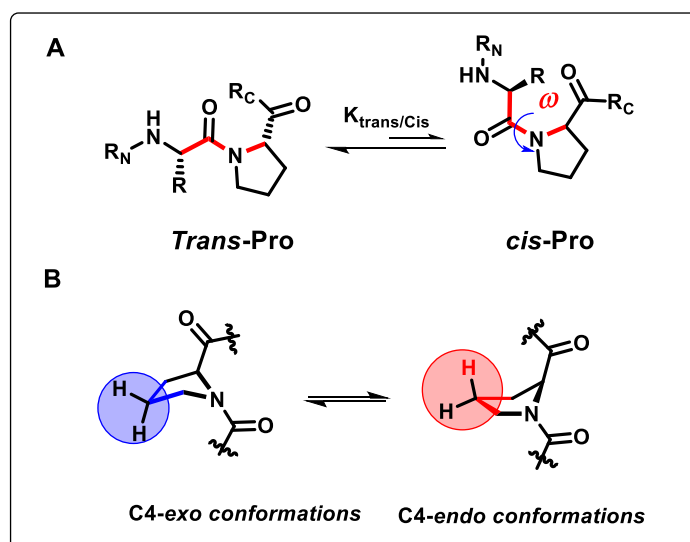
Figure 18. **A)** *Cis-trans* isomerism of prolyl amide bond **B)** *Exo* and *endo* ring pucker of proline.[69]

1.2.4b The $n \rightarrow \pi^*$ interaction

The $n \rightarrow \pi^*$ interaction is a weak non-covalent electronic interaction. Raines *et al.*[66] suggested that the backbone $n \rightarrow \pi^*$ electronic interaction could play a key role in stabilizing the PP-II helices. Increasing stereoelectronic effects, favor the *trans* amide bond and increase the folding propensity of the triple-helical collagen structure which comprised of PP-II helices. Using short polyproline peptides, it has been shown that the electron withdrawing substituent at C4 position on proline has impact on polyproline conformation. The electron

withdrawing substitution of proline such as 4*R*-hydroxyproline (Hyp) or 4*R*-Fluoroproline (Flp) was found to increase the backbone $n \rightarrow \pi^*$ interaction and stabilize PP-II conformation. However, 4*S*-hydroxyproline (hyp) or 4*S*-fluoroproline (flp) destabilizes PP-II conformation (Figure 19).[66]
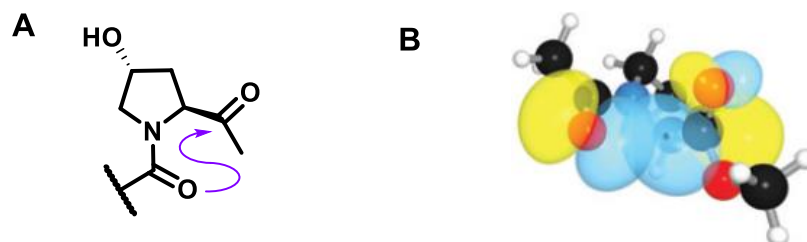
Figure 19. A) $n \rightarrow \pi^*$ interaction stabilizes the *trans* isomer **B)** Overlap of n and π^* bond orbitals.[66]

1.2.4c Gauche effect

The complex balance of non-covalent interactions, steric hindrance and stereoelectronic effects determine the conformations of flexible molecules. In the absence above mentioned effects, weak stereo electronic effects, such as "gauche effect" can also have large influence on the conformation of peptides. The "gauche effect" describes the hyperconjugative electron donation of the sigma (σ) bonding orbital into the (σ*) antibonding orbital (Figure 20A, 20B).
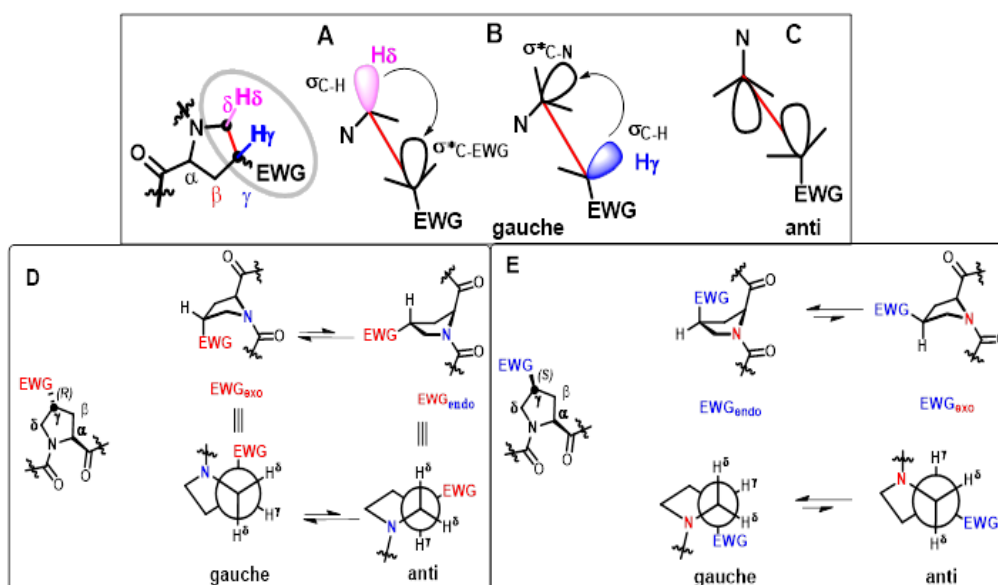
Figure 20. A&B) Gauche conformation **C)** Anti gauche conformation **D)** 4*R*-substituent proline favors gauche **E)** 4*S*-substituted proline favors C^{γ}-C^{δ}-bond gauche between the amine and electron withdrawing group.

In proline, it has been shown that electron withdrawing groups in the C4 inductively withdraw electron density from the peptide bond and reduce the bond order of the C-N linkage. In the gauche conformation of proline, electron withdrawing 4*R*-substitution leads to a strong preference for a C$^\gamma$-*exo* puckering (Figure 20A), whereas, 4*S*-substitution leads to a strong preference for C$^\gamma$-*endo* ring puckering (Figure 20A and 20E).[70]

1.2.5 Effect of solvents on PP-II conformation

1.2.5a Aliphatic alcohols

The nature of solvent plays an important role in dictating the peptide conformation.[71] In hydrophilic solvents such as water, polyprolines adopt PP-II conformation whereas, in hydrophobic solvents such as aliphatic alcohol PP-I conformation is favourable (Figure 21). PP-II conformation is stabilized by solvation of the backbone through water molecules, but the way in which it influences to adopt a PP-II conformation is still not well understood.[72]
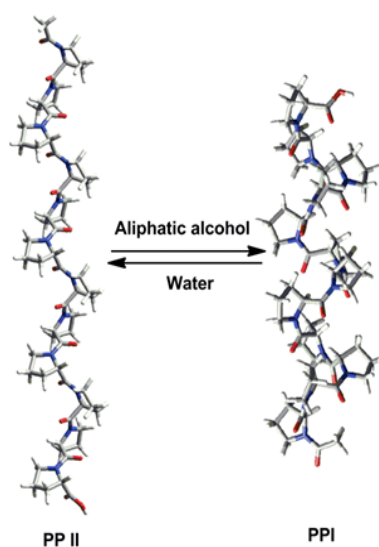
Figure 21. Solvent dependent switching between PP-II and PP-I.

1.2.5b Trifluoroethanol

Trifluoroethanol is known to break the helix by removing hydration sphere around the peptides backbone.[73] The solvent dependent switching of conformation between α-helix to PP-II to the random coil is reported by Mahalakshmi *et al.*[74] A conformational change between PP-II and *β*-structure in case of polypeptides of *cis*-(2*S*,4*S*)-L-amino and *cis*-(2*S*,4*S*)-L-hydroxy polyprolines (figure 22) has been demonstrated by Ganesh *et. al.*[75] It occurs by change of *intra*-molecular hydrogen bonding to *inter*-molecular hydrogen bonding. In

hydrophilic solvent water, the 4S-OH/NH$_2$ groups form a hydrogen bond with carbonyl of the same residue (*intra*-molecular) leading to PP-II structure. In hydrophobic solvent like trifluoroethanol, *intra*-chain switches to *inter*-chain hydrogen bonds, leading to β-structures (Figure 22).
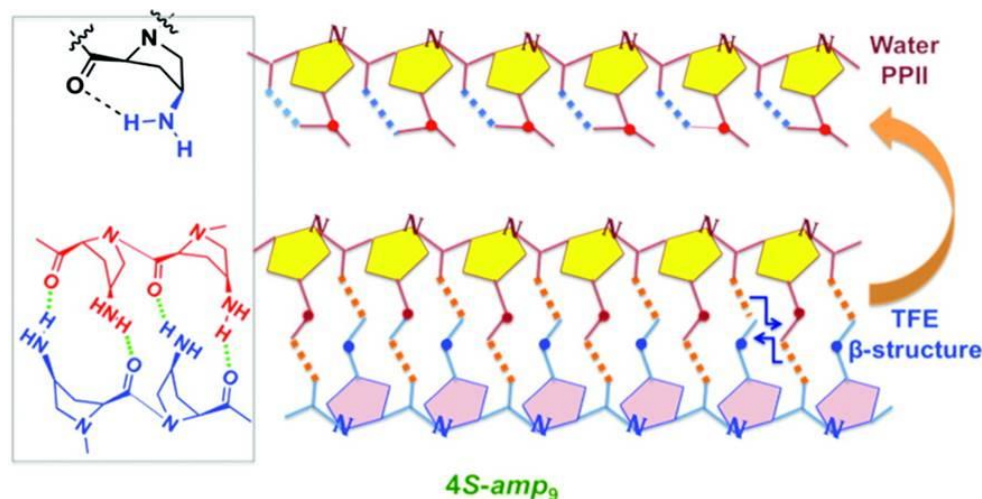
Figure 22. Water-induced switching between PPII$\leftrightarrow$ β-structures.[75]

1.2.5c Effects of terminal functional groups

It has been shown both experimentally and theoretically that the protected and free terminus of C and N-terminus has direct impact on stability of the PP-II helix.[68] The conversion of PP-II to PP-I was studied by the CD spectroscopic technique. The study concluded that free N-terminus with positive charged and free C-terminus with a negatively charged amino acid, destabilize the PP-II helix and favor the PP-I helix, while the protected termini favor the PP-II helix. (Figure 23, a-d).

a: X = Ac; Y = NH$_2$; AcN-[Pro]$_{12}$-CONH$_2$
b: X = H; Y = NH$_2$; HN-[Pro]$_{12}$-CONH$_2$
c: X = Ac; Y = OH; AcN-[Pro]$_{12}$-COOH
d: X = H; Y = OH; HN-[Pro]$_{12}$-COOH
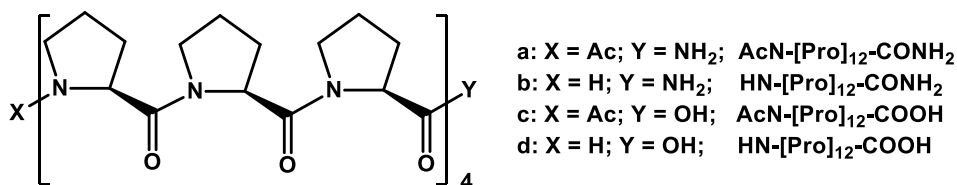
Figure 23. Oligoproline peptide with different groups at the C and N-terminal.

1.2.6 Significance of PP-II conformations in therapeutics

PP-II conformation is well-defined, non-flexible, stable secondary structure and acts as a rigid rod. Due to this, uses of PP-II conformations are ranging from material science to

the medical science.[68] Molecular self-assembly based on PP-II conformation as spacers attracted special attention because of easy synthesis and mimicking various natural amino acid side chains. Five consecutive prolines are enough to fold into a stable structure and do not show any conformational effect on functionalizing large ligand on it.

1.2.6a Cell-penetrating agents

Due to its easy amenability for chemical modifications, various functional groups can be installed on 4-substituted proline and mimic the modified side chains of natural amino acids. Proline-rich peptides and proline dendrimer are known to internalize into the eukaryotic cells.[76] Royo *et al.*[77] synthesized the *cis-γ*-amino-L-proline oligomers and showed that *γ*-peptides enter into different types of cells by usual endocytosis mechanism. In addition, the short length peptides give advantages over the well-known cell penetrating TAT peptide in various respects such as toxicity, resistance towards enzymes.

Polyproline PP-II conformation is rigid and Chimielewski *et al.*[78] took advantage of rigidity of PP-II conformation and synthesized oligoproline peptide containing cationic and hydrophobic functional groups. It was observed that uptake of peptide was more in MCF-7 cells (Figure 24).[88]
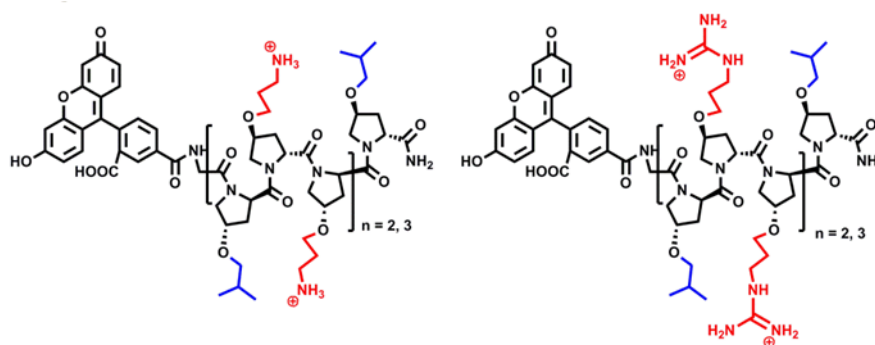
Figure 24. Oligoproline peptides with amino, guanidinium and isobutyl functionality.[78]

Cyclic nature of proline residue induces conformational constraints in the pyrrolidine ring. The proline rich peptide sequences form rigid helical rod structures in aqueous medium. Three hydrophobic methylene groups are present at the outer part of the rigid PP-II structure. Based on these facts, Lee *et al.*[79] hypothesized that the rigid rod like nature of helix and the hydrophobic character of the outer surface of the PP-II helix might show microphase separation (Figure 25). A rigid rod of hydrophobic character with conjugation of hydrophilic peptide enables microphase separation. The slightly hydrophobic nature of PP-II and the

hydrophilic peptide, leads to self-assembled nano capsule structures, which are stable enough to cross the cytoplasmic membrane barrier of the cell.
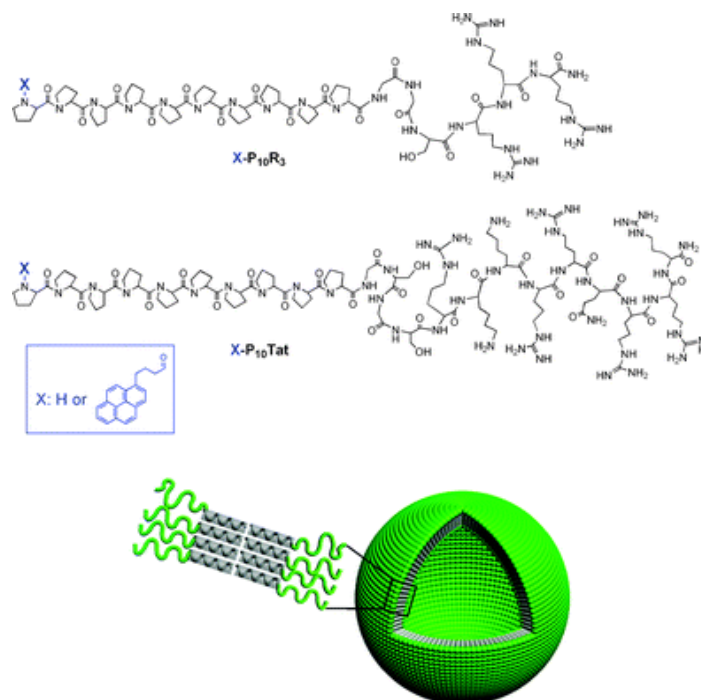
Figure 25. Structure of the peptides rod–coil and it's self-assembly into nano capsule. [79]

1.2.6b Drug delivery agents

A common challenge in drug development is the *in vivo* cellular distribution in the treatment of disease. Cell-penetrating peptides (CPPs) are promising candidates for the delivery of drugs to both bacterial and eukaryotic cells.[80] Although CPPs are potential drug delivery candidates, they can display cytotoxicity depending on cargo used and cargo linkage position.[81] However, proline-rich peptides are translocated across cellular membranes without inducing lysis or causing damage and display much less toxicity to mammalian cells. Thus, these peptides may have significant potential as CPPs or transport systems to deliver drugs to the target cells but may also be used to enhance antimicrobial activity. Proline-rich peptides are capable of penetrating cell membranes and cross blood-brain barrier as novel potential carriers for drug delivery.[82]

1.2.7 Self-assembly based on PP-II conformation

Wennemers et al.[83] demonstrated the value of functionalizable peptidic scaffolds that have no tendency to self-aggregate but govern the spatial orientation between π-systems for

directed self-assembly (Figure 26). The length of the conjugate and the absolute configuration of stereocenters at the outside of the helix, allowed for tuning the supramolecular aggregation.
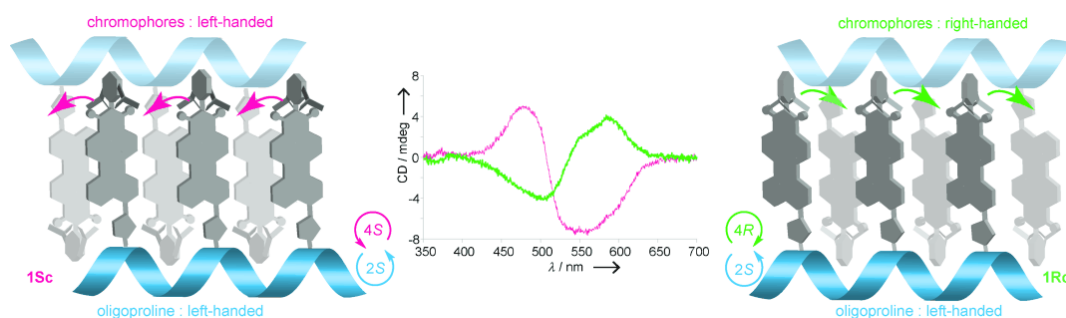
Figure 26. CD spectra of diastereoisomers in THF/H$_2$O (30:70, 50 μM, 294 K; middle), Representation of the counter-clockwise and clockwise orientation of chromophores.[83]

With increasing length of the oligoproline-π-system conjugates, higher ordered nanostructures form that range from flexible worm-like threads *via* fibrils to nano sheets and nano ribbons. Same building blocks have been used to synthesize the triaxial supramolecular weave which are practically hard to prepare. The distance between two monoimide chromophore was increased to 18 Å. Upon self-assembling, the π-stacking of the chromophores feature voids at regular distances. Further, these voids accommodate new building blocks by providing the crossing points through CH-π interactions and forms triaxial woven superstructures which results into uniform hexagonal pores. This material has been shown to capture iridium nanoparticles.[84]
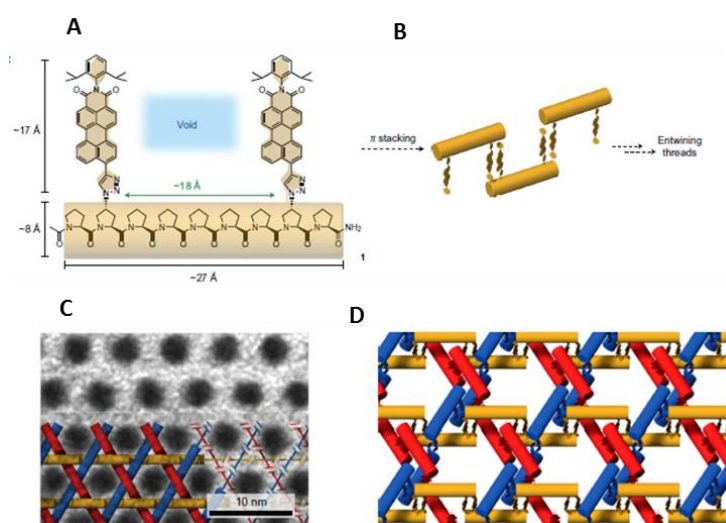
Figure 27. A) Void between two monoimide chromophore at 18 A^0 distance **B)** CH-π interactions **C)** Uniform hexagonal assembly **D)** Triaxial weave packing.[84]

Ganesh *et al.*[75] established the stereospecific and solvent dependent effect on PP-II conformation. A stretch of *cis*-(4*S*,2*S*)-aminopolyproline or *cis*-(4*S*,2*S*)-hydroxypolyproline forms antiparallel *β* structures in solvent trifluoroethanol. 4S-hydroxy-L-prolyl polypeptide (*hyp₉*) forms nanorods in TFE (Figure 28) upon conjugation with different fatty acid chains to the N-terminus, which cooperatively increases the hydrophobic and hydrophilic interactions among the peptides and self-assembled into long nanowires
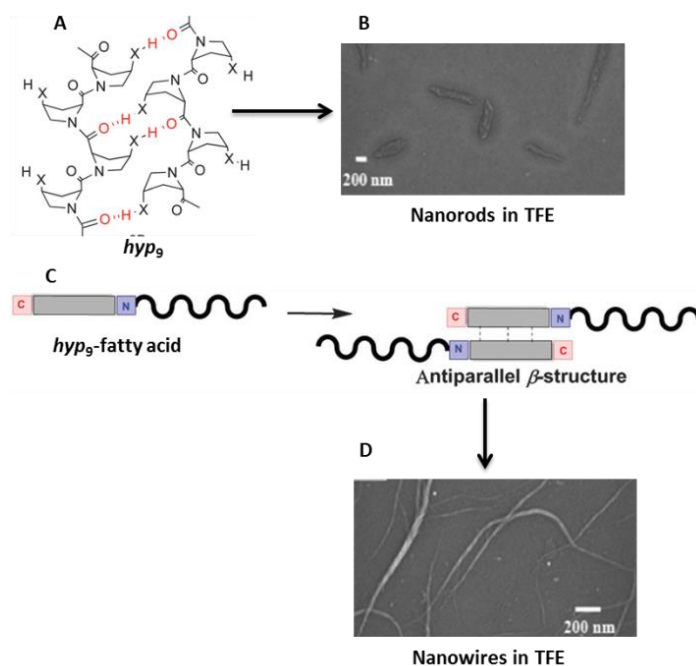
Figure 28. A) *hyp₉* forms antiparallel *β*-structures in TFE **B)** nanorods formation in TFE **C** and **D)** Fatty acid conjugation leads to nanowires.[75]

1.3 Collagen

Collagen is an ancient, abundant structural protein found in all mammals. Collagen is present in all connective tissue such as skin, bone, cartilage, tendon, basement membrane, blood vessels and forms a major component of extra cellular matrix (ECM). The term 'Collagen' is derived from the Greek word meaning 'glue' which refers to the compounds early use in the process of boiling the skin and tendons of horses to obtain the glue. Collagen is an important class of structural proteins which can self-assembly from individual peptide chains to a canonical triple helix. Collagen triple helices are having innate tendency to form higher ordered structures which are mostly fibrous in nature (Figure 29).

In the human body, collagen consists of one-third part of all proteins and is a prevalent component of extracellular matrix (ECM). The collagen belongs to an important family of

proteins, which forms fibrillar network in the ECM around the cell, provides support to the tissues and tightly regulate the cellular functions. There are twenty-eight different types of genes conserved in the genome for the synthesis of the collagen proteins. The collagen proteins are synthesized in the endoplasmic reticulum (ER) and are then secreted into the extracellular matrix.
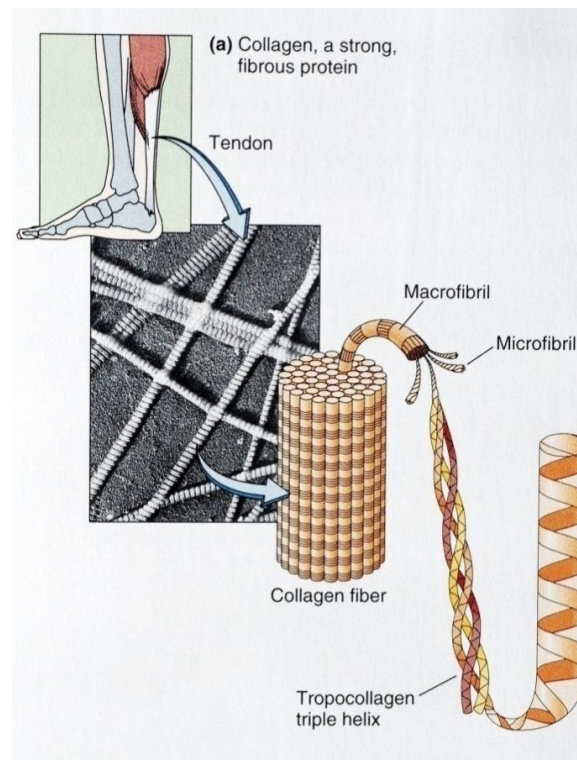
Figure 29. Collagen in the human body.

The most defining and important structural motif of the collagen proteins is a right-handed triple helix, where three parallel left-handed polyproline-II type (PP-II) helices with $\varphi= -75^o$, $\psi= 145^o$, and $\omega= 180^o$ are intertwined around one another on a common axis. These three strands are held together by hydrogen bonding, originating from NH (H-bond donor) of glycine and CO (H-bond acceptor) of next proline from different strand with one residue staggered, to form a right-handed super helix.[85] The primary structure of collagen is composed of X-Y-Gly repeat, the amino acids in the X and Y positions in collagen are predominantly (2S)-L-proline (Pro, 28%) and (2S, 4R)-L-4-hydroxyproline (Hyp 38%) respectively. These amino acids account for 20% of the total amino acids composition of natural collagen. The other commonly found amino acids are Ala, Lys, Arg, Leu, Val, Ser, and Thr.[86] Hydroxyl group in hydroxyproline (Hyp) provides exceptional mechanical strength,

broad resistance to the proteolytic enzyme and thermal stability to the triple-helical structure of collagen.

1.3.1 Collagen Mimetics

Synthetic collagen models, such as collagen mimetic peptides (CMPs), have been very useful in extracting the information about the collagen structure and finding the factors responsible for the stabilization of the triple helix. Among them, CMPs based on (Pro-Pro-Gly)$_n$ and (Pro-Hyp-Gly)$_n$ is most studied trimers. Natural collagen protein on melting converts into gelatin where it regains the little fraction (less than 10%) of its original triple helical content. CMPs are mostly studied because it exhibited reversible melting behavior due to their small size when heat denatured completely and on cooling regain its original triple helical structure. This property of CMPs provide us full information about the thermodynamic characterization of folding and unfolding processes which is very important to understand the natural collagen structure.

The thermal stability of CMPs is modulated by both the number of trimeric repeats and the amino acid composition. Longer peptides exhibit higher thermal stability with Tm of (Pro-Hyp-Gly)n rising from 37 ^{o}C for $n = 7$ to 43 ^{o}C and 69 ^{o}C for $n = 8$ and 10, respectively.[87] Raines *et.al.*[88] reported that the thermal stability of a CMP could be enhanced by incorporation of 4R-fluoroproline (Flp) in place of 4R-hydroxyproline (Hyp). This work suggests how important the stereoelectronic effect of Hyp in collagen stability.

1.3.2 Collagen mimetics with unnatural amino acids

In attempts to understand and modify the triple-helical strength of collagen, several unnatural amino acids have been tested at the X and Y positions of collagen sequence (Figure 30). To elucidate the importance of stereochemistry of 4-hydroxyl group 4S-hydroxyproline (hyp) containing peptides (Pro-hyp-Gly)$_{10}$, (hyp-Pro-Gly)$_{10}$ have been synthesized and studied for their triple-helix forming abilities. Variable temperature polarimetry and CD spectroscopy have shown that these peptides do not form triple helices.[89] Several studies have evaluated the propensity of different amino acids to adopt the triple-helical conformation. A high proportion of charged residues is found in the sequence of the triple-helical domain and is presumed to participate in folding interactions.[90]
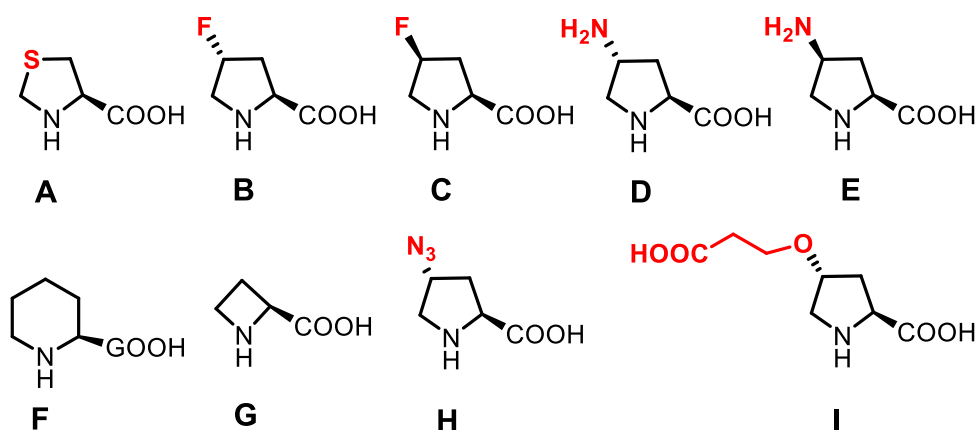
Figure 30: Various proline surrogates incorporated in collagen sequence. **A)** Thiozilidine (Thz), **B)** 4*R*-Fluoroproline (Flp), **C)** 4*S*-Fluroproline (flp), **D)** 4*R*-aminoproline (Amp), [93] **E)** 4*S*-aminoproline (amp),[94] **F)** L-piperidine-2-carboxylic acid (Pipec), **G)** Azitidine (Aze). **H)** 4*R*Azidoproline (Azp), **I)** 4*R*-2-carboxyethoxy proline.

Since residues in the X and Y are partially exposed to the solvent; charged residue has a potential for *intra* and *inter* molecular interactions. Modeling studies indicate that oppositely charged residues within a single chain form salt bridges when separated by one or two residues.[91] Electrostatic interactions between opposite residues are sterically possible between the collagen polypeptide chains when separated by one residue along the chain.[92]

Ganesh *et.al*.[93] first time incorporated ionizable 4R-aminoproline (Amp) at Y position and demonstrated that at all pH range it forms stable collagen triple helix. Subsequently, from the same group, it had been shown that incorporation of 4*S*-amino (amp), 4*R*-aminoproline (Amp) at X and Y position respectively forms stable collagen triple helix.[94,95] Chmielewski *et.al*.[96] engineered a pH-responsive collagen triple helix peptide by introducing carboxylate groups at 4*R* position which protonated under acidic conditions. This design is complementary to the use of electrostatic interactions to promote the stabilization of triple helical peptides. Wennemers *et.al*.[97] incorporated 4*R*-azidoproline and showed that it has a similar stabilizing effect on the collagen triple helix as 4*R*-hydroxyproline and functionalization of collagen peptides are easy by 'click' chemistry.

1.3.3 Collagen in Aging and Disease

The overall shape and function, in terms of flexibility and locomotion of the skeletal system, depends on a basic framework of collagen fibers.[98] Collagen fibers provide mechanical strength to various organs of the body. The biological diversity in the function of

collagenous tissue is primarily due to several genetically distinct classes of collagens that are tissue-specific. During aging (over a period of time), several chemical changes occur in the collagen framework. These changes reflect in the physical properties of the fibers, such as stiffness of skin, tendon, bone, joints and also decreases the elasticity and increases the brittleness of the tissue.[99] Collagen synthesis decreases steadily with age and drops down 10-fold in the majority of tissues.

Cross-linking is essential for the strength of the collagenous tissue. It is carried out in a controlled fashion by the enzyme *lysyl oxidase* during maturation of the tissue. The *lysyl oxidase* oxidatively determines the lysine or hydroxyproline residue in the N-terminal regions of one peptide to an aldehyde. This aldehyde, in turn, reacts with the ε-amino group of lysine residues in the C-terminal region of the peptide in the adjacent fiber to form a reduced Schiff base, thus resulting in cross-linking. However, the decreased metabolic turnover of collagen with aging allows a second indirect cross-linking to occur through the reaction with glucose and its oxidation product, a process referred to as *glycation*. The open chain aldehyde form of glucose reacts with the free ε-amino acid side chain of lysine in the collagen peptides to form a *glycosyl*-lysine.[100]

Deficiencies in the post-translational modification of the collagen are also known to cause several heritable disorders. For examples, in Ehlers-Danlos syndrome type VI, the collagen fiber fragility arises from the hydroxylation deficiency. Several subtypes of Alport syndrome, Bethlem myopathy, a certain subtype of Epidermolysis bullosa, Knobloch syndrome, Arterial aneurysms, Osteroarthrosis and Intervertebral disk disease have also been ascribed to the imperfections in the collagenous tissue.

1.3.4 Biomedical Applications of Collagen

Collagen is one of the most useful biomaterials because of its superior biocompatibility and weak antigenicity along with this its biodegradable nature made it a primary source for medical applications. In pharmaceutics, the main applications of collagen are for drug delivery vehicle. Sponges for burns, shields in ophthalmology, mini-pellets/tablets are used for protein delivery. In gel formulation such as combination of collagen with liposomes is used for sustainable drug delivery. Along with delivery vehicles, it can also be used to engineered the tissues such as skin replacement, bone substitutes, and artificial blood vessels.[101,102]

1.3.6 Disadvantages of collagen in biomedical applications

Cost for pure collagen is very high because, during isolation various forms of collagen are getting isolated. It has variability in enzymatic degradation rate as compared to hydrolytic degradation and complex to handle. There are chances of getting contamination, of several diseases such as bovine sponge form encephalopathy (BSF) because collagen source is animals.

1.3.7 Scope of present work

Proteins are important biopolymers made up of L-amino acids with uniform chirality. If we replace even a single L-amino acid with a D-amino acid, the protein loses its structure and biological functions. However, inverting all L-amino acids into D-amino acids, results in a mirror image structure. Understanding the role of chirality in determining the stability of protein structure is crucial.

Short peptides are suitable and convenient models to study the effects of the backbone conformation on the overall structure of the protein and its function. In this study designed polyproline and collagen mimetic peptides are synthesized to explore the role of chirality of constituent amino acid residues in the formation of basic secondary structures. Proline rich peptides adopt common polyproline type conformations PP-I & PP-II. PP-II has been recognized for its presence in both folded and unfolded protein structures. Collagen is an abundant structural proline rich protein which occurs predominantly in PP-II conformation. Short collagen mimetic peptides mimic the natural protein and are amenable to chemical functionalization. Hence polyproline and collagen peptides are ideal candidates to study the chirality dependent structural changes in proteins.

Chapter 2: Self-assembly of 4(*R/S*)-D-Aminopolyproline

Chapter 2 is directed towards a comparative study of 4(*R/S*)-amino-D-prolyl polypeptides and unsubstituted polyproline peptides to understand the effect of stereochemistry at C2 position of proline on chirality (handedness) of the helix. This study emphasizes the importance of stereochemistry at both C2 and C4 positions to understand the effect of H-bonding substituents of proline on conformation in water and fluoroalcohol. CD spectroscopic technique is used to investigate the conformation adopted by these polypeptides.
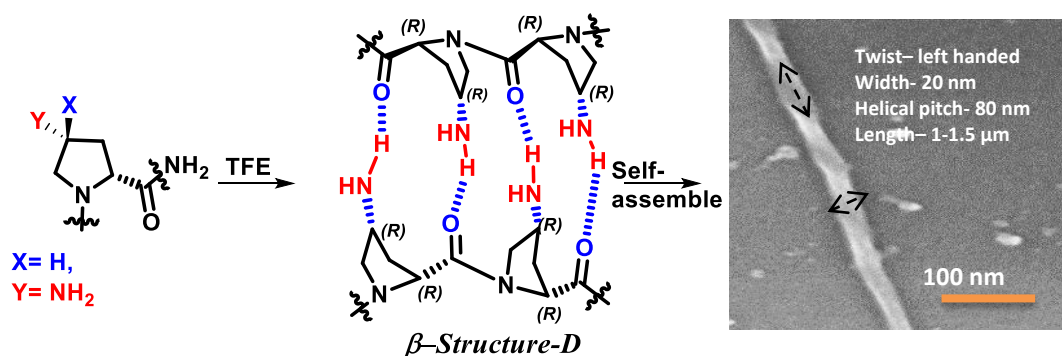
β–Structure-D

Chapter 3: Alternate and Block Heterochiral Polypeptides from 4(*R/S*)-Hydroxy L/D Proline

Chapter 3 deals with the conformational study of heterochiral alternate and block prolyl polypeptides. Such studies lead to understand the importance of 4(*R/S*)-OH group on proline and stereochemistry at C2 position in prolyl polypeptides. The target polypeptides for this work are as follows.

Alternate polyproline peptides
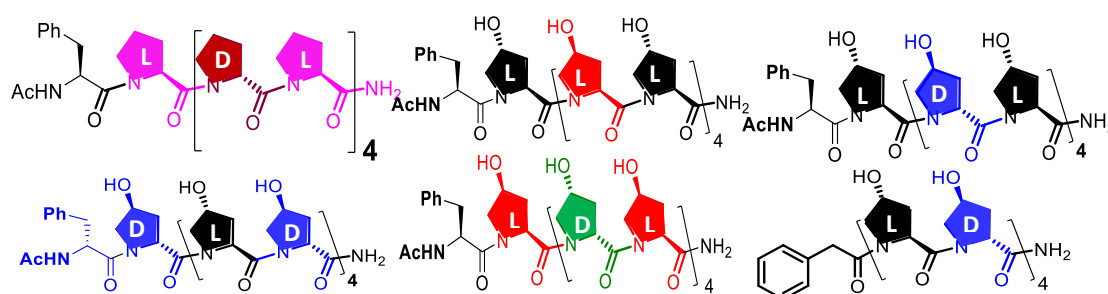
Block polyproline peptides
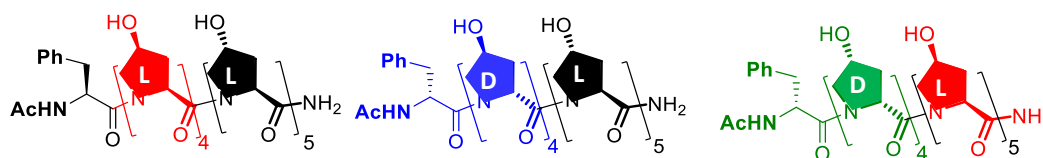
Chapter 4: Self-assembly of 4*R/S*-Hydroxy/Amino Collagen Peptide Spiegelomers

Chapter 4 is divided in two sections. Section A is comparative study of L/D collagen peptides **P1** & **P2**. Section B is comprised of 4*R/S*-amino L/D-proline substituted collagen

peptides **P3** & **P4**. Secondary structure and thermal stability of these peptides in various physical environments were investigated by CD spectroscopic technique. AFM and FE-SEM microscopic techniques were used to find out the self-assembled nanostructures.

L-*Phe*-[-(2*S*)-L-*Pro*-(2*S*, 4*R*)-L-*Hyp*-*Gly*-]₆

L-Collagen peptide P1

D-*Phe*-[-(2*R*)-D-*Pro*-(2*R*, 4*S*)-D-*hyp*-*Gly*-]₆

D-Collagen peptide P2

P3, (L-Amino collagen peptide)

L-Phe[-(2*S*)-L-*Pro*-(2*S*,4*R*)-L-*Amp*-*Gly*]

P4, (D-Amino collagen peptide)

D-Phe[-(2*R*)-D-Pro-(2*R*,4*S*)-D-*amp*-Gly]
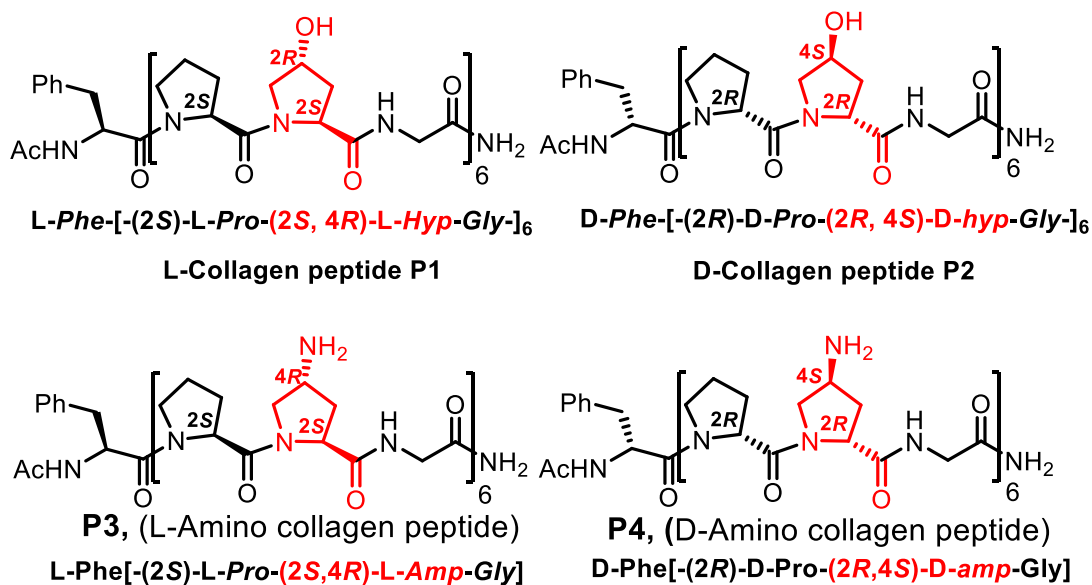
1.3.8 References:

1) Turner, R. D.; Vollmer, W.; Foster, S. J., Different walls for rods and balls: The diversity of peptidoglycan. *Mol. Microbiol.,* **2014,** *91*, 862-874.

2) Wolosker, H.; Blackshaw, S.; Snyder, S. H., Serine racemase: A glial enzyme synthesizing d-serine to regulate glutamate-n-methyld-aspartate neurotransmission. *Proc. Natl. Acad. Sci. U.S.A.,* **1999**, *96*, 13409-13414; (b) Kim, P. M.; Duan, X.; Huang, A. S.; Liu, C.Y.; Ming, G.; Song, H.; Snyder, S. H., Aspartate racemase, generating neuronal d-aspartate, regulates adult neurogenesis. *Proc. Natl. Acad. Sci. U.S.A.,* **2010,** *107*, 3175-3179.

3) Kreil, G., D-amino acids in animal peptides. *Annu Rev Biochem*, **1997**, *66*, 337-345.

4) Craig, G.; Bandyopadhyay, P.; Olivera, B. M., Post-translationally modified neuropeptides from conus venoms. *Eur J Biochem*, **1999**, *264*, 271-275.

5) Li, J.; Gao, Y.; Kuang, Y.; Shi, J.; Du, X.; Zhou, J.; Wang, H.; Yang, Z.; Xu, B., Dephosphorylation of D-peptide derivatives to form biofunctional, supramolecular nanofibers/hydrogels and their potential applications for intracellular imaging and intratumoral chemotherapy. *J. Am. Chem. Soc.,* **2013,** *135*,, 9907-9914.

6) (a) Thomas, H.; Ma, J. G.; Yolanda, S.; Ernest, G., D-Amino acids in protein de novo design. II. Protein-diastereomerism versus protein-enantiomerism. *Letters in Peptide Science,* **1997,** 4, 377-386. (b) Mason, S.F., *chirality*, **1991**, 3, 223.

7) Susheel, D., Protein Design with L- and D-amino acid structures as the alphabet. *Acc. Chem. Res.* **2008,** 41, 1301-13195.

8) Milton, R. C.; Milton, S. C.; Kent, S. B., Total chemical synthesis of a D-enzyme: the enantiomers of HIV-1 protease show demonstration of reciprocal chiral substrate specificity. *Science,* **1992**, *256*, 1445-1448.

9) (a) Taolei, S.; Dong, H.; Kristina, R.; Lifeng, C.; Harald, F., Stereospecific interaction between immune cells and chiral surfaces. *J. Am. Chem. Soc.* **2007**, *129*, 1496. (b) Saghatelian, A.; Yokobayashi, Y.; Soltani, K.; Ghadiri, M. R., A chiroselective peptide replicator. *Nature*, **2001**, *409*, 797-801. (c) Chung, D. M.; Nowick, J. S., Enantioselective molecular recognition between β-sheets. *J. Am. Chem. Soc.,* **2004**, *126*, 3062-3063.

10) Fuhrhop, J. H.; Krull, M.; Buldt, G., Precipitates with β-pleated sheet structure between by mixing aqueous solution of helical poly (D-lysine) and poly (L-lysine). *Angew. Chem., Int. Ed. Engl.*, **1987**, *26*, 699-700.

11) Ramagopal, U. A.; Ramakumar, S.; Mathur, P.; Joshi, R.; Chauhan, V. S., Dehydrophenylalanine zippers: strong helix-helix clamping through a network of weak interactions. *Protein Eng.*, **2002**, *15*, 331-335.

12) (a) Gerber, D.; Shai, Y., Chirality-independent protein-protein recognition between transmembrane domains in *vivo*. *J. Mol. Biol.*, **2002**, *322*,, 491-495. (b) Pentelute, B. L.; Gates, Z. P.; Tereshko, V.; Dashnau, J. L.; Vanderkooi, J. M.; Kossiakoff, A. A.; Kent, S. B., X-ray structure of snow-flea antifreeze protein determined by racemic crystallization of synthetic protein enantiomers. *J. Am. Chem. Soc.*, **2008**, *130*, 9695-9701.

13) Hirst, A. R.; Smith, D. K.; Feiters, M. G.; Geurts, H. P. M., Two-component dendritic gel: effect of stereochemistry on the supramolecular chiral assembl. *Chem. Eur. J.*, **2004**, *10*, 5901-5910.

14) (a) Luo, X.; Liu, B.; Liang, Y., Self-assembled organogels formed by mono-chain I-alanine derivatives. *Chem. Commun.*, **2001**, *17*, 1556-1557. (b) Beceril, J.; Escuder, B.; Miravet, J. F.; Gavara, R.; Luis, S. V., Understanding the expression of molecular chirality in the self-assembly of a peptidomimetic organogelator. *Eur. J. Org. Chem.* **2005**, *3*, 481-485.

15) Brizard, A.; Oda, R.; Huc, I. *Top. Curr. Chem.*, **2005**, *256*, 814.

16) Marc, B. T.; Yue, F.; Boualem, H.; Laura, L. H.; Bruce, Y. *Chem. Mater*, **2012**, *24,* 2299.

17) Hirst, A. R.; Huang, B.; Castelletto, V.; Hamley, I. W.; Smith, D. K., Self-organization in the assembly of gels from mixtures of different dendritic peptide building blocks. *Chem. Eur. J*., **2007**, *13*, 2180-2188.

18) (a) Frkanec, L.; Zinic, M., Chiral bis(amino acid) and bis(amino alcohol) oxalamide gelators. Gelation properties, self-assembly motifs and chirality effects. *Chem. Commun.,* **2010**, *46,*, 522-537. (b) Makarvic, J.; Jokic, M.; Frkanec, L.; Vujicic, N.; Zinic, M., Oxalyl retro-peptide gelators. Synthesis, gelation properties and stereochemical effects. *Beilstein J. Org. Chem.* **2010**, *6*, 945-959.

19) Peng, W.; Motonaga, M.; Koe, J. R., Chirality control in optically active polysilane aggregates. *J. Am. Chem. Soc*. **2004**, *126*, 13822-13826.

20) (a) Suzuki, N.; Fujiki, M.; Kimpinde-Kalunga, R.; Koe, J. R., Chiroptical inversion in helical Si-Si bond polymer aggregates. *J. Am. Chem. Soc.* **2013**, *135*, 13073-13079. (b) Li, J.; Fan, K.; Guan, X.; Yu, Y.; Song, J., Self-Assembly mechanism of 1,3:2,4-Di(3,4-dichlorobenzylidene)-D-sorbitol and control of the supramolecular chirality. *Langmuir*, **2014**, *30*, 13422-13429.

21) Li, Y.; Li, B.; Fu, Y.; Lin, S.; Yang, Y., Solvent-Induced Handedness Inversion of Dipeptide Sodium Salts Derived from Alanine. *Langmuir*, **2013**, *29*, 9721-9726.

22) (a) Duan, P.; Qin, L.; Zhu, X.; Liu, M., Hierarchical self-assembly of amphiphilic peptide dendrons: evolution of diverse chiral nanostructures through hydrogel formation over a wide pH range. *Chem. Eur. J*., **2011**, *17*, 6389-6395. (b) Kumar, J.; Nakashima, T.; Kawai, T., Inversion of supra molecular chirality in bichromophoric perylene bisimide: influence of temperature and ultrasound. *Langmuir*, **2014**, *30*, 6030-6037.

23) Anfinsen, C. B. Principles that govern the folding of protein chains. *Science* **1973,** *181* (4096), 223-230.

24) Voet, D.; Pratt, C. W.; Voet, J. G., *Principles of Biochemistry.* Wiley: 2012

25) (a) Mahalakshami, R.; Balaram, P., The use of D amino acids in peptide design. Book Chapter 5.9, A new frontier in amino acid and protein research, **2006,** *Nova Science Publishers*. (b) Venkatraman, J., Shankaramma, S. C.; Balaram, P., Design of folded peptides. *Chem Rev*,

2001, *101*, 3131-3152. (c) Aravinda, S., Shamala, N., Roy, R. S.; Balaram, P., Non-protein amino acids in peptide design. *Proc Indian Acad Sci (Chem Sci)*, **2003**, *115*, 373-400.

26) Sibanda, B. L.; Blundell, T. L.; Thornton, J. M., Conformation of *β*-hairpins in protein structures: A systematic classification with applications to modelling by homology, electron density fitting and protein engineering. *J. Mol. Biol.* **1989,** *206*, 759-777.

27) (a) Wilmot, C. M.; Thornton, J. M. Analysis and prediction of the different types of β-turn in proteins. *J Mol Biol*, **1988**, *203*, 221-232. (b) Creighton, T. E. Proteins: structure and molecular properties (2nd edition), **1997**, New York, NY: Freeman Press.

28) Karle, I. L.; Awasthi, S. K.; Balaram, P., A designed β-hairpin peptide in crystals. *Proc Natl Acad Sci USA*, **1996**, *93*, 8189-8193

29) (a) Karle, I. L.; Awasthi, S. K.; Balaram, P., A designed β-hairpin peptide in crystals. *Proc Natl Acad Sci USA*, **1996**, *93*, 8189-8193. (b) Stanger, H. E.; Gellman, S. H., Rules for antiparallel β-sheet design: D-Pro-Gly is superior to L-Asn-Gly for β-hairpin nucleation. *J Am Chem Soc*, **1998**, *120*, 4236-4237.

30) Das, C.; Raghothama, S.; Balaram, P. A designed three stranded β-sheet peptide. *J Am Chem Soc*, **1998**, *120*, 5812-5813.

31) Das, C.; Raghothama, S.; Balaram, P., A four stranded β-sheet structure in a designed synthetic polypeptide. *Chem Commun*, **1999**, 967-968

32) Salick, D. A.; Kretsinger, J. K.; Pochan, D. J.; Schneider, J. P., Inherent antibacterial activity of a peptide-based β-hairpin hydrogel. *J. Am. Chem. Soc.,* **2007**, *129*,, 14793-14799.

33) Xinming, Li.; Xuewen, D.; Jiayang, L.; Yuan, G.; Yue, P.; Junfeng, S.; Ning, Z.; Bing, X., Introducing D−Amino acid or simple glycoside into small peptides to enable supramolecular hydrogelators to resist proteolysis. *Langmuir*, **2012**, *28*, 13512−13517.

34) Zhongli, L.; Shunkang, W.; Shuguang, Z. Fabrication of self-assembling D-form peptide nanofiber scaffold d-EAK16 for rapid hemostasis. *Biomaterials* **2011**, *32*, 2013-2020.

35) Michele, M.; Styan, K. E.; Marchesan, S., The unexpected advantages of using D-amino acids for peptide self-assembly into nantostructured hydrogels for medicine. *Current Topics in Medicinal Chemistry,* **2016**, *16*, 2009-2018.

36) Valeria, C.; Ge, C.; Ian, W. H., Amyloid peptides incorporating a core sequence from the amyloid beta peptide and gamma amino acids: relating bioactivity to self-assembly. *Chem. Commun.*, **2011**, *47*, 12470–12472.

37) Zhongli, L.; Xiaojun, Z.; Shuguang, Z., Structural Dynamic of a Self-Assembling Peptide d-EAK-16 Made of Only D-Amino Acids. *PLoS One*, **2003**, 3,, 2364

38) Robert, W.; Mikhail, T.; Karolina, C.; Priyanka, M.; Mirko, N.; Uwe, F.; Christoph, N.; Carsten, W.; Yixin, Z., Minimal peptide motif for non-covalent peptide−heparin hydrogels. *J. Am. Chem. Soc.,* **2013**, *135,* 2919−2922.

39) Fairman, R.; Anthony-Cahill, S. J.; DeGrado, W. F., The helix-forming propensity of D-alanine in a right-handed α-helix. *J. Am. Chem. Soc.,* **1992**, *114*, 5458-5459.

40) Aravinda, S.; Shamala, N.; Bandyopadhyay, A.; Balaram, P. Probing the role of the C-H...O hydrogen bond stabilized polypeptide chain reversal at the C-terminus of designed peptide helices. Structural characterization of three decapeptides. *J Am Chem Soc.*, **2003**, *125*, 15065-15075.

41) Subrayashastry, A.; Narayanaswamy, S.; Shrilakshmi, D.; Balaram, P., A right handed peptide helix containing a central double D-amino acid segment. *Chem. Commun.*, **2002**, 2454–2455

42) Srinivasan, N.; Anuradha, V. S.; Ramakrishnan, C.; Sowdhamini, R.; Balaram, P., Conformational characteristics of asparginyl residues in proteins. *Int J Peptide Protein Res*, **1994**, *44*, 112-122.

43) Banerjee, A.; Raghothama, S. R.; Karle, I. L.; Balaram, P., Ambidextrous molecules: Cylindrical peptide structures formed by fusing left and right-handed helices. *Biopolymers*, **1996**, *39*, 279- 285.

44) (a) Ramachandran, G. N.; Chandrasekaran, R., Conformation of peptide chains containing both L and D-residues: Part I-helical structures with alternating L and D-residues with special reference to the LD-ribbon and the LD-helices. *Indian J. Biochem Biophys*, **1972**, *9*, 1-11. (b) Hesselink, F.T.; Sheraga, H. A., On the possible existence of α-helical structure of regular sequence D,L-copolymers of amino acid. Conformational energy calculations. *Micromolecules,* **1972**, 5, 455-463. (c) Colona-Cesari, F.; Pramilat, S.; Heitz, F., Helical structures of poly (D-L-peptides). A conformational energy analysis. *Micromolecules*, **1977**, 10, 1284-1288. (d) Townsley, L. E.; Tucker, A.; Sham, S.; Hinton, J. F., Structures of gramicidins A, B and C incorporated in sodium dodecyl sulfate micelles. *Biochemistry*, **2001**, *40*, 11676-11686. (e) Langs, D. A., Three-dimensional structure at 0.86Å of the uncomplexed form of the

transmembrane ion channel peptide gramicidin A. *Science*, **1988**, *241*, 188-191. (f) Bunkoczi, G.; Vertesy, L.; Sheldrick, G. M., The antiviral antibiotic feglymycin: First direct-methods solution of a 1000+ equal-atom structure. *Angew Chem Int Ed*, **2005**, *44*, 1340-1342.

45) Linus, Pauling and Robert B. Corey, Two rippled-sheet configuration of polypeptide chains, and a note about the pleated sheets. *PNAS,* **1953**, *39*, 253-255.

46) Shuwei, L.; Jiaming, Q.; Yi, L.; Baoong, L.; Yonggang, Y. Chirality-driven parallel and antiparallel β-sheet secondary structures of Phe-Ala lipodipeptides. *Langmuir*, **2017**, *33*, 8246-8252.

47) Yoshida, T.; Sakurai, S.; Okuda, T.; Takagi, Y. *J. Am. Chem. Soc.***1962**, *84*, 3590.

48) Fuhrhop, J. H.; Krull, M.; Büldt, G., *Angew. Chem. Int. Ed. Engl.***1987**, *26*, 699.

49) Dzwolk, W.; Ravindra, R.; Nicolini, C.; Jansen, R.; Winter, R., The distereomeric assembly of polylysine is the low-volume pathway for preferential formation of β sheet aggregates. *J. Am. Chem. Soc*. **2004,** *126*, 3762-3768.

50) Fei, X.; Khan, I. J.; Kenneth, M.; Avanish, S. P.; Teresita, S.; Sanjeeva, M.; Vikas Nanda. *J. Am. Chem. Soc.***2013**, *135*, 18762.

51) Katelyn, J. N.; Michael, C. G.; Albert, J.; Darrin, J. P.; Schneider, J. P. *J. Am. Chem. Soc.***2011**, *133*, 14975

52) Rai, J. S.; T. M. DiMaio.; Charles, J. B.; Bradley L. Nilsson. *J. Am. Chem. Soc.***2012**, *134*, 5556.

53) Regenmortel, M.; Muller, S., D-peptides as immunogens and diagnostic reagents. *Curr. Opin. Biotechnol*, **1998**, *9*, 377-382.

54) Li, P.; Li, X.; Saravanan, R.; Li, C. M.; Leong, S. S. J., Antimicrobial macromolecules: Synthesis methods and future applications. *RSC Adv.,* **2012,** *2*, 4031-4044.

55) Marchesan, S.; Qu, Y.; Waddington, L. J.; Easton, C. D.; Glattauer, V.; Lithgow, T. J.; McLean, K. M.; Forsythe, J. S.; Hartley, P. G., Self-Assembly of ciprofloxacin and a tripeptide into an antimicrobial nanostructured hydrogel. *Biomaterials,* **2013,** *34*, 3678-3687.

56) Hamley, I. W., The amyloid beta peptide: A chemist's perspective. Role in Alzheimer's and fibrillization. *Chem. Rev*. **2012**, *112*, 5147−5192.

57) Marta, J. K.; Valeria, C.; Antonios, K.; Hamley, I. W.; Rohan, A. H.; Darrin, J. P., Self-Assembly and hydrogelation of an amyloid peptide fragment. *Biochemistry* **2008**, *47*, 4597–4605.

58) Valeria C.; Ge, C.; Hamley, I. W., Amyloid peptides incorporating a core sequence from the amyloid beta peptide and gamma amino acids: relating bioactivity to self- assembly. *Chem. Comm.,* **2011**, *47*, 12470–12472.

59) Subrata, D.; Alejandro, R. F.; Christopher, J. A.; Warner, X. Z.; Marco, R.; Benjamin, A.; Jevgenij, A. R. *Angew. Chem.* **2017**, *129*, 11664 –11668**.**

60) Li, J.; Kuang, Y.; Gao, Y.; Du, X.; Shi, J.; Xu, B., D-amino acids boost the selectivity and confer supramolecular hydrogels of a nonsteroidal anti-inflammatory drug. *J. Am. Chem. Soc.,* **2012,** *135*, 542-545.

61) Altunbas, A.; Lee, S. J.; Rajasekaran, S. A.; Schneider, J. P.; Pochan, D. J., Encapsulation of curcumin in self-assembling peptide hydrogels as injectable drug delivery vehicles. *Biomaterials,* **2011,** *32*, 5906-5914.

62) Liu, J.; Liu, J.; Chu, L.; Zhang, Y.; Xu, H.; Kong, D.; Yang, Z.; Yang, C.; Ding, D., Self-assembling peptide of d-amino acids boosts selectivity and antitumor efficacy of 10-hydroxycamptothecin. *ACS Appl. Mater. Interfaces,* **2014,** *6*, 5558-5565.

63) Deber, C. M.; Brodsky, B.; Rath, A., Proline Residues in Proteins. In *eLS*, John Wiley & Sons, Ltd: **2001**.

64) Wilhelm, P.; Lewandowski, B.; Trapp, N.; Wennemers, H., A Crystal Structure of an Oligoproline PP-II-Helix, at Last. *J. Am. Chem. Soc.,***2014**, *136*, 15829-15832.

65) Shi, Z.; Woody, R. W.; Kallenbach, N. R., Is polyproline II a major backbone conformation in unfolded proteins? *Adv.protein chem.* **2002**, *62*, 163-240.

66) Hodges, J. A.; Raines, R. T., Energetics of an n→π* interaction that impacts protein structure. *Org. Lett.* **2006**, *8*, 4695-4697.

67) (a) Zafra-Ruano, A.; Luque, I., Interfacial water molecules in SH3 interactions: Getting the full picture on polyproline recognition by protein-protein interaction domains. *FEBS Lett.* **2012**, *586*, 2619-2630; (b) Adzhubei, A. A.; Sternberg, M. J. E.; Makarov, A. A., Polyproline-II Helix in Proteins: Structure and Function. *J. Mol. Biol.* **2013**, *425*, 2100-213271) Kuemin, M.; Schweizer, S.; Ochsenfeld, C.; Wennemers, H., Effects of terminal functional groups on the

stability of the polyproline II structure: a combined experimental and theoretical study. *J. Am. Chem. Soc.* **2009**, *131*, 15474-82.

68) Lynn, E. B.; Cara, L. J.; Taylor, K. M.; Michele, L. D.; Raines, R. T. Conformational stability of collagen relies on a stereoelectronic effect. *J. Am. Chem. Soc.* **2001**, *123*, 777-778.

69) (a) Oh, K. I.; Kim, W.; Joo, C.; Yoo, D.-G.; Han, H.; Hwang, G. S.; Cho, M., Azido Gauche Effect on the Backbone Conformation of *β*-Azidoalanine Peptides. *J. Phys. Chem. B* **2010**, *114*, 13021-13029; (b) Sonntag, L. S.; Schweizer, S.; Ochsenfeld, C.; Wennemers, H., The "Azido Gauche Effect" Implications for the Conformation of Azidoprolines. *J. Am. Chem. Soc.* **2006**, *128*, 14697-14703.

70) (a) Alexander, N. D.; Alan, G.; Rohit, V. P. *J. Am. Chem. Soc.*, **2004**, *126*, 2574–2581. (b) Ninad, P.; Kim, S. *Chem Rev.* **2006,** *106*, 1616–1623.

71) Rucker, A. L.; Creamer, T. P., Polyproline II helical structure in protein unfolded states: Lysine peptides revisited. *Protein Scienc : A Publication of the Protein Society* **2002**, *11* , 980-985.

72) Kelly, M. A.; Chellgren, B. W.; Rucker, A. L.; Troutman, J. M.; Fried, M. G.; Miller, A. F.; Creamer, T. P., Host-guest study of left-handed polyproline-II helix formation. *Biochemistry* **2001**, *40*, 14376-14383.

73) (a) Goodman, M.; Neider, F.; Toniolo, C. *Biopolymer.* **1971**, *10,* 1719-1730. (b) Sonnichsen, F. D.; Van Eky, J. C.; Hodges, R. S.; Sykes, B. D. *Biochemistry*. **1992,** *31*, 8790-8798.

74) Muralikrishna, L.; Radhakrishnan Mahalakshmi. *Biopolymer* (*Pep. Sci)* **2017**, *108*, 1-10.

75) (a) Mahesh, V. S.; Krishna, N. Ganesh. *Org. Lett*, **2010**, *12*, 5390-5393. (b) Nitin, D. B.; Madhanagopal, B.; Mahesh, V. S.; Krishna, N. Ganesh. *Peptide Science,* **2017**, *108*, 22981. (c) Nitin, D. B.; Mahesh, V. S.; Krishna, N. Ganesh. *Chem. Commun.,* **2016**, 52, 4884-4887.

76) (a) Li, W.; Tailhades, J.; O'Brien-Simpson, N.; Separovic, F.; Otvos, L., Jr.; Hossain, M. A.; Wade, J., Proline-rich antimicrobial peptides: potential therapeutics against antibiotic-resistant bacteria. *Amino Acids* **2014**, *46*, 2287-2294; (b) Sadler, K.; Eom, K. D.; Yang, J. L.; Dimitrova, Y.; Tam, J. P., Translocating proline-rich peptides from the antimicrobial peptide bactenecin 7. *Biochemistry* **2002**, *41*, 14150-14157.

77) Farrera-Sinfreu, J.; Giralt, E.; Castel, S.; Albericio, F.; Royo, M., Cell-penetrating cis-gamma-amino-l-proline-derived peptides. *J. Am. Chem. Soc.* **2005**, *127*, 9459-68.

78) (a) Fillon, Y. A.; Anderson, J. P.; Chmielewski, J., Cell Penetrating Agents Based on a Polyproline Helix Scaffold. *J. Am. Chem. Soc.* **2005**, *127*, 11798-11803. (b) Geisler, I.; Chmielewski, J., Probing length effects and mechanism of cell penetrating agents mounted on a polyproline helix scaffold. *Bioorg. Med. Chem. Lett.* **2007**, *17*, 2765-2768.

79) (a) Yoon, Y.-R.; Lim, Y.-b.; Lee, E.; Lee, M., Self-assembly of a peptide rod-coil: a polyproline rod and a cell-penetrating peptide Tat coil. *Chem. Commun.* **2008**, 16, 1892-1894; (b) Lim, Y.-b.; Moon, K.-S.; Lee, M., Recent advances in functional supramolecular nanostructures assembled from bioactive building blocks. *Chem. Soc. Rev.* **2009**, *38*, 925-934.

80) Stewart, K. M.; Horton, K. L.; Kelley, S. O., Cell-penetrating peptides as delivery vehicles for biology and medicine. *Org. Biomol. Chem.* **2008**, *6*, 2242-2255.

81) El-Andaloussi, S.; Jarver, P.; Johansson, H. J.; Langel, U., Cargo-dependent cytotoxicity and delivery efficacy of cell-penetrating peptides: a comparative study. *Biochem. J.* **2007**, *407*, 285-92.

82) (a) Otvos, L., Jr., The short proline-rich antibacterial peptide family. *Cell. mol.life sci. : CMLS* **2002**, *59* , 1138-50; (b) Li, W.; Tailhades, J.; O'Brien-Simpson, N. M.; Separovic, F.; Otvos, L., Jr.; Hossain, M. A.; Wade, J. D., Proline-rich antimicrobial peptides: potential therapeutics against antibiotic-resistant bacteria. *Amino Acids,* **2014**, *46*, 2287-94.

83) Lewandowska, U.; Zajaczkowski, W.; Chen, L.; Bouillière, F.; Wang, D.; Koynov, K.; Pisula, W.; Müllen, K.; Wennemers, H., Hierarchical Supramolecular Assembly of Sterically Demanding π-Systems by Conjugation with Oligoprolines. *Angew. Chem. Int. Ed.* **2014**, *53*, 12537-12541.

84) Urszula, L.; Wojciech, Z.; Stefano, C.; Junki, T.; Ruediger, B.; Edmondo, M. B.; Sebastian, S.;Kohei, W.; Nellie, A. K. O.; Robin, S.; Chen, L.; Eiji, Y.; Wojciech, P.; Klaus, M.; Wennemers, H. A triaxial supramolecular weave. *Nature chemistry*, **2017**, *9*, 1068–1072.

85) Engel, J., *Science* **1997**, *277*, 1787-1786.

86) (a) Brinckmann, J. *Top. Curr. Chem.* **2005**, 247, 1–6. (b) Veit, G.; Kobbe, B.; Keene, D. R.; Paulsson, M.; Koch, M.; Wagener R., Collagen XXVIII, a novel von Willebrand factor A domain-containing protein with many imperfections in the collagenous domain. *J. Biol. Chem.,* **2006**, *281*, 3494–504.

87) Brodsky, B.; Thiagarajan, G.; Madhan, B.; Kar K., Triple-helical peptides: an approach to collagen conformation, stability, and self-association. *Biopolymers*, **2008**, *89*, 345–353.

88) (a) Holmgren, S. K.; Taylor, K. M.; Bretscher, L. E.; Raines R. T., Code for collagen's stability deciphered. *Nature*, **1998**, *392*, 666–667. (b) Holmgren, S. K.; Taylor, K. M.; Bretscher, L. E.; Raines R. T. *Chem. Biol.*, **1999**, *6*, 63–70.

89) Inouye, K.; Sasakibara, S.; Prockop, D. J. *Biochim. Biophys. Acta,* **1976**, *420*, 133-141.

90) Zagari, A.; Nemethy, G.; Scheraga, H. A. *Biopolymers,* **1990**, *30*, 967.

91) Li S-T.; Golub, E.; Katz, E. P. *J. Mol. Biol.* **1975**, *98*, 791.

92) Katz, E. P.; David, C. W. *Biopolymers* **1990**, *29*, 791.

93) Babu, R. I.; Ganesh, K. N., Enhanced Triple Helix Stability of Collagen Peptides with 4*R*-Aminoprolyl (Amp) Residues: Relative Roles of Electrostatic and Hydrogen Bonding Effects. *J. Am. Chem. Soc.* **2001**, *123,* 2079.

94) Umashankar, M., Babu, R. I., Ganesh, K. N., Two prolines with a difference: contrasting stereoelectronic effects of 4*R*/*S*-aminoproline on triplex stability in collagen peptides [Pro(X)-Pro(Y)-Gly]$_n$ *Chem.Commun*. **2003**, 2606.

95) Umashankar, M., Sonar, M. V., Bansode, N. D., Ganesh, K. N.*,* Orchestration of Structural, Stereoelectronic, and Hydrogen-Bonding Effects in Stabilizing Triplexes from Engineered Chimeric Collagen Peptides (Pro^X-Pro^Y-Gly)$_6$ Incorporating 4(*R*/*S*)-Aminoproline. *J. Org. Chem.* **2015**, *80*,8552.

96) Lee S. G., Lee J. Y., and Chmielewski J., *Angew. Chem. Int. Ed.* **2008**, *47*, 8429 –8432.

97) Erdmann R. S. and Wennemers H., *J. Am. Chem. Soc*. **2010**, *132*, 13957–13959.

98) Alexander, R. M. *Sci. Prog*. **1981**, *67*, 109-130.

99) (a) Trop,S.; Arridge, R. S. C.; Armenides, C. D.; Baer, E. In Structure of Fibrous *Biopolymers* Atkins, E. D. T.; Keller, A. Eds. **1975**, 26, pp. 197-221, Butterworth, London. (b) Uitto, *J. Dermatol.Clin*. **1986**, *4,* 433-436.

100) (a) Robins, S. P.; Bailey, A. *J. Biocem. Biophys. Res. Commun.* **1972**, *48*, 76-84. (b) Siegel, R. C.; *Int. Rev. Connect. Tissue Res*. **1979**, *8*, 73-188.

101) Lee, C. H.; Singla, A.; Lee, Y. *Inte. J. Phar.*, **2001,** *221*, 1–22.

102) Auger, F.A.; Rouabhia, M.; Goulet, F.; Berthod, F.; Moulin, V.; Germain, L. *Med. Biol. Eng.Comput*. **1998**, *36*, 801–812.

Chapter 2

Self-Assembly of 4(R/S)-D-Aminopolyproline

2.0 Introduction

Biomolecules such as nucleic acids, proteins are an excellent source of inspiration in the design of stimulus responsive materials. Proteins and peptides that encompass in biomolecules forming variety of functional structures should be good as building blocks for design of materials. They have the ability to respond to environmental change such as pH, solvent, temperature etc. Peptides are small, rigid unit that have protein mimicking properties.

The properties of peptides are basically defined by the nature of amino acids present in the sequence and length of the peptide. The different amino acids with varying side chains such as ionisable, aromatic, acidic, basic, hydrophobic etc, provide diversity via non-covalent interactions like aromatic stacking, hydrogen bonding, disulfide bridges and electrostatic interactions. The individual interactions are weak, but as an ensemble they give rise to stable secondary and tertiary structures essential for function.

2.1 General secondary structure in proteins

The polyproline helix is one of the common types of secondary structures prevalent in proteins. Among the naturally occurring amino acids, proline is the only amino acid in which the side chain folds back to form a five-membered ring. The secondary amine involved in peptide bond does not have any NH proton available for hydrogen bonding. Thus, polyproline secondary structures are formed without any backbone H-bonding (due to lack of NH proton) and the structural rigidity arises from cyclic side chain restricting the flexibility of φ and ψ angles forcing the peptide chain to form polyproline helices. This form is prevalent in collagen protein where three polyproline helices intertwine to form a triplex helix. Polyproline structure is considered as one of the predominant structures in many folded and unfolded proteins.[1]

There are two types of polyproline helical structures: polyproline-I (PP-I) and polyproline-II (PP-II). Polyproline PP-II helix is left-handed and fully extended with all amide bonds in *trans* conformation and exists in polar (hydrophilic) solvents like water. PP-I is a more compact right-handed, structure in which all amide bonds are in *cis* form and exists in relatively less polar (hydrophobic) solvent such as aliphatic alcohols. It is known that PP-II conformation plays a vital role in a wide variety of biological processes which includes signal transduction, transcription, immune response and cell motility.[2]

The classical PP-II and PP-I structures adopted by polyproline has no intra-helical H-bonding, unlike other forms of helices in proteins. Thus polyprolines cannot adopt any β-structures or β-sheets which need a H-bond donor. H-bonding substituents can be placed at C4 position of proline (C4-NH$_2$/OH/SH) to explore if the nature of secondary structure is altered. Previous work from this laboratory demonstrated that *cis*-(2*S*,4*S*)-aminopolyproline[3] and *cis*-(2*S*,4*S*)-hydroxypolyproline[4] (4*S*-amp$_9$/hyp$_9$) switch to an unusual β-structure (Figure 1) in TFE, while both skow PPII form in water.. In contrast, *trans*-(2*S*,4*R*)-4-Aminopolyproline and *trans*-(2*S*,4*R*)-4-hydroxypolyproline (4*R*-Amp$_9$/Hyp$_9$) do not undergo any conformational transition in TFE and remain in PP-II form in both water and TFE. This was postulated to occur through conversion of H-bonds from an intra-chain to inter-chain mode. This inter-chain association of two chains to β-structure extends into long micro-meter fiber morphology as clearly seen in FE-SEM images.
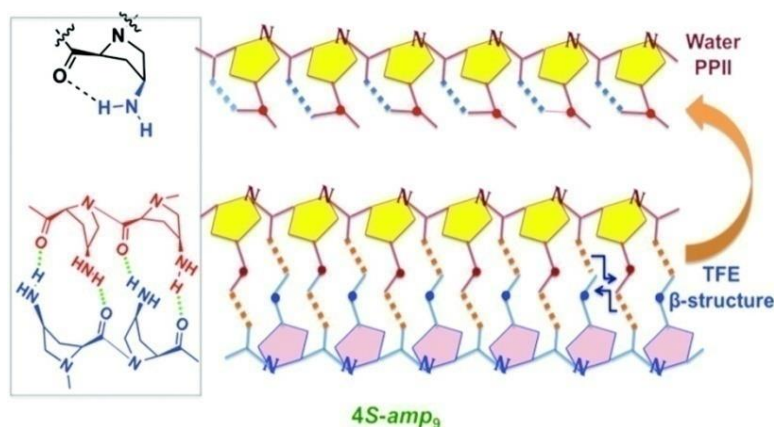

Figure 1. Water-induced switching β-structure to PP-II conformation in peptide 4*S*-amp$_9$[3]

The orientational nature of β-structure as to parallel or antiparallel polyproline chains was addressed by fluorescence resonance energy transfer (FRET) by labelling the peptides in appropriate configurations (N-terminal tryptophan/ C-terminal dansyl). Through suitable mixing of peptide chains, it was demonstrated that the peptide forms antiparallel β-structure. To support this finding by another method, 4*S*-hyp$_9$ peptide was conjugated to a long chain fatty acid of varying lengths and based on hydrophobic associations originating from fatty acids chains, long micro-meter fibers were observed, suggesting antiparallel orientation of the β-structure.[4]
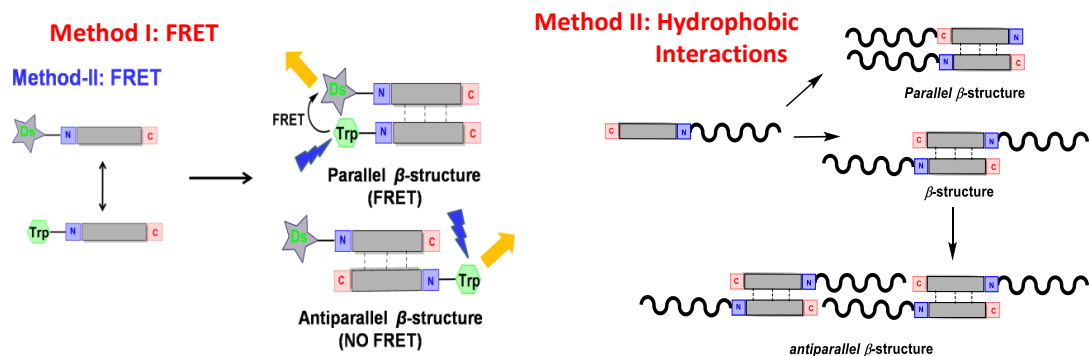
Figure 2. Antiparallel β-structure[4]

2.2 Present work: Rationale and objective

It was established that substitution at C4 in prolines has a primary effect on the hydrogen bonding patterns and backbone torsion angles in these polyproline mimics. Hydrogen bonding substituents (NH$_2$/OH/NHCHO) and the stereochemistry at C4(S) shows solvent specific formation of β-structure through side chain backbone hydrogen bonding.[5] Solvent-dependent switching of conformation between PP-II and β-structure was observed in case of both polypeptides derived from cis-(2S,4S)-amino[3] and cis-(2S,4S)-hydroxy prolines[4] which form antiparallel β-sheet in TFE. For this to be observed, cis disposition of substituents at C2 and C4 seems mandatory. Hence it will be interesting to see if by inverting both centers from (2S,4S) to (2R,4R), one obtains mirror image β-structure with opposite handedness.

With this rationale, it was decided to synthesize and study homo oligo-polyproline peptides derived from D-Proline corresponding to cis-(2R,4R)-aminopolyproline and $trans$-(2S,4R)-aminopolyproline which should result in mirror image PP-II structures in water and mirror image β-structures in TFE. One can then explore the possibilities of generating combinatorial stereoblocks of peptide to generate a variety of chiral supra molecular assemblies. Such associations may be modulated by conjugation with fatty acids to further superorganize the peptides into interesting varieties of β-structures. Peptides conjugated to aliphatic lipid chain may induce continuous fibers based on the hydrophobic interactions of alkyl chains in addition to H-bonding in prolyl residues.

Thus the main objective of this work is to synthesize, characterize and carry out biophysical studies 4(R/S)-NH$_2$-(2R)-D-prolyl polypeptides to examine the range of

morphological structure controlled by stereochemical disposition of 2-carboxyl 4-amino substitution.

The specific objectives of the present proposed work are as follows.

❖ Synthesis of (2R,4R) and (2R,4S), N^1-Fmoc-4-NH(Boc)-aminoproline monomers from 4(R/S)-amino (2R)D-proline

❖ Solid phase synthesis, purification & characterization of polyproline peptides

❖ Investigation of the conformation of polyproline peptides **P1**-**P4** folding into PP-II helix and *β*-structure by CD-spectroscopy.

❖ Morphological study of self-assembly of polypeptides through imaging techniques AFM, FE-SEM, TEM

P1 (2*S*)-L-*Pro*9   P2 (2*R*)-D-*Pro*9

P3 c*is*-(2*R*,4*R*)-D-*Amp*9   P4 t*rans*-(2*R*,4*S*)-D-*amp*9
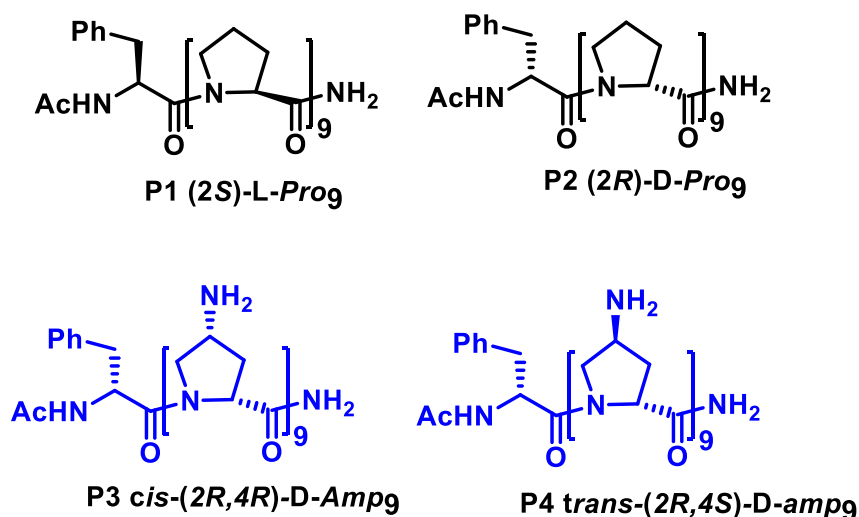
2.3 Synthesis of monomers 8 & 13

The monomers **8** and **13** as shown below and required for assembly of various polypeptides were synthesized by following standard protection and de-protection chemistry.

(8)   (13)
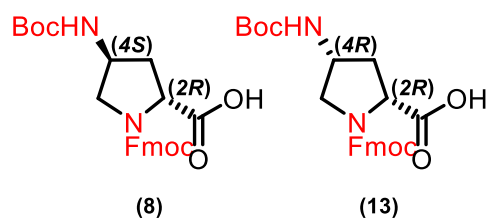
2.3.1 Synthesis of (*2R,4S*) aminoproline monomer (**8**)

The *cis*-(2R,4R)-hydroxy-D-proline **1** was synthesized from the commercially available *trans*-(2S,4S)-hydroxy-L-proline by inversion of stereochemistry at C2. This was achieved by reacting *trans*-(2S,4R)-hydroxy-L-proline with acetic anhydride and hydrochloric acid to obtain *cis*-(2R,4R)-hydroxy-D-proline. The inversion of configuration was confirmed by optical rotation $[\alpha]^D_{20}$ $+59^0$ (lit. $[\alpha]^D_{20,}$ $+59^0$).[6] The compound (2R,4R)-N[1]-(benzyloxycarbonyl)-4-hydroxy-D-proline methyl ester **3** was synthesized by reacting *cis*-(2R,4R)-hydroxy-D-proline **1** with Cbz-Cl in the presence of mild base aq. NaHCO$_3$ and esterified by using dimethyl sulphate.

Scheme 1: *Synthesis of (2R,4S) aminoproline monomer* **8**
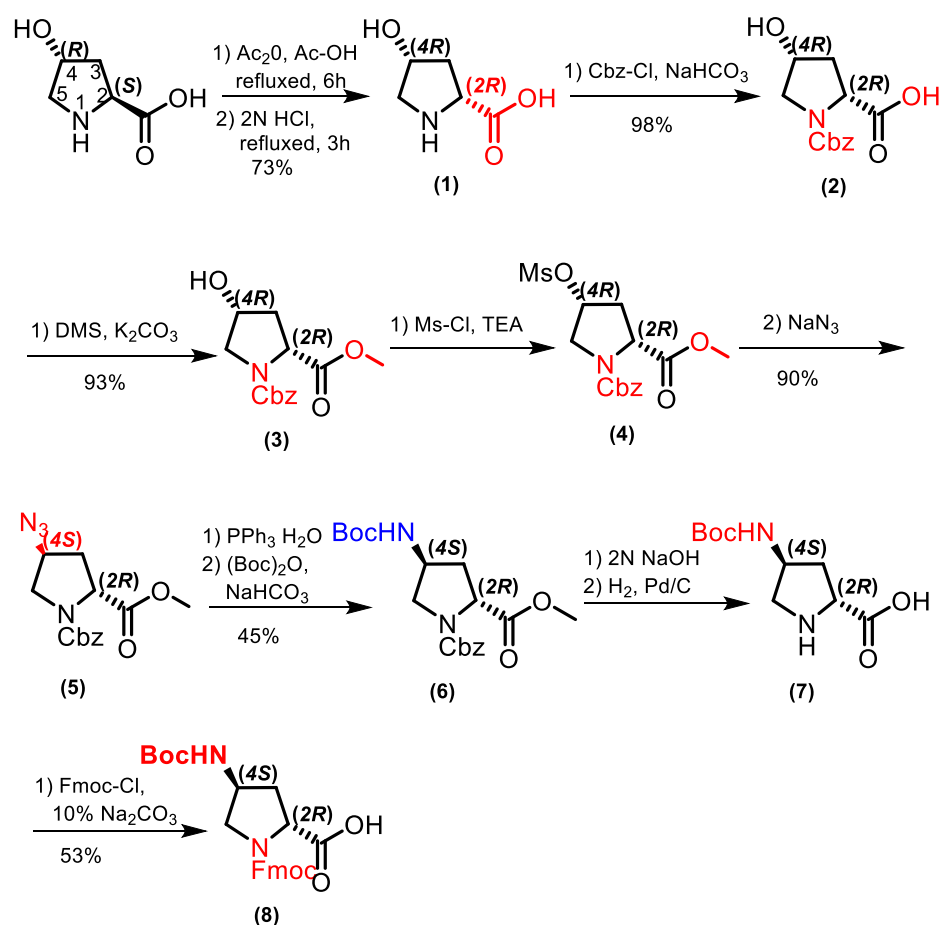
To generate amino functionality at C4 position on proline with inversion in stereochemistry, 4R-OH compound **3** was reacted with mesyl chloride in the presence of triethylamine to obtain 4R-OMs compound **4**, which was subsequently reacted with sodium azide to get the 4S-azido compound **5**. This was characterized by IR to identify the azide stretching frequency at 2104 cm^{-1}. The 4S-azido compound **5** was reduced by Staudinger

reaction to obtain the 4S-NH$_2$ compound, that was *in situ* protected as Boc derivative to obtain (4S-NHBoc) **6**. This was followed by hydrolysis of ester with aq. LiOH. The deprotection of NHCbz in **6** was done under hydrogenation to yield the N^1-amine **7**, which was reacted with Fmoc-Cl to yield the desired monomer **8** (2R,4S)-N^1-(Fmoc)-N^4-(Boc)-D-Proline.

2.3.2 Synthesis of (*2R,4R*) 4-Aminoproline monomer (13)

Synthesis of *cis*-(*2R,4R*)-aminoproline monomer **(13)** started from the previously synthesized compound **3**. To obtain the amino functionality at C4 position on proline with retention in configuration (4R), compound **3** (2R,4R)-N^1-(Cbz)-4-hydroxy-D-proline methyl ester **3** was treated with triphenyl phosphine, methyl-*p*-toluenesulfonate and diethyl azodicarboxylate to get 4S-OTs compound **9** with inversion at C4. This was subsequently reacted with sodium azide to get the 4R-azido compound **10** that was characterized by IR spectroscopy and proton NMR. The azido derivative **10** was reduced by Staudinger reaction to yield the 4R-NH$_2$ compound, which was *in situ* protected as Boc derivative (4R-NHBoc) **11**. This was hydrolysed with aq. LiOH followed by deprotection of N^1-Cbz by hydrogenation to get compound **12**. The final monomer **13** (2R,4R)-N^1-(Fmoc)-N^4-(Boc)-D-proline was obtained by reacting amine **12** with Fmoc-Cl. All compounds were characterized by ^{1}H NMR, IR and mass spectrometry.

Scheme 2: *Synthesis of (2R,4R) aminoproline monomer 13*
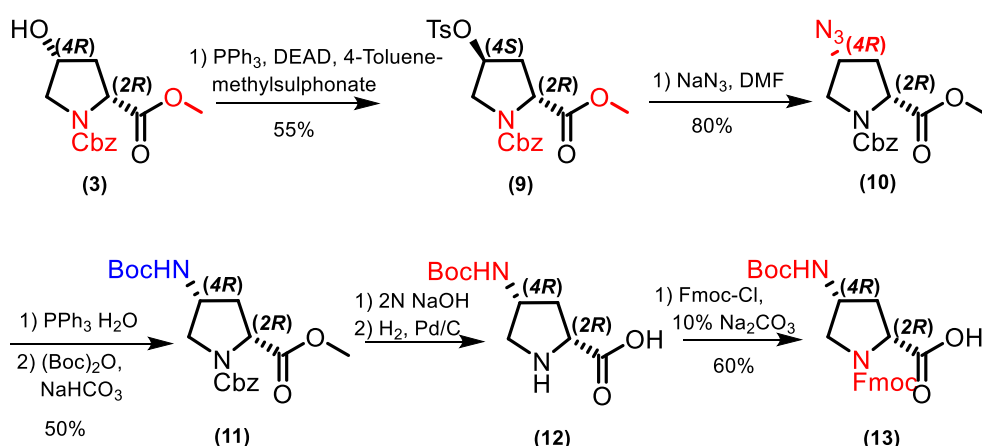
2.3.3 Solid phase peptide synthesis

The desired peptides of present study were synthesized manually on a solid phase by using standard Fmoc protocol, on commercial Rink amide resin (Nova biochem 100-200

mesh) carrying amine substitution of 0.61 mmol/g. The loading on resin was reduced to 0.3 mmol/g by partial capping of resin with acetic anhydride in pyridine.

The Fmoc group on resin was removed by 20% piperidine in DMF, and the free acid monomers were coupled sequentially using *in situ* activation of amino acid (3 eq) in the presence of HBTU as a coupling reagent, HOBt as racemisation suppressor and DIPEA as a catalyst in DMF. For the quantitative determination of peptides aromatic amino acid phenylalanine was coupled to the N-terminus and followed by end capping by acetylatation with acetic anhydride in pyridine. The synthesized peptides were cleaved from the solid support by treating with 90% TFA in DCM containing triisopropylsilane.

Scheme 3: *Solid phase synthesis of peptides (**P1**-**P4**)*
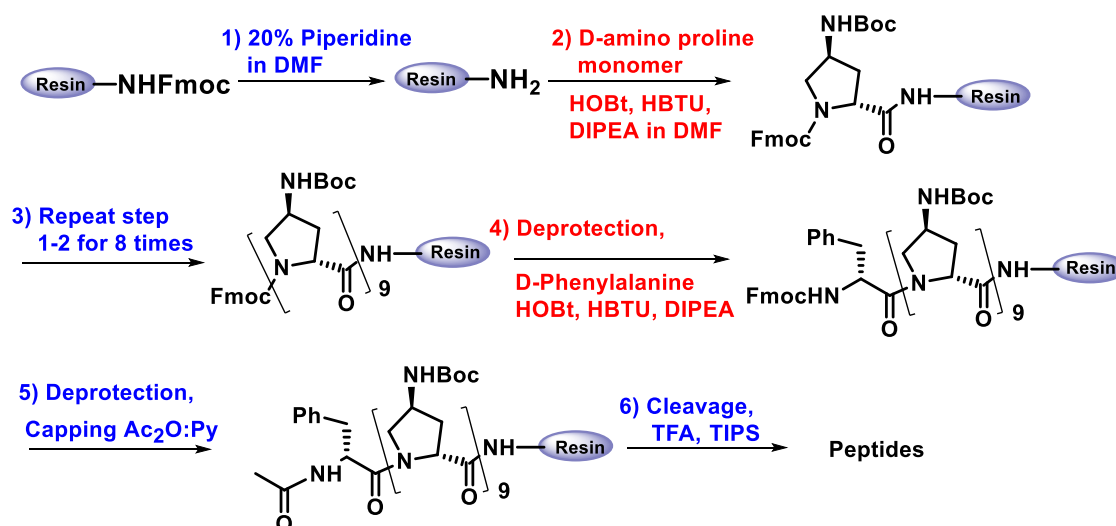
The various proline polypeptides **P1**-**P4** were synthesized by solid phase peptide synthesis using appropriate monomers. After the synthesis, the peptides **P1**-**P4** were cleaved from solid support and purified by HPLC and characterized by MALDI-TOF.
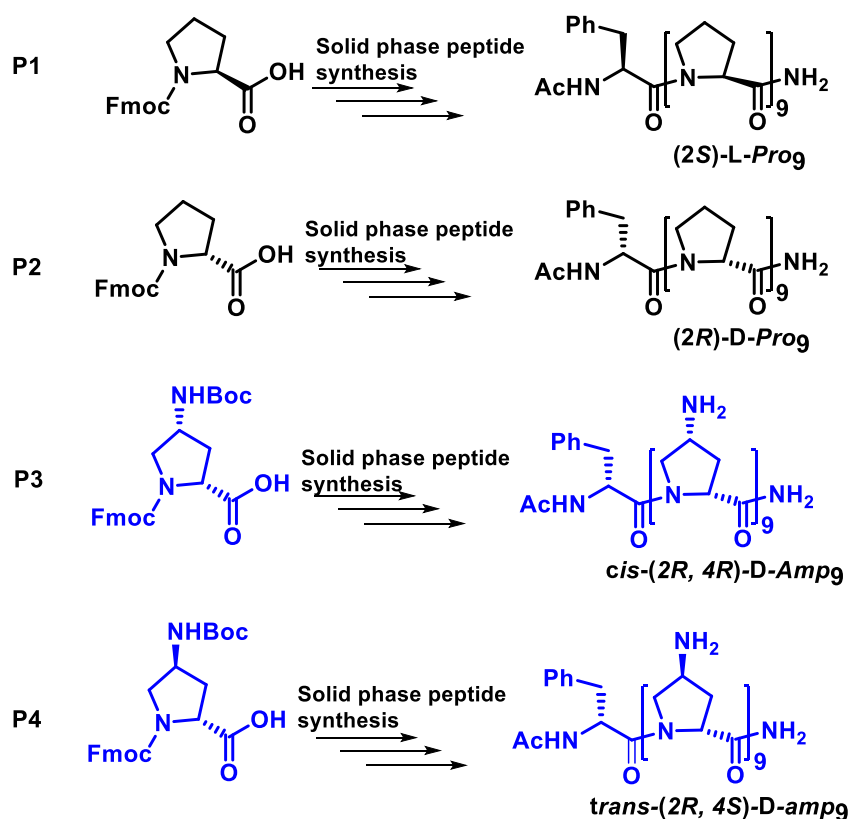
Table 1: HPLC retention time and MALDI-TOF characterization of peptides **P1**-**P4**

Sequence	Ret. time	Mol. Formula	Cal. Mass	Obs. Mass
P1 AcNH-L-Phe-[-L-Pro-]$_9$-NH$_2$	19.2	$C_{56}H_{77}N_{11}O_{11}Na$	1102.57	1102.50
		$C_{56}H_{77}N_{11}O_{11}K$	1118.54	1118.50
P2 AcNH-D-Phe-[-D-Pro-]$_9$-NH$_2$	19.3	$C_{56}H_{77}N_{11}O_{11}Na$	1102.57	1102.60
		$C_{56}H_{77}N_{11}O_{11}K$	1118.54	1118.58
P3 AcNH-D-Phe-[-D-Amp-]$_9$-NH$_2$	14.1	$C_{56}H_{86}N_{20}O_{11}Na$	1238.42	1238.40
		$C_{56}H_{86}N_{20}O_{11}K$	1254.53	1254.50
P4 AcNH-D-Phe-[-D-amp-]$_9$-NH$_2$	14.6	$C_{56}H_{86}N_{20}O_{11}Na$	1238.42	1237.87
		$C_{56}H_{86}N_{20}O_{11}K$	1254.53	1253.82

2.3.4 Synthesis of fatty acid conjugated peptides P5-P10

By following the above described solid phase peptide synthesis protocol, peptides *cis*-(2R,4R)-D-*Amp₉*, and *trans*-(2R,4S)-D-*amp₉*, peptides were synthesised and coupled on the resin with the fatty acids lauric acid (C$_{12}$), myristic acids (C$_{14}$) and palmitic acid (C$_{16}$) to

result in conjugated peptides **P5**-**P10.** These were cleaved from the solid support, purified by reverse phase HPLC and characterized by MALDI-TOF analysis.

2.4 Determination of the peptide concentration in stock solution

To determine the concentrations of the synthesised peptides, the aromatic amino acid phenylalanine (Phe) was incorporated at the N-terminus side of peptides **P1-P10**. The concentration of peptide stock-solutions were determined by UV absorption maximum of phenylalanine at 257 nm and extinction coefficient of 195 $M^{-1}cm^{-1}$.

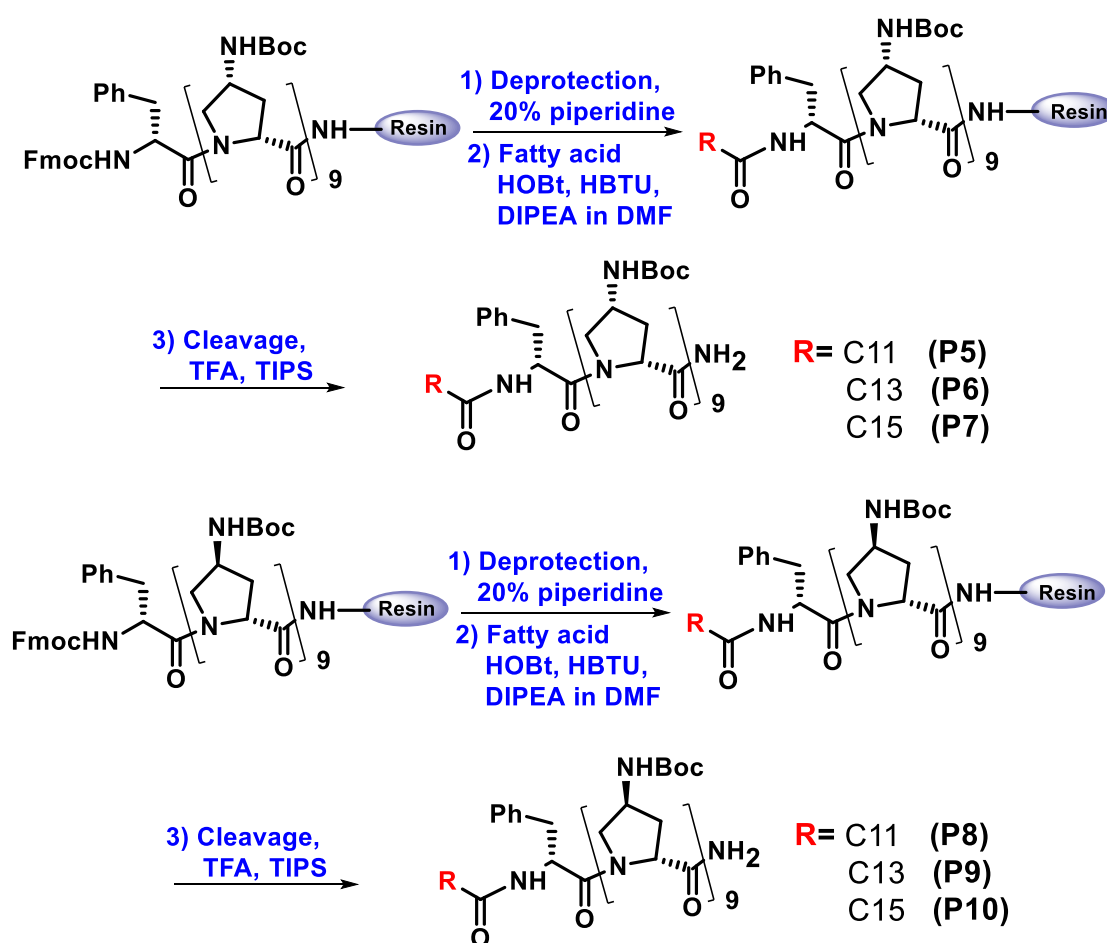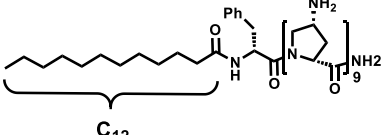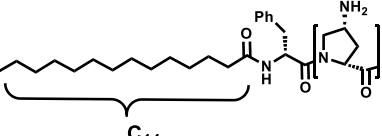Scheme 4: *Solid phase peptides synthesis of peptide (**P5-P10**) conjugation of fatty acid.*
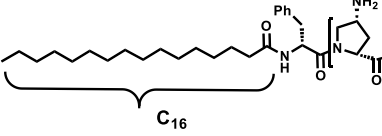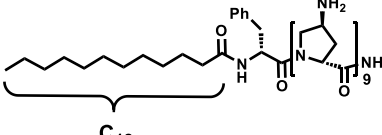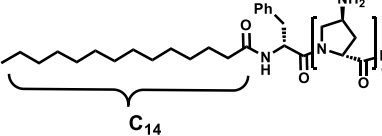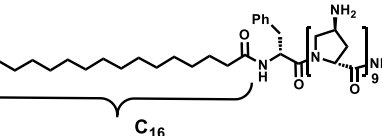
Table 2: Characterization of fatty acid conjugated polyproline peptide **(P5-P10)**

No.	Peptides	Mol. Formula	Mass (cal.)	Mass (obs.)
P5	P5 C$_{12}$-*cis*-(2R, 4R)-D-amp$_9$	C$_{66}$H$_{106}$N$_{20}$O$_{11}$Na C$_{66}$H$_{106}$N$_{20}$O$_{11}$K	1377.82 1393.79	1378.57 1393.53
P6	P6 C$_{14}$-*cis*-(2R, 4R)-DAmp$_9$	C$_{68}$H$_{110}$N$_{20}$O$_{11}$Na C$_{68}$H$_{110}$N$_{20}$O$_{11}$K	1405.85 1421.83	1405.54 1421.51
P7	P7 C$_{16}$-*cis*-(2R, 4R)-D-Amp$_9$	C$_{70}$H$_{115}$N$_{20}$O$_{11}$Na C$_{70}$H$_{115}$N$_{20}$O$_{11}$K	1433.88 1449.86	1434.47 1449.43
P8	P8 C$_{12}$-*trans*-(2R, 4S)-D-amp$_9$	C$_{66}$H$_{106}$N$_{20}$O$_{11}$Na C$_{66}$H$_{106}$N$_{20}$O$_{11}$K	1377.8248 1393.7987	1378.52 1393.51
P9	P9 C$_{14}$-*trans*-(2R, 4S)-D-amp$_9$	C$_{68}$H$_{110}$N$_{20}$O$_{11}$Na C$_{68}$H$_{110}$N$_{20}$O$_{11}$K	1405.8561 1421.8300	1405.55 1421.40
P10	P10 C$_{16}$-*trans*-(2R, 4S)-D-amp$_9$	C$_{70}$H$_{115}$N$_{20}$O$_{11}$Na C$_{70}$H$_{115}$N$_{20}$O$_{11}$K	1433.8874 1449.8613	1433.58 1449.53

2.5 RESULTS AND DISCUSION

CD spectroscopy is a versatile technique for determining the conformation of peptides. To find out the solvent dependent secondary structure of the synthesized peptides **P1**-**P10**, CD spectroscopic studies were carried out in aqueous buffer and in TFE.

2.5.1 Conformational study of peptides P1 (L-*Pro₉*) and P2 (D-*Pro₉*) in buffer

A single strand of L-polyproline peptide is known to adopt left-handed polyproline-II (PP-II) helix. In CD-spectroscopy polyproline-II (PP-II) helix gives characteristic positive CD band at 225 nm and a negative CD band at 205 nm. Figure 3A and 3B show concentration-dependent CD spectra of enantiomeric peptides **P1** (L-*Pro₉*) and **P2** (D-*Pro₉*) in phosphate buffer in the concentration range 50-300 μM. For (2*S*)-L-*Pro₉* peptide, the observed large negative band at 205 nm and a less intense positive band at 230 nm with cross over at 220 nm is characteristic of left handed PP-II helix (Figure 3A). The enantiomeric peptide (2*R*)-D-*Pro₉* shows CD spectra of right handed PP-II helix (Figure 3B) which is a mirror image with larger positive band at 205 nm and small negative band at ~225 nm. The CD spectra show exact mirror image inversion of signals for oppositely handed PP-II helix conformations (Figure 3C) both in sign and in amplitude. Concentration dependent CD spectra were recorded to find out the effect of concentration on conformation. It was observed that no change in intensity of CD band occurred as a function of concentration of both L and D-polyprolyl peptides.
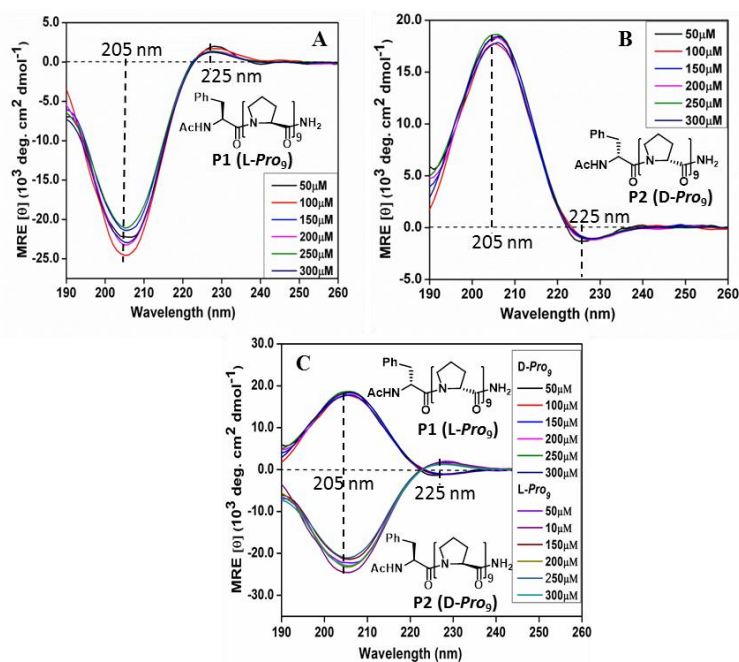

Figure 3. CD spectra of peptides **P1** and **P2**. **A)** **P1** (L-*Pro₉*), **B)** **P2** (D-*Pro₉*) and **C)** superimposed spectra of **P1** and **P2** at 25⁰ C, concentration 50-300 μM in 10 mM phosphate buffer pH 7.2.

2.5.2 Conformational study of peptides P3 [*cis-*(*2R,4R*)-D-*Amp9*] & P4 [*trans-*(*2R,4S*)-D-*amp9*] in phosphate buffer

Figures 4A and 4B show the CD spectra of diastereomeric peptides **P3** (*cis-*(*2R, 4R*)-D-*Amp9*) and **P4** (*trans-*(*2R,4S*)-D-*amp9*) respectively in phosphate buffer (pH 7.2) in the concentration range 50-300 μM. These peptides are diastereomers derived from D-enantiomer. Hence they form right handed PP-II helix. Both the spectra show a weak negative signal at 225 nm and a strong positive signal at 205 nm suggesting no major changes in helical structure.
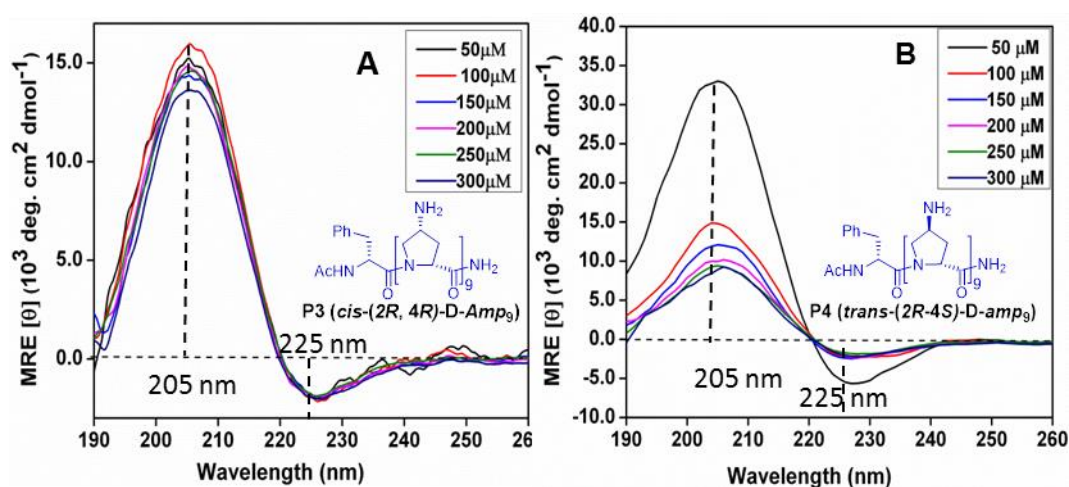

Figure 4. CD spectra of peptides **P3** and **P4**. **A)** **P3** (*cis-*(*2R,4R*)-D-*Amp9*), **B)** **P4** (*trans-*(*2R,4S*)-D-*amp9*) at 25⁰ C, concentration range 50-300 μM in 10 mM Sodium phosphate buffer pH 7.2

2.5.3 Conformational study of lipidated *cis*-D-peptides P5-P7 in phosphate buffer

Figures 5 (A-C) are the CD spectra of peptides **P5** [C_{12}-*cis-*(*2R,4R*)-D-*Amp9*], **P6** [C_{14}-*cis-*(*2R,4R*)-D-*Amp9*] and **P7** [C_{16}-*cis-*(*2R,4R*)-D-*Amp9*] in the concentration range 50-300 μM in phosphate buffer. The peptide **P5** with fatty acid chain adopts right handed PP-II conformation as seen for **P3** *without the chain.* The negative CD band at 225 nm and the positive band at 205 nm remain at the same position indicating that conjugation with fatty acids of different chain lengths (C_{12}, C_{14} and C_{16}) do not alter its conformation and there is no effect of concentration on conformation.
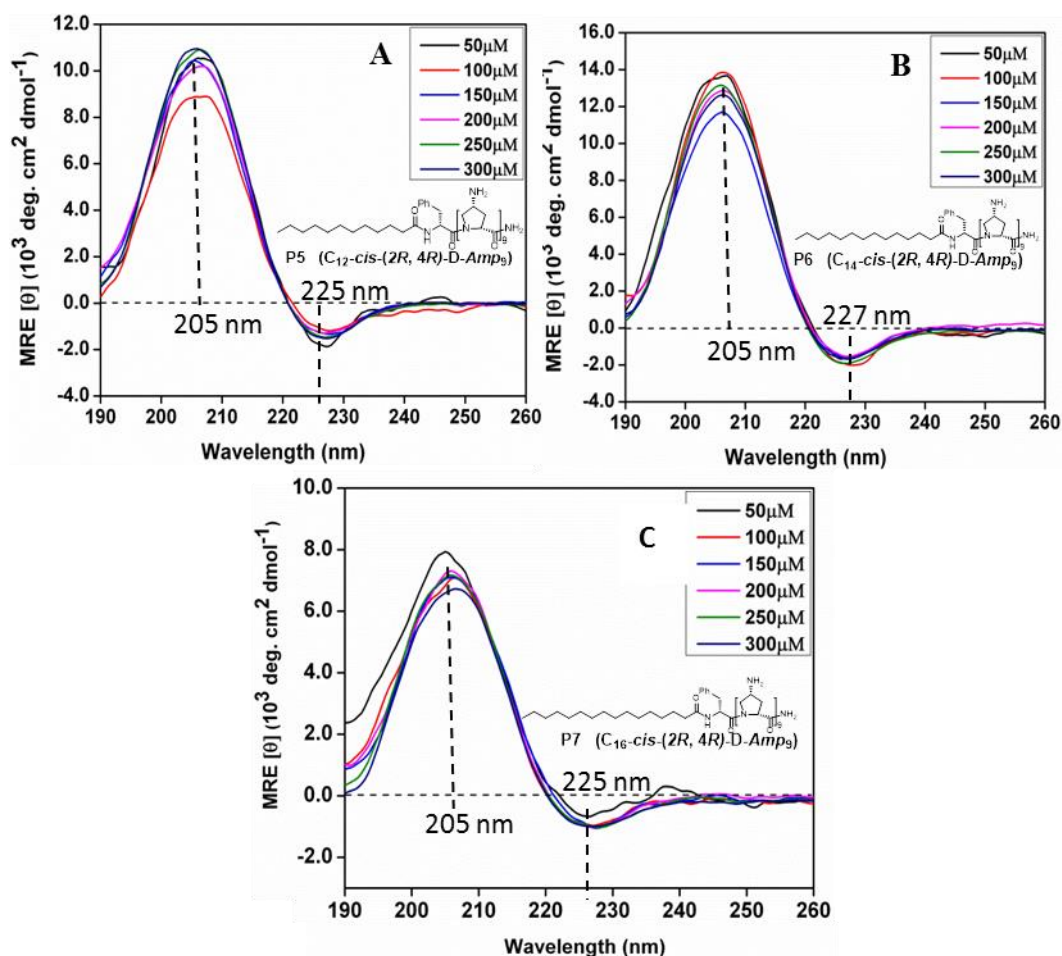
Figure 5. CD spectra of peptide **A) P5** (C$_{12}$-*cis*-(2R,4R)-D-*Amp$_9$*), **B) P6** (C$_{14}$-*cis*-(2R,4R)-D-*Amp$_9$*), **C) P7** (C$_{16}$-*cis*-(2R,4R)-D-*Amp$_9$*) at 25^0 C, concentrations 50-300 uM in phosphate buffer pH-7.2

2.5.4 Conformational study of lipidated *trans*-D-peptides P8-P10 in phosphate buffer

Figures 6 (A-C) are the CD spectra of lipidated *trans*-D-peptides **P8** [C$_{12}$-*trans*-(2R,4S)-D-*amp$_9$*], **P9** [C$_{14}$-*trans*-(2R,4S)-D-*amp$_9$*] and **P10** [C$_{16}$-*trans*-(2R,4S)-D-*amp$_9$*] respectively in phosphate buffer in the concentration range 50-300 μM. The negative CD band at 225 nm for enantiomeric polyproline peptides and the strong positive CD band at 205 nm remain unaltered indicating that conjugation of different fatty acid chains (C$_{12}$, C$_{14}$, and C$_{16}$) do not alter the conformation and all exist in PP-II conformation. The CD band intensities remain same for all fatty acid conjugated peptides throughout the concentration range 50-300 μM suggesting that peptides form well defined right handed PP-II structures.
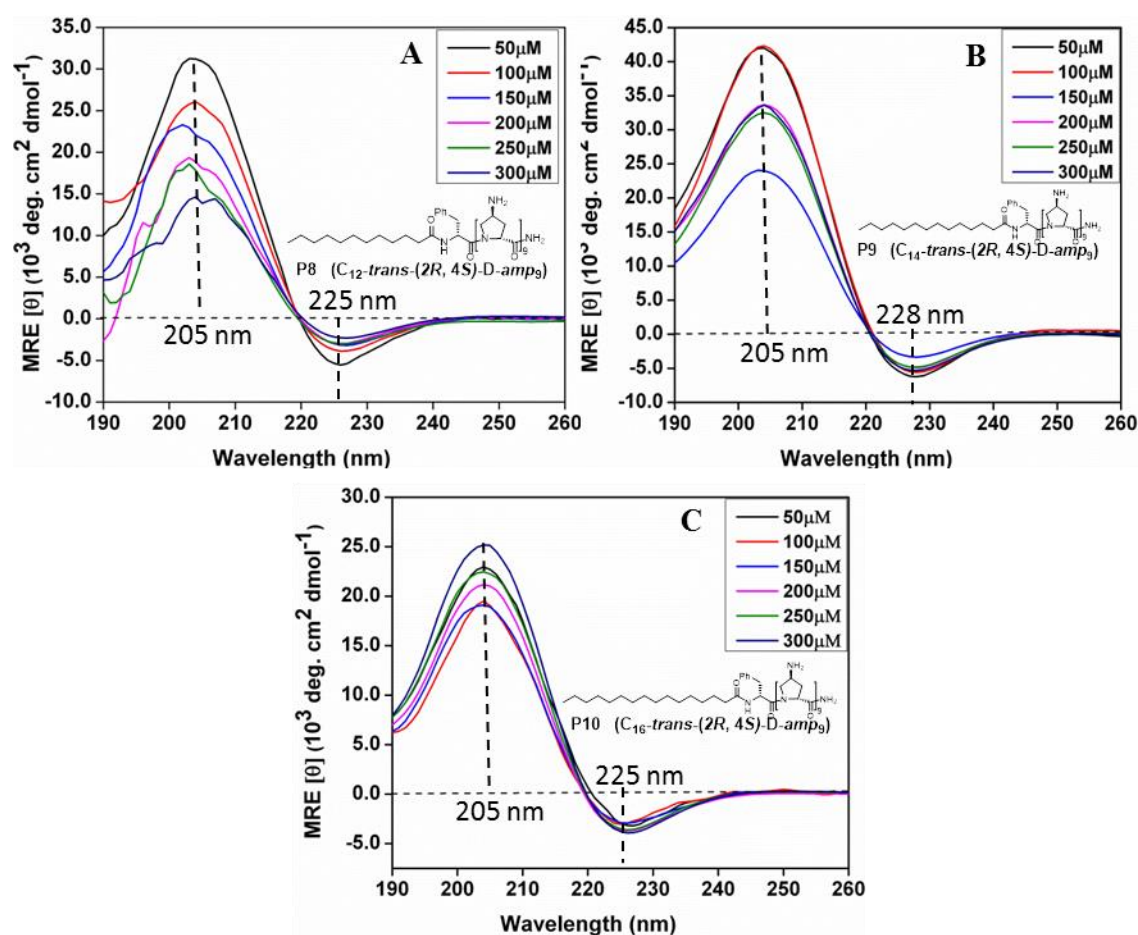
Figure 6. CD spectra of peptides **P9-P10. A) P8** [C_{12}-*trans*-(*2R,4S*)-D-*amp_9*], **B)** **P9** [C_{14}-*trans*-(*2R,4S*)-D-*amp_9*] and **C) P10** [C_{16}-*trans*-(*2R,4S*)-D-*amp_9*] at 25^0 C, concentration 50-300 uM in phosphate buffer pH-7.2

2.6 Solvent effects on the conformation of peptides P11-P14

The peptide conformation is dependent on the nature of solvent.[7] TFE is known to break the helix by removing hydration sphere around the peptide backbone.[8] It is known in the literature that in less polar solvents like alcohols polyproline peptide adopts PP-I form while in aqueous solvent, it exhibits PP-II form. The rate of conversion of PP-I to PP-II form is very slow.[9] The solvent dependent switching of conformation from α helix to PP-II to the random coil is well known.[10] A conformational change between PP-II and *β* structures in case of polypeptides of **P11** (*cis*-(*2S,4S*)-L-*amp_9*) and **P13** (*cis*-(*2S,4S*)-L-*hyp_9*) (figure 7A) has been observed in our group.[3,4] It occurs by change of *intra*-molecular hydrogen bonding in PP-II to *inter*-molecular hydrogen bonding in *β*-structures. In hydrophilic solvent water, the 4S-OH/NH$_2$ groups form a hydrogen bond with carbonyl of the same residue (*intra*-molecular) favouring PP-II structure. In a hydrophobic solvent like TFE, *intra*-chain H-

bonding switches to *inter*-chain H-bonds, leading to *β*-structure (Figure 7B). In the diastereomric peptides **P12** (*trans*-(2*S*,4*R*)-L-*Amp₉*) and **P14** (*trans*-(2*S*,4*R*)-L-*Hyp₉*) where the C2 and C4 substituents are in *trans* position, intraresidue H-bond is not possible and may not favour inter-chain bonding also hence do not show lead to formation of *β*-structure.
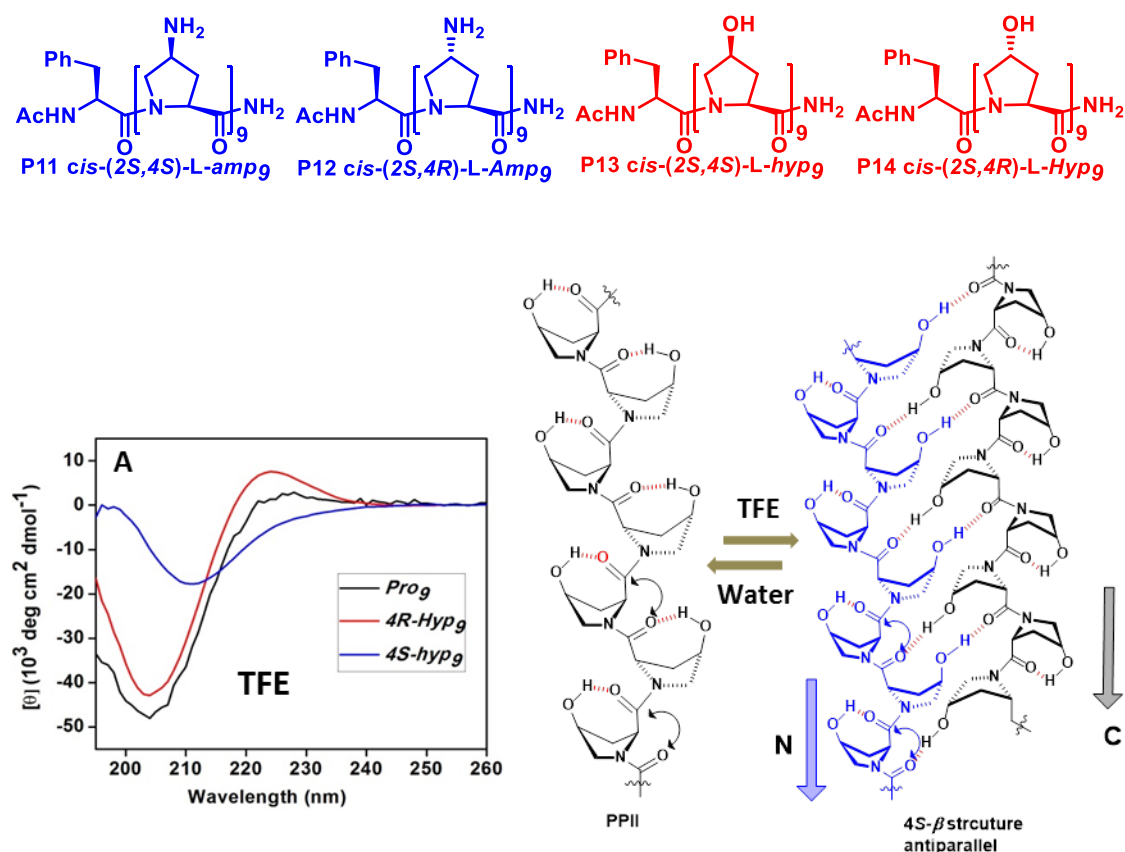

Figure 7 CD Spectra of peptides **P1**, **P13** and **P14, A)** in TFE and **B)** schematics of *intra*-molecular H-bonding favoring the PPII form *via* enriching the *trans* amide geometry in water and *inter*-chain H- bonds involving *4S*-OH in *β*-structure in TFE.

Since the conformations of peptides reported earlier are for the L-peptides, it would be interesting to examine if similar effects are present in the corresponding enantiomeric D-peptides.

2.6.1 Conformational study of peptides P1 (L-*Pro₉*) and P2 (D-*Pro₉*) in TFE

Figures 8A and 8B are the CD spectra of unsubstituted prolyl peptides **P1** (L-*Pro₉*) and **P2** (D-*Pro₉*) respectively in trifluoroethanol in the concentration range 50-300 μM. Figure 8A shows a weak positive band at 225 nm and strong negative band at 205 nm. Figure 8B is the CD spectra enantiomer of its enantiomeric peptide **P2** (D-*Pro₉*) which is opposite in handedness to that of peptide **P1** (L-*Pro₉*) with negative band at 225 nm and strong positive

band at 205 nm, forming a right-handed PP-II conformation. Figure 8C shows superimposed CD spectra of the two peptides **P1** and **P2** in TFE which are mirror images of each other

Concentration dependent CD spectra were recorded to find out its effect on conformation. It is observed that, there is no change in intensity of CD band as a function of concentration.
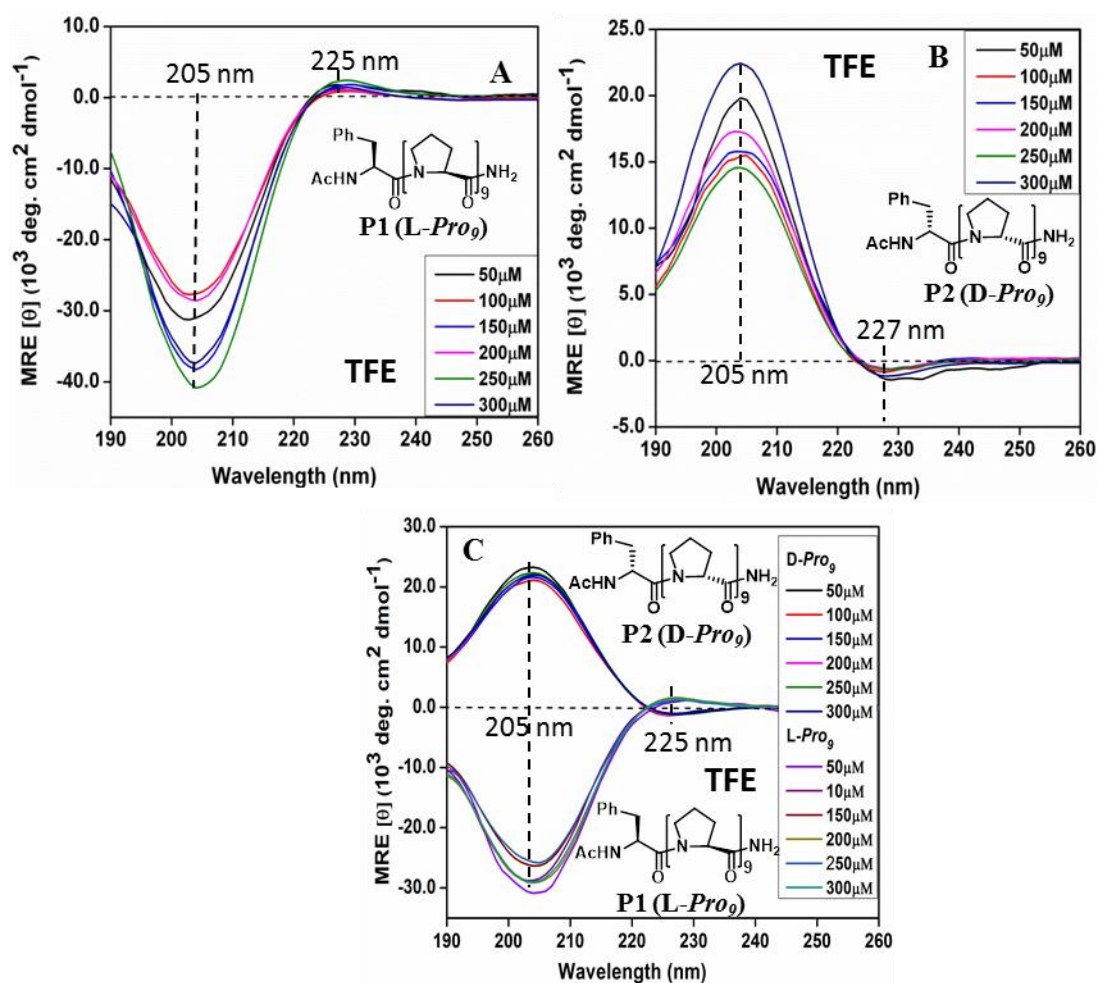

Figure 8. CD spectra of peptides **P1** and **P2. A) P1** (L-*Pro$_9$*), **B) P2** (D-*Pro$_9$*) and **C)** super imposed spectra **from A** and **B.** Spectra recorded in TFE at 25^0 C in the concentration range 50-300 μM.

2.6.2 Conformational study of peptides P3 [*cis*-(*2R,4R*)-D-Amp$_9$] & P4 [*trans*-(*2R,4S*)-D-amp$_9$] in TFE

Figures 9A and 9B are the CD spectra of peptides **P3** [*cis*-(*2R,4R*)-D-Amp$_9$] and **P4** [*trans*-(*2R,4S*)-D-amp$_9$ respectively in TFE in the concentration range 50-300 μM. The peptide **P3** [*cis*-(*2R,4R*)-D-Amp$_9$] undergoes a conformational change in solvent TFE (Figure

9A). Two new CD bands appear, one positive at 218 nm and a negative band at 200 nm which correspond to β-structure. It is important to note that the observed effect of TFE is similar for both L and D enantiomers. This brings the importance of hydrogen bonding substitution at the C4 position, possible only in (*cis*) 4*R* peptide that shows change in CD, while and (*trans*) 4*S* peptide does not.

In the peptide **P4** (*trans*-(*2R,4S*)-D-*amp₉*) the negative CD band at 225 nm and the positive CD band at 205 nm remain at the same position in TFE as that observed in phosphate buffer (Figure 9B). This shows that there is no effect of TFE on its conformation, suggesting that peptide **P4** [*trans*-(*2R,4S*)-D-*amp₉*] remains in right handed PP-II conformation in TFE.
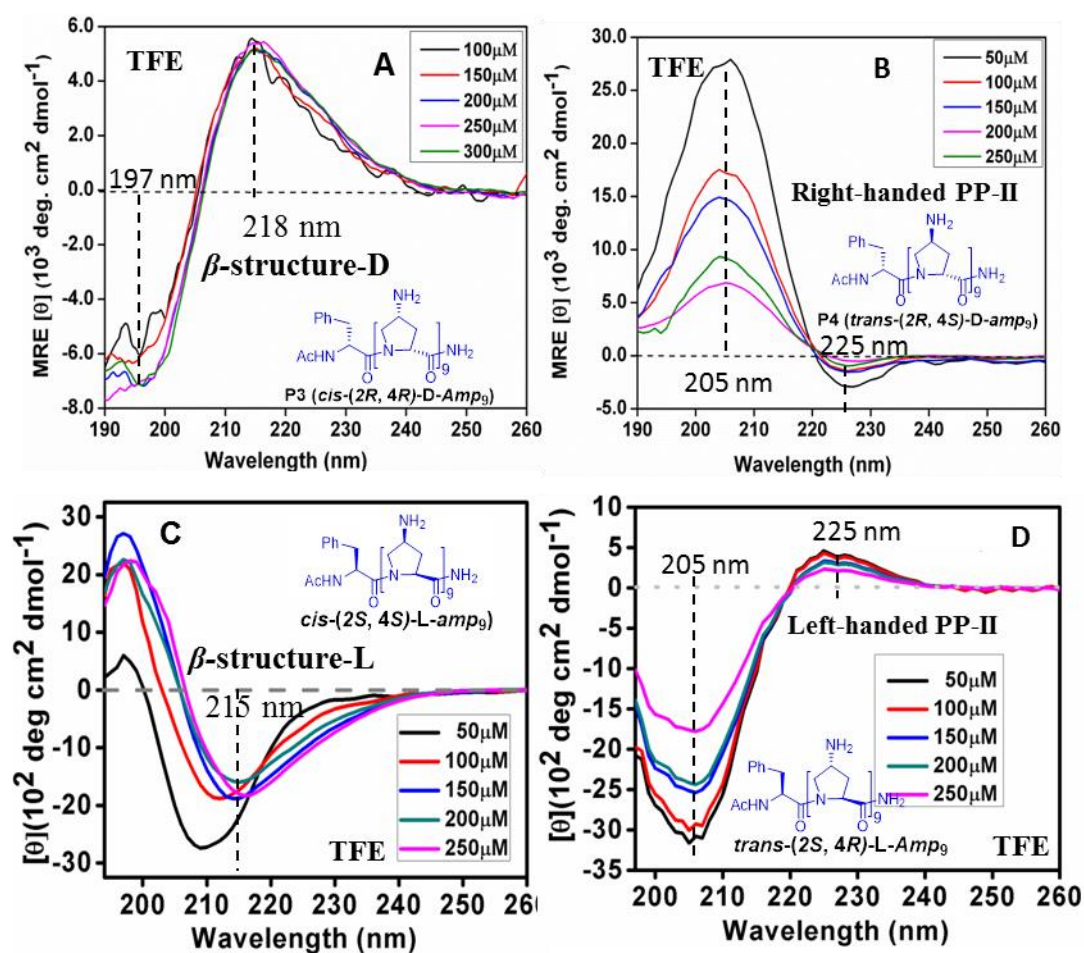

Figure 9. CD spectra of peptides **P3**, **P4**, **P11** and **P12** in TFE. **A) P3** [*cis*-(*2R,4R*)-D-*Amp₉*] **B) P4** [*trans*-(*2R,4S*)-D-*amp₉*], **C) P11** [*cis*-(*2S,4S*)-L-*amp₉*][5] and **D) P12** ([*rans*-(*2S,4R*)-L-*Amp₉*][5] in _the_ concentration range 50-300 μM. For comparison **C** and **D** graphs taken from reference no 5.

It is observed that the CD spectra recorded for the peptides **P3** and **P4** in solvent TFE are opposite (mirror image) to that of L-enantiomer **P11** [*cis*-(2*S*,4*S*)-L-*amp₉*] and **P12** [*trans*-(2*S*,4*R*)-L-*Amp₉*] which forms *β*-structure-L and left-handed PP-II helix in TFE and in water respectively.

2.6.3 CD spectra of peptides P2 (D-*Pro₉*), P3 [*cis*-(2*R*,4*R*)-D-*Amp₉*] & P4 [*trans*-(2*R*,4*S*)-D-*amp₉*] in buffer and in TFE

Figure 10(A) shows the CD spectra of peptides **P2** (D-*Pro₉*), **P3** [*cis*-(2*R*, 4*R*)-D-*Amp₉*] & **P4** [*trans*-(2*R*, 4*S*)-D-*amp₉*] in phosphate buffer (pH 7.2) concentration 300 µM. All these peptides show right handed PP-II structure in buffer, with a negative CD band at 225 nm and a strong positive CD band at 205 nm. Figure 10(B) is the CD spectra of **P2** (D-*Pro₉*), **P3** [*cis*-(2*R*, 4*R*)-D-*Amp₉*] & **P4** [*trans*-(2*R*, 4*S*)-D-*amp₉*] in TFE at concentration 300 µM. The peptides **P2** (D-*Pro₉*) and **P4** [*trans*-(2*R*, 4*S*)-D-*amp₉*] show right handed PP-II structure in TFE, with a negative CD band at 225 nm and a strong positive CD band at 205 nm. Only the peptide **P3** [*cis*-(2*R*, 4*R*)-D-*Amp₉*] shows a conformational change from PP-II to *β* structure on going from water to TFE
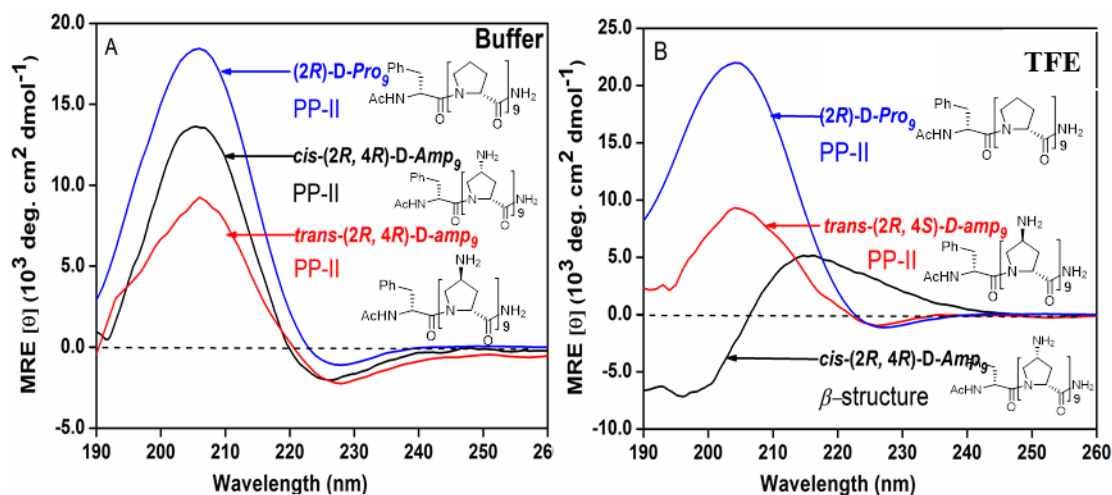

Figure 10. CD Spectra of peptides **P2** (D-*Pro₉*), **P3** [*cis*-(2*R*, 4*R*)-D-*Amp₉*] & **P4** [*trans*-(2*R*, 4*S*)-D-*amp₉*] **A)** in buffer and **B)** in TFE at concentration of 300 µM.

2.6.4 Mirror image CD spectra of P3 [*cis*-(2*R*,4*R*)-D-*Amp₉*] and P11 [*cis*-(2*S*,4*S*)-L-*amp₉*] in buffer and in TFE

Figure 11(A) is the CD spectra of **P3** [*cis*-(*2R,4R*)-D-*Amp₉*] and **P11** [*cis*-(*2S,4S*)-L-*amp₉*] in phosphate buffer at 150 µM, which indicates that these peptides being enantiomers of each other, show exact mirror image CD spectra. The peptide **P11** [*cis*-(*2S,4S*)-L-*amp₉*] forms left handed PP-II conformation while peptide **P3** [*cis*-(*2R,4R*)-D-*Amp₉*] forms right handed PP-II conformation with little change in signal intensity. The CD spectra recorded for peptide **P3** [*cis*-(*2R,4R*)-D-*Amp₉*] had inverted negative band at 225 nm and a positive band at 205 nm.

Figure 11(B) depicts the CD spectra of **P3** (*cis*-(*2R,4R*)-D-*Amp₉*) and **P11** (*cis*-(*2S,4S*)-L-*amp₉*) in TFE. Both these peptides exhibit mirror image *β*-structure for each other with opposie signs, but a small difference in intensities. Negative band at 220 nm in CD spectra of peptide **P11** [*cis*-(*2S,4S*)-L-*amp₉*] is inverted CD spectra of peptide **P3** [*cis*-(*2R,4R*)-D-*Amp₉*] and appears at 218 nm with 2 nm shift in shorter wavelength.
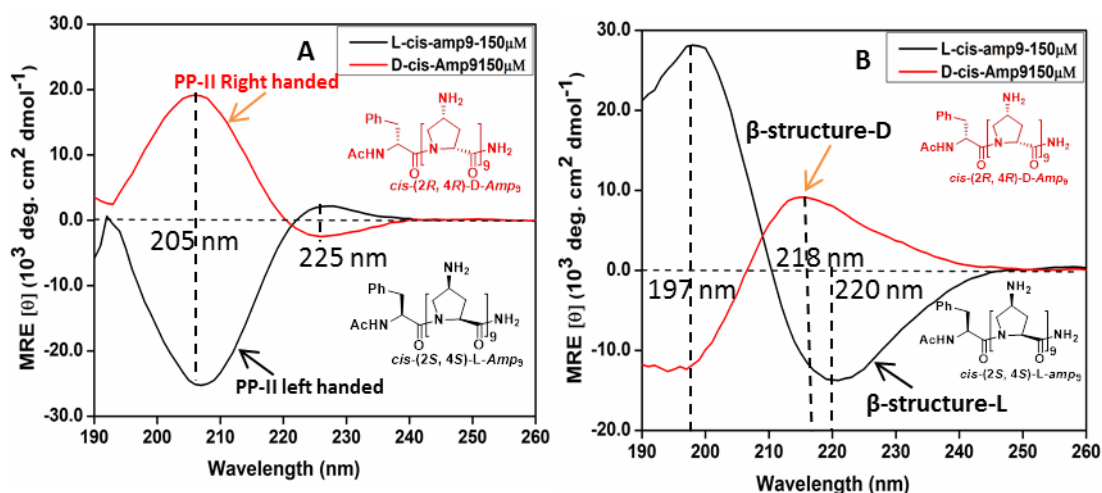

Figure 11. CD spectra of peptides P3 and P11 in TFE. **A) P3** [*cis*-(*2R, 4R*)-D-*Amp₉*] and **P11** [*cis*-(*2S,4S*)-L-*amp₉*] in buffer **B) P3** [*cis*-(*2R, 4R*)-D-*Amp₉*] and **P11** (*cis*-(*2S,4S*)-L-*amp₉*) at 25⁰ C at concentration of 150 µM.

2.6.5 CD study of lipidated *cis*-D-peptides P5-P7 in TFE

Figures 12 (A-C) are the CD spectra of lipidated *cis*-D-peptides **P5** [C_{12}-*cis*-(*2R,4R*)-D-*Amp₉*], **P6** [C_{14}-*cis*-(*2R,4R*)-D-*Amp₉*] and **P7** [C_{16}-*cis*-(*2R,4R*)-D-*Amp₉*] in TFE at concentration range from 50-300 µM. As explained in earlier section *cis*-peptide **P3** [*cis*-(*2R,4R*)-D-*Amp₉*] adopts *β*-structure in TFE. The peptides **P5-P7** are *cis*-peptides with C12, C14 and C16 fatty acid conjugation. These peptides also undergo a conformational change in

solvent TFE (Figure 12 A-C). Two new CD bands appear a positive band at 218 nm and a negative band at 197 nm. The effect of TFE on lipidated peptide **P5**-**P7** is similar to peptide **P3** without fatty acid conjugation. All fatty acid chain conjugated peptides adopt β-structure in TFE at all concentration range.
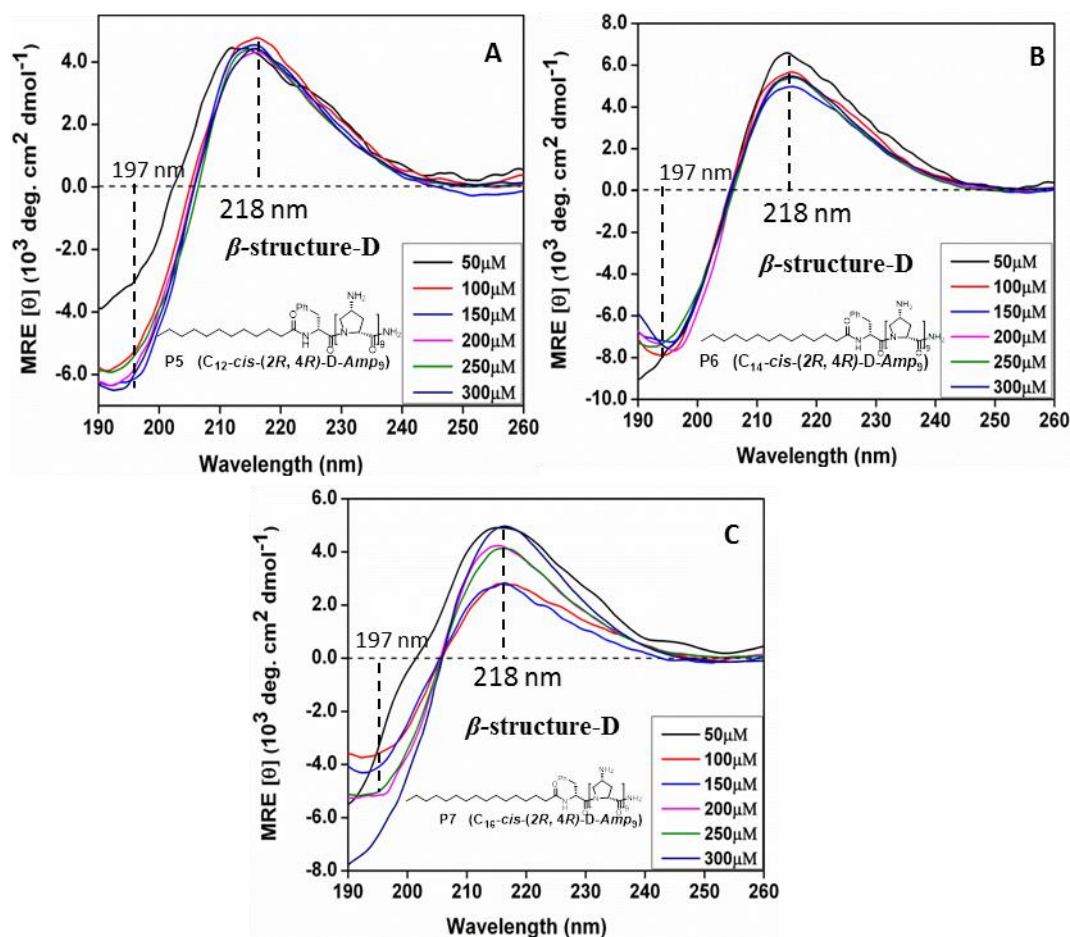

Figure 12. CD spectra of peptides P5-P7 in TFE. **A)** P5 [C_{12}-*cis*-(2R,4R)-D-Amp_9], **B)** P6 [C_{14}-*cis*-(2R,4R)-D-Amp_9] and **C)** P7 [C_{16}-*cis*-(2R,4R)-D-Amp_9] at 25^0 C, concentrations 50-300 uM

2.6.6 CD study of lipidated *trans*-peptides P8-P10 in TFE

Figures 13 (A-C) are the CD spectra of lipidated *trans*-D-peptides **P8** [C_{12}-*trans*-(2R,4S)-D-amp_9], **P9** [C_{14}-*trans*-(2R,4S)-D-amp_9] and **P10** [C_{16}-*trans*-(2R,4S)-D-amp_9] respectively in TFE in the concentration range 50-300 μM. The negative CD band at 225 nm for enantiomeric polyproline peptides and the strong positive CD band at 205 nm remain at the same position indicating that conjugation of different fatty acid chains (C_{12}, C_{14} and C_{16}) do not alter the conformation, and all exist in PP-II conformation.
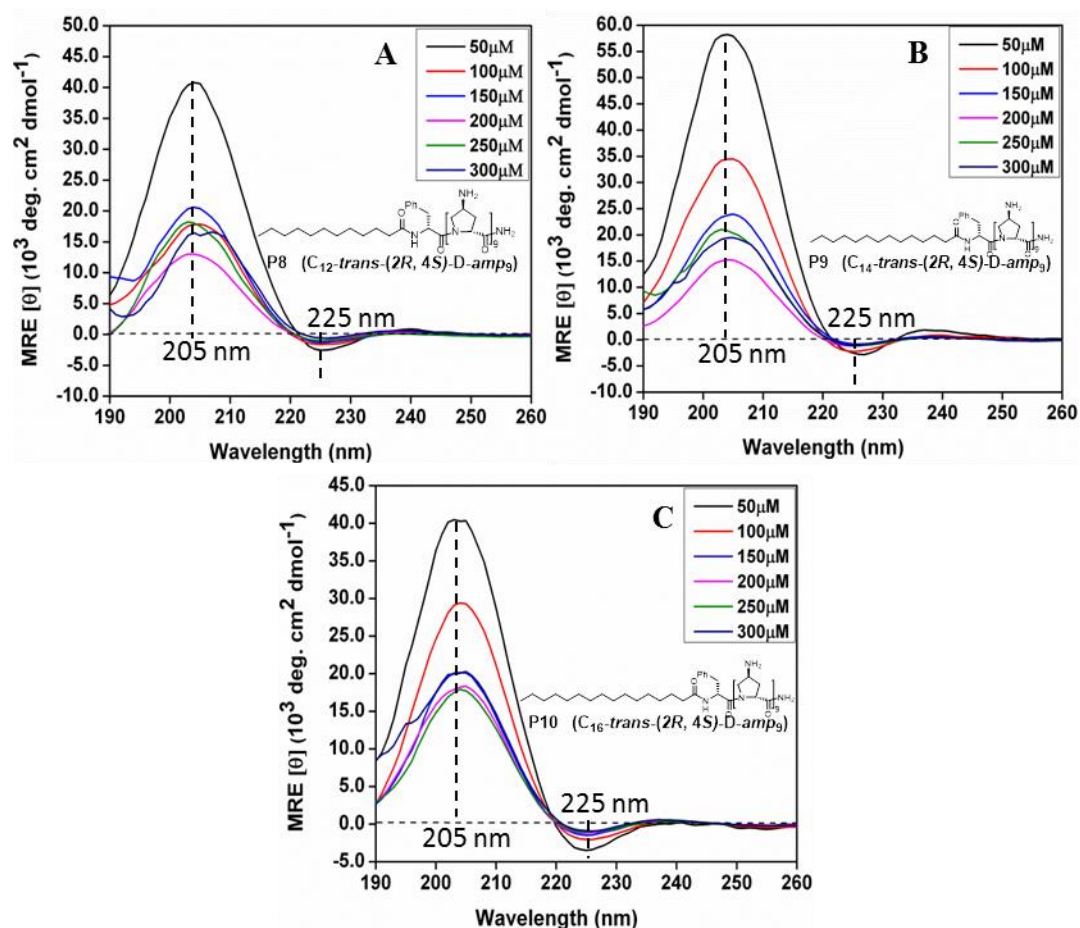
Figure 13. CD spectra of lipidated *trans*-D-peptides in TFE. . **A) P8** [C_{12}-*trans*-(*2R,4S*)-D-*amp$_9$*]**,,B)** [C_{14}*trans*-(*2R,4S*)-*amp$_9$*] and **C) P10** [C_{16}-*trans*-(*2R,4S*)-D-*amp$_9$*], concentration 50-300 μM.

2.7 Field Emission-Scanning Electron Microscopy (FE-SEM)

Previous work from this laboratory demonstrated that the peptides (4*S*)-L-*amp$_9$*/*hyp$_9$* (**P11/P13**) peptides show *β*-structure in TFE which self-assembles to form nano fibers. Fatty acid conjugation increases the interaction between molecules through additional hydrophobic interactions resulting into longer fibers. To examine the morphologies of self assembled structure of chiral peptides with and without fatty acid conjugation, FE-SEM imaging was carried out for each of these peptides. Samples were prepared in respective solvent as described below.

Polyproline peptides (300 μM) were taken into microfuge tube from the stock solution, and water was evaporated under vaccum. The desired solvent was added to it and solution was vortexed for 1 min, centrifuged and kept for two days. The supernatant solution

(3 μL) was then drop cast on silicon wafer and allowed to dry at room temperature before imaging after coating with gold.

2.7.1 Peptide P1 (L-*Pro₉*) & P2 (D- *Pro₉*) in water and in TFE

Figure 14 shows morphologies of unsubstituted peptides **P1** (L-*Pro₉*) and **P2** (D-*Pro₉*) in water and trifluoroethanol and as seen by the CD, the peptides adopt PP-II structure in both solvents. Both peptides exhibited needle structure in both water and trifluoroethanol.
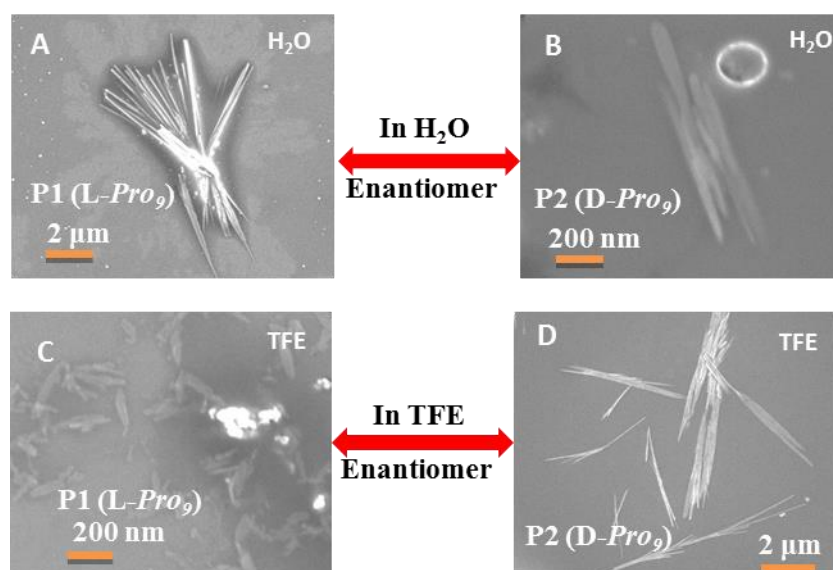

Figure 14. FE-SEM images of peptide **P1** (L-*Pro₉*) & **P2** (D-*Pro₉*) in **A)** and **B)** in water, **C) and D)** in TFE at 300 μM.

2.7.2 Peptide P3 [*cis*-(*2R*,*4R*)-D-*Amp₉*], P4 [*trans*-(*2R*,*4S*)-D-*amp₉*], P11 [*cis*-(*2S*,*4S*)-L-*amp₉*] & P12 [*trans*-(*2S*,*4R*)-L-*Amp₉*] in water and in TFE

Figure 15 (A-D) show SEM images of peptides **P3** [*cis*-(*2R*,*4R*)-D-*Amp₉*] and **P4** [*trans*-(*2R*,*4S*)-D-*amp₉*] in water and compared with that earlier reported for peptide **P11** [*cis*-(*2S*,*4S*)-L-*amp₉*] & **P12** [*trans*-(*2S*,*4R*)-L-*Amp₉*] in water at concentration of 300 μM. The diastereomeric peptides **P3** [*cis*-(*2R*,*4R*)-D-*Amp₉*], **P4** [*trans*-(*2R*,*4S*)-D-*amp₉*] and their respective enantiomeric peptides **P11** [*cis*-(*2S*,*4S*)-L-*amp₉*] & **P12** [*trans*-(*2S*,*4R*)-L-*Amp₉*] aggregate to form nano-spheres in water. Among these, only *cis*-peptides **P3** [*cis*-(*2R*,*4R*)-D-*Amp₉*] and **P11** [*cis*-(*2S*,*4S*)-L-*amp₉*] form *β*-structure as shown by CD spectra in TFE.

Figure 15. FE-SEM images of peptides **P3** [*cis*-(*2R*,4*R*)-D-*Amp₉*] and **P11** [*cis*-(*2S*,4*S*)-L-*amp₉*]
A) and **B)** in water; **P4** [*trans*-(*2R*,4*S*)-D-*amp₉*] and **P12** [*trans*-(*2S*,4*R*)-L-*Amp₉*] **C)** and **D)**
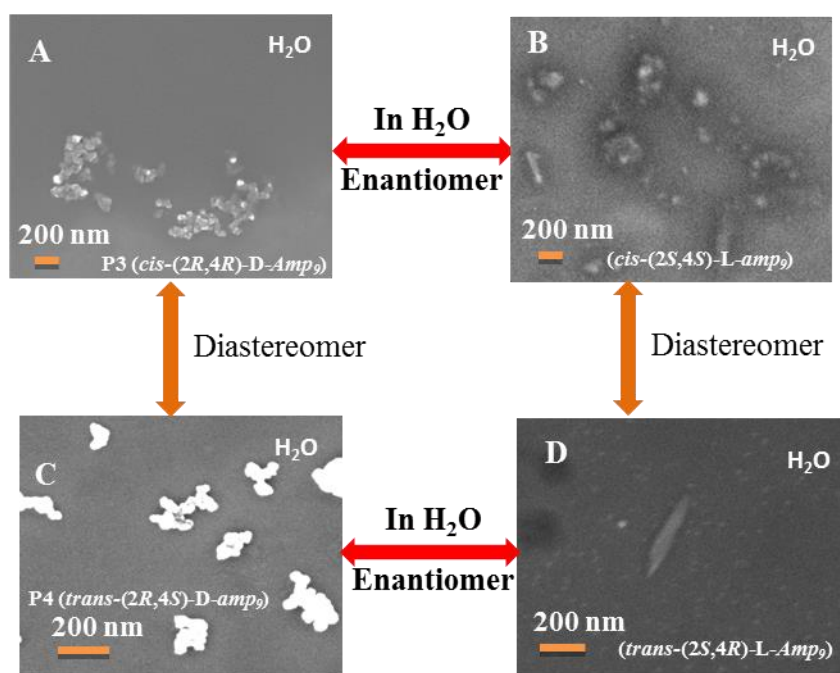in water.

Figure 16. FE-SEM images of peptides **P3** [*cis*-(*2R*,4*R*)-D-*Amp₉*] and **P11** [*cis*-(*2S*,4*S*)-L-*amp₉*]
A) and **B)** in TFE; **P4** [*trans*-(*2R*,4*S*)-D-*amp₉*] and **P12** [*trans*-(*2S*,4*R*)-L-*Amp₉*] **C)** and **D)**
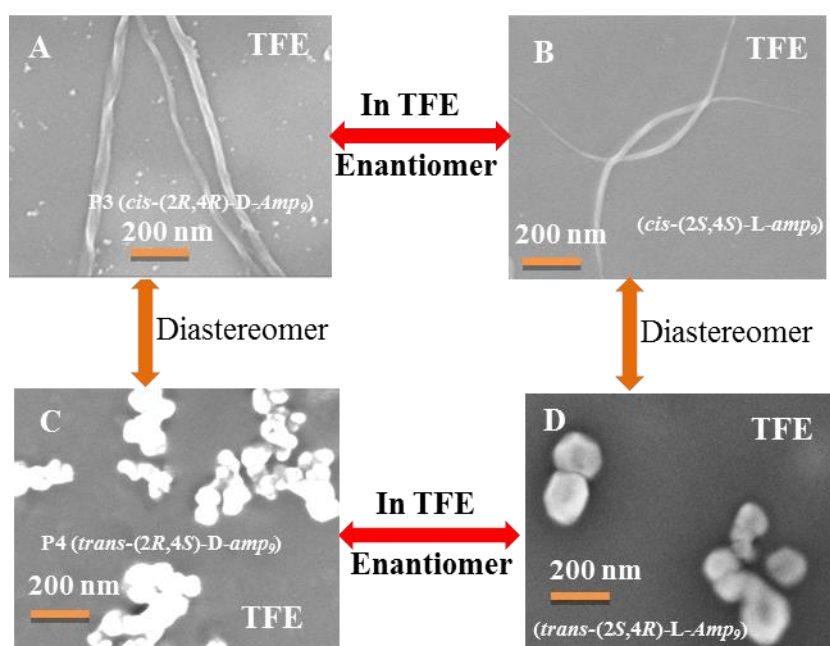in TFE.

In FE-SEM only these peptides assemble into long left-handed twisted nanofibers with
20 nm in width, around 80 nm in helical pitch and 1-1.5 μm in length. The *trans*-peptides **P4**

[*trans*-(*2R*,4*S*)-D-*amp₉*] & **P12** [*trans*-(*2S*,4*R*)-L-*Amp₉*] that form PP-II structure show irregular bundles of nano spheres with 100 nm in diameter both in water and in TFE (Figure 16 A-D).

2.7.3 Mixture of P3 [*cis*-(*2R,4R*)-D-*Amp₉*] and P11 [*cis*-(2*S*,4*S*)-L-*amp₉*] in TFE

Since both *cis*-peptides **P3** [*cis*-(*2R,4R*)-D-*Amp₉*] and **P11** [*cis*-(4*S*,2*S*)-L-*amp₉*] show nano-fiber structures, it was thought to mix these enantiomeric peptides to examine the resultant morphology. Figure 17(A) shows the self-assembly of peptides **P11** [*cis*-(4*S*,2*S*)-L-*amp₉*], Figure 17(B) shows self assembly of a 1:1 mixture of **P3** [*cis*-(*2R,4R*)-D-*Amp₉*] and **P11** [*cis*-(4*S*,2*S*)-L-*amp₉*] and Figure 17(C) is image of **P3** [*cis*-(*2R,4R*)-D-*Amp₉*] peptide alone in TFE. The chirality of amino acid has primary effects on the handedness of nanostructure self-assembly.[11] The purpose of this experiment was to examine if left-handed and right-handed nano-fibers are formed in isolation or result in hybrid nanofibers.

The peptide **P11** (*cis*-(4*S*,2*S*)-L-*amp₉*), forms left-handed twisted fibers with 22 nm width, around 100 nm helical twists and 1-2 μm in length. The enantiomer **P3** (*cis*-(*2R,4R*)-D-*Amp₉*) also forms left-handed twisted fibers with 20 nm width, around 80 nm helical pitch and 1-1.5 μm length, although they are showing opposite handedness in CD spectra.

On mixing the two enantiomeric peptides **P3** (*cis*-(*2R,4R*)-D-*Amp₉*) and **P11** (*cis*-(4*S*,2*S*)-L-*amp₉*) in identical concentrations, increased number of fibers were seen with more twists and less helical pitch. Figure 17 (B) is the mixed *β*-structure co-assembled into left-handed fibrils with large aggregates as compared to that of each pure enantiomer.
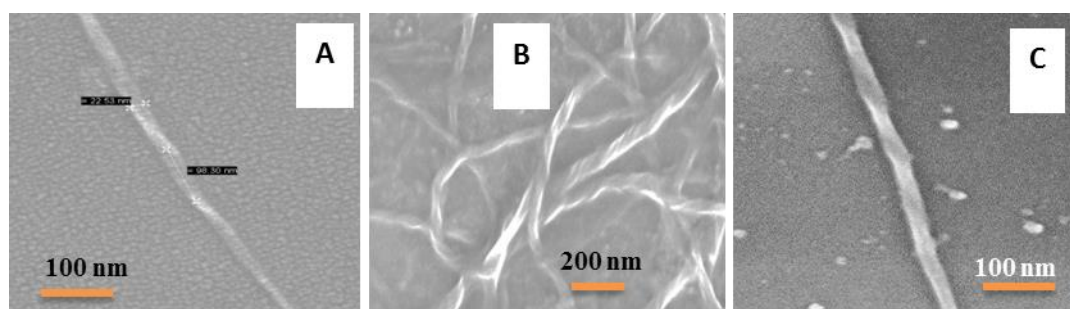

Figure 17. FE-SEM images of **A)** **P11** *cis*-(4*S*,2*S*)-L-*amp₉*, **B)** mixing of **P3** *cis*-(*2R,4R*)-D-*Amp₉* + **P11** *cis*-(4*S*,2*S*)-L-*amp₉*, **C)** **P3** *cis*-(*2R,4R*)-D-*Amp₉*, at 200 μM in TFE.

2.7.4 Lipidated *cis*-D-peptides P3, P5-P7 in water and in TFE

Figure 18 is the self-assembly of *cis* peptides **P3** [*cis-(2R,4R)*-D-*Amp9*], **P5** [C$_{12}$-*cis-*(*2R,4R*)-D-*Amp9*], **P6** [C$_{14}$-*cis-(2R,4R)*-D-*Amp9*] and **P7** [C$_{16}$-*cis-(2R,4R)*-D-*Amp9*] respectively, with samples prepared in water at concentration of 300 μM. The peptide **P3** [*cis-*(*2R,4R*)-D-*Amp9*] showed spherical morphology (Figure 18A) and the fatty acid conjugated peptides **P5-P7** show nanorods of 1-2 μm size, with the size decreasing as the number of carbons increases (Figure 18 B-D).
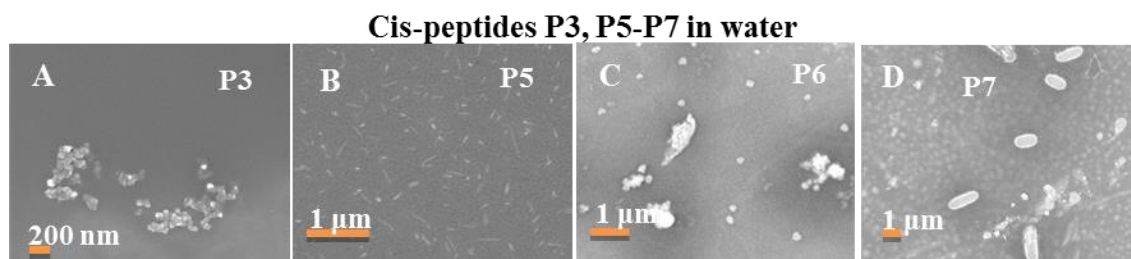

Figure 18. FE-SEM images of peptides in water. **A) P3** [*cis-(2R,4R)*-D-*Amp9*], **B) P5** [C$_{12}$-*cis-*(*2R,4R*)-D-*Amp9*], **C) P6** [C$_{14}$-*cis-(2R,4R)*-D-*Amp9*], **D) P7** (C$_{16}$-*cis-(2R,4R)*-D-*Amp9*).

Figure 19A-D shows morphologies of cis-peptides **P3** [*cis-(2R,4R)*-D-*Amp9*], **P5** [C$_{12}$-*cis-(2R,4R)*-D-*Amp9*], **P6** [C$_{14}$-*cis-(2R,4R)*-D-*Amp9*] and **P7** [C$_{16}$-*cis-(2R,4R)*-D-*Amp9*] respectively, with samples prepared in TFE at concentration of 300 μM. All these *cis*-peptides exhibit *β*-structure in CD spectra and assemble into long nano fibers when processed in TFE. The dimensions of fibers of left-handed twisted are around 100 nm helical twist, 20 nm in width and 1-2 μm in length.

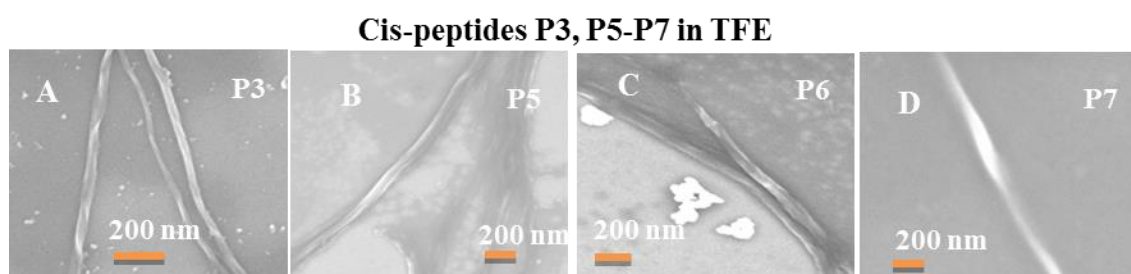**Figure 19.** FE-SEM images of peptides in TFE. **A) P3** [*cis-(2R,4R)*-D-*Amp9*], **B) P5** [C$_{12}$-*cis-(2R,4R)*-D-*Amp9*], **C) P6** [C$_{14}$-*cis-(2R,4R)*-D-*Amp9*], **D) P7** [C$_{16}$-*cis-(2R,4R)*-D-*Amp9*]

Only *cis*-peptides form nano fibers, while *trans*-peptides and unsubstituted polyproline peptides that do not undergo any solvent dependent change in CD did not exhibit any self-

assembled nano fiber structure. This brings the importance of stereospecific hydrogen bonding substitution at C4 of proline in inducing morphology.

2.7.5 Lipidated *trans*-peptides P4, P8-P10 in water and in TFE

Figure 20 shows self-assembly of peptides **P4** [*trans*-(*2R,4S*)-D-*amp*₉], **P8** [C₁₂-*trans*-(*2R,4S*)-D-*amp*₉], **P9** [C₁₄-*trans*-(*2R,4S*)-D-*amp*₉], **P10** [C₁₆-*trans*-(*2R,4S*)-D-*amp*₉] at concentration of 300 μM in water. The peptides conjugated with shorter chains (C₁₂ and C₁₄) show disordered nanoparticles with 0.5-1 μm in length, while peptide **P10 with** C₁₆ conjugation shows ordered core shell morphology with 100 nm in diameter.
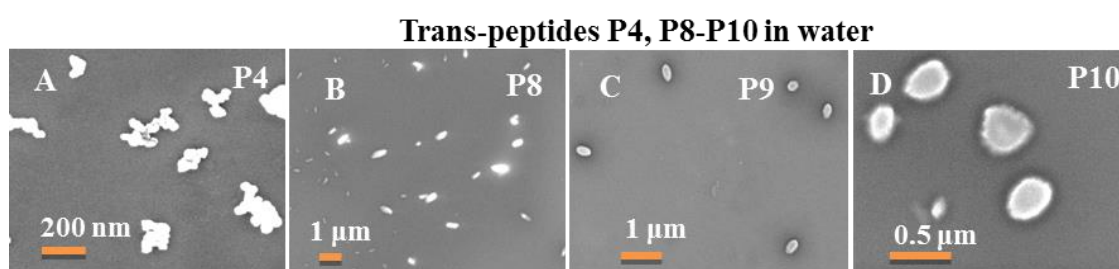

Figure 20. FE-SEM images of peptides in water. **A)** **P4** [*trans*-(*2R,4S*)-D-*amp*₉],, **B)** **P8** [C₁₂-*trans*-(*2R,4S*]-D-*amp*₉}, **C)** **P9** [C₁₄-*trans*-(*2R,4S*)-D-*amp*₉], and **D)** **P10** [C₁₆-*trans*-(*2R,4S*)-D-*amp*₉]

Figures 21(A-D) show morphologies of *trans*-peptides **P4** [*trans*-(*2R,4S*)-D-*amp*₉], **P8** [C₁₂-*trans*-(*2R,4S*)-D-*amp*₉], **P9** [C₁₄-*trans*-(*2R,4S*)-D-*amp*₉], **P10** [C₁₆-*trans*-(*2R,4S*)-D-*amp*₉] in TFE at concentration of 300 μM. The peptide **P4** [*trans*-(*2R,4S*)-D-*amp*₉] showed ordered spherical morphology with 100 nm in diameter (Figure 21A), while the conjugated peptide **P8** [C₁₂-*trans*-(*2R,4S*)-D-*amp*₉], showed sharp needle structure (Figure 21B) and peptide **P9** (C₁₄) & **P10** (C₁₆) exhibited disordered particles of around 1μm in length (Figure 21C and D).
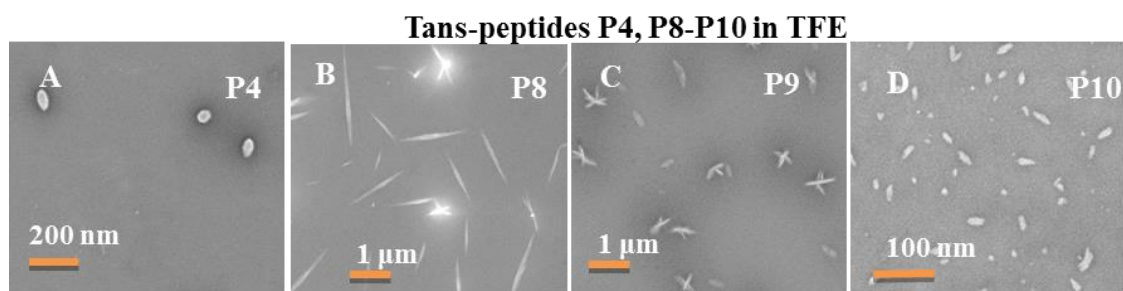
Figure 21. FE-SEM images of peptides in TFE. **A) P4** [*trans*-(*2R,4S*)-D-*amp*$_9$], **B) P8** [C$_{12}$-*trans*-(*2R,4S*)-D-*amp*$_9$], **C) P9** [C$_{14}$-*trans*-(*2R,4S*)-D-*amp*$_9$], **D) P10** [C$_{16}$-*trans*-(*2R,4S*)-D-*amp*$_9$]

2.8 Atomic Force Microscopy (AFM)

Atomic force microscopy (AFM) allows us to find morphology and measure dimensions of the materials with high resolution and accuracy. Images are captured in a small region of 5 nm to large region 100 μm or even larger than that is possible. AFM is mainly useful to measure roughness and morphology of the surface in particular, the height of the sample. Contact imaging via tapping mode using the microscopic probe on the surface of a sample accompanied by measurements of force deflection of the cantilever on which the probe is mounted generates the readout of the surface morphology.

2.8.1 Peptides P3 & P4 in water and in TFE

Figures 22(A-B) show morphologies of peptide **P3** [*cis*-(*2R,4R*)-D-*Amp*$_9$] and **P4** [*trans*-(*2R,4S*)-D-*amp*$_9$] in water. Figures 22(C-D) are images of peptides in TFE at 300 μM concentration. Peptides **P3** and **P4** show aggregates of nanospheres in water. It is seen in AFM image that the only peptide **P3** [*cis*-(*2R,4R*)-D-*Amp*$_9$] which forms β-structure in TFE results into long nanofibers with height of fibers around 10 nm and length of 2-4 μm seen.
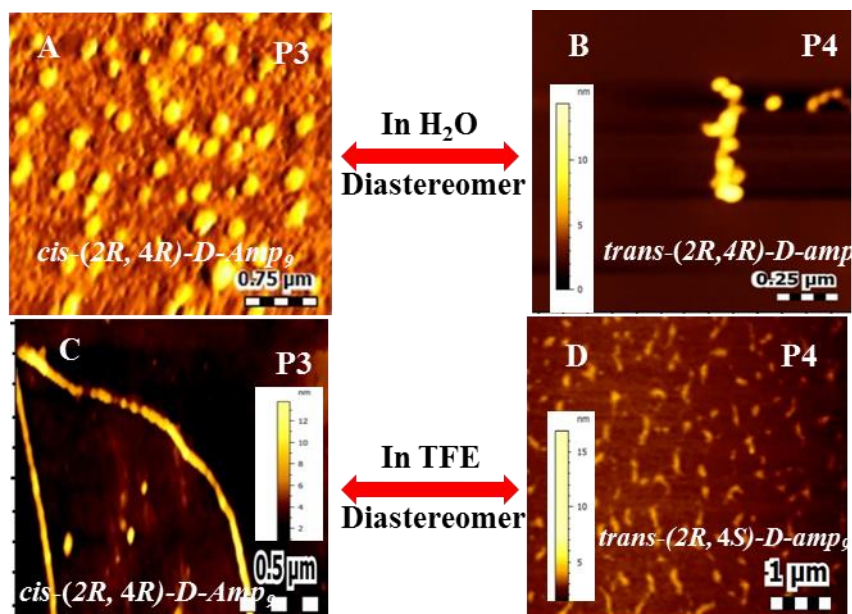
Figure 22. AFM images of peptides **P3** [*cis*-(2*R*,4*R)*-D-*Amp*₉] and **P4** [*trans*-(2*R*,4*S*)-D-*amp*₉] **A, B)** in water and **C, D)** in TFE

.

2.8.2 Lipidated *cis*-D-peptides P3, P5-P7 in water

Figures 23(A-D) show morphologies of *cis*-peptides **P3** [*cis*-(*2R,4R*)-D-*Amp₉*], **P5** [C₁₂-*cis*-(*2R,4R*)-D-*Amp₉*], **P6** [C₁₄-*cis*-(*2R,4R*)-D-*Amp₉*] and **P7** [C₁₆-*cis*-(*2R,4R*)-D-*Amp₉*] in water at concentration of 300 μM. The *cis*-peptide **P3** shows spherical morphology and the corresponding fatty acid conjugated peptides **P5**-**P7** show solid nanospheres with 200 nm in diameter and about 20 nm in height. The peptide **P5** [C₁₂-*cis*-(*2R,4R*)-D-*Amp₉*] gave spheres of diameter 400 nm and the size of these spheres decrease with increasing number of carbons, **P5** [C₁₂-*cis*-(*2R,4R*)-D-*Amp₉*] 400 nm, **P6** [C₁₄-*cis*-(*2R,4R*)-D-*Amp₉*] around 300 nm diameter and **P7** [C₁₆-*cis*-(*2R,4R*)-D-*Amp₉*] of about 200 nm in diameter.

All in water

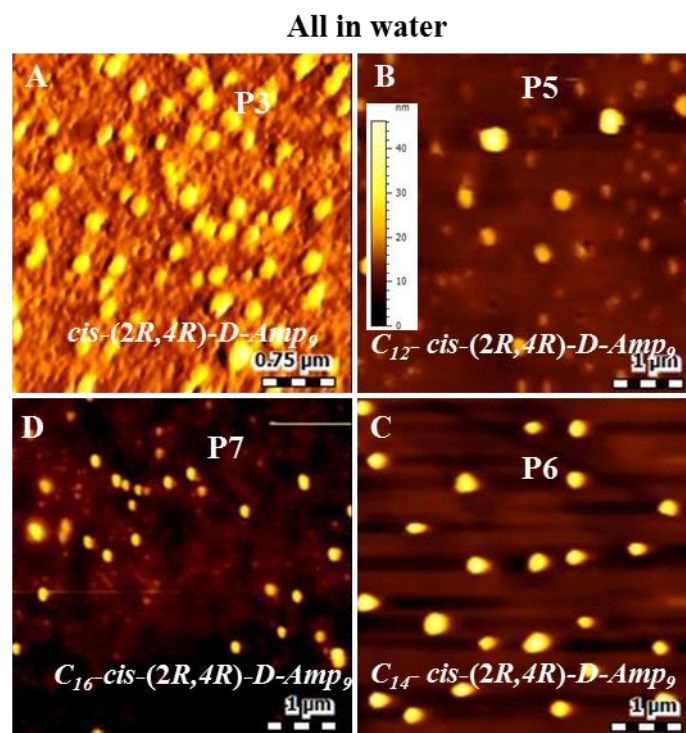**Figure 23.** AFM images of *cis*-peptides **A) P3** [*cis*-(*2R,4R*)-D-*Amp*₉], **B) P5** [C₁₂-*cis*-(*2R,4R*)-D-*Amp*₉], **C) P6** [C₁₄-*cis*-(*2R,4R*)-D-*Amp*₉] and **D) P7** [C₁₆-*cis*-(*2R,4R*)-D-*Amp*₉] in water at concentration of 300 μM.

2.8.3 Lipidated *trans*-peptides P4, P8-P10 in water

Figures 24(A-D) show AFM images of *trans*-peptides **P4** [*trans*-(*2R,4S*)-D-*amp*₉], **P8** [C₁₂-*trans*-(*2R,4S*)-D-*amp*₉], **P9** [C₁₄-*trans*-(*2R,4S*)-D-*amp*₉], and **P10** [C₁₆-*trans*-(*2R,4S*)-D-*amp*₉] in water at concentration of 300 μM. The peptide **P4** [*trans*-(*2R,4S*)-D-*amp*₉] shows spherical morphology of diameter around 100 nm and height of 6-8 nm, while the corresponding fatty acid conjugated peptides **P8**-**P10** show disordered nanoparticles.
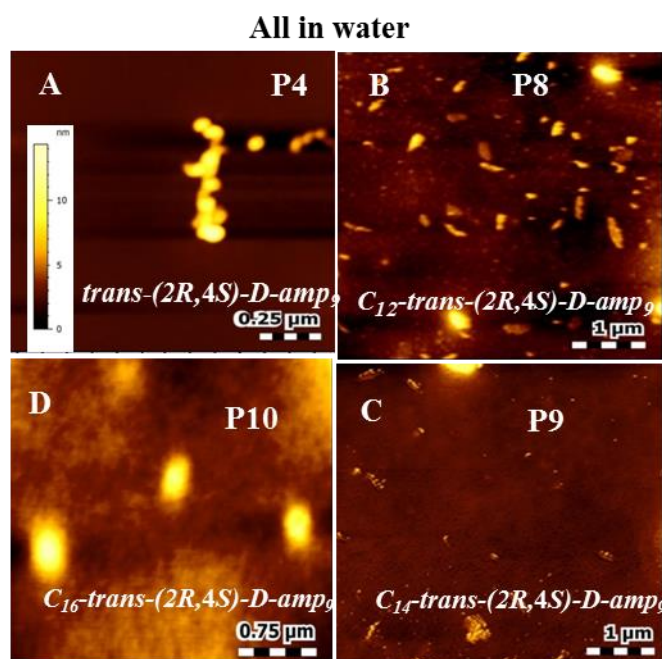
Figure 24. AFM images of peptides **A)** **P4** [*trans*-(*2R,4S*)-D-*amp₉*], **B)** **P8** [C₁₂-*trans*-(*2R,4S*)-D-*amp₉*], **C)** **P9** [C₁₄-*trans*-(*2R,4S*)-D-*amp₉*] and **D)** **P10** [C₁₆-*trans*-(*2R,4S*)-D-*amp₉*] in water.

2.8.4 Lipidated *trans*-peptides P4, P8-P10 in TFE

Figures 25(A-D) show AFM images of *trans*-peptides **P4** [*trans*-(*2R,4S*)-D-*amp₉*], **P8** [C₁₂-*trans*-(*2R,4S*)-D-*amp₉*], **P9** [C₁₄-*trans*-(*2R,4S*)-D-*amp₉*] and **P10** [C₁₆-*trans*-(*2R,4S*)-D-*amp₉*] in water at concentration of 300 μM in TFE. The *trans*-peptide **P4** [*trans*-(*2R,4S*)-D-*amp₉*] shows spherical morphology of diameter 100 nm, while the corresponding fatty acid conjugated peptides **P8**-**P10** show sharp nanorods with 1-2 μm in size, with height of these rods being 10-15 nm. The size of these nanorods decreased with increasing number of carbon atoms in the chain.
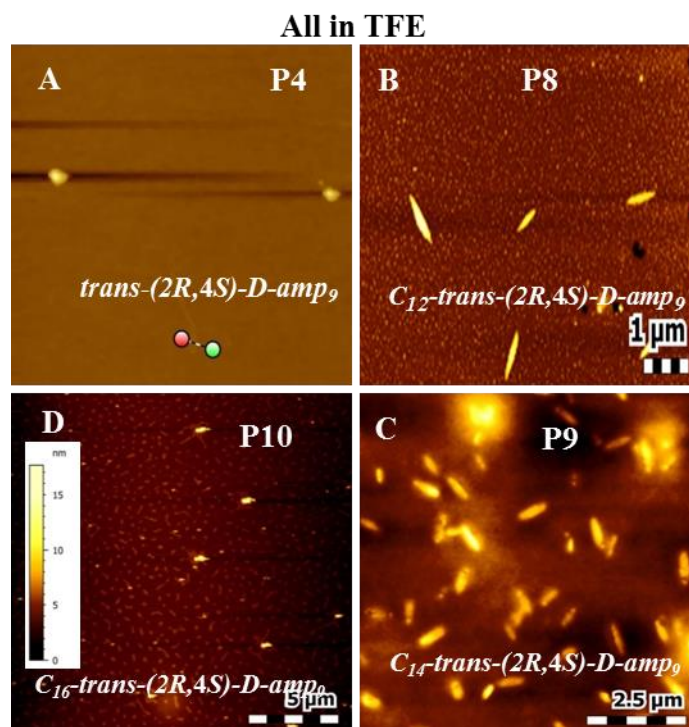
All in TFE

Figure 25. AFM images of peptides **A) P4** [*trans*-(*2R,4S*)-D-*amp₉*], **B) P8** [C₁₂-*trans*-(*2R,4S*)-D-*amp₉*], **C) P9** [C₁₄-*trans*-(*2R,4S*)-D-*amp₉*] and **D) P10** [C₁₆-*trans*-(*2R,4S*)-D-*amp₉*] in TFE.

2.9 Summary

In this chapter, circular dichroism spectroscopic studies were used to demonstrate that the peptide **P3** [*cis*-(*2R,4R*)-D-*Amp₉*] and its enantiomeric peptide **P11** [*cis*-(*2S,4S*)-L-*amp₉*] adopt PP-II conformation in water that were exact mirror image of each other. In TFE they adopt *β*-structures that were also mirror images. The *β*-structure arises from *inter*chain H-bonds involving 4*R/S*-NH₂ and amide carbonyl at C2 (*R/S*), which break in water and rearrange to *intra*molecular H-bonding favouring a PPII conformation. A plausible molecular *β*-structure for peptide **P3** (*cis*-(*2R,4R*)-D-*Amp₉*) is depicted in (Figure 26).

The self-assembling studies revealed that both the enantiomeric *cis*-peptide **P3** [*cis*-(*2R,4R*)-D-*Amp₉*] and **P11** [*cis*-(*2S,4S*)-L-*amp₉*] exhibit similar nanofibrous morphology but with same left-handed twist and similar dimensions. The racemic mixture of two cis peptides **P3** [*cis*-(*2R,4R*)-D-*Amp₉*] and **P11** [*cis*-(*2S,4S*)-L-*amp₉*] in identical concentrations resulted in thicker fibers with more twists (2-3 twists per 100 nm length) and less helical pitch (20-40 nm). Large aggregates of fibrils were observed in the racemic mixture as compared to pure enantiomers.

Generation of mirror images of PP-II and β-structure from polyprolyl peptides serve as novel secondary structural motifs for engineering peptide based biomaterials, and contribute to new design principles for developing novel nanoassemblies.
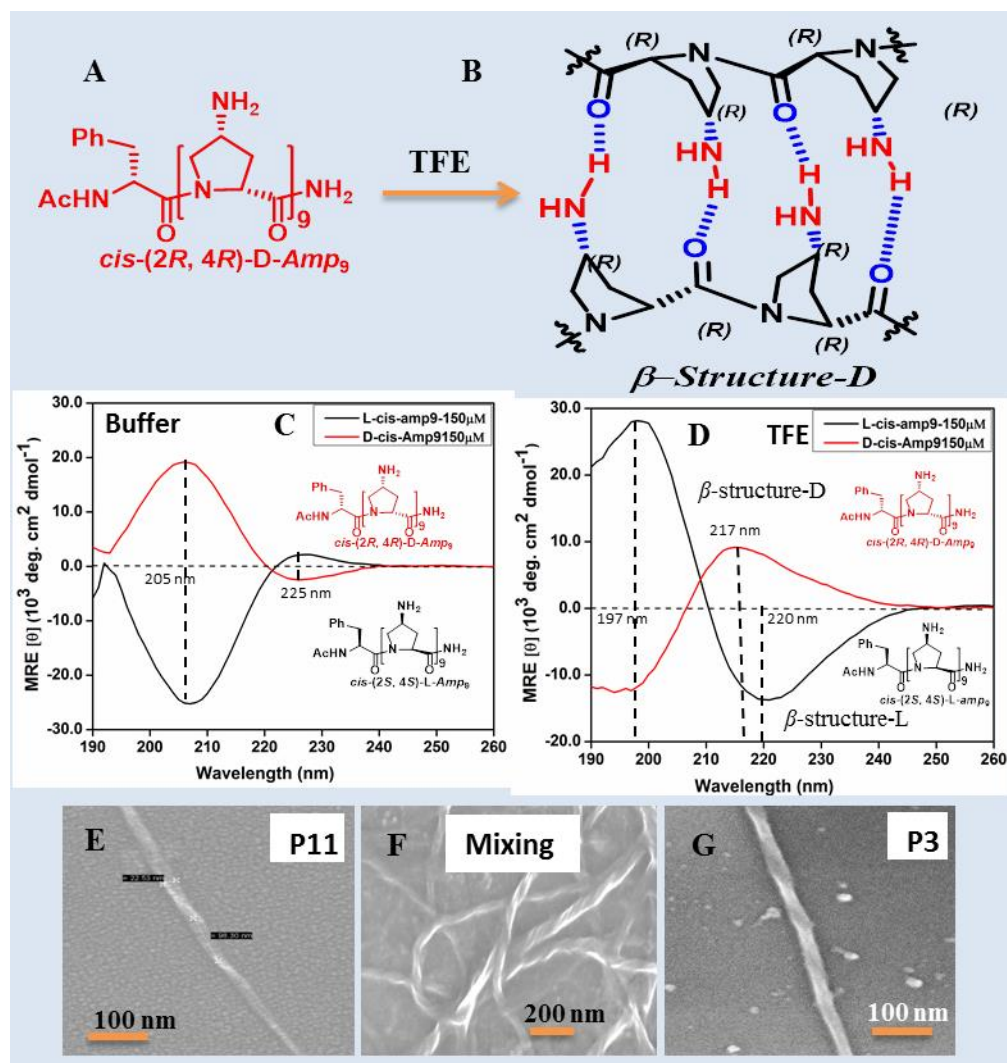

Figure 22. A) and **B)** Intra and interchain H-bonding in water and TFE in peptide **P3** [*cis*-(*2R,4R*)-D-*Amp₉*]**, C)** and **D)** CD spectra of enantiomeric peptides in water and TFE**, E)** and **G)** FE-SEM images of peptides **P11** and **P3** respectively **F)** FE-SEM image Mixture of peptides **P11** and **P3**

2.10 Experimental section

2.10.1 General methods for peptide synthesis

The desired peptides were synthesized manually on solid phase by using standard Fmoc strategy, using readially available Novabiochem (German) Rink amide resin (100-200 mesh) having substitution of 0.61 mmol/g. The resin bound Fmoc group was first deprotected

with 20% piperidine in dry DMF, and coupling reactions were carried out using *in situ* generation of active ester, using HBTU in presence of DIPEA as a base and HOBt as a recemization suppresser. Recoupling was done in N-Methyl-2-pyrrolidone (NMP) as a solvent. Piperidine, HOBt (Spectrochem) HBTU, DIPEA were purchased from (Sigma-Aldrich) and were used as such

2.10.2 Procedure for acetylation

Pyridine (2 mL) and acetic anhydride (1 mL) were added to the resin. The mixture was kept for 1 h followed by purging with N_2 for 10 min and washed with DMF and DCM 3 times each. In case of peptides conjugated with fatty chains, respective fatty acid was added along with coupling agent.

2.10.3 Procedure for cleavage of peptides from solid support

Peptides were cleaved from the solid support by treating them with 90% trifluoroacetic acid (TFA) in DCM in which 0.2 ml of triisopropylsilane (TIPS) was added as a scavenger to prevent alkylation. Furthermore, these peptides were purified by HPLC using RP-C18 column in an acetonitrile-water solvent system containing 0.1% TFA.

2.10.4 High-performance liquid chromatography

All peptides were purified by reverse phase-HPLC using semi-preparative RP-C18 columns (250x10 mm). The elution solvent system comprised of acetonitrile:water, with following compositions.

Solvent A: Acetonitrile:water (5:95) with 0.1% TFA.

Solvent B: Acetonitrile:water (50:50) with 0.1% TFA. A gradient system running 0-100% with flow rate of 2 mL/min to elute the peptide, and the elutants were monitored at 220 nm (peptides bond) and 254 (phenylalanine). In case of fatty acid conjugated peptide solvent B: acetonitrile: water (95:5) is used.

2.10.5 MALDI-TOF characterization

MALDI-TOF mass spectra were obtained on either Voyager-Elite instrument (PerSeptive Biosystems Inc., Farmingham, MA) equipped with delayed extraction or on Voyager-De-STR (Applied Biosystems) instrument. Sinapinic acid or α-cyano-4-

hydroxycinnamic acid (CHCA) were used as matrices for peptides of which CHCA was found to give satisfactory results. A solution of matrix was spotted on the metal plate along with the oligomers and allowed to co-crystallize. The metal plate was loaded into the instrument and then accelerated by an applying high voltage (15-25 kV) in reflector mode, separated in a field-free flight tube and detected as an electrical signal at the end of the flight tube. HPLC purified peptides were characterized through this method and were observed to give good spectra, with most of them gshowing molecular ion peak.

2.10.6 Circular dichroism spectroscopy

CD spectra were recorded on JASCO J-715 spectropolarimeter using quartz cell (1 mm path length), with sample holder connected to Julabo water cooling circulator. CD spectra were recorded using spectral bandwidth of 1.0 nm at 25 °C with a time constant of 1 s and a step resolution of 1 nm. All spectra were corrected for respective buffer signals and recorded as the average of 3-5 scans. Each spectra is the result of 3-5 accumulations. A quartz cell with a path length of 1 mm was used with solutions containing approximately 0.2 mL (50-300 μM) peptide solutions. For the blank spectrum, buffer and only TFE were recorded and subtracted from the subsequent spectra of samples. All samples were equilibrated for at least 24 h before measurement.
Resolution, 0.1- 1 nm; Bandwidth, 1.0 nm; Sensitivity (standard); Response, 1 sec; Speed, 50 nm/min; Accumulation, 3-5 scans.

2.10.7 Field Emission Scanning Electron Microscopy (FE-SEM)

FE-SEM imaging was performed using ZEISS *ULTRA PLUS* electron microscope operating at 30 kV. Polyproline peptides were taken in Eppendorf tube from the stock solution, and water was evaporated by using speed vac concentrator. The desired solvent was added to it and solution was vortexed for 1 min and centrifuged. Supernatant solution (3 μL) was then drop cast on silicon vapor. Samples were allowed to dry at room temperature and then kept under ordinary light for 4 h for complete drying and before imaging coated with gold.

2.10.8 Atomic Force Microscopy (AFM)

Atomic force microscopy imaging was carried out on AFM instrument model number key sight-5500 using tapping mode cantilever, which was auto-tuned for 190 KHz frequency.

Desired sample (5 µL) was spotted on fresh mica allowed to dry at room temperature followed by complete drying under an ordinary lamp for 4 h.

2.11 Synthesis of compounds 1-13

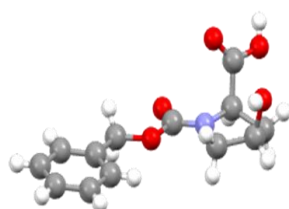**(2*R*,4*R*)-*cis*-4-hydroxy-D-proline (1)**

1
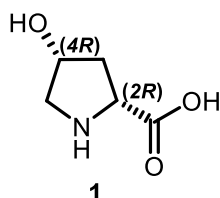
Conversion of *trans*-4-hydroxy-L-proline to *cis*-4-hydroxy-D-Proline has been done by following literature procedure. Commercially available *trans*-4-hydroxy-L-proline (6.55 g, 50.0 mM) was added to a mixture of acetic anhydride (50 ml) and glacial acetic acid, (100 ml) and refluxed for 5.5 h. at boiling temperature of acetic anhydride. The dark solution was cooled and evaporated under reduced pressure to yield thick oil. Obtained oil was dissolved in 2 M HCl (125 ml), and the solution was refluxed for 3 h, decolourised with charcoal and filtered. The filtrate was concentrated under reduced pressure to yield light yellow oil. Trituration with diethyl ether leads to precipitate which is epimeric hydrochloride salts. Recrystallisation from ethanol gave a crystalline colourless solid.

Recrystallisation: Hydrochloride salt (5g, 30.0 mmol) was dissolved in water (20 ml), and triethylamine (10 ml) and absolute ethanol (400 ml) were added. The solution was stored at room temperature until crystallisation was complete. The crystals were washed with ethanol to give pure *cis*-4-hydroxy-D-prolie needles (3.5 g, 54% yield); HRMS (ESI-MS): Molecular formula $C_5H_9NO_3$ $[M+H]^+$ 132.0662 found 132.0660; Specific rotation: $[\alpha]^D_{22}$ +59 (c 2.0%,H_2O)   {lit. $[\alpha]^D_{25}$ +60 (c 2.0%, H_2O)}; ^1H NMR: (Methanol-d_4, 400 MHz) δ 4.57-4.54 (m, 1H), 4.21-4.17 (m, 1H), 3.46-3.42 (m, 1H), 3.37-3.32 (m, 1H), 2.52-2.44 (m, 1H), 2.25-2.20 (m, 1H); ^{13}C NMR: (400 MHz, $CDCl_3$) δ 174.5, 69.2, 59.7, 53.0, 37.2; Crystal structure of *cis*-4-hydroxy-D-Proline:
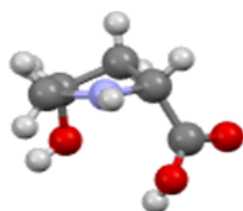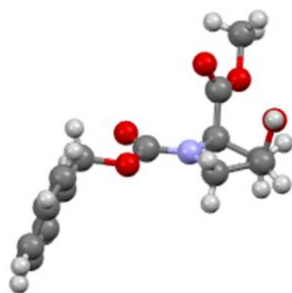
(2*R*,4*R*)-N[1]-(benzyloxycarbonyl)-*cis*-4-hydroxy-D-proline (2)
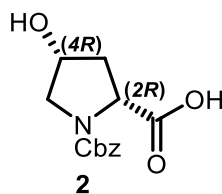
A solution of compound **1** (4g, 30.5 mmol) in 10% aq. NaHCO$_3$ (40 ml) was cooled on ice bath, 50% solution of Cbz-Cl in toluene was added (11 ml) slowly and stirred for 12 h, at RT. Toluene was removed under reduced pressure, the aqueous solution extracted with hexane 3-4 times to remove unreacted Cbz-Cl. The aqueous layer was acidified to pH 3 with saturated KHSO$_4$ and extracted with ethyl acetate. The organic layers ware washed with brine solution, dried over anhydrous Na$_2$SO$_4$ and concentrated to yield white sticky solid compound. Yield: 6.5g; 80%; HRMS (ESI-MS): Molecular formula (C$_{13}$H$_{15}$NO$_5$) Calculated mass (M+K) 304; observed 304; ^{1}H NMR (CDCl$_3$, 400 MHz) δ: 2.16-2.6 (m, 2H), 3.53-3.61 (m, 2H), 4.3(m, 1H), 4.45 (m, 1H), 5.1- 5.27(m, 2H), 7.26-7.36 (m, 5H); ^{13}C NMR δ: 37.6, 38.6, 55.1, 58.6, 67.7, 69.6, 70.9, 127.5, 128.1, 128.9, 136.2, 154.8, 155.3, 175.8; Crystal structure: (2*R*,4*R*)-N[1]-((benzyloxy) carbonyl)-*cis*-4-hydroxy-D-proline (2)


(2*R*,4*R*)-N[1]-(benzyloxycarbonyl)-*cis*-4-hydroxy-D-proline methyl ester (3)
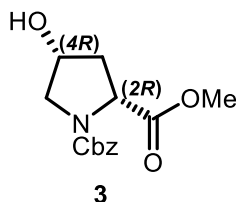
The stirred solution of compound **2** (13g, 49 mmol) in anhydrous acetone 75 ml, (16.9g, 122 mmol) of anhydrous K$_2$CO$_3$ and dimethylsulphate 5.6 ml (58.8 mmol) was added. The reaction mixture was refluxed under nitrogen for 4 h. The reaction mixture was concentrated and extracted three times with ethyl acetate. The combined organic layers ware washed with brine solution, dried over Na$_2$SO$_4$ and concentrated under vacuum. The crude

material was purified by silica gel chromatography (30% ethyl acetate/hexane) afford compound as colourless thick oil. Yield: 13.52g; 98%; Specific rotation: $[\alpha]^D_{22}$ +36 (c 2.0, CH_2Cl_2); HRMS(ESI-MS): Molecular formula ($C_{14}H_{17}NO_5$) calculated mass (M+Na), = 302.1004, observed 302.1002; ^1H NMR (CDCl$_3$, 400 MHz) δ: 2.08-2.15 (m, 1H), 2.29-2.35(m, 1H), 3.58-3.76 (m, 5H), 4.36-4.43 (m, 2H), 4.96-5.18 (m, 2H), 7.26-7.32 (m, 5H); ^{13}C NMR δ: 37.7, 39.0, 52.5, 56.0, 58.3, 67.4, 70.5, 71.4, 127.7, 128.5, 136.9, 154.9, 155.2, 174.9; Crystal structure: (2*R*, 4*R*)-N^1-((benzyloxy) carbonyl)-*cis*-4-hydroxy-D-proline methyl ester (3)


**(2*R*,4*R*)-N^1-(benzyloxycarbonyl)-4-(methanesulfonyloxy) proline methyl ester (4)**
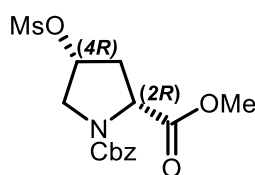
The solution of compound **3** (4 g, 14.3mmol) and triethylamine (3 ml 21mmol) in dry dichloromethane (50 ml) was cooled to 0°C under inert condition. Methanesulfonyl chloride (1.7 ml, 22mmol) was added dropwise over a period of 1 h at 0°C. After completion of reaction, mixture was washed with water followed by brine solution. The organic layer was dried over anhydrous Na$_2$SO$_4$ and concentrated under vacuum. The crude compound 4 was used for next step.

**(2*R*,4*S*)-N^1-(benzyloxycarbonyl)-4-azidoproline methylester (5)**
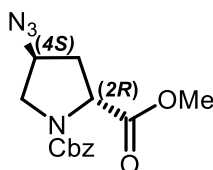
A solution of compound **4** (5.1 g, 14.3 mmol) and NaN_3 (10 g, 153.6 mmol) in dry DMF (50 ml) was stirred at 60 °C for 8 h under nitrogen. DMF was removed under vacuum, and the residue was dissolved in water. The aqueous layer was extracted three times with ethyl acetate. The organic layers ware combined, washed with brine, dried over anhydrous Na_2SO_4 and concentrated under reduced pressure. The azide compound **4** was purified by silica gel chromatography (20% ethyl acetate/hexane) to afford as colourless thick oil. Yield: 3.8g; 83%; HRMS (ESI-MS): Molecular formula ($C_{14}H_{16}N_4O_4$) calculated mass (M+Na) 327.1069; observed mass 327.1068; Specific rotation: $[\alpha]^D_{25}$ +45.2 (c, 2%, MeOH); ^1H NMR (CDCl3, 400 MHz) δ: 2.15-2.25 (1H, m), 2.30-2.40 (1H, m), 3.52-3.58 (2H, m), 3.60-3.68 (1H, m), 3.71-3.79 (3H, m), 4.15-4.25 (1H, m), 4.39-4.50 (1H, m), 5.50-5.20 (2H, m), 7.27-7.36 (5H, m); ^{13}C NMR δ: 35.3, 36.7, 52.6, 57.5, 58.8, 59.4, 67.5, 127.7, 128.7, 136.3, 153.7, 154.5, 172.5.

(2*R*,4*S*)-N^1-(benzyloxycarbonyl)-4-Aminoproline methyl ester
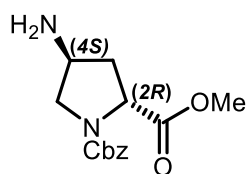
Staudinger reduction: compound **5** (4 g, 12.5 mmol) was reacted with PPh$_3$ (5 g, 19.2 mmol) in dry THF (40 ml), solution was stirred overnight when complete consumption of azide observed, 4 ml water was added and stirred for another 2h, THF was evaporated and crude product without purification used for next step.

(2*R*,4*S*)-N^1-(benzyloxycarbonyl)-4-(*t*-butoxycarbonylamino)-proline methyl ester (6)
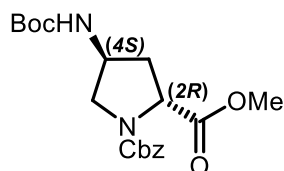
In order to protect 4*S*-NH$_2$ compound, (3.65g, 13 mmol) was reacted with (Boc)$_2$O (3.45g, 16 mmol) in 1:1 dioxane-water containing $NaHCO_3$ for 4h. After completion of reaction dioxane was evaporated under vacuum and extracted three times with ethyl acetate. Combined organic layers were collected and dried over Na_2SO_4. Product was purified by column chromatography. Yield: 2.0g, 41%. HRMS (ESI-MS): Molecular formula ($C_{19}H_{26}N_2O_6$) calculated mass (M+Na) 401.1688; observed mass 401.1689; Specific rotation:

$[\alpha]^D_{25}$ +15 (c, 2%, MeOH); ^{1}H NMR (CDCl$_3$, 400 MHz) δ: 1.59(9H, s), 2.15-2.25 (2H, m), 3.25-3.27 (1H, m), 3.52- 3.75 (3H, m), 3.86 (1H, m), 4.24-4.33 (1H, bs), 4.36-4.45 (1H, m), 4.99-5.18 (2H, m), 7.26-7.35 (5H, m); ^{13}C NMR δ: 28.0, 35.9, 36.8, 52.6, 57.8, 67.5, 127.7, 129.1, 136, 154.0, 155.8, 172.1, 172.8.

## (2*R*,4*S*)-N^1-Fmoc-4-Boc-aminoproline (8)
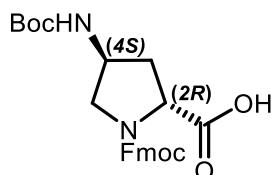
Compound **6** (1 g, 4.3 mmol) was subjected to hydrolysis using aq. LiOH 2N (in THF : water 20 ml, 1:1) for 1 h. THF was removed under reduced pressure, and the aqueous layer was washed with ethyl acetate (3 x 20 mL) to remove THF and organic impurity. Aqueous layer acidified with KHSO$_4$ and extracted with ethyl acetate, crude product (acid) dissolved in dry methanol (15 mL) to which of 10% Pd/C (0.5 g) was added. The mixture was subjected to hydrogenation under H$_2$ gas in a balloon for 6 h. The reaction mixture was filtered through celite. The filtrate was concentrated under reduced pressure. The product obtained as a white solid powder was dissolved in water: dioxane, 1:1 (60 mL). The pH was maintained at 9 by addition of 10% Na$_2$CO$_3$. The reaction mixture was stirred at 0 ^{o}C for 15 minutes. Fmoc-Cl (1.46 g, 5.6 mmol) was added over a period of 30 min, and stirred at 0 ^{o}C for 4 h, and then overnight.

The dioxane was removed under vacuum, and the aqueous layer was washed with diethyl ether (20 mL) to remove unreacted Fmoc-Cl. The aqueous layer was acidified with KHSO$_4$ to pH 4 followed by extraction with ethyl acetate (3 x 50 mL). The concentration of solvent gave the crude product which was purified by silica gel chromatography to afford compound as white solid. Yield: 1g 53(%); HRMS (ESI-MS): Molecular Formula (C$_{25}$H$_{28}$N$_2$NaO$_6$) calculated mass (M+Na) 475.1845, observed 475.1850; Specific rotation: $[\alpha]^D_{25}$ +1 (c, 2%, MeOH); ^{1}H NMR (CDCl$_3$, 400 MHz) δ: 1.46 (9H, s), 2.15-2.20 (1H, m), 2.33-2.36 (1H, m), 3.32-3.36 (1H, m), 3.81- 3.85 (1H, m), 4.15-4.46 (5H, m), 4.754-4.80 (1H, m), 6.07 (2H, bs), 7.28-7.41 (4H, m), 7.53-7.59 (2H, m), 7.70-7.76 (2H, m); ^{13}C NMR δ: 28.44, 29.72, 35.71, 37.03, 47.08, 49.27, 51.97, 55.00, 57.92, 68.01, 80.27, 120.07, 125.18, 127.21, 127.85, 141.38, 143.65, 154.07, 155.38, 172.01, 172.8

**(2R,4S)-N¹-(t-butoxycarbonyl)–4-(p-toluenesulfonyloxy)proline methyl ester (9)**
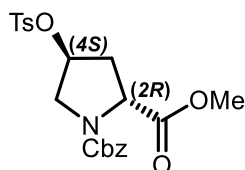
Compound **3** (1.2 g, 4.3 mmol), PPh$_3$ (1.35g, 5.1 mmol) and methyl-toluenesulfonate(0.8 mL, 5.1 mmol) was dissolved in dry THF (10 mL) and cooled to 0$^\text{o}$C on ice bath under nitrogen. The mixture was stirred for 30 min at 0$^\text{o}$C. Diethyl azodicarboxylate (0.8 mL, 5.1 mmol) was added slowly with a syringe. The reaction mixture was stirred at 0$^\text{o}$C for first 4 h then stirred at room temperature for 8 h after which THF was removed under reduced pressure. The resulting orange colored thick oil was dissolved in ethyl acetate (10 mL) to which petroleum ether (100 mL) was added. After triturating with a spatula, the solution was kept at room temperature for 2 h. The white powder settled was filtered, and then the filtrate was concentrated and purified by column chromatography. Yield:1g,56(%); HRMS (ESI-MS): Molecular Formula (C$_{21}$H$_{23}$NO$_7$S) Calculated mass (M+Na) 456.1092, observed mass 456.1087; Specific rotation: [α]$^\text{D}_{25}$ +4$^\text{o}$ (c, 2%, MeOH); ^{1}H NMR (CDCl$_3$, 400 MHz) δ: 2.30-2.45 (3H, m), 3.20-3.25 (1H, m), 3.45-3.75 (7H, m), 4.40-4.55 (1H, m), 4.95-5.20 (4H, m), 7.28-7.35 (8H, m), 7.71-7.75 (2H, m); ^{13}C NMR δ: 21, 30, 36, 38, 53, 55, 57, 68, 128, 128.2, 128.9, 130, 133, 136, 154, 171.

(2R,4R)-N¹-(benzyloxycarbonyl)-4-azidoprolinemethylester (10)
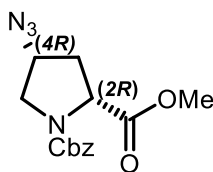
The compound **9** (0.8 g, 1.8 mmol) and NaN$_3$ (1.4 g, 22 mmol) were dissolved in dry DMF (10 mL), and stirred for 8 h at 55-60 ^{0}C under a nitrogen atmosphere. Water (100 mL) was added to reaction mixture, and the aqueous layer was extracted with ethyl acetate (3 x 50 mL). The combined organic layers ware washed with water (3 x 50 mL) followed by brine and dried over anhydrous Na$_2$SO$_4$. The crude product obtained was purified by silica gel chromatography (20% ethyl acetate/hexane) to afford as colorless thick oil. Yield: 0.4 g, 71 (%); HRMS (ESI-MS): Molecular Formula (C$_{14}$H$_{16}$N$_4$O$_4$) Calculated mass (M+Na) 327.1069,

observed mass 327.1072; Specific rotation: $[\alpha]^D_{25}$ +17 (c, 2%, MeOH); ^{1}H NMR (CDCl$_3$, 400 MHz) δ: 2.20-2.2 (1H, m), 2.40-2.50 (1H, m), 3.64 (1H, s), 3.70-3.81 (3H, m), 4.15-4.21 (1H, m), 4.40-4.50 (1H, m), 5-5.21 (2H, m), 7.27-7.36 (5H, m); ^{13}C NMR δ: 35.0, 35.5, 51.2, 52.5, 57.8, 58.3, 59.5, 67.5, 128.2, 128.6, 136.0, 171.0.

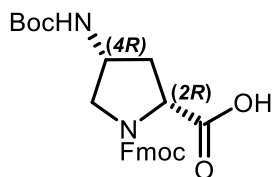**(2*R*,4*R*)-N^1-(benzyloxycarbonyl)-4-Aminoproline methyl ester**
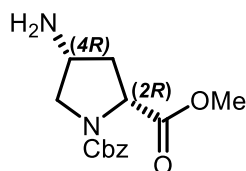
Staudinger reduction; compound **10** (4 g, 12.5 mmol) was reacted with PPh$_3$ (5 g, 19.2 mmol) in dry THF (40 ml). The resulting solution was stirred overnight when complete consumption of azide observed then water (4 ml) was added and stirred for another 2h and then THF evaporated. Same product without purification used for next step.

(2*R*,4*R*)-N1-(Cbz)-N^4-(*t*-butoxycarbonyl) aminoproline methyl ester (11)
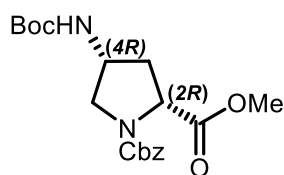
(2*R*,4*R*)-N^1-(benzyloxycarbonyl)-4-aminoprolinemethylester (3.65g, 13 mmol) was taken RB without purified, and 1:1 dioxane-water was added in that then NaHCO$_3$ (1 g) followed by slow addition of (Boc)$_2$O (3.45g, 16 mmol) and stirred for another 4h during this reaction was monitored by TLC. After 4h TLC showed the maximum conversion of the product then removed from stirrer, dioxane was evaporated under vacuum then water was added in that and extracted with ethyl acetate. Combined organic layers were dried by adding Na$_2$SO$_4$.

Product purified by column chromatography. Yield: 2.0g, (41%); Molecular formula(C$_{19}$H$_{26}$N$_2$O$_6$); HRMS (ESI-MS): Calculated mass (M+Na) 401.1688; observed 401.1689; Specific rotation: $[\alpha]^D_{25}$ +9 (c, 2%, MeOH); ^{1}H NMR (CDCl$_3$, 400 MHz) δ: 1.41(9H, m), 1.94-2.03(1H, m), 2.44-2.48 (1H, m), 3.55-3.78 (5H, m), 4.32-4.38 (2H, m), 5.00-5.19 (2H, m), 7.29-7.35 (5H, m); ^{13}C NMR δ: 28.0, 35.9, 36.8, 52.6, 57.8, 67.5, 127.7, 129.1, 136, 154.0, 155.8, 172.1.

(2R,4R)-N1-Fmoc-N⁴-(t-butoxycarbonyl) aminoproline (13)

(2R,4R)-N1-Fmoc-N[4]-(t-butoxycarbonyl) aminoproline (13)

The methyl ester, (2R,4R)-N[1]-(benzyloxycarbonyl)-4-(t-butoxycarbonylamino) proline methyl ester (1 g, 4.3 mmol) was subjected to hydrolysis using NaOH 2N 20 ml for 1 h. THF was removed under vacuum, and the aqueous layer was washed with ethyl acetate (3 x 20 mL) to remove THF and unreacted organic compound. The crude product obtained was dissolved in dry methanol (15 mL) to which of 10% Pd/C was added. The mixture was subjected to hydrogenation under H_2 gas in a balloon for 6 h in. The reaction mixture was filtered through celite. The filtrate was concentrated under reduced pressure. The product obtained as a white solid powder was dissolved in water: dioxane, 1:1 (60 mL). The pH was maintained at 10 by addition of 10% Na_2CO_3. The reaction mixture was stirred at 0°C for 15 minutes. Fmoc-Cl (1.46 g, 5.6 mmol) was added in portion-wise during 45 minutes maintained the temperature for first 4 h and then allowed to come to room temperature at 0°C and stirred for 18 h.

The dioxane was removed under vacuum, and the aqueous layer was washed with diethyl ether (20 mL) to remove unreacted Fmoc-Cl. The aqueous layer was acidified with $KHSO_4$ to pH 2 followed by extraction with ethyl acetate (3 x 50 mL). The concentration of solvent gave the crude product which was purified by column chromatography to afford compound as white solid. Yield: 1g, 53(%); HRMS (ESI-MS): Molecular Formula ($C_{25}H_{28}N_2NaO_6$) calculated mass (M+Na) 475.1845, observed 475.1850; Specific rotation: $[\alpha]^D_{25}$ +3 (c, 2%, MeOH); ^1H NMR (CDCl$_3$, 400 MHz) δ: 1.47 (9H, s), 2.28-2.38 (1H, m), 2.40-2.46 (1H, m), 3.54-3.56 (1H, m), 3.69- 3.73 (1H, m), 4.25-4.52 (5H, m), 5.32-5.37 (1H, m), 7.28-7.41 (4H, m), 7.56-7.61 (2H, m), 7.74-7.79 (2H, m); ^{13}C NMR δ: 28.10, 28.45, 31.04, 34.73, 37.25, 47.10, 53.41, 53.70, 58.52, 68.05, 68.36, 79.87, 120.07, 125.08, 125.21, 127.20, 127.85, 141.47, 143.89, 155.44, 175.01.

2.12 References

(1) Cowan, P. M.; Mcgavin, S., Structure of Poly-L-Proline. *Nature*, **1955**, *176,* 501-503. (b) Traub, W.; Shmulei, U., Structure of Poly-L-Proline-I. *Nature*, **1963**, *198,* 1165-1166.

(2) (a) Rath, A.; Davidson, R.; Deber, C. M., The Structure of "Unstructured" Regions in peptides and proteins: role of the polyrproline-II helix in protein folding and recognition. *Biopolymers* **2005**, *80*, 179–185. (b) Holt, M. R.; Koffer, A., Cell motility: proline-rich proteins promote protrusions. *Trends Cell Biol.* **2001**, *11*, 38–46. (c) Kay, B. K.; Williamson, M. P.; Sudol, M., The importance of being proline: the interaction of proline-rich motifs in signalling proteins with their cognate domains. *FASEB J.* **2000**, *14*, 231–241.

(3) Mahesh, V. S.; Krishna, N. G., Water induced switching of beta-structure to polyproline II conformation in the 4S-amino proline polypeptide *via* H-bond rearrengment. *Org. Lett*, **2010**, *12*, 5390-5393.

(4) Nitin, D. B.; Mahesh, V. S.; Ganesh. K. N., A nanofiber assembly directed by the non-classical antiparallel beta-structure from 4S(OH) proline polypeptides. *chem. Commun.,* **2016**, *52*, 4884-4887.

(5) Nitin, D. B.; Madhanagopal, B.; Mahesh, V. S.; Krishna, N. Ganesh., Stereo dependent and solvent-specific formation of unusual β-structure through side chain-backbone H-bonding in C4(S)-(NH$_2$/OH/NHCHO)-L-prolyl polypeptides. *Peptide. Science,* **2017**, *108*, 22981-22992.

(6) Piero, D. C.; Concetta, L. R., Stereoselective synthesis of (1R,4R)-N-acyl-2-OOxa-5-aza-bicyclo[2.2.1]heptane-3-ones via mesoionic compounds. An improved synthesis of cis-4-hydroxy-D-proline. *Tetrahedron: Asymmetry*, **2002**, *13*, 197-201.

(7) (a) Alexander, N. D.; Alan, G.; Rohit, V. P., Role of Solvent in Determining Conformational Preferences of Alanine Dipeptide in Water. *J. Am. Chem. Soc.*, **2004**, *126*, 2574–2581. (b) Ninad, P.; Kim, S., Solvent-Protein interactions. *Chem Rev.* **2006,** *106*, 1616–1623.

(8) (a) Goodman, M.; Neider, F.; Toniolo, C., Circular dichroism studies of isoleucine oligopeptides in solution. *Biopolymer.* **1971**, *10,* 1719-1730. (b) Sonnichsen, F. D.; Van Eky, J. C.; Hodges, R. S.; Sykes, B. D., Effect of Trifluoroethanol on Proteins Secondary Structure: An NMR and CD Study Using a Synthetic Actin Peptides. *Biochemistry*. **1992,** *31*, 8790-8798.

(9) Michael A. Young.; E. S. Pysh., Vacuum Ultraviolet Circular Dichroism of Poly(L-Proline) I and II. *J. Am. Chem. Soc.* **1975,** *97*, 5100-5103.

(10) Muralikrishna, L.; Radhakrishnan M., Solvent Driven Conformational Transitions in the Second Transmembrane Domain of Mycobacteriophage Holin. *Biopolymer* (*Pep. Sci)* **2017**, *108*, 1-10.

(11) (a) Meng, W.; Peng, Z.; Jiqian, W. Y.; Zhao, H. M.; Jian, R. L.; Hai Xu., Left or Right How Does Amino Acid Chirality Affect the Handedness of Nanostructures Self-Assembled from Short amphiphilic Peptides? *J. Am. Chem. Soc.* **2017,** *139*, 4185−4194. (b) Noa, R.; Emanuel, P.; Michal, G.; Mati, F.; Lia Addadi., Chirality of Amyloid Suprastructure. *J. Am. Chem. Soc.* **2008,** *130*, 4602−4603. (c) Chothia, C., Conformation of twisted beta-pleated sheets in proteins. *J. Mol. Biol.* **1973**, *75*, 295-302. (d) Richardson, J. S., The anatomy and taxonomy of protein structure. *Adv.Protein Chem.* **1981**, *34*, 167-339.(e) Kuo-Chen, C.; Harold, A. S., Origin of the right-handed twist of beta-sheets of poly (L-Val) chains. *Pro. Nat. Acad. Sci.* **1982**, *79*, 7047-7051.

2.13 Appendix1: Characterization data of synthesized compound and peptides

2.13a ^{1}H and ^{13}C NMR spectrum of compounds (**1-13**)

2.13b HPLC and MALDI-TOF of peptides (**1-10**)

H^1 NMR of compound *cis*-(2*R*,4*R*)-4-hydroxy-D-proline (1)
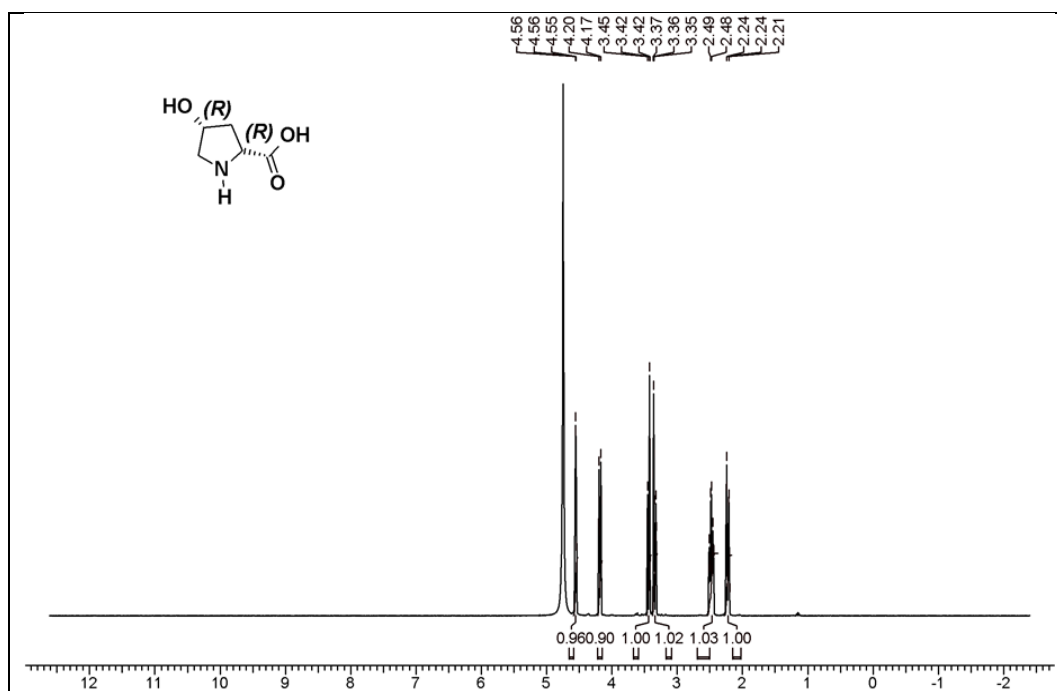
C^{13} NMR of compound *cis*-(2*R*,4*R*)-4-hydroxy-D-proline (1)
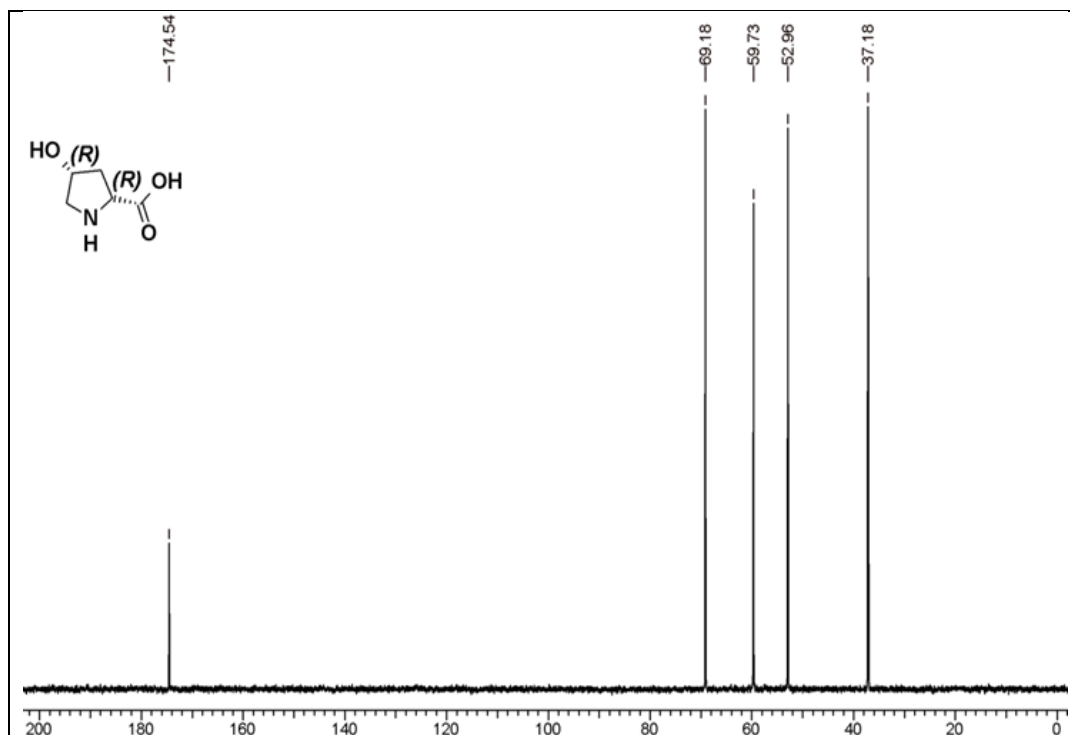
H[1] NMR of compound *cis*-(2*R*,4*R*)-N1–(benzyloxycarbonyl)-4-hydroxy-D-proline (2)
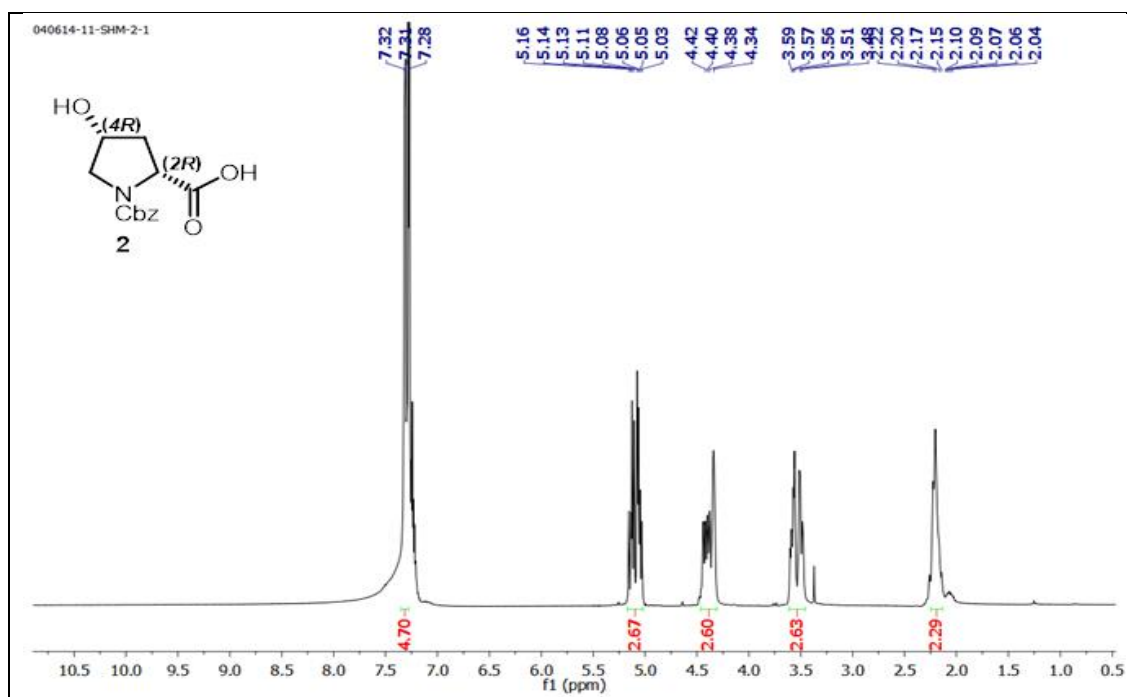
C[13] NMR of compound *cis*-(2*R*,4*R*)-N1–(benzyloxycarbonyl)-4-hydroxy-D-proline (2)
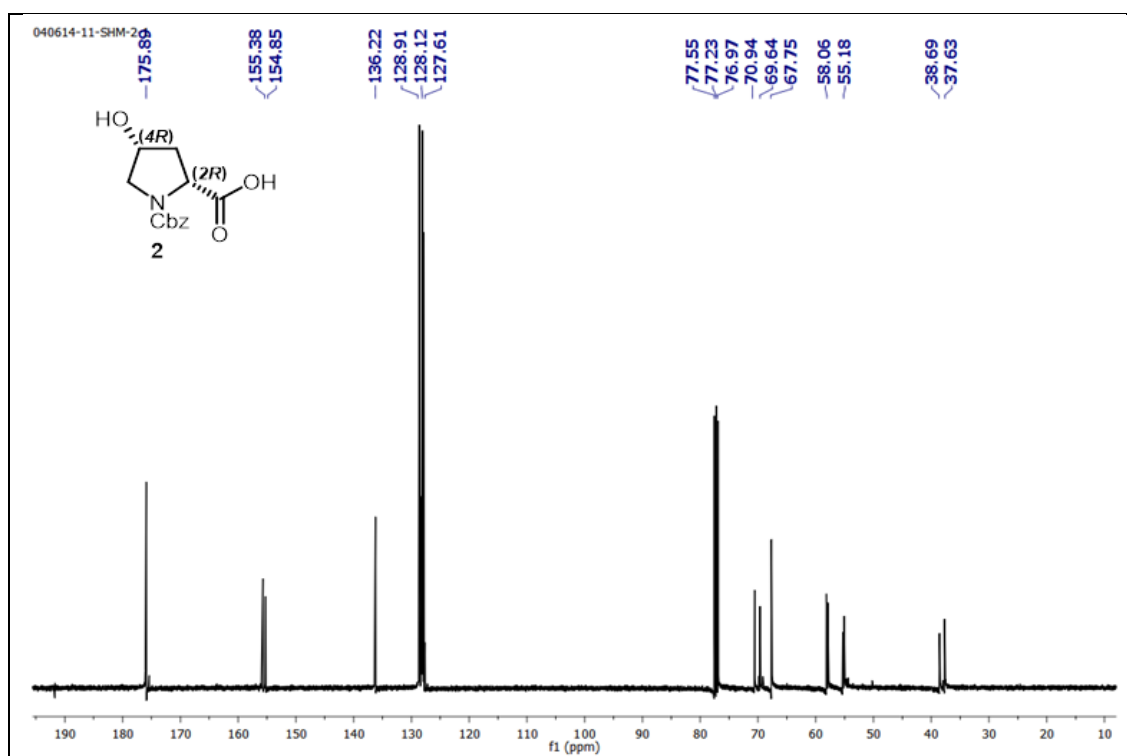
H¹ NMR of compound *cis*-(2*R*,4*R*)-N1-(benzyloxycarbonyl)-4-hydroxy-D-proline methyl ester (3)
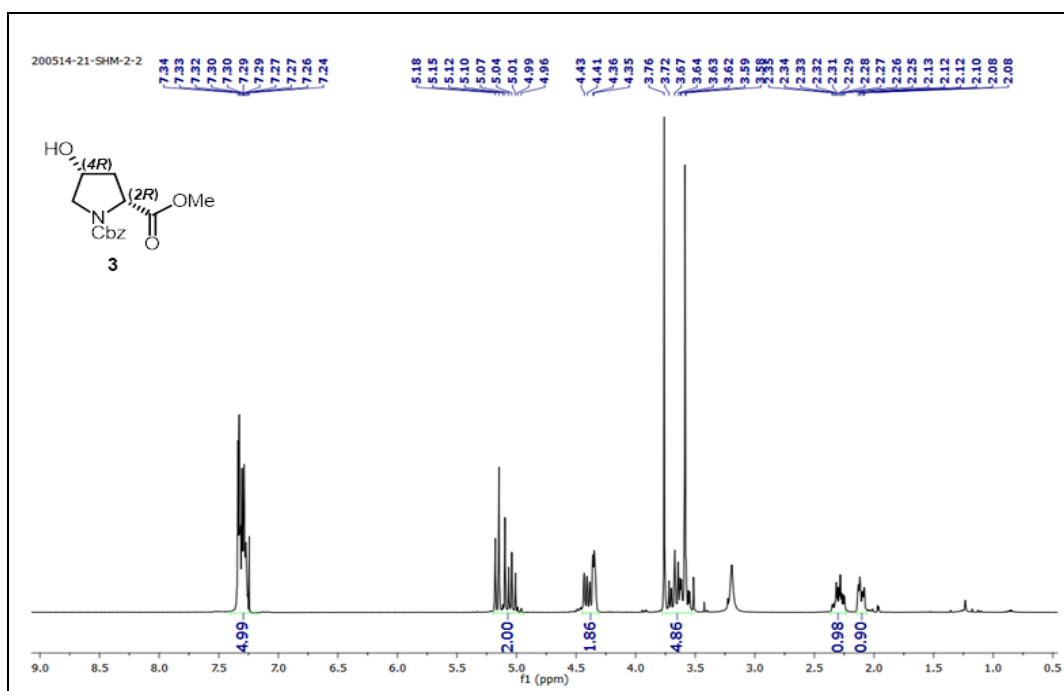
C¹³ NMR of compound *cis*-(2*R*,4*R*)-N1-(benzyloxycarbonyl)-4-hydroxy-D-proline methyl ester (3)
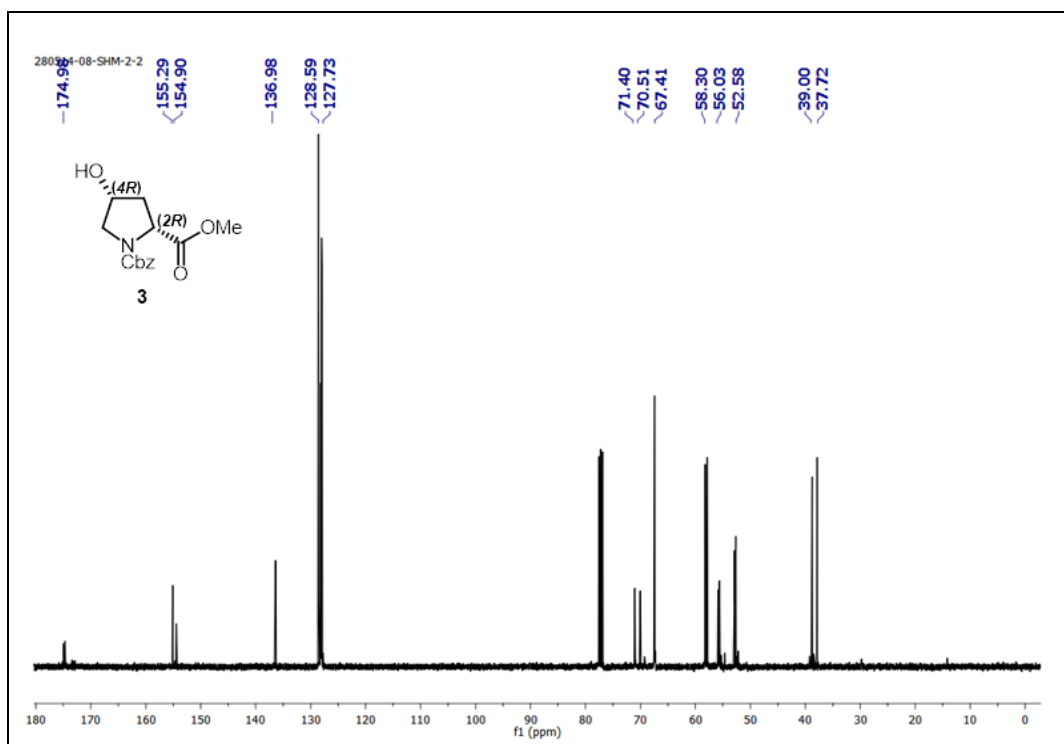
H^1 NMR of compound (2*R*,4*S*)-N1-(benzyloxycarbonyl)-4-azidoprolinemethylester (5)
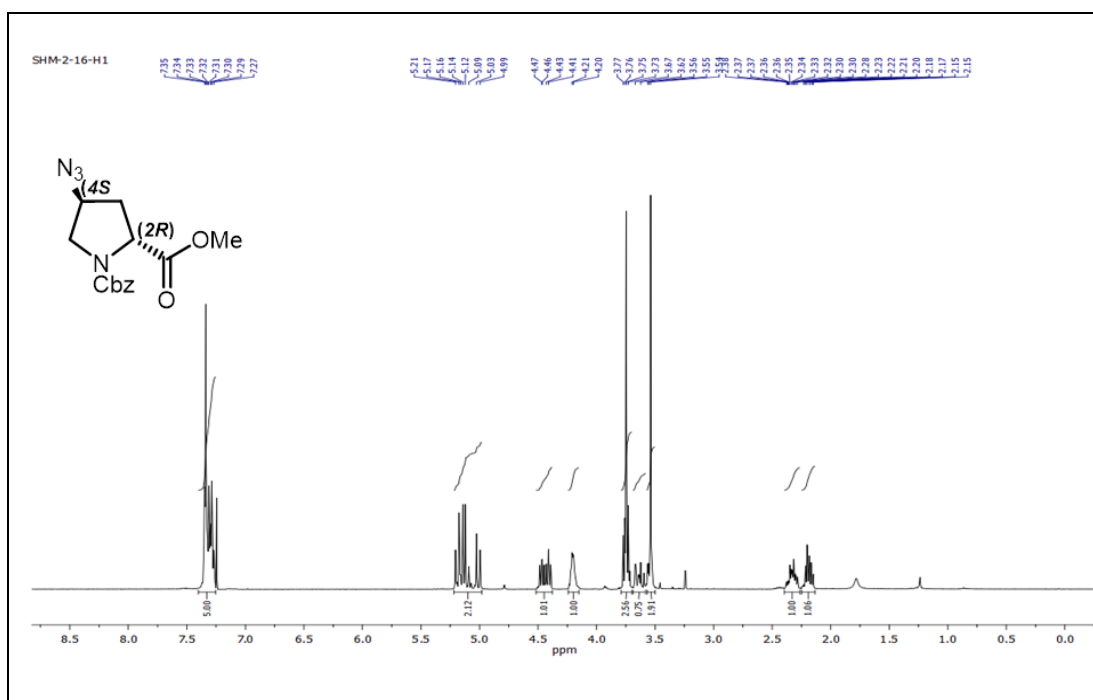
C^{13} NMR of compound (2*R*,4*S*)-N1-(benzyloxycarbonyl)-4-azidoprolinemethylester (5)
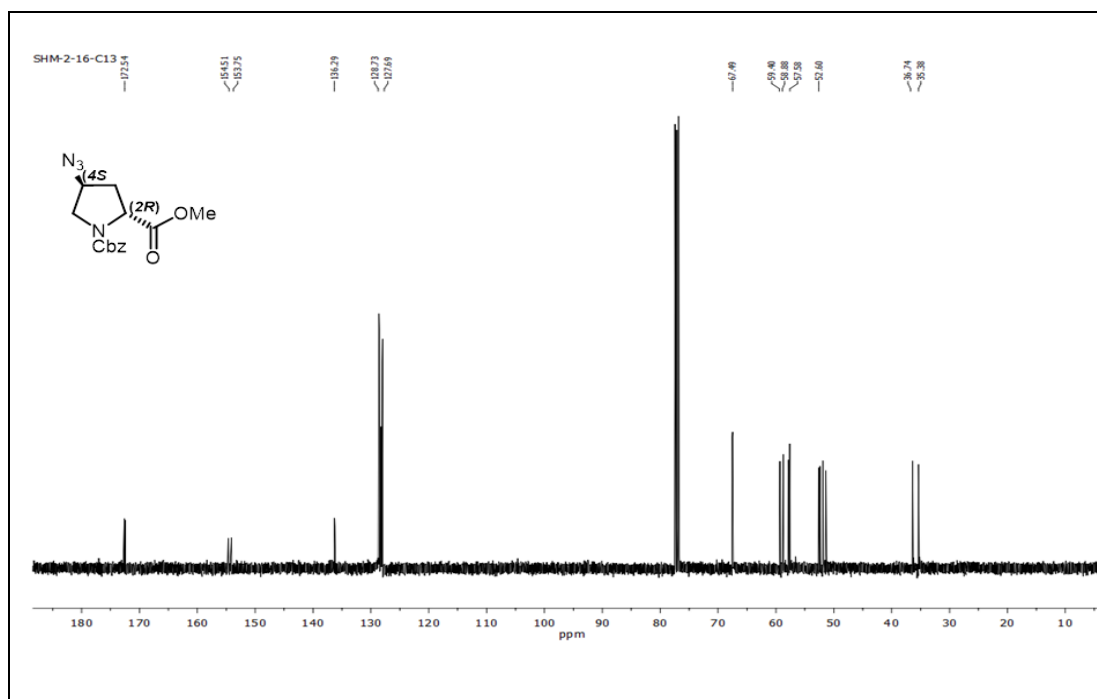
H^1 NMR of compound (2*R*,4*S*)-N1-(benzyloxycarbonyl)-N^4-(*t*-butoxycarbonyl) amino proline methyl ester (6)
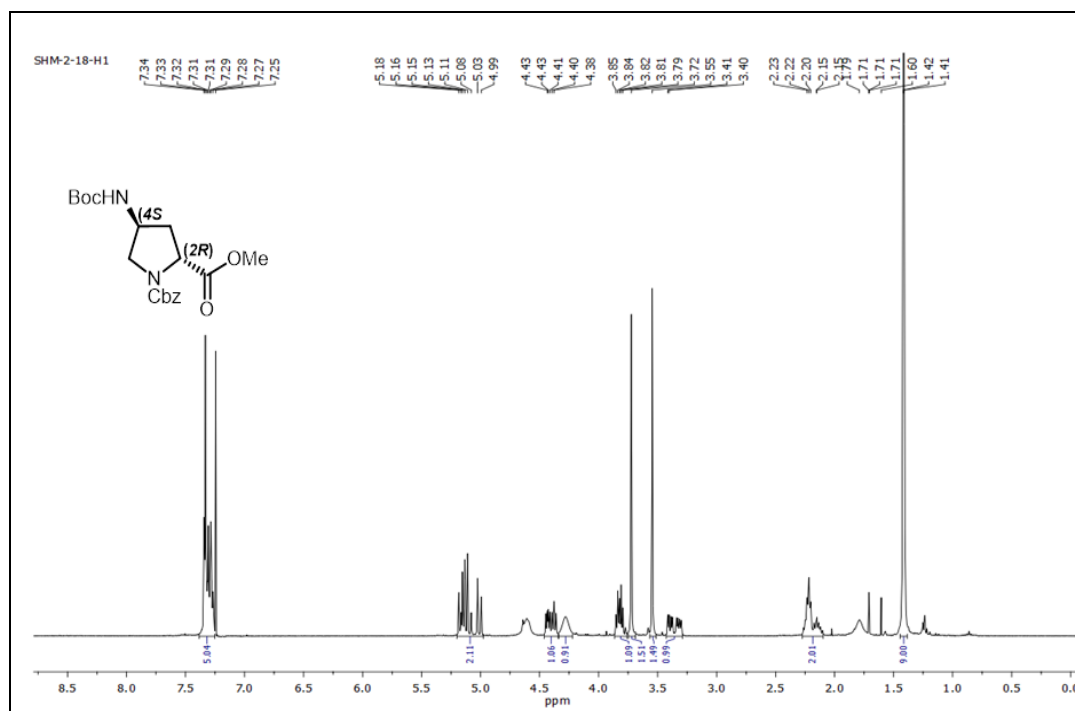
C^{13} NMR of compound (2*R*,4*S*)-N1-(benzyloxycarbonyl)-N^4-(*t*-butoxycarbonyl) amino proline methyl ester (6)
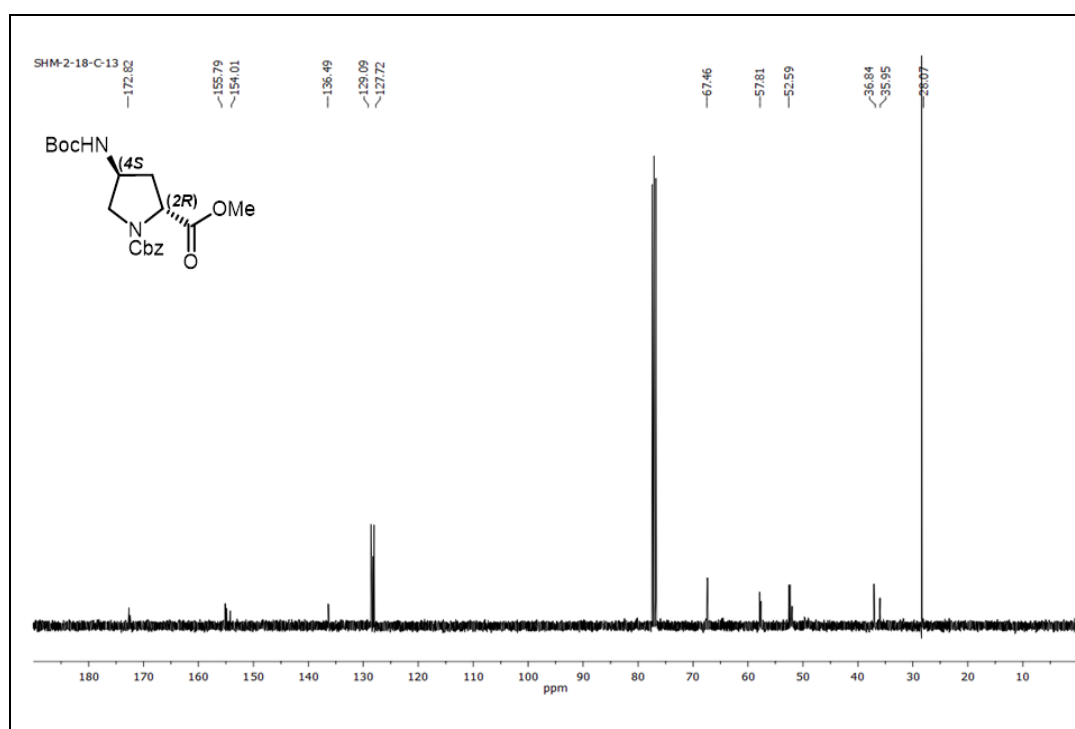
H^1 NMR of compound (2*R*,4*S*)-N1-(Fmoc)-N^4-(t-butoxycarbonyl) aminoproline (8)
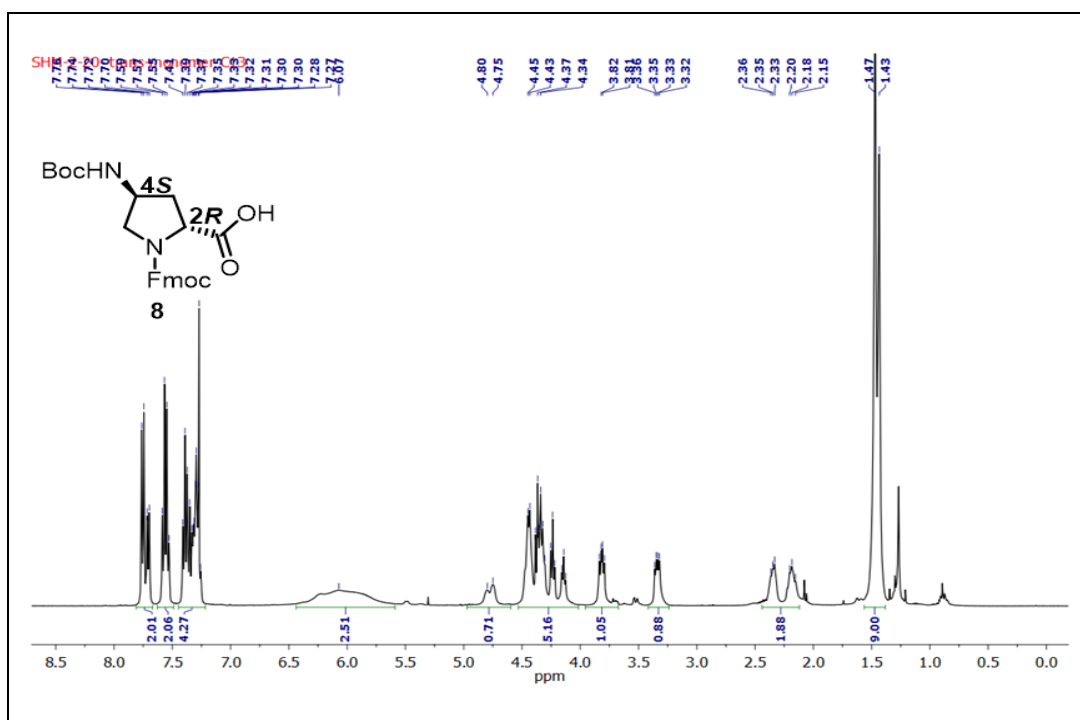
C^{13} NMR of compound (2*R*,4*S*)-N1-(Fmoc)-N^4-(t-butoxycarbonyl) aminoproline (8)
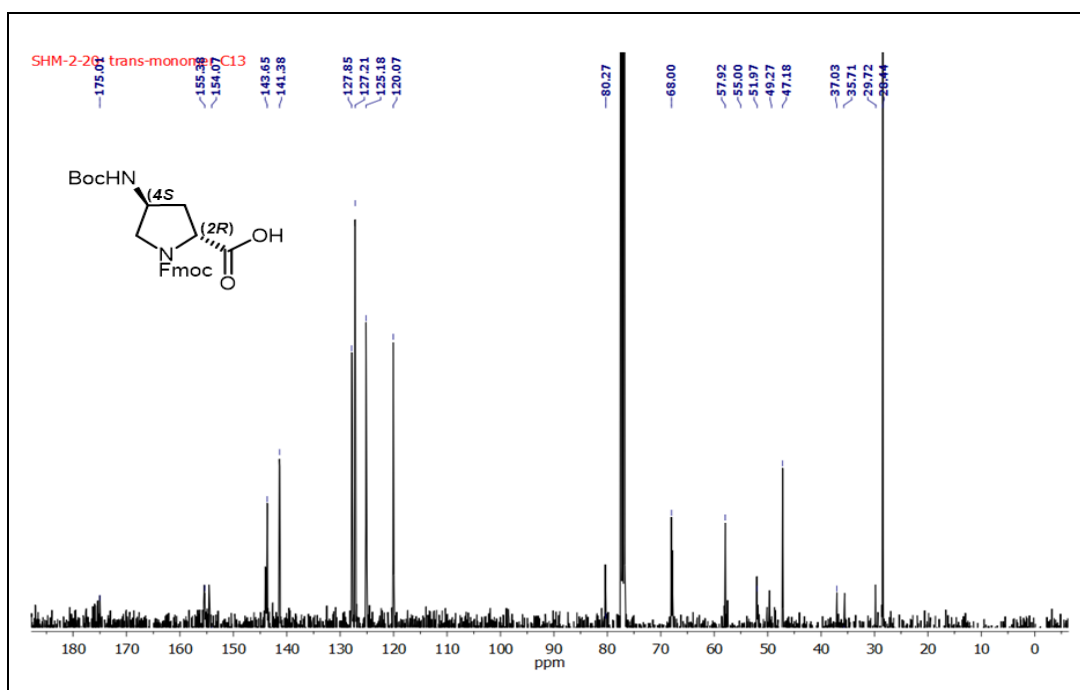
H^1 NMR of compound (2*R*,4*R*)-N1-(benzyloxycarbonyl)-4-azidoprolinemethylester (10)
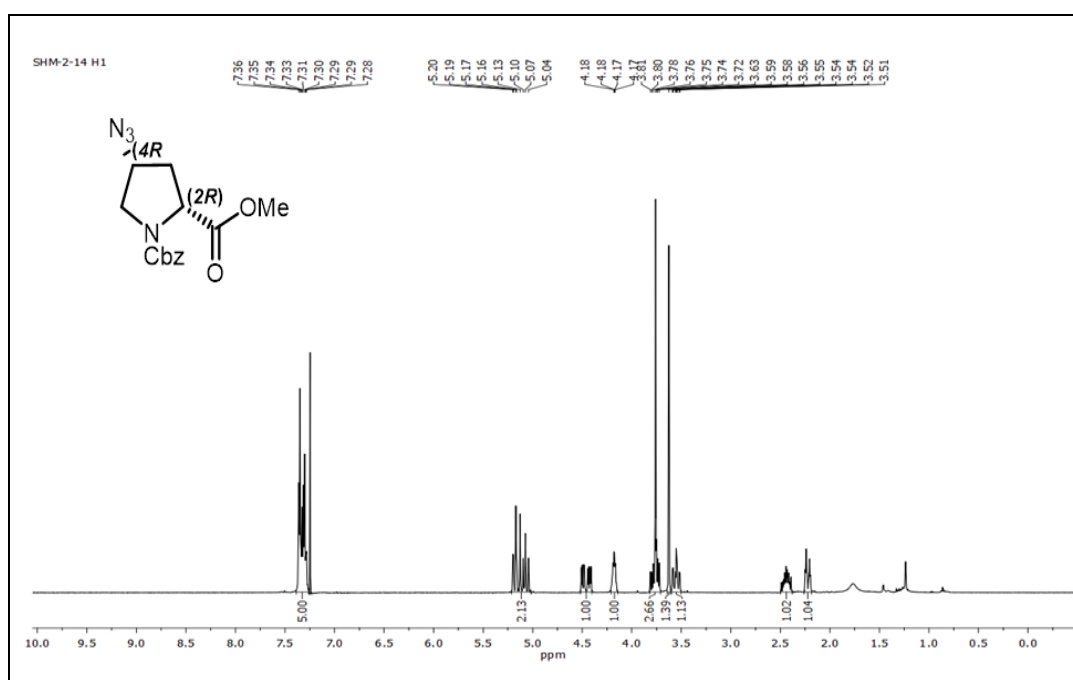
C^{13} NMR of compound (2*R*,4*R*)-N^1-(benzyloxycarbonyl)-4-azidoprolinemethylester (10)
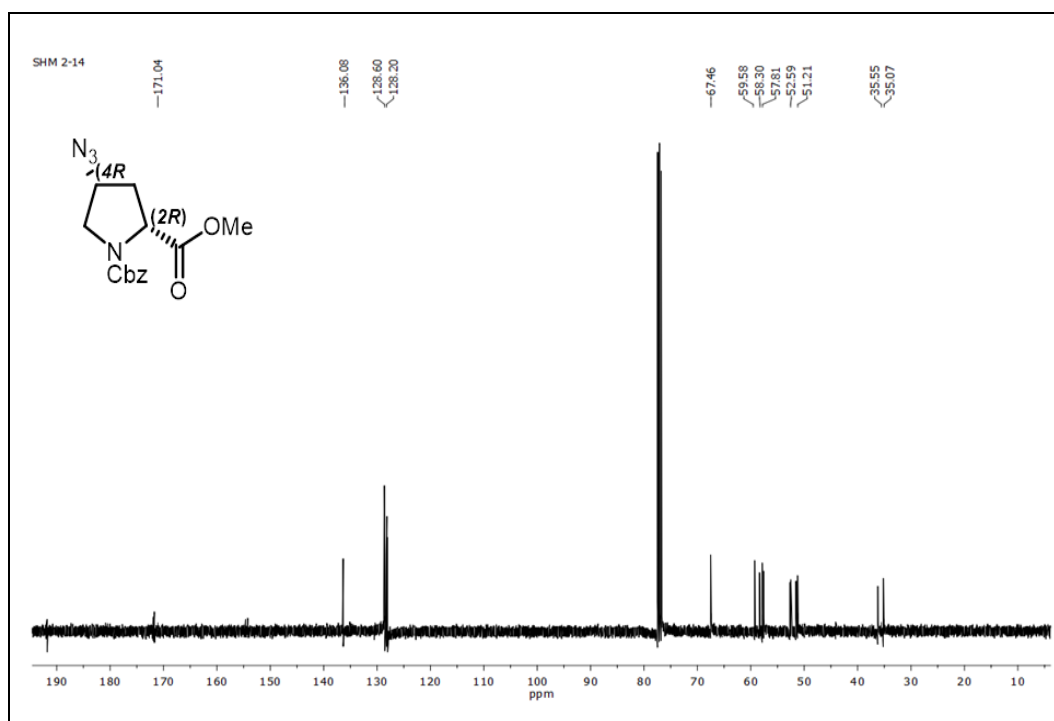
H^1 NMR of (2*R*,4*R*)-N1-(benzyloxycarbonyl)-4-(*t*-butoxycarbonyl) aminoproline methyl ester (11)
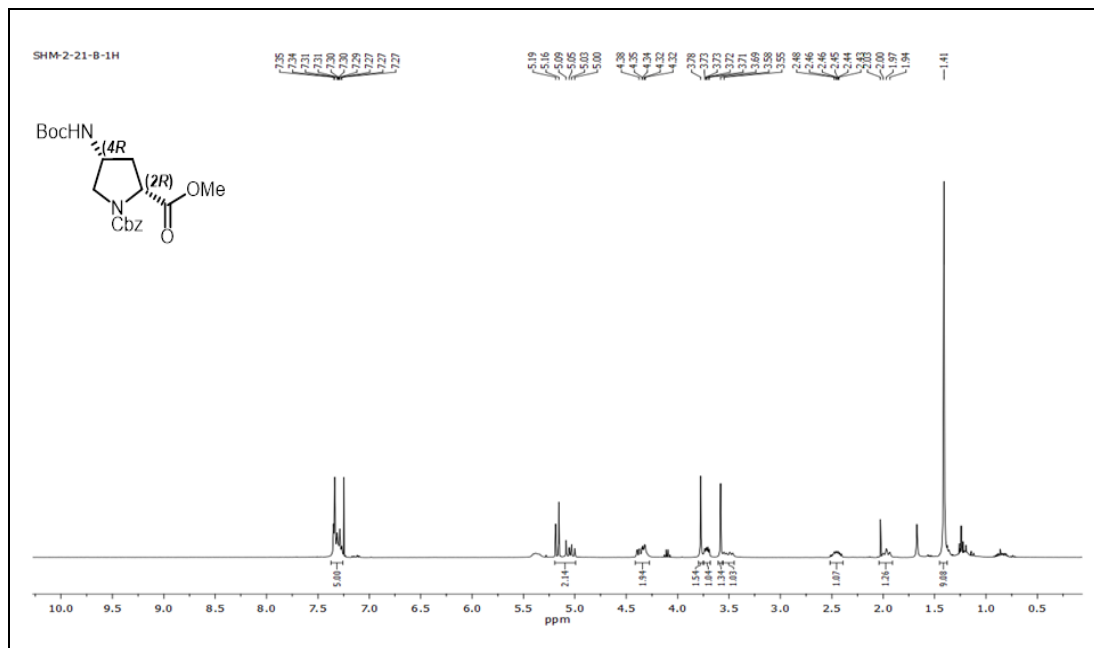
C^{13} NMR of (2*R*,4*R*)-N1-(benzyloxycarbonyl)-N^4-(*t*-butoxycarbonyl) aminoproline methyl ester (11)
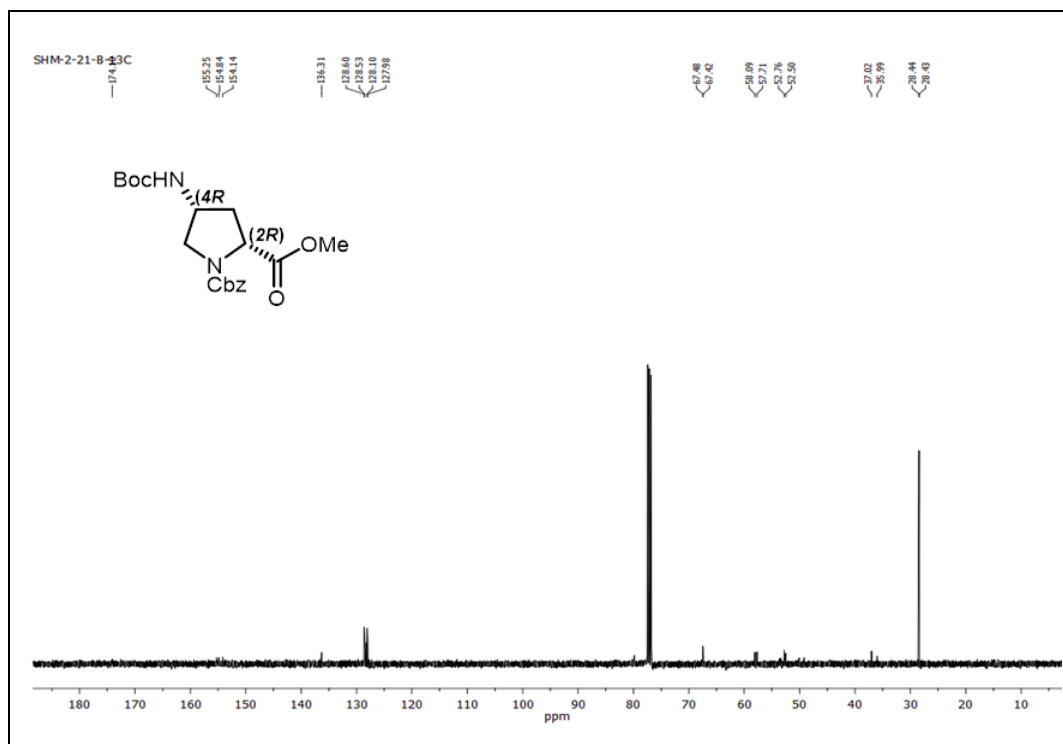
H¹ NMR of compound (2*R*,4*R*)-N1-(Fmoc)-N⁴-(t-butoxycarbonyl) aminoproline (13)
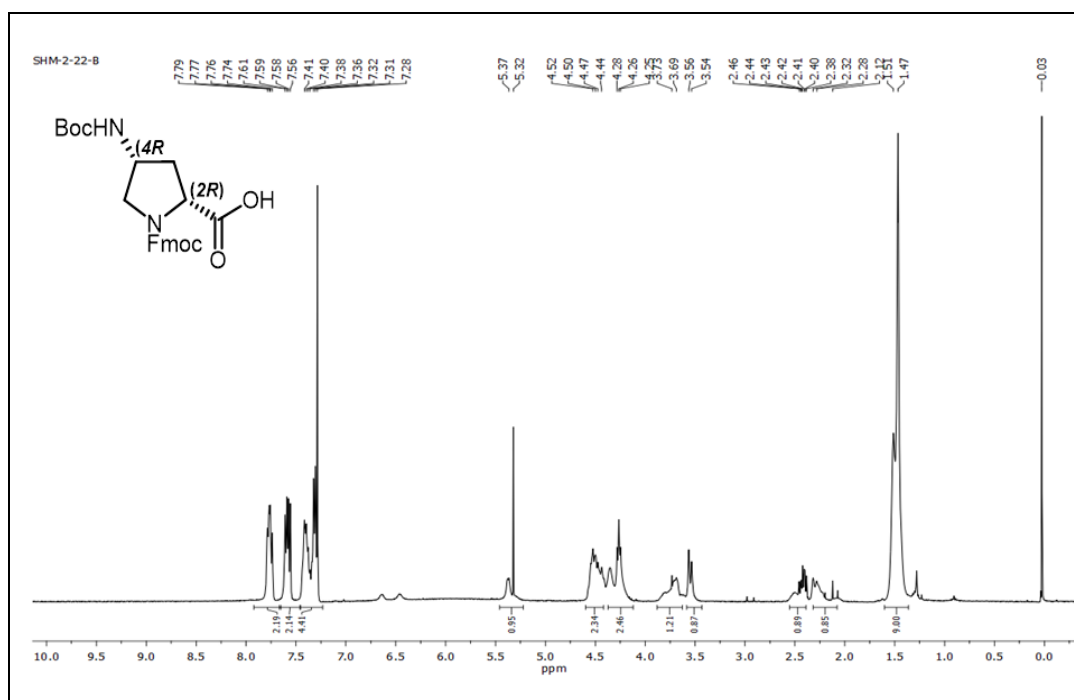
C¹³ NMR of compound (2*R*,4*R*)-N1-(Fmoc)-N⁴-(t-butoxycarbonyl) aminoproline (13)
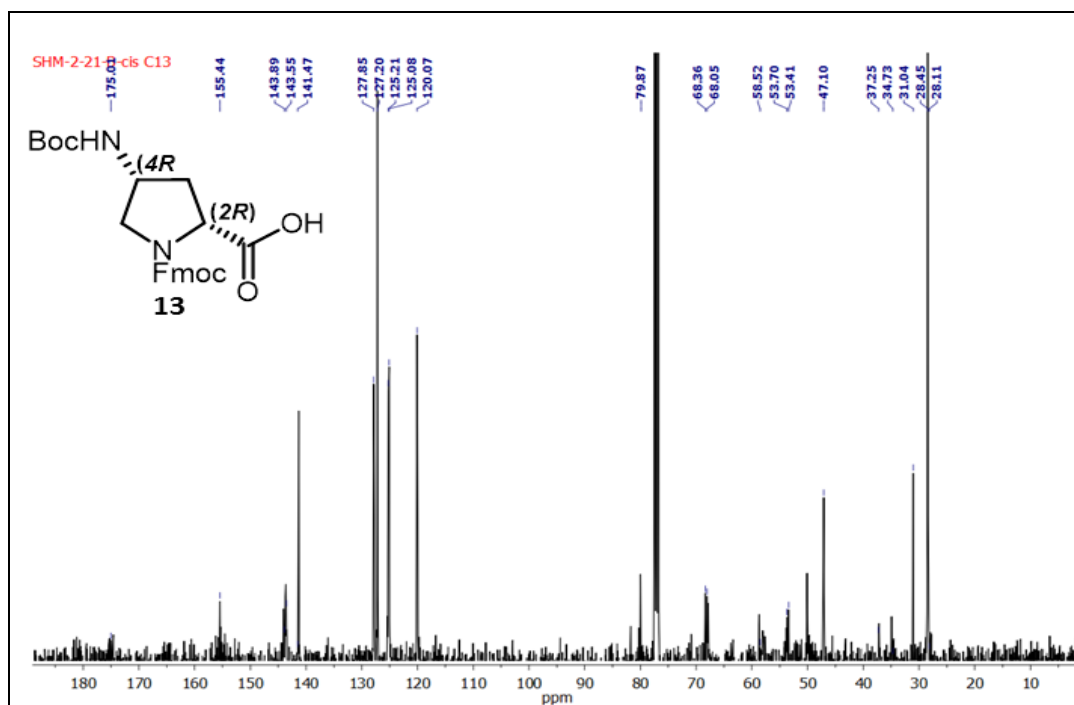
HPLC profile of L-*Pro₉* P1
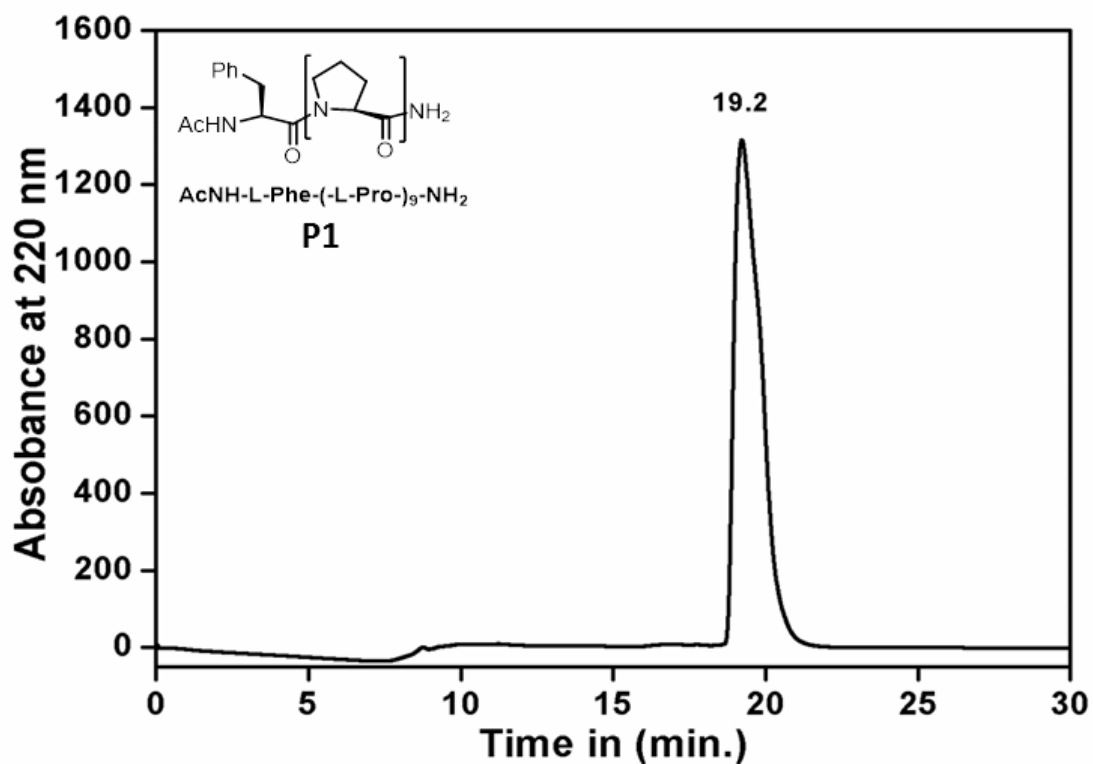
MALDI-TOF spectra of L-*Pro₉* (P1)
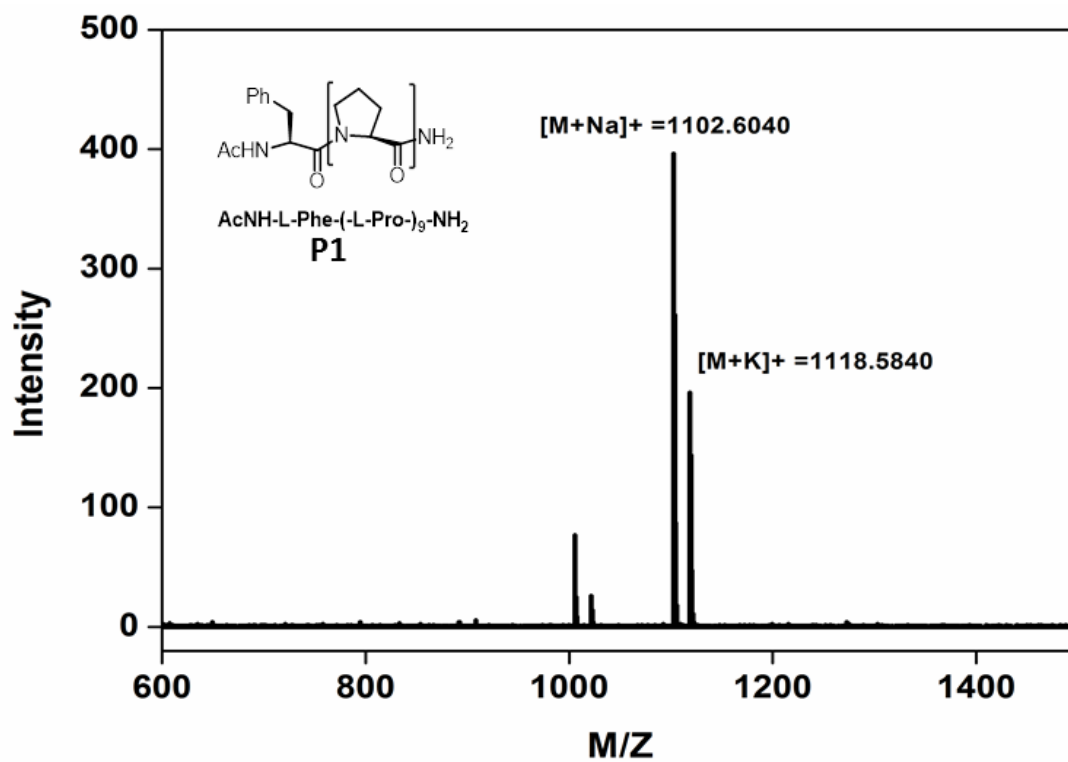
HPLC Profile of D-*Pro₉* (P2)
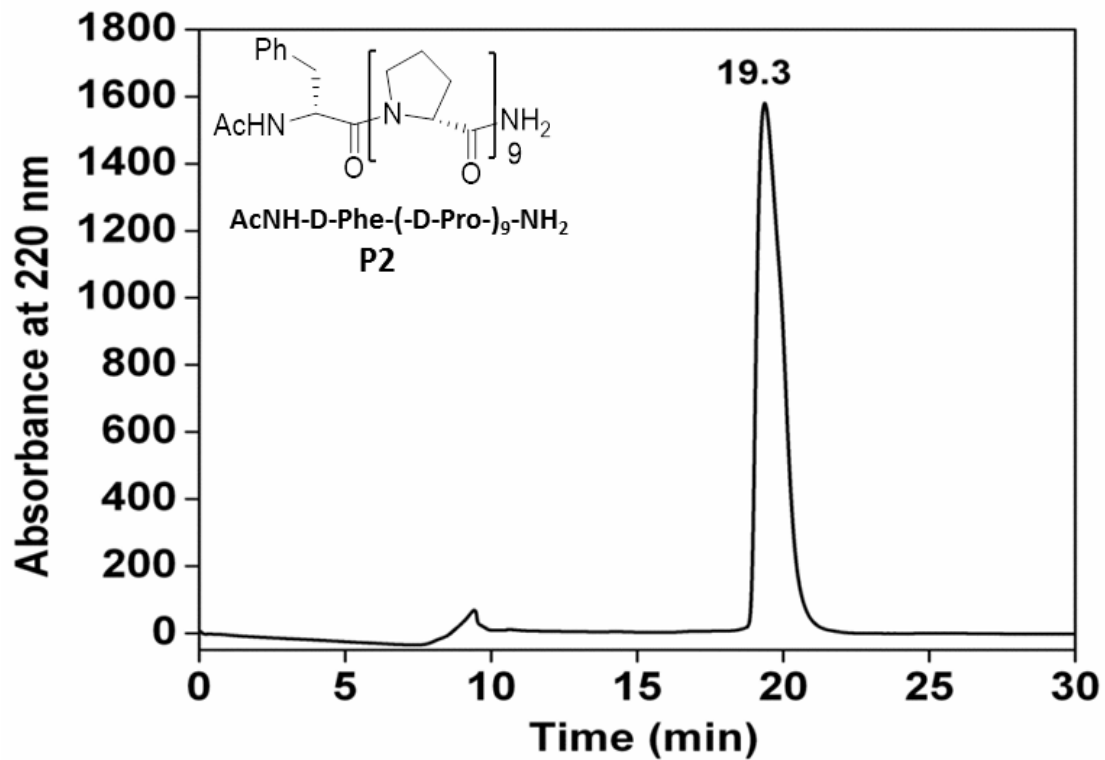
MALD-TOF Spectra of D-*Pro₉* (P2)
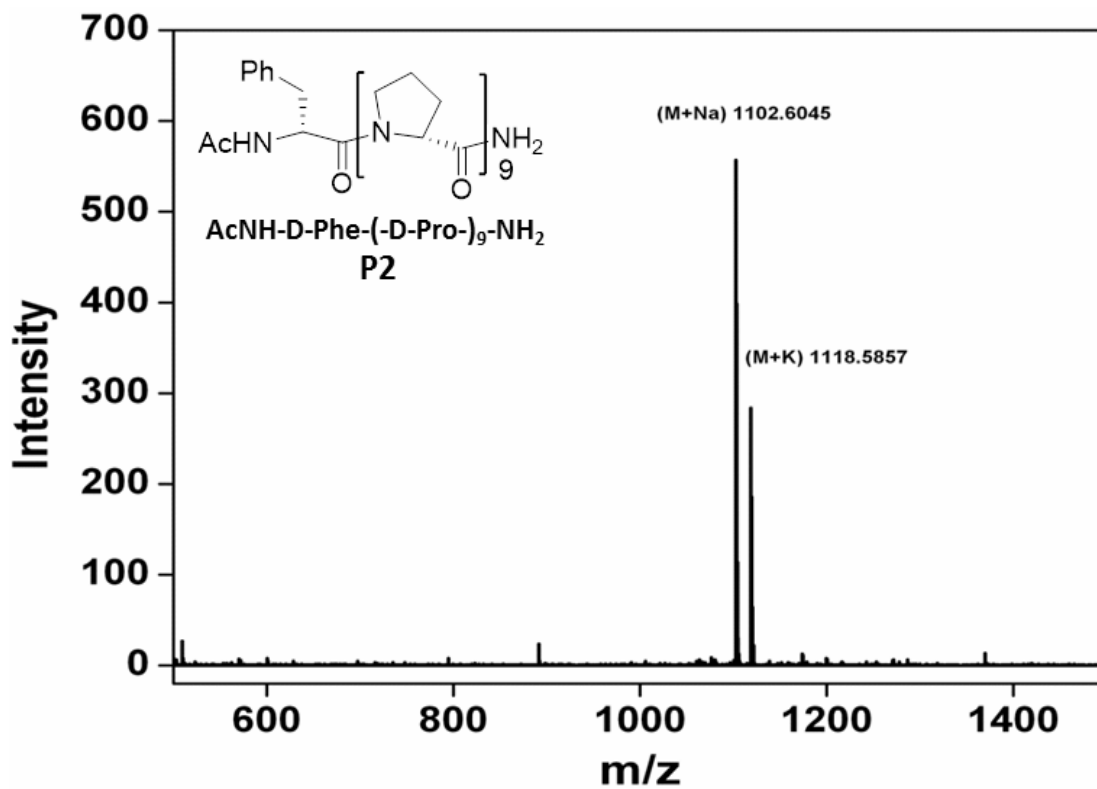
HPLC-Profile of *cis*-(2*R*,4*R*)-D-*Amp₉* (P3)
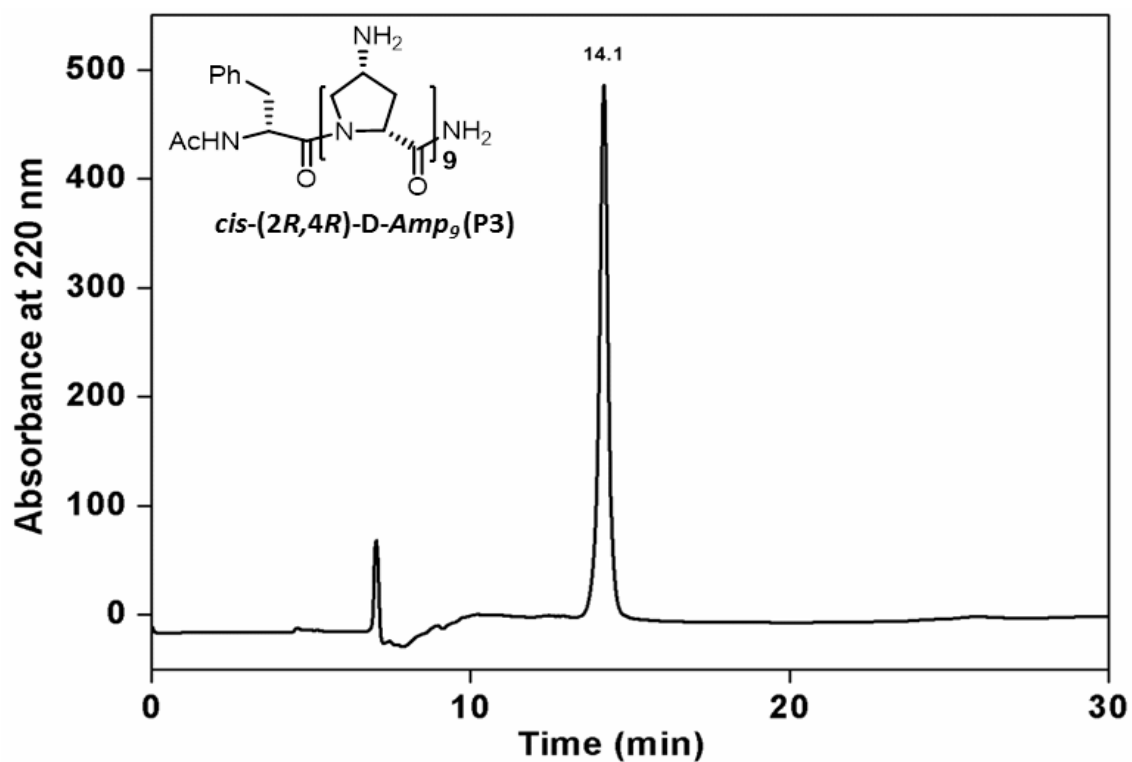
MALDI-TOF spectra of *cis*-(2*R*,4*R*)-D-*Amp₉* (P3)
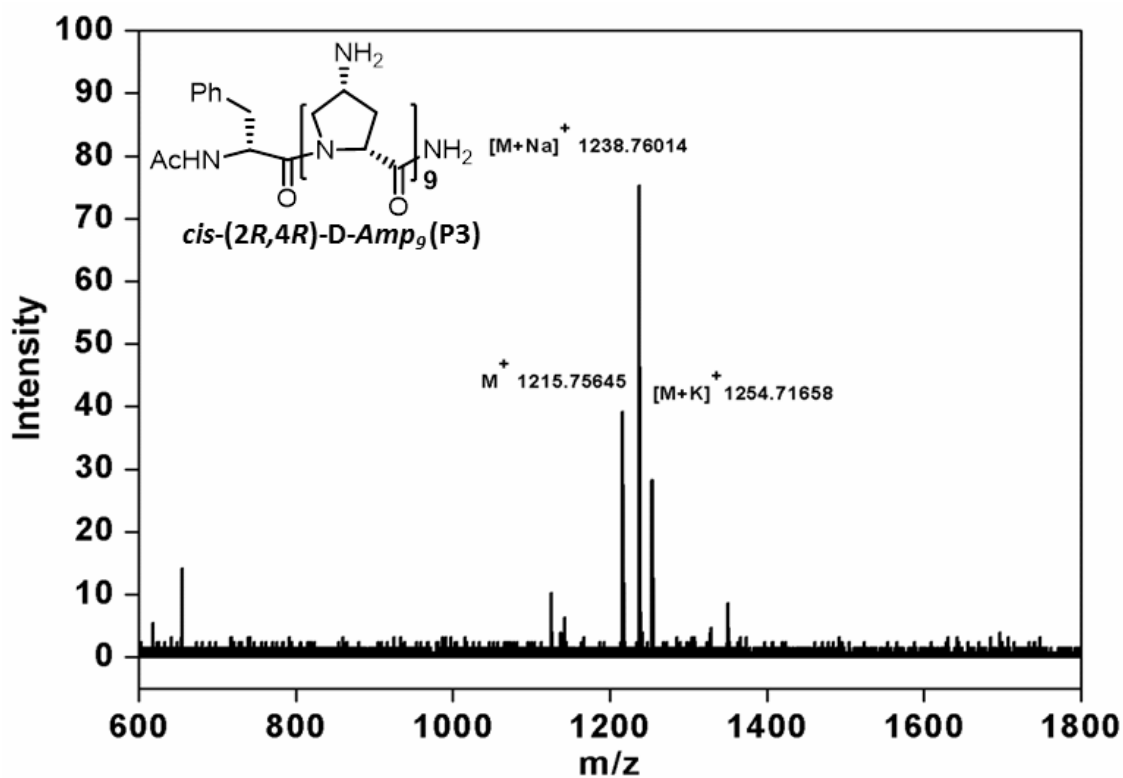
HPLC profile of C$_{12}$-*cis*-(2*R*,4*R*)-D-*Amp$_9$* (P5)
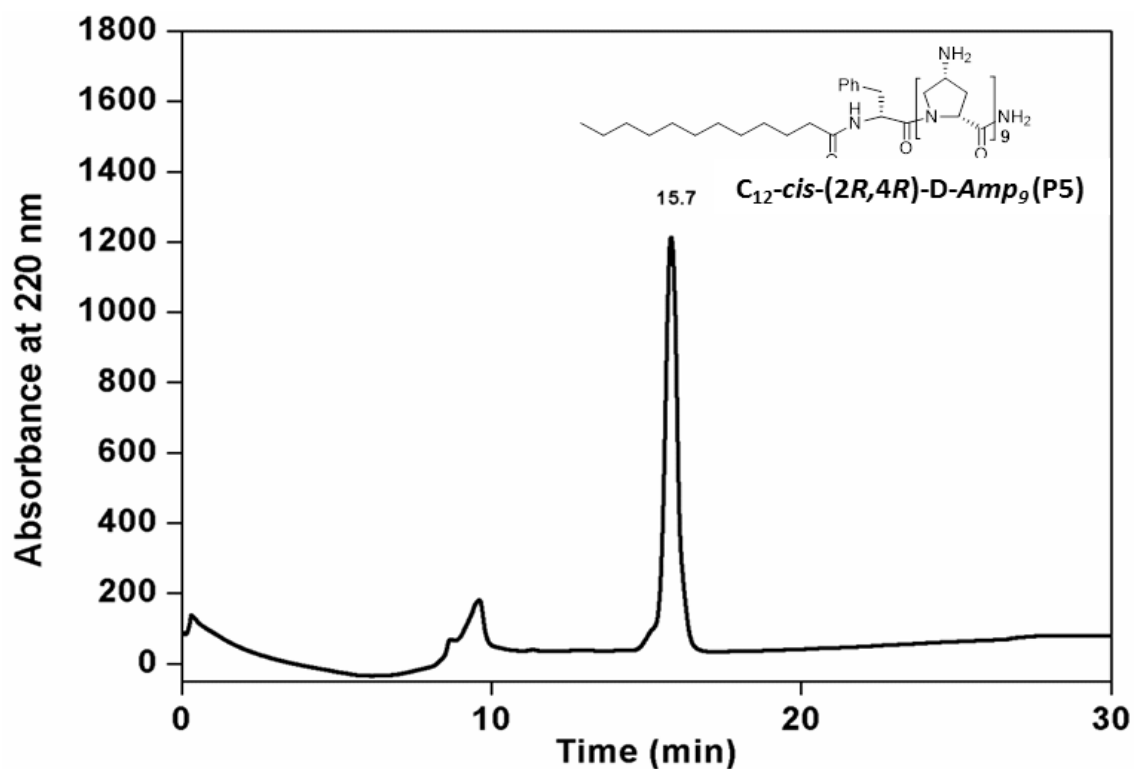
MALDI-TOF of C$_{12}$-*cis*-(2*R*,4*R*)-D-*Amp$_9$* (P5)
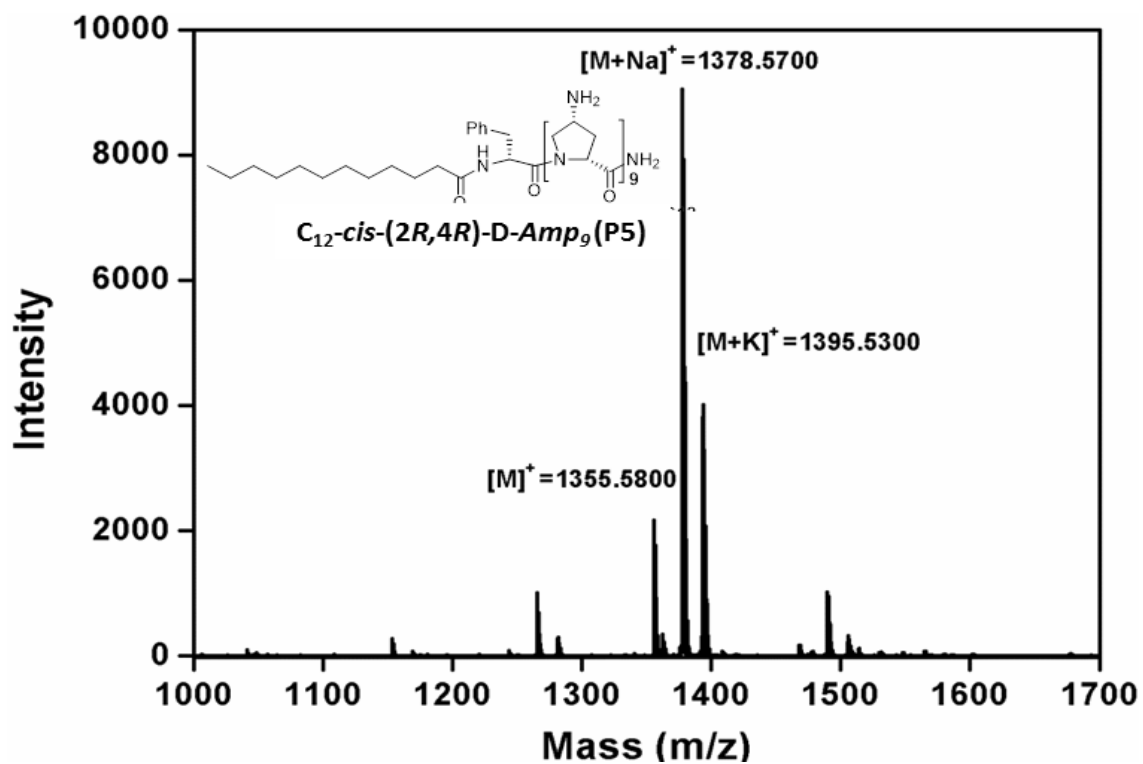
HPLC of C$_{14}$-*cis*-(2*R*,4*R*)-D-*Amp$_9$* (P6)
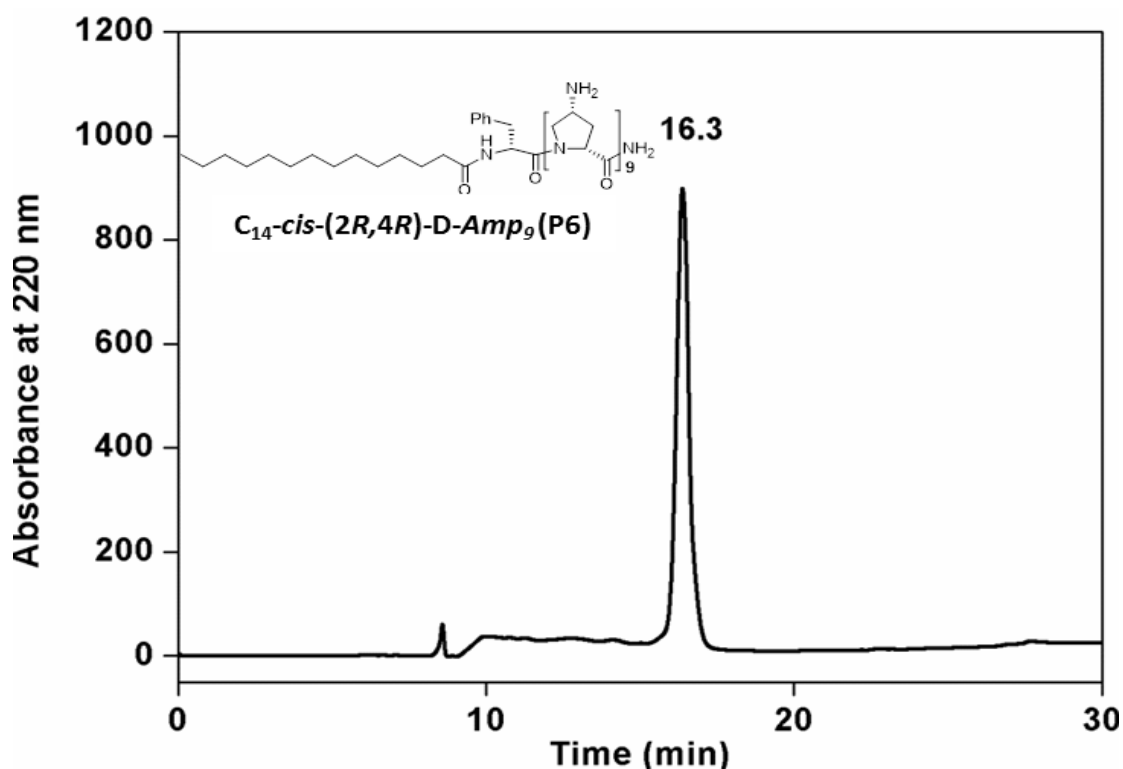
MALDI-TOF of C$_{14}$-*cis*-(2*R*,4*R*)-D-*Amp$_9$* (P6)
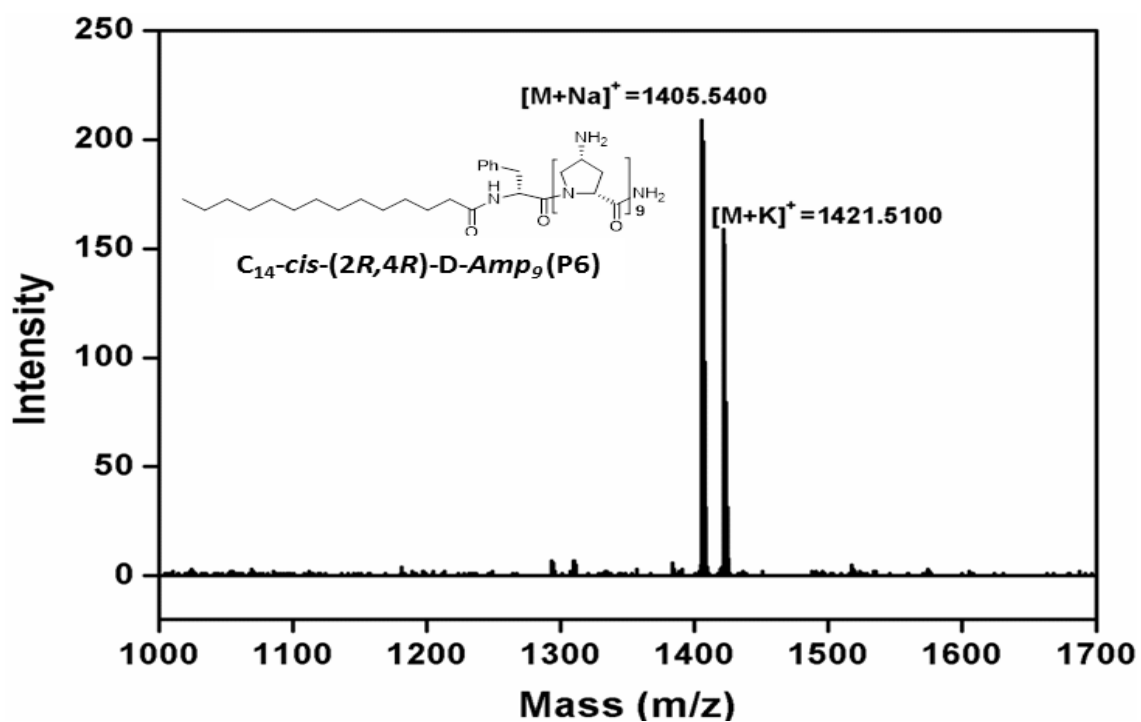
HPLC of C$_{16}$-*cis*-(2R,4R)-D-*Amp$_9$* (P7)
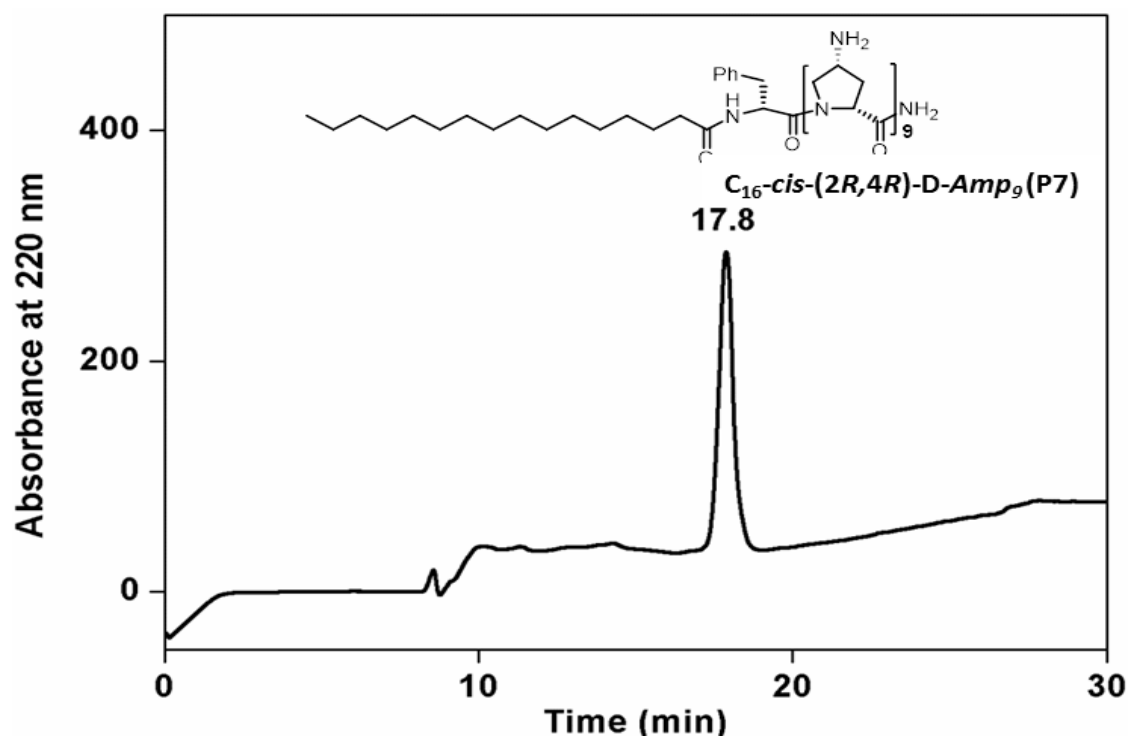
MALDI-TOF of C$_{16}$-*cis*-(2R,4R)-D-*Amp$_9$* (P7)
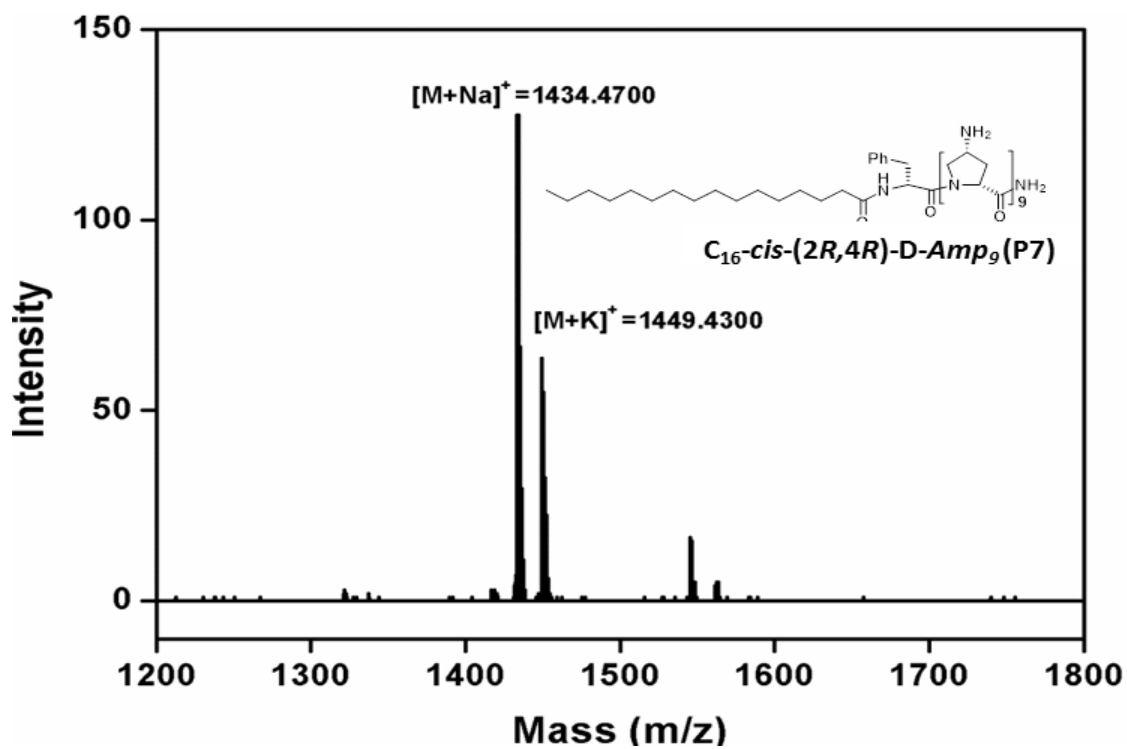
HPLC profile of *trans*-(2*R*,4*S*)-D-*amp*$_9$ (P4)
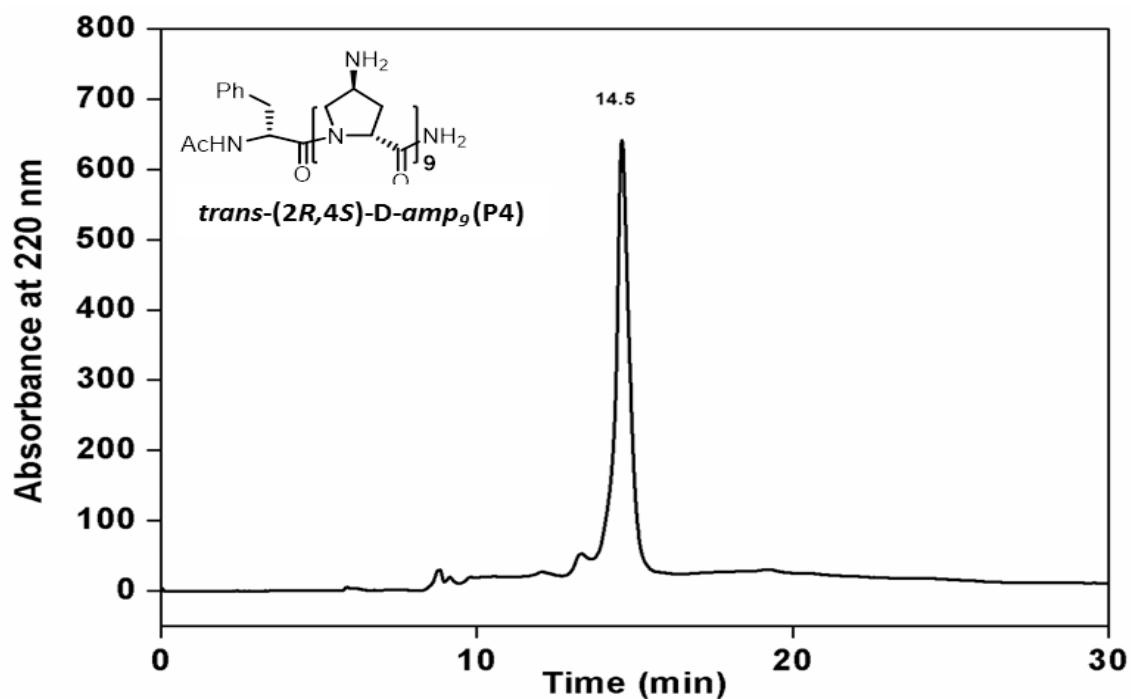
MALDI-TOF of *trans*-(2*R*,4*S*)-D-*amp*$_9$ (P4)
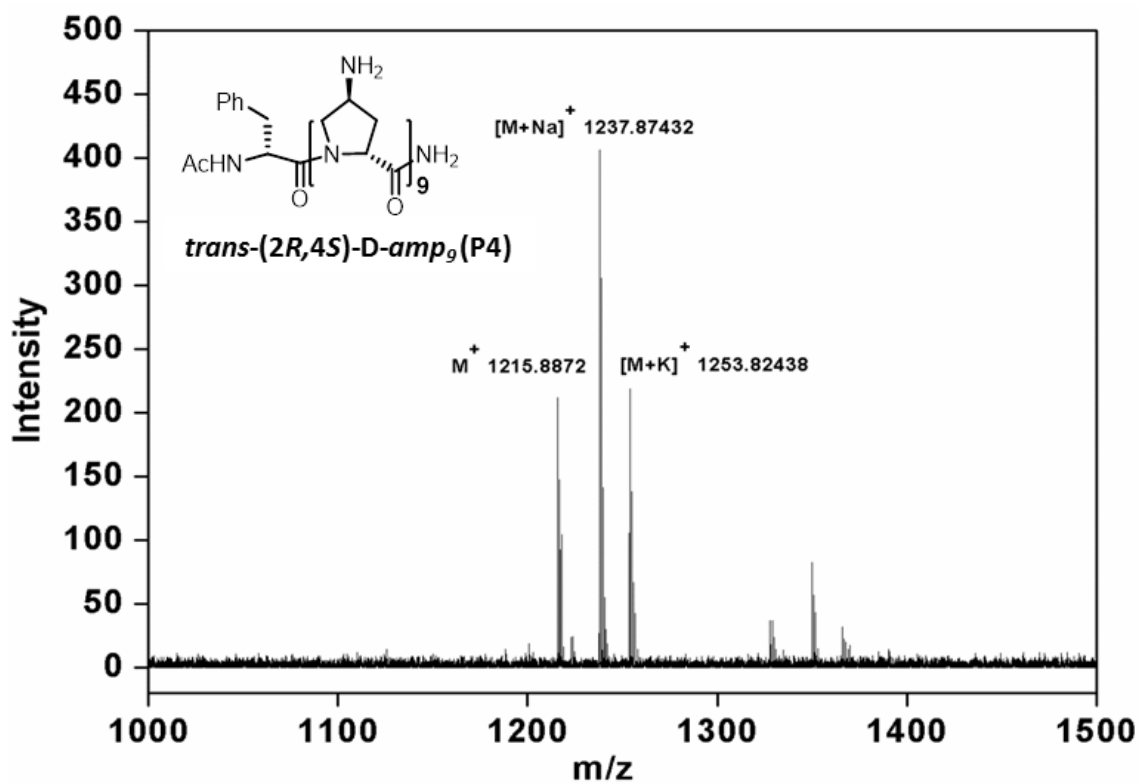
HPLC-profile of C$_{12}$-*trans*-(2R,4S)-D-*amp*$_9$ (P8)
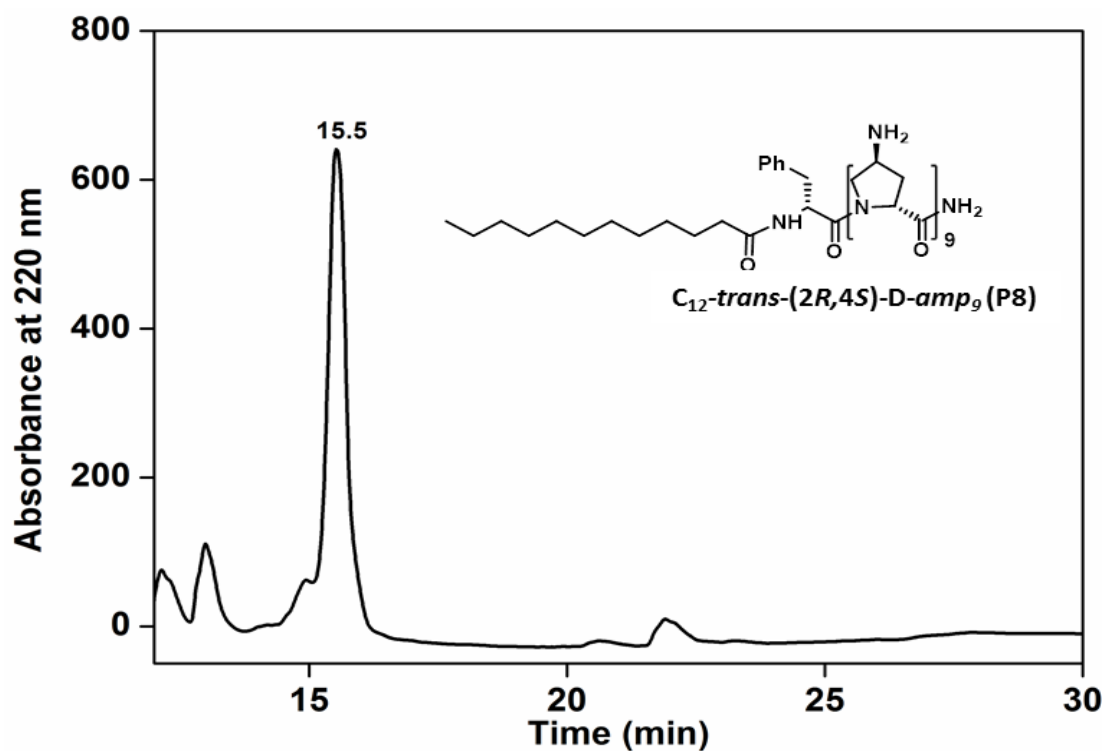
MALDI-TOF of C$_{12}$-*trans*-(2R,4S)-D-*amp*$_9$ (P8)
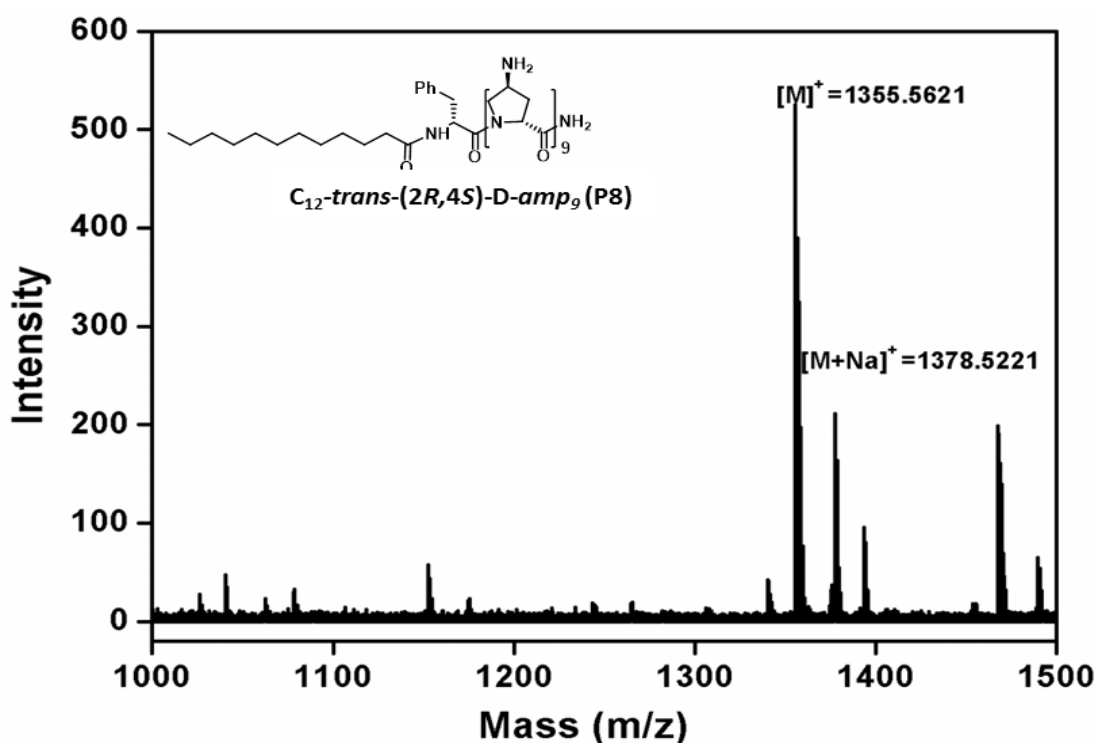
HPLC-profile of C$_{14}$-*trans*-(2*R*,4*S*)-D-*amp$_9$* (P9)
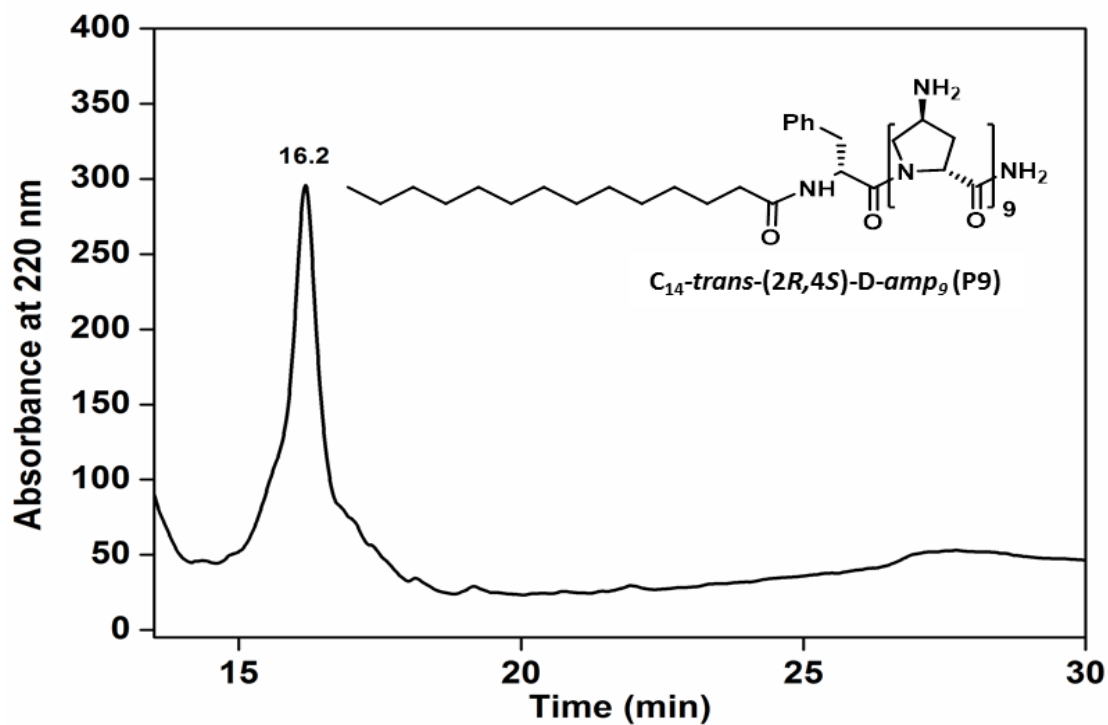
MALDI-TOF of C$_{14}$-*trans*-(2*R*,4*S*)-D-*amp$_9$* (P9)
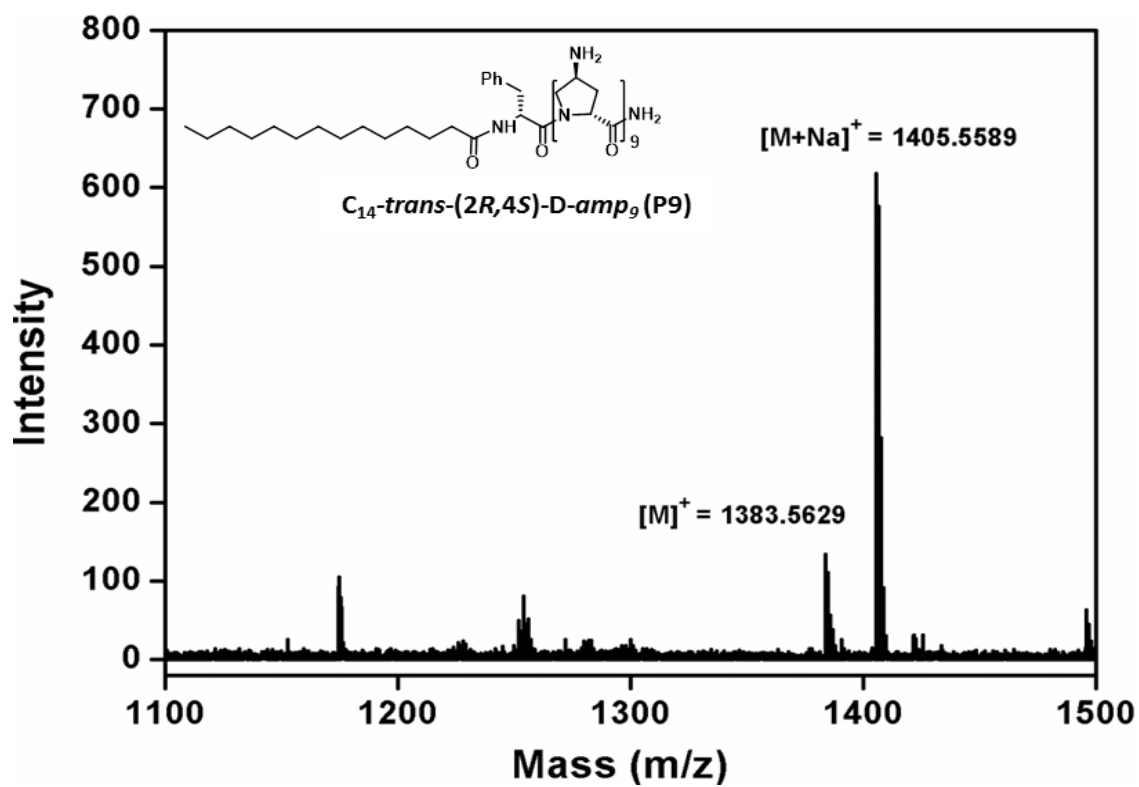
HPLC-profile of C$_{16}$-*trans*-(2*R*,4*S*)-D-*amp$_9$* (P10)
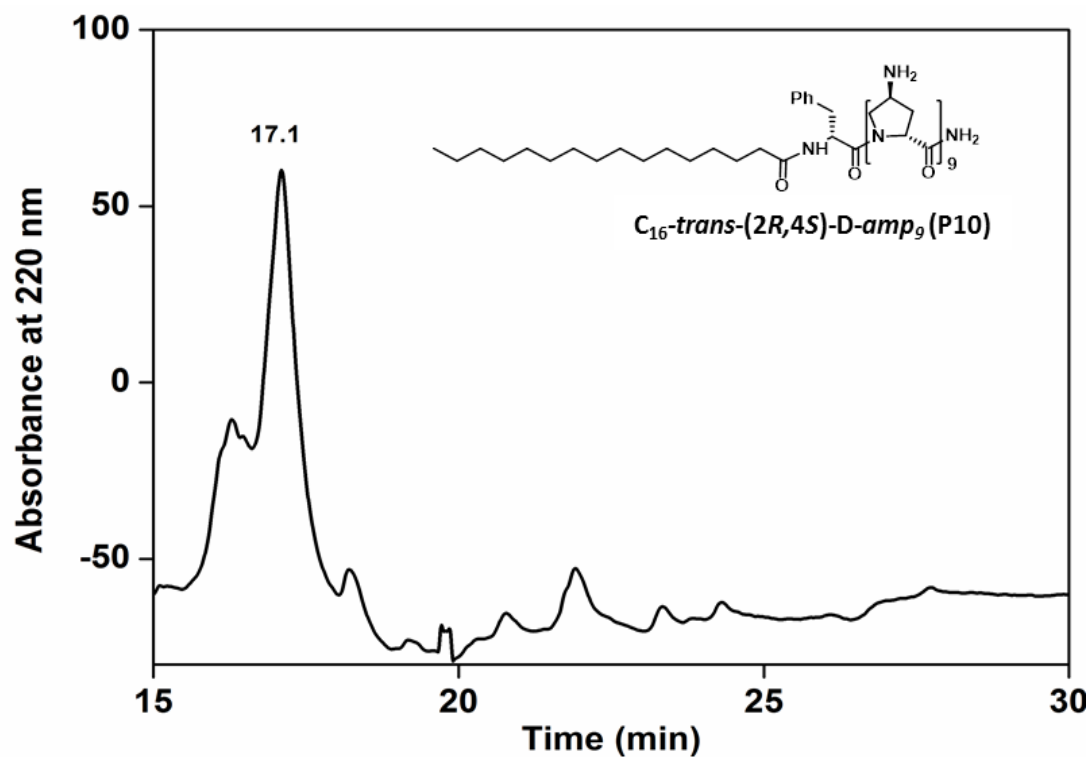
MALDI-TOF of C$_{16}$-*trans*-(2*R*,4*S*)-D-*amp$_9$* (P10)
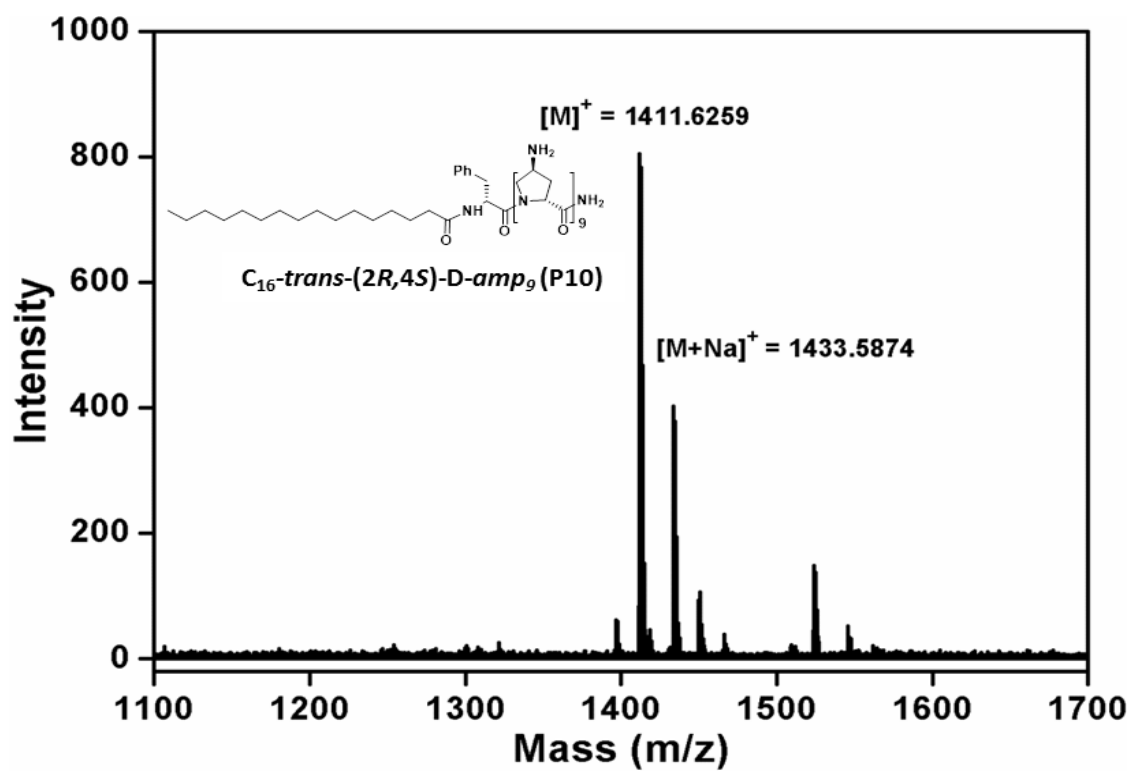
Chapter 3

Alternate and Block Heterochiral Polypeptides from 4(R/S)-Hydroxy-L/D-Proline

3.0 Introduction to chirality in biomolecules

There has been a lot of speculations and debate about the origin of chirality in biomolecules like proteins and nucleic acids. Why and how the amino acid in proteins have L-configuration while the sugars, ribose and deoxyribose, in nucleic acids have D-configuration is not known.[1,2] It is generally understood that homochirality was needed in the pre-biotic world so that proteins and nucleic acids could have their well-defined structure and carry out their specific functions properly. It is not desirable to keep structure and functions of these bio-polymers intact with a random mixture of L and D amino acid enantiomers in conjunction. Change in configuration from L to D amino acid in proteins or D to L-sugar in nucleic acids even at one monomer level results in the collapse of structure and function. But it is possible to construct the whole protein by inverting all L-amino acids to D-amino acids and such total configurational inversion of the structure (including chirality and handedness of helix) results in mirror image proteins.[3]

Specificity in biomolecular recognition is a very well-studied phenomenon. This molecular recognition happens in different ways. DNA nucleobases recognize each other by H bonding and in proteins, it occurs either through H-bonding, electrostatics interactions, hydrophobic forces or helix-helix recognition, and which are very specific interactions. Similarly, chiral recognition enables biomolecules to recognize their correct substrates.[3] Recognition properties and derived functions associated with chirality vary from point to point. There are peptides and proteins in which recognition happens through homochirality,[4-6] for e.g. in some peptides such as poly-L-lysine, poly-D-lysine where ambidextrous, recognition occurs in heterochiral species.[7,8] There are a few examples in literature where there is no specificity in recognition between homochiral and heterochiral species.[9,10]

One of the ways of expression of homochirality and heterochirality is in terms of gel formation. There are instances where homo and heterochirality are individually responsible for better gelling ability.[11-16] In one of examples, homochirality confers mechanical strength, while heterochirality influences kinetics of gel formation.[14] However, there are cases where gel formation is independent of chirality. It is possible to tune the mechanical strength and kinetics of such supramolecular aggregates by taking advantage of several factors including

chirality, side chains, temperature, etc. It is reported that chirality of supramolecular aggregates can be fine-tuned by achiral alkyl groups,[17,18] changing the solvent,[19,20] modulating the pH values,[21] ultra-sonication, and temperature.[22,23]

3.1 Naturally occurring cyclic antibiotic peptide containing L, D amino acids

In nature, several antibiotic peptides, synthesized by bacteria contain unnatural amino acids in their sequence. Tyrocidine and gramicidin D contain mixture of peptides synthesized by bacteria *Bacillus brevis*, that are antibiotics.[24] In this class of antibiotic peptides, several uncommon amino acids are present such as D-Leu, D-Val, D-Phe, ornithine. In gramicidin S (Figure 1), a dimer of two pentapeptides joined to form a cyclic decapeptide, two unnatural amino acids D-Phe and ornithine are present. This peptide is effective against gram-positive as well as gram-negative bacteria.
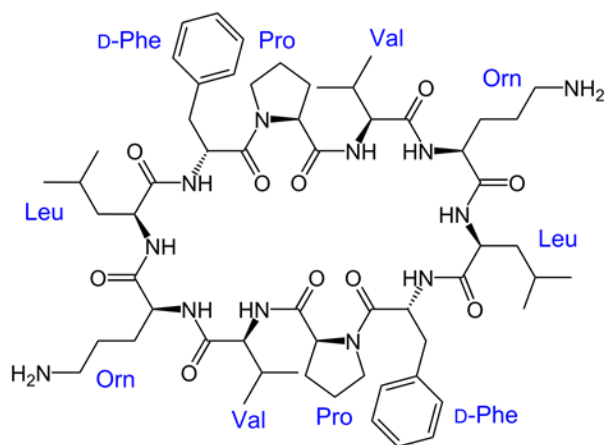
Figure 1: Chemical structure of gramicidin S.

3.2 A cyclic heterochiral peptide containing alternate L, D amino acids

Ghadiri *et al.*[25] designed and synthesized cyclic octapeptide of sequence cyclo[-(D-Ala-L-Glu-D-Ala-L-Gln)$_2$] with alternate L and D amino acids. Under protonated conditions, the peptide crystallized into a long tubular structure. Based on this, they designed new cyclic peptide which acts as artificial transmembrane ion channel due to the self-assembling property to form nanotubes.[26]
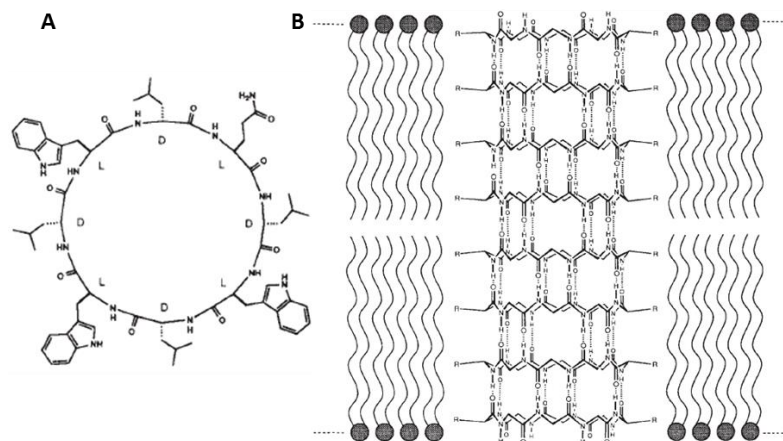
Figure 2: A) Cyclic peptide[-(D-Ala-L-Glu-D-Ala-L-Gln)$_2$] with alternate LD amino acids **B)** Nanotube formation of the cyclic octapeptide.[26]

3.3 Linear heterochiral peptide containing L, D amino acids in the sequence

Yang *et al.*[27] synthesized homochiral and heterochiral dipeptides containing phenylalanine and alanine (Phe-Ala) and conjugated lipid chain at the end. In this study, they observed that homochiral lipopeptides self-assemble into parallel β sheets whereas heterochiral lipopeptides self-assemble into antiparallel β sheet structures.
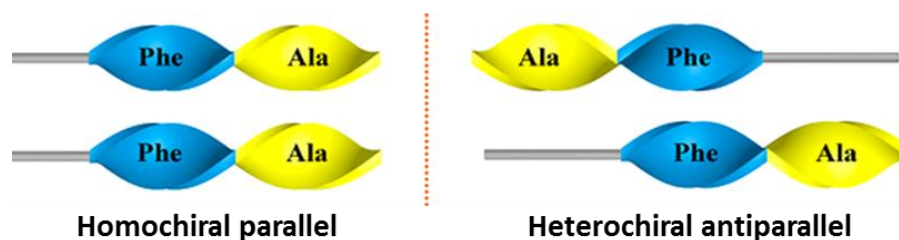
Figure 3: Packing of homochiral and heterochiral lipodipeptides.[27]

3.4 Linear heterochiral peptides containing L, D amino acids

Blood brain barrier (BBB) protects the brain against external agents by regulating molecular transport through it and not allowing the therapeutic molecules to pass through. For this reason, treatment of the brain related diseases are hard and hence to overcome this problem, diverse approaches have been made to induce crossing of BBB.

Giralt *et. al.*[28] used chirality approach to address BBB problem. They designed and synthesized phenyl proline (Phe-Pro)$_4$ based 16 stereoisomers of tetrapeptide and conjugated therapeutically relevant cargos nipecotic acid and L-3,4-dihydroxyphenylalanine (L-DOPA). Using conformational and chiral effects originating from these different stereoisomers, they were successful to make them cross the lipid bilayer of BBB. In this study, it was observed that peptides with homochirality (LLLL/DDDD) have the highest values of transport while heterochiral (LDDL/DLLD) have the lowest values of transport. Alternate heterochiral tetrapeptide (LDLD/DLDL) show moderate transport values between enantiomers.
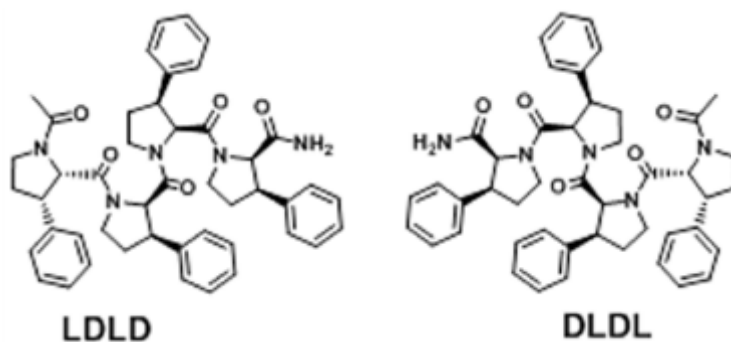
Figure 4: Chemical structure of heterochiral (PhePro)$_4$ peptides.[28]

3.5 Linear homochiral polypeptides of 4(*R/S*) hydroxyl/amino substituted L/D proline

Ganesh *et al.*[29-31] established that hydrogen bonding substituents such as (NH$_2$/OH/NHCHO) at C4 position on proline and in *cis* stereochemistry with respect to C2 show solvent specific switching and form *β*-structure in TFE through side chain hydrogen bonding. Solvent-dependent switching of conformation between PP-II in water and *β*-structure in TFE has been observed in case of various proline polypeptides of *cis*-(2*S*,4*S*)-L-*amp*$_9$ (**P11**), *cis*-(2*R*,4*R*)-D-*Amp*$_9$ (**P3**), *cis*-(2*S*,4*S*)-L-*hyp*$_9$ (**P13**) and *cis*-(2*R*,4*R*)-D-*hyp*$_9$ which form antiparallel *β*-sheet in TFE (chapter 2). However, this observed only when substituents at C2 and C4 are in *cis* disposition.[29-31] Further, it was shown that when 4-hydroxyproline peptide *cis*-(2*S*,4*S*)-L-*hyp*$_9$ (**P13**) is, conjugated with fatty acids, self-assembly in TFE leads to nanofibers (Figure 5A). Without fatty acid conjugation, hydroxyl proline peptide self-assembles to form nanospheres. Hydrophobic groups like fatty carbon chain are needed to enhance the molecular interaction to have well-defined self-assembled

nanofibres.[31] In contrast, the peptide **P16** *cis*-(2*R*,4*R*)-D-*Hyp*$_9$ on conjugation with different lengths of fatty acids does not self-assemble into nanofibres and remain as aggregates of nanospheres (Figure 5C).
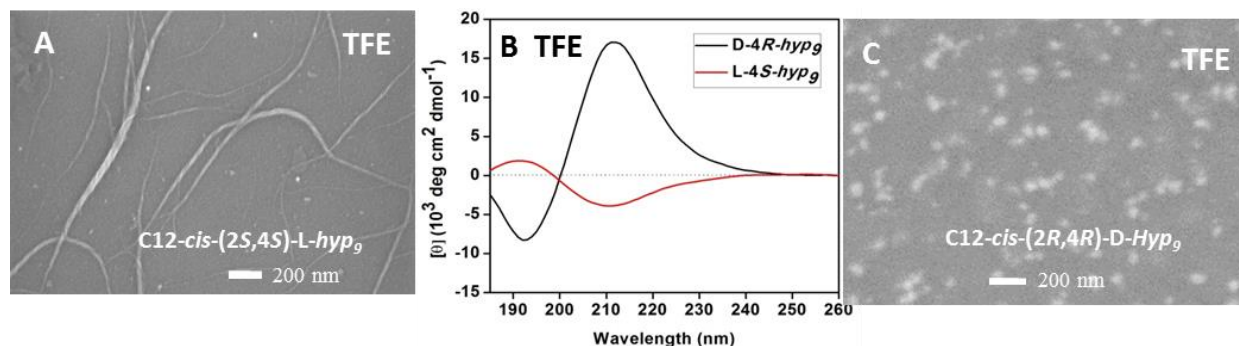
Figure 5A & C: FE-SEM images of **P15** C$_{12}$-*cis*-(2*S*,4*S*)-L-*hyp*$_9$,[31] and **P17** C$_{12}$-*cis*-(2*R*,4*R*)-D-*Hyp*$_9$ in TFE. **B)** CD spectra of **P13** *cis*-(2*S*,4*S*)-L-*hyp*$_9$ and **P16** *cis*-(2*R*,4*R*)-D-*Hyp*$_9$ in TFE.

3.6 Rationale and objectives of the present work

In 1953, Linus Pauling proposed structural models for polypeptides in the form of α-helix and β-sheet. In β-sheets two types are possible i.e. pleated and rippled sheet structure with parallel and antiparallel orientations.[32] The structure described are applicable for polypeptides constructed entirely from L-amino acids or of D-amino acid residues (homochiral peptides). He proposed that similar rippled sheet structures could be constructed with polypeptide chains having alternate D and L amino acid residues (heterochiral).

Helices from peptides with alternate L, D amino acids have been described by several authors.[33-36] These regular structures have basic D, L-dipeptide repeating units form either single or double stranded helices.[35] Such structures observed experimentally and supported by theoretical calculations are composed with torsional angles of the enantiomers located in respective *β* regions of Ramachandran plot.

With this rationale, it was thought to synthesize and study heterochiral alternate, and block prolyl polypeptides derived from L-proline and D-proline with 4(*R*/S) hydroxyl substitutions at C4 position. As hypothesized in literature, one can expect specific

conformational states adopted by these peptides to result in interesting orderly self-assembled structures.

Thus the main objective of this work is to synthesize, characterize and carry out conformational studies of heterochiral alternate and block polyproline peptides and examine the range of morphological structures controlled by stereochemistry at C2 and C4 of proline.

Specific objectives are:

❖ Synthesis of (2R,4R) / (2R,4S) / (2S,4S), N1-(Fmoc)-4-O-(*t-butoxycarbonyl*)-D/L-proline monomers.

❖ Solid phase synthesis of various polyprolyl peptides, purification & characterization.

❖ Investigation of the conformation of alternate and block polyproline peptides **P1-P12** by CD-spectroscopy.

❖ Self-assembly of peptides studied by imaging techniques AFM, FE-SEM.

P1

Alternate-L-Phe-L-Pro[L-*Pro*-D-*Pro*]₄

P2

Alternate-L-Phe-*trans*-(2S,4R)-L-*Hyp*[-*trans*-(2S,4R)-L-*Hyp*-*cis*-(2S,4R)-L-*hyp*]₄

P3

Alternate L-Phe-*trans*-(2S,4R)-L-*Hyp*[*trans*-(2S,4R)-L-*Hyp*-*trans*-(2R.4S)-D-*hyp*]₄

P4

Alternate-D-Phe-*trans*-(2R,4S)-D-*hyp*[*trans*-(2R,4S)-D-*hyp*-*trans*-(2S,4R)-L-*Hyp*]₄

P5

Alternate-L-Phe-*cis*-(2S,4S)-L-*hyp*[*cis*-(2S,4S)-L-*hyp*-*cis*-(2R,4R)D-*Hyp*]₄

P6

Alternate-D-Phe-*trans*-(2S,4R)-L-*Hyp*[*trans*-(2R,4S)-D-*hyp*-*trans*-(2S,4R)-L-*Hyp*]₄

P7

Alternate-L-Phe-*trans*-(2R,4S)-D-*hyp*-[*trans*-(2S,4R)-L-*Hyp*-*trans*-(2R,4S)-D-*hyp*]₄

P8

Alternate *Phenylacyl*-[*trans*-(2S,4R)-L-*Hyp*-*trans*-(2R,4S)-D-*hyp*-]₄

P9

Block-L-Phe-[*cis*-(2S,4S)-L-*hyp*]₄-[*trans*-(2S,4R)-L-*Hyp*]₄

P10

Block D-Phe-[*trans*-(2R,4S)-D-*hyp*]₄-*trans*-(2S,4R)-L-*Hyp*]₅

P11

Block D-Phe-[*cis*-(2R,4R)-D-*Hyp*]₄-[*cis*-(2S,4S)-L-*hyp*]₅

P12

Alternate C₁₄-L-Phe-*trans*-(2S,4R)-L-*Hyp*[-*trans*-(2R.4S)-D-*hyp*-*trans*-(2S,4R)-L-*Hyp*]₄

3.7 Synthesis of monomers 18, 21 and peptides P1-P12

The monomers 1**8** and **21** required for assembly of various polypeptides were synthesized by following standard protection and de-protection chemistry. Compound **3** *cis*-(2*R*,4*R*)-N1-(benzyloxycarbonyl)-4-hydroxy-D-proline methyl ester was synthesized as described in previous Chapter 2.

(18)   (21)
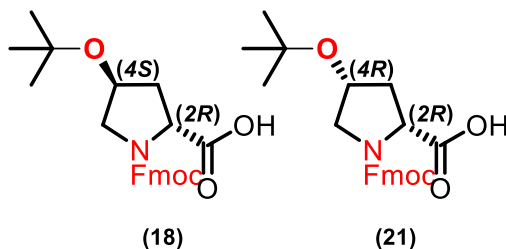
3.7.1 Synthesis of *trans*-(*2R,4S*)-4-hydroxyl-D-proline monomer (18)

The synthesis of 4*S*-OH-proline (**14**) from 4*R*-OH proline **3** was done by reacting **3** with DCC in presence of a catalytic amount of CuCl followed by treatment with formic acid. Hydrolysis with aq. NaOH yielded *trans*-(2*R*,4*S*)-4-hydroxy-D-proline acid **14**. This was esterified to compound **15** and 4*S*-hydroxyl group was protected with *tert*-butylbromide to compound **16**, followed by hydrolysis of ester with aq. LiOH. The deprotection of Cbz in **16** was done by hydrogenation condition to yield 4*S*-O-*t*-butyl acid **17.** This was reacted with Fmoc-Cl to obtained monomer **18** *trans*-(2*R*,4*S*)-4-hydroxy-D-proline. All compounds were characterized by ^{1}H NMR and mass spectrometry.

Scheme 1: *Synthesis of trans-(2R,4S)-4-hydroxyl-D-proline monomer 18*

117
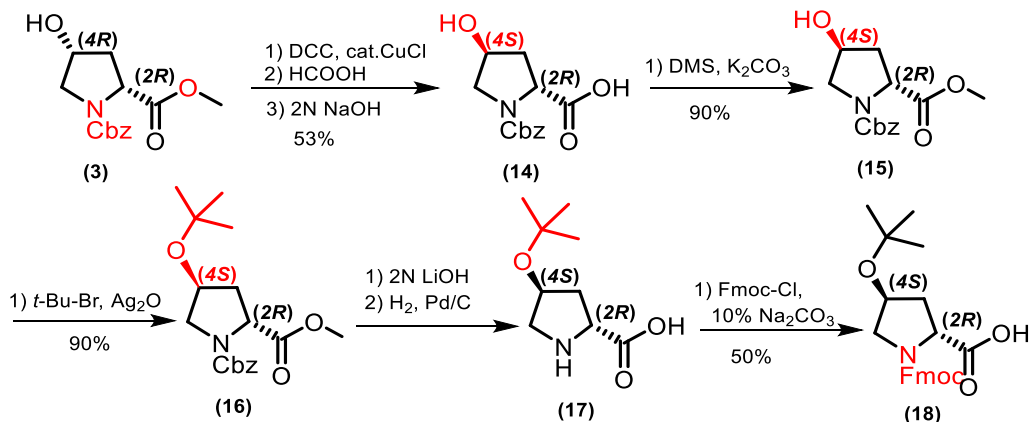
3.7.2 Synthesis of *cis*-(*2R,4R*)-4-hydroxyl-D-proline monomer (21)

cis-(*2R,4R*)-4-(OH)-D-proline monomer **21** was synthesized from compound **3** as follows. 4*R*-hydroxyl group in compound **3** was protected with *tert*-butylbromide to obtain compound **19**, followed by hydrolysis of ester with aq. LiOH. The deprotection of Cbz group was done under hydrogenation condition to yield 4*R*-O-*t*-butyl acid **20**. The desired monomer **21** [N1-Fmoc-4*R*-(O-*t*-butyl)-(2*R*)-D-proline] was synthesized from compound **10** by reacting with Fmoc-Cl. Corresponding *cis*-L-monomer **22** [N1-Fmoc-4*S*-(O-*t*-butyl)-(2*S*)-L-proline] was synthesized by a known procedure reported in literature.[31]

Scheme 2: *Synthesis of (2R,4R)-4-hydroxyl-D-proline monomer 21*
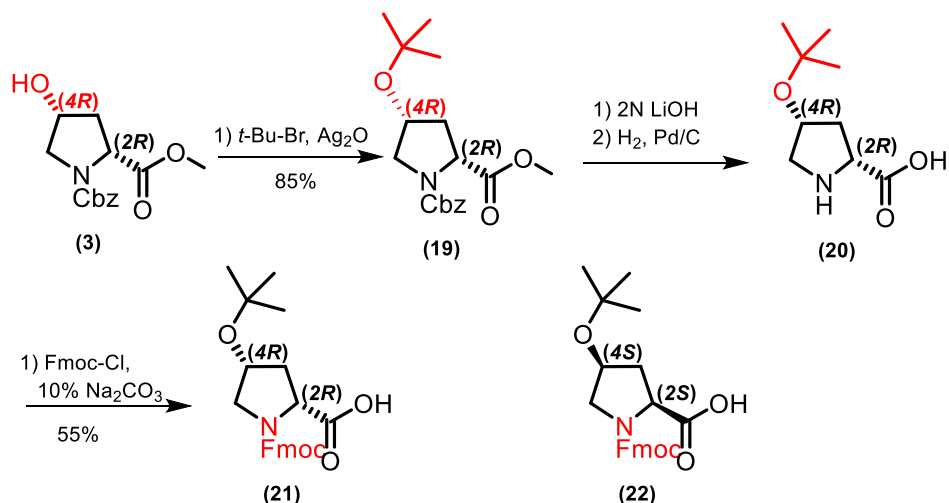
3.7.3 Solid phase peptide synthesis of P1-P12

The desired peptides **P1-P12** were synthesized manually on a solid phase by using standard Fmoc strategy, using readily available Nova biochem rink amide resin. Fmoc group on resin was deprotected by 20% piperidine in DMF, and the appropriate proline acid monomers were coupled by using HBTU coupling agent, with HOBt as racemization suppressor and DIPEA as a catalyst in DMF solvent. This was followed by coupling with subsequent monomers in the order of peptide sequence to reach the desired length. For the quantitative determination of peptides UV-absorbing aromatic amino acid (L/D) phenylalanine was attached to the N-terminus end and the peptide was acetylated using acetic anhydride in pyridine.

The synthesized peptides were cleaved from the solid support by treatment with 90% trifluoroacetic acid (TFA) in DCM containing triisopropylsilane (TIPS) used as a scavenger to prevent N-alkylation. The peptides were purified by HPLC using RP-C18 column in an acetonitrile-water solvent system containing 0.1% TFA.

Scheme 3: *Solid phase synthesis protocol for alternate peptides (**P1-P8** & **P12**)*
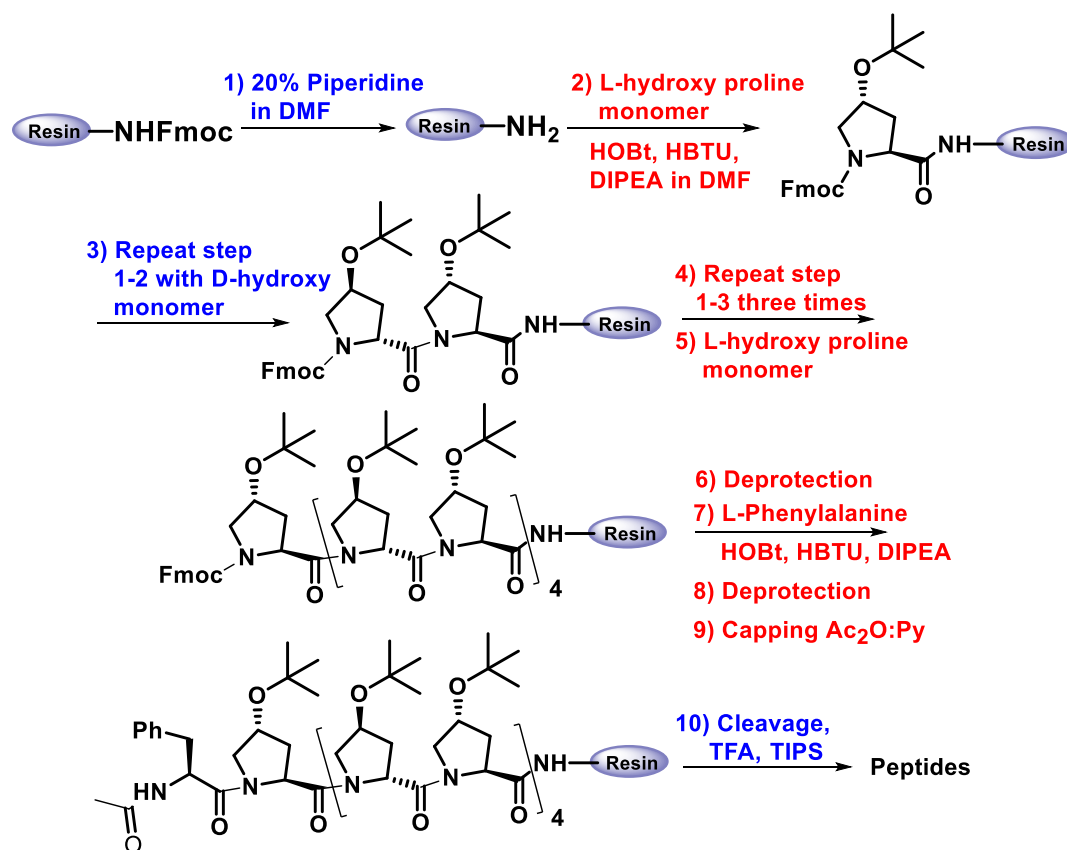
The various 4-substituted prolyl polypeptides **P1-P8** with alternating chiral monomers or block peptides were synthesized by solid phase peptide synthesis using appropriate monomers. Peptides **P1-P3** & **P7** were coupled with L-phenylalanine, whereas the peptides **P4** and **P6** were coupled with D-phenylalanine. In case of peptide **P8** achiral phenyl acetic acid was coupled to N-terminus. The peptide **P3** was conjugated to myristic acid (C14) to get peptide **P12**.

The block polyproline peptides **P9-P11** were synthesized in similar manner by using the same monomer repeated to half-length and then switching to the next appropriate monomer to get the desired length. The peptides **P1**-**P12** were successfully cleaved from solid support, purified by reverse phase HPLC and characterized by MALDI-TOF analysis. The retention time and observed masses of **P1-P12** are given in Table 1.
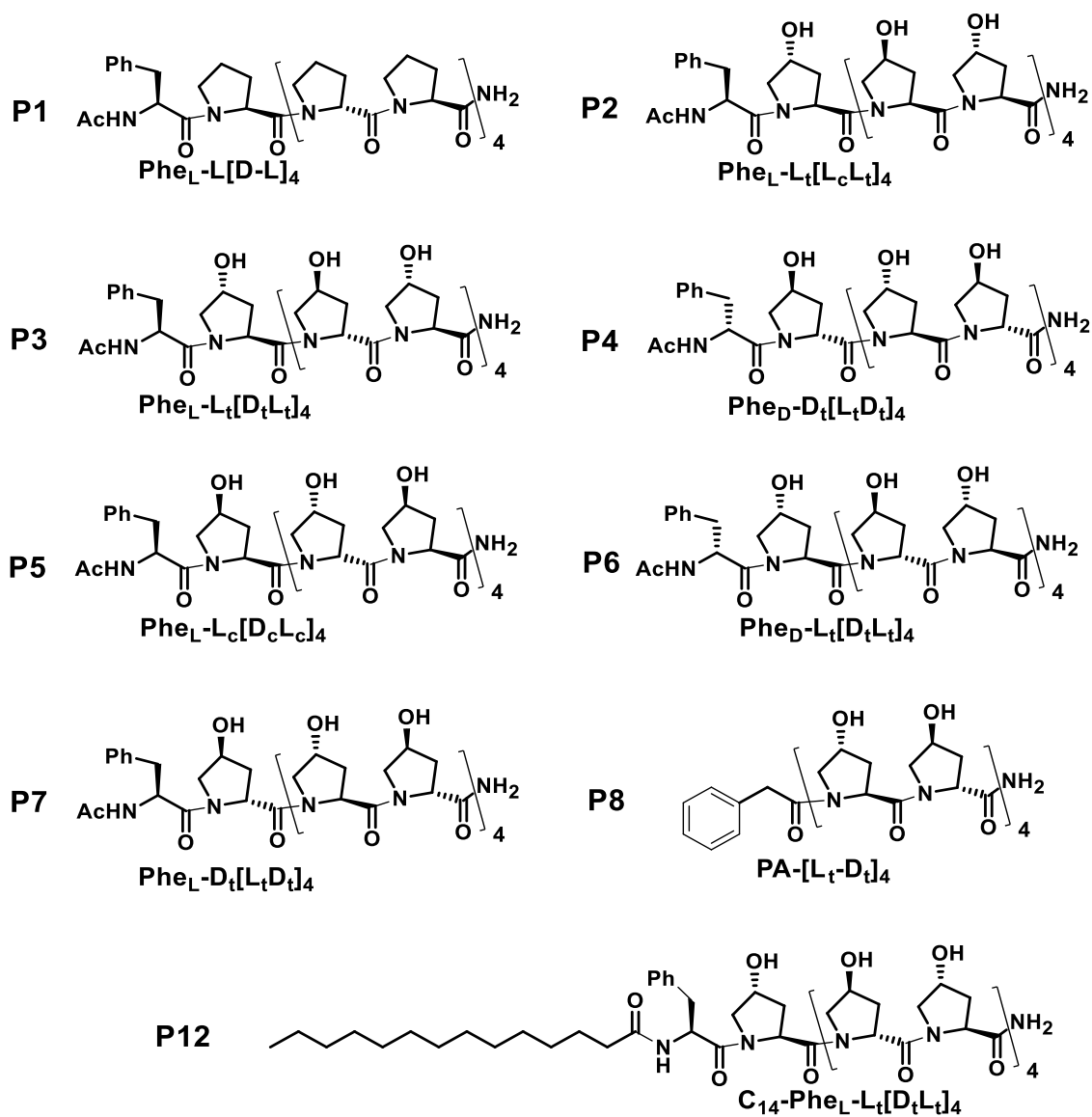
Scheme 4: *Solid phase synthesis protocol for block peptides (**P9-P11**)*

$$Phe_L[L_c]_4[L_t]_5$$

$$Phe_D[D_t]_4[L_t]_5$$

$$Phe_D[D_c]_4[L_c]_5$$
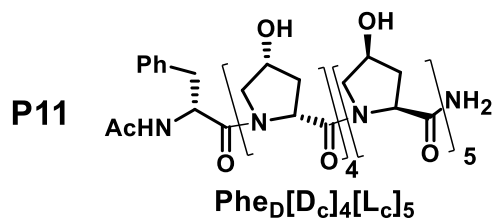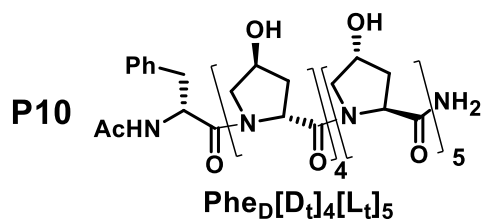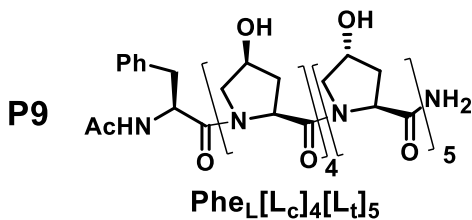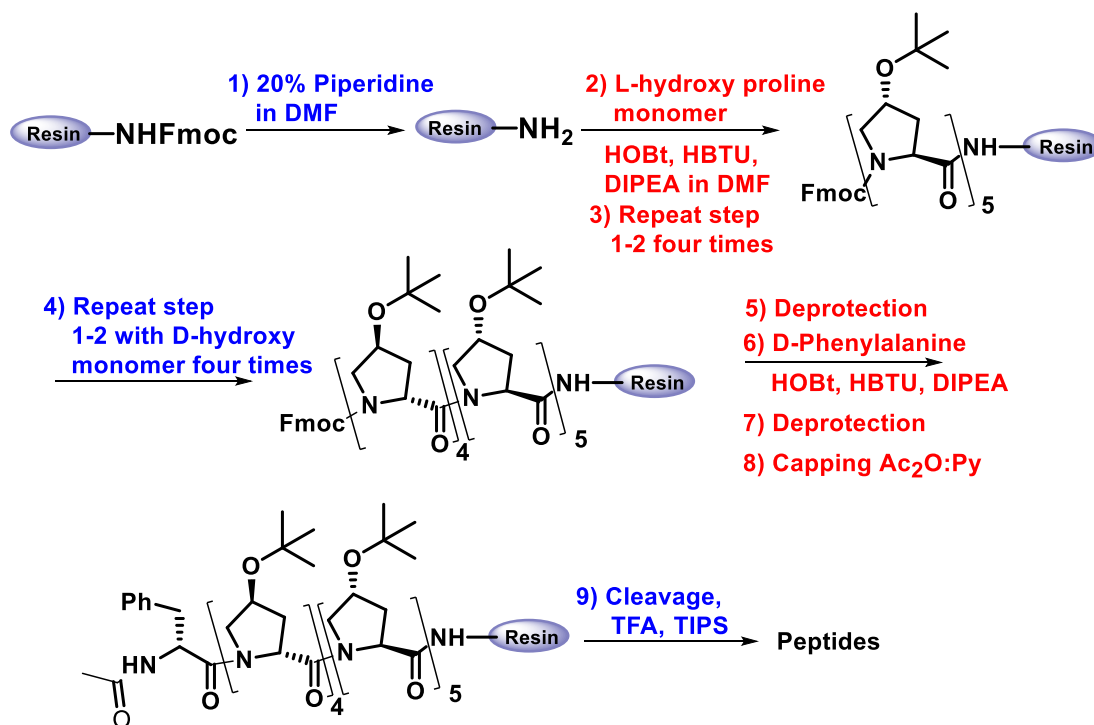
Table1: Purification and characterization of peptides **P1-P12**

Pep. No	Peptide Name	Ret. Time	Calculated Mass	Observed Mass
P1	Phe_L-$L[DL]_4$	22.3	[M+Na] 1102.5700	1102.6429
			[M+K] 1118.5400	1118.6012
P2	Phe_L-$L_t[L_cL_t]_4$	15.0	[M+Na] 1246.5244	1246.7220
			[M+K] 1262.4983	1262.6910
P3	Phe_L-$L_t[D_tL_t]_4$	14.5	[M+Na] 1246.5244	1246.4721
			[M+K] 1262.4983	1262.4335
P4	Phe_D-$D_t[L_tD_t]_4$	15.1	[M+Na] 1246.5244	1246.4721
			[M+K] 1262.4983	1262.4335
P5	Phe_L-$L_c[D_cL_c]_4$	15.5	[M+Na] 1246.5244	1247.1100
			[M+K] 1262.4983	1263.0850
P6	Phe_D-$L_t[D_tL_t]_4$	15.0	[M+Na] 1246.5244	1246.6644
			[M+K] 1262.4983	1262.6229
P7	Phe_L-$D_t[L_tD_t]_4$	15.5	[M+Na] 1246.5244	1246.6740
			[M+K] 1262.4983	1262.6544
P8	PA-$[L_tD_t]_4$	14.5	[M+Na] 1062.4396	1062.6208
			[M+K] 1078.4135	1078.6100
P9	Phe_L-$[L_c]_4[L_t]_5$	15.2	[M+Na] 1246.5244	1246.4841
			[M+K] 1262.4983	1262.4410
P10	Phe_D-$[D_t]_4[L_t]_5$	14.6	[M+Na] 1246.5244	1246.2311
			[M+K] 1262.4983	1262.2140
P11	Phe_D-$[D_c]_4[L_c]_5$	15.2	[M+Na] 1246.5244	1246.2341
			[M+K] 1262.4983	1262.2140
P12	C_{14}-$Phe_LL_t[D_tL_t]_4$	13.1	[M+Na] 1414.7122	1414.8835
			[M+K] 1430.6861	1430.8544

3.7.4 Determination of the peptide concentration in the stock solution

To determine the concentrations of the peptides, the UV-absorbing aromatic amino acid phenylalanine (L/D-Phe) was incorporated at the N-terminus. The concentrations of peptide stock-solutions were determined by absorbance of phenylalanine at 257 nm and using extinction coefficient of 195 $M^{-1}cm^{-1}$. The choice of employing D or L-phenylalanine depends on the sequence to maintain homochirality over the complete peptide or in blocks. Since all peptides contained phenylalanine at N-terminus, any effect from this residue on polyproline helix would be same for all peptides.

3.8 RESULTS AND DISCUSSION

In this chapter CD spectroscopic technique was used to determine the secondary strucutures of synthesized heterochiral alternate and block prolyl polypeptides **P1**-**P12**.

3.9 Circular dichroism study of peptides: Role of solvents

The peptide conformation is dependent on the nature of solvent.[38] The effect of trifluoroethanol,[39] in terms of causing the transition from PP-II to *β*-structure in case of peptide **P11** *cis*-(2S,4S)-L-*amp*9,[29] **P13** *cis*-(2S,4S)-L-*hyp*9[31] and **P15** *cis*-(2R,4R)-D-*Amp*9 is described in the previous Chapter 2. The reported peptides are homochiral, made from purely L or D proline. The effect of a hydrophobic solvent such as TFE was studied on the conformations of heterochiral alternating and heterochiral block peptides.

Among the synthesized alternating heterochiral peptides, **P1** (Phe$_L$-L[L-D]$_4$), **P2** (Phe$_L$-L$_t$[L$_c$L$_t$]$_4$), **P4** (Phe$_D$-D$_t$[L$_t$D$_t$]$_4$), **P5** (Phe$_L$-L$_c$[D$_c$L$_c$]$_4$), **P7** (Phe$_L$-D$_t$[L$_t$D$_t$]$_4$) and block heterochiral peptides **P9** (Phe$_L$-[L$_c$]$_4$[L$_t$]$_5$), **P10** (Phe$_D$-[D$_t$]$_4$[L$_t$]$_5$) and **P11** (Phe$_D$-[D$_c$]$_4$[L$_c$]$_5$) exhibited solvent dependent conformational change. In aqueous medium (sodium phosphate buffer) these peptides adopt left-handed PP-II conformation and in TFE they show random conformation and not *β*-structure as was seen in homochiral cis-peptides.

3.9.1 CD spectra of peptide P1 (Phe$_L$-L[LD]$_4$)

In the previous chapter, it was shown that unsubstituted L-*Pro*$_9$ shows less intense positive band at 225 nm and a strong negative CD band at 210 nm with crossover at 220 nm in sodium phosphate buffer, which is characteristic feature of left-handed PP-II. The CD spectra of peptide **P1** having alternate L-*Pro*-D-*Pro* in sodium phosphate buffer in the concentration range from 50-200 μM is shown in (Figure 6A). A small positive CD band at 225 nm, relatively less intense negative CD band at 208 nm with crossover around 220 nm were seen suggesting left-handed PP-II structures. This spectra is similar to that seen for L-*Pro*$_9$. It was also observed that change in concentration has no effect on conformation.

The CD spectra of peptide **P1** (Phe$_L$-L[LD]$_4$) in the concentration range 50-200 μM in TFE shows a strong negative band around 213 nm and absence of any band at 225 nm suggesting that peptide **P1** adopts random type conformation. In hydrophilic solvent like water, peptide **P1** (Phe$_L$-L[LD]$_4$) showed PP-II left-handed conformation, whereas in TFE it showed random conformation (Figure 6B). Alternate stereochemistry (*S/R*) at the C2 position in polyproline seems to have effect on the conformation in hydrophobic solvent.
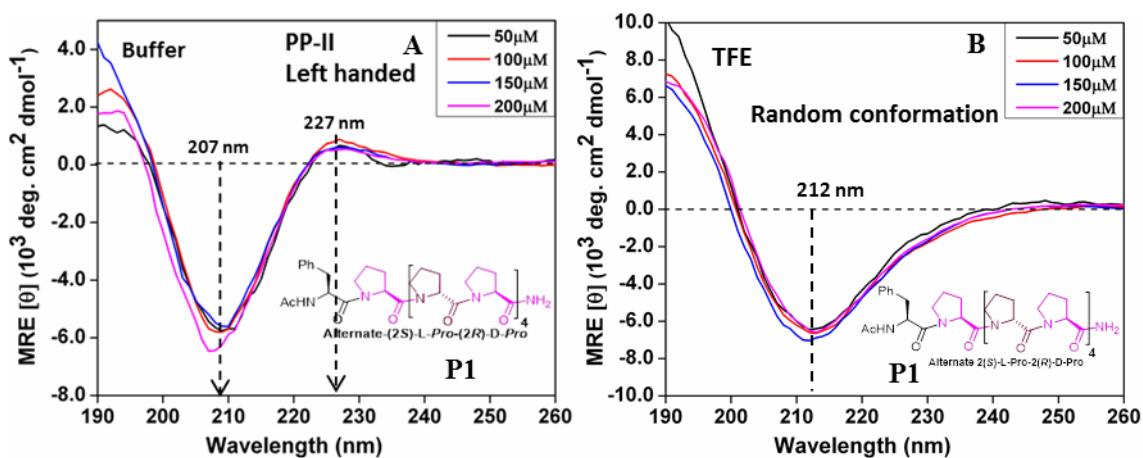
Figure 6: CD spectra of the peptide **P1** (Phe$_L$-L[LD]$_4$) in the concentration range 50-200 μM **A)** in buffer and **B)** in TFE.

3.9.2 CD spectra of peptide P4 (Phe$_D$-D$_t$[L$_t$D$_t$]$_4$)

The L/D alternating peptide **P4** (Phe$_D$-D$_t$[L$_t$D$_t$]$_4$) shows a positive CD band at 225 nm and a less intense negative CD band at 200 nm, which is indicative of weak PP-II left-handed conformation in buffer (Figure 7A). In comparision, in TFE, the positive CD band at 225 nm disappeared and only one strong positive CD band at 214 nm was observed suggesting that the peptide **P4** (Phe$_D$-D$_t$[L$_t$D$_t$]$_4$) adopts random conformation in TFE (Figure 7B).
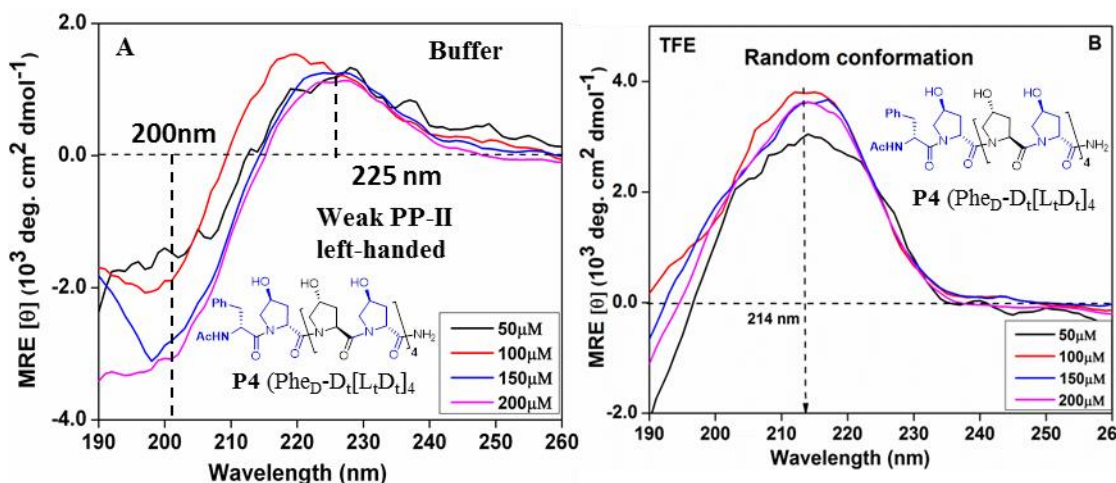
Figure 7: CD spectra of the peptide **P4** (Phe$_D$-D$_t$[L$_t$D$_t$]$_4$) in the concentration range 50-200 μM **A)** in buffer and **B)** in TFE.

3.9.3 CD spectra of peptide P5 (Phe$_L$-L$_c$[D$_c$L$_c$]$_4$)

Figure 8 shows the CD spectra of peptide **P5** (Phe$_L$-L$_c$[D$_c$L$_c$]$_4$), in the concentration range 50-200 μM. In sodium phosphate buffer, peptide **P5** (Phe$_L$-L$_c$[D$_c$L$_c$]$_4$) shows a strong negative CD band at 208 nm and negligible positive band at 220 nm, indicating no defined conformation for the peptide **P5** (Figure 8A). The peptide **P5** (Phe$_L$-L$_c$[D$_c$L$_c$]$_4$) in TFE shows an intense negative CD band at 215 nm and the absence of any CD band at higher wavelength indicates a random conformation for this peptide (Figure 8B).
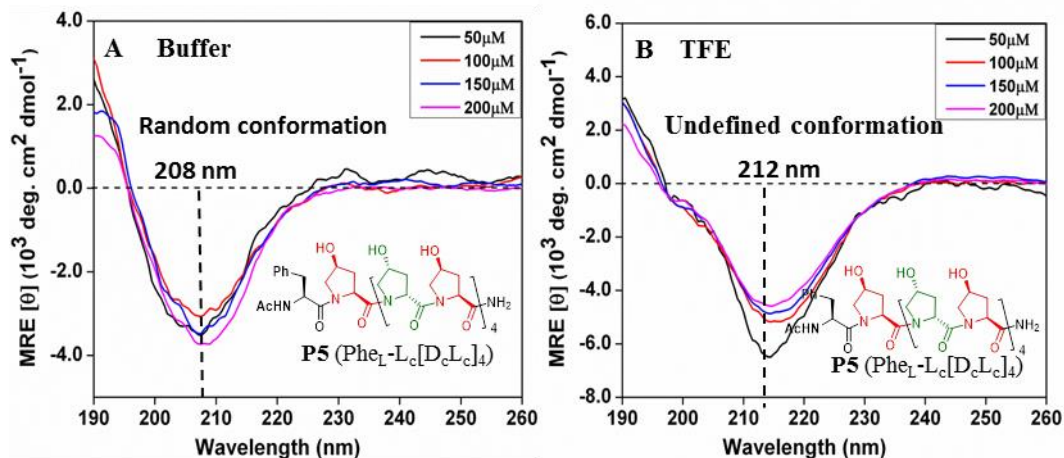
Figure 8: CD spectra of peptide **P5** (Phe$_L$-L$_c$[D$_c$L$_c$]$_4$), in the concentration range 50-200 μM **A)** in buffer and **B)** in TFE

3.9.4 CD spectra of heterochiral peptide P7 (Phe$_l$-D$_t$[L$_t$D$_t$]$_4$)

Figures 9A-B are the CD spectra of peptide **P7** (Phe$_L$-D$_t$[L$_t$D$_t$]$_4$) in the concentration range 50-200 μM. In buffer, the peptide **P7** shows a strong negative CD band at 205 nm and absance of positive CD band around 220 nm which indicates that the peptide **P7** (Phe$_L$-D$_t$[L$_t$D$_t$]$_4$) has random conformation in buffer (Figure 9A). In TFE, the peptide **P7** (Phe$_L$-D$_t$[L$_t$D$_t$]$_4$) shows one strong negative CD band at 218 nm indicating that peptide **P7** has no recognisable conformation (Figure 9B).
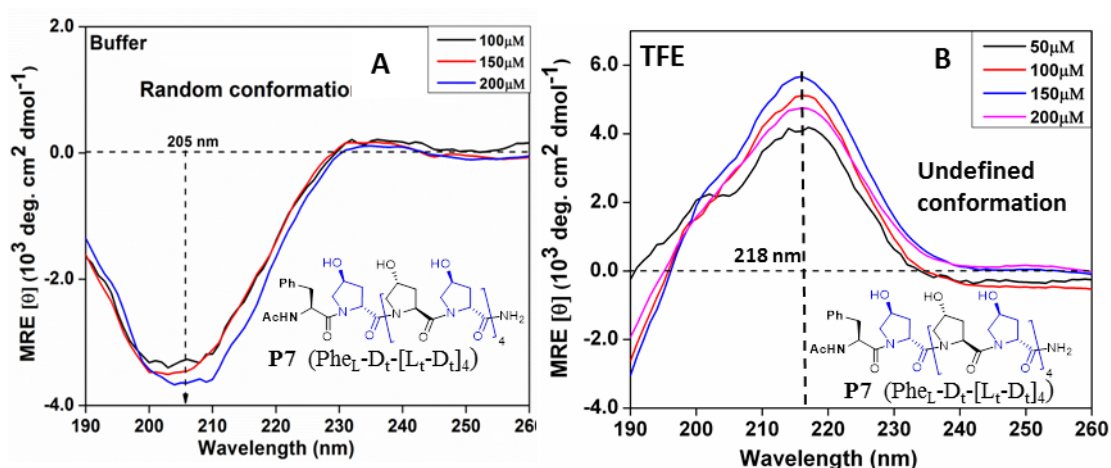
Figure 9: CD spectra of peptide **P7** (Phe$_L$-D$_t$[L$_t$D$_t$]$_4$) in the concentration range 50-200 μM **A)** in buffer and **B)** in TFE

3.9.5 CD spectra of homo oligomeric peptide P2 (Phe$_L$-L$_t$[L$_t$L$_c$]$_4$)

In order to examine the stereospecific effect of 4(*R/S*)-OH group on proline, peptide **P2**, with alternating *trans*-(2*S*,4*R*)-L-*Hyp*-*cis*-(2*S*,4*S*)-L-*hyp* unit was examined. The CD spectra of homo oligomeric peptide **P2** (Phe$_L$-L$_t$[L$_t$L$_c$]$_4$) with alternating chirality in the concentration range 50-200 μM shows a positive CD band at 225 nm and a strong negative CD band at 205 nm. These are characteristics of left-handed PP-II conformation (Figure 10A). Thus peptide **P2** with alternating *R/S* stereochemistry at C4 position does not show any difference in peptide conformation compared to homochiral peptide.

Figure 10B shows the CD spectra of peptide **P2** (Phe$_L$-L$_t$[L$_t$L$_c$]$_4$) with alternating chirality (*R/S*) at C4 in TFE. The spectra exhibited a strong negative CD band at 207 nm suggesting disordered conformation in TFE for this peptide (Figure 10B). Alternate *R/S* stereochemistry at C4 on proline thus causes transition in conformation from PP-II to random in TFE. Hence alternate residues of *cis*-(2*S*,4*S*)-*hydroxy* proline in polypeptide stretch is not enough to retain *β*–structure in TFE and induces random form.
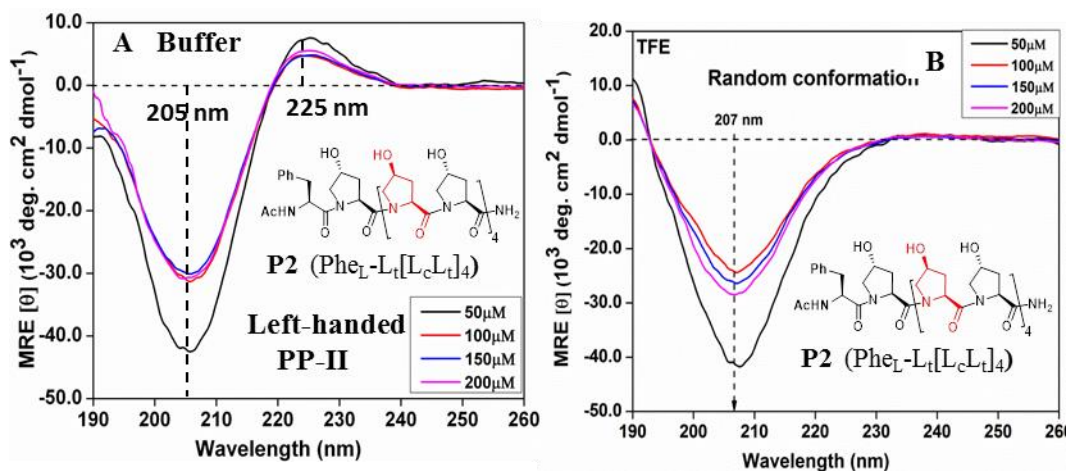
Figure 10: CD spectra of peptide **P2** (Phe$_L$-L$_t$[L$_t$L$_c$]$_4$) in the concentration range 50-200 μM **A)** in buffer and **B)** in TFE

3.9.6 CD Spectra of the block peptides P9-P11

Figures 11E-F are the CD spectra of block peptides **P9** (Phe$_L$-[L$_c$]$_4$[L$_t$]$_5$), **P10** (Phe$_D$-[D$_t$]$_4$[L$_t$]$_5$) and **P11** (Phe$_D$-[D$_c$]$_4$-[L$_c$]$_5$) in the concentration range of 50-200 μM. The peptide

P9 (Figure 11A) adapted left-handed PP-II conformation, showing two characteristic CD bands around 225 nm (positive) and 205 nm (negative), which suggests that stereochemistry at C4(R/S) of prolines in alternating peptide **P2** (Phe$_L$-L$_t$[L$_t$L$_c$]$_4$) and block peptide **P9** (Phe$_L$-[L$_c$]$_4$[L$_t$]$_5$) conform to PP-II structure in water. In TFE, the *cis-trans* alternating peptide **P2** (Phe$_L$-L$_t$[L$_t$L$_c$]$_4$) and block peptide **P9** (Phe$_L$-[L$_c$]$_4$[L$_t$]$_5$) show random conformation. The block peptides **P10** and **P11** in (Figures 11 C-F) had disordered conformation in both water and TFE.
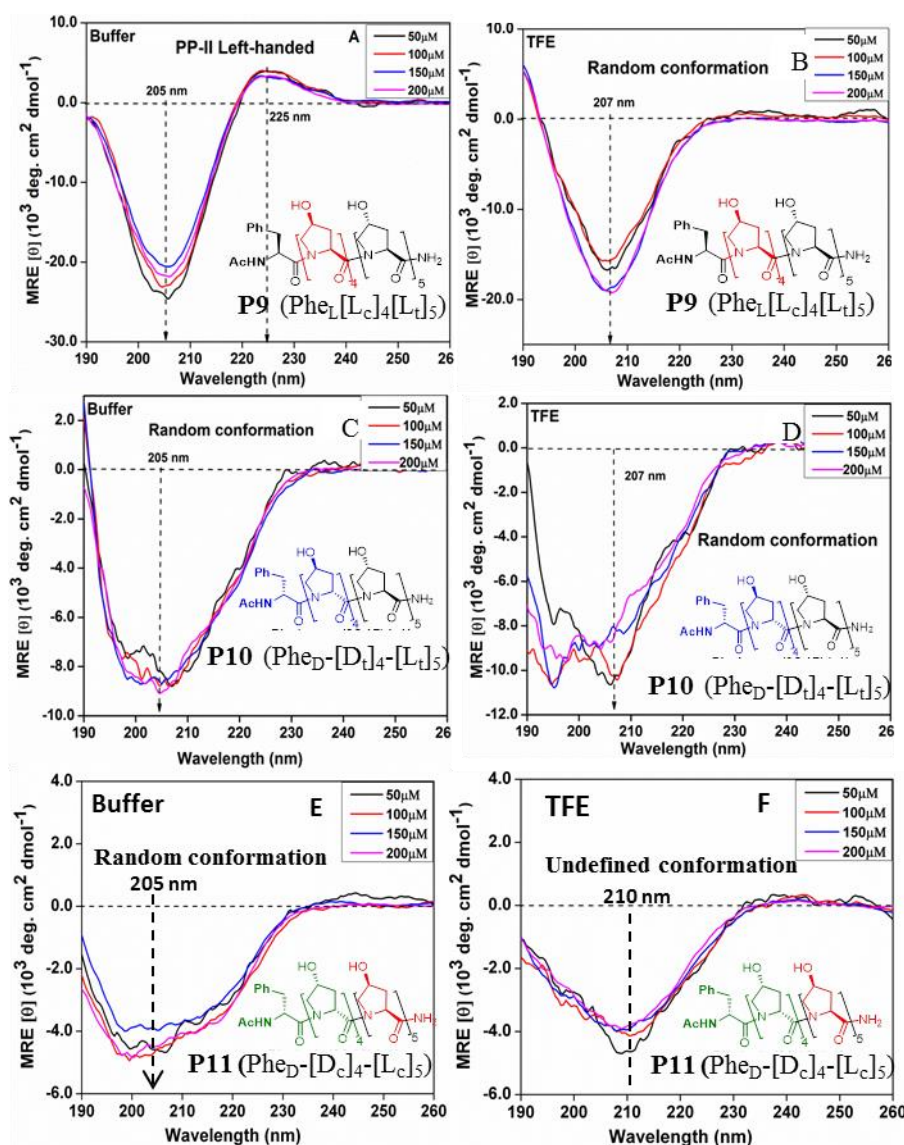
Figure 11: CD spectra of **block** peptides **P9** (Phe$_L$-[L$_c$]$_4$[L$_t$]$_5$), **P10** (Phe$_D$-[D$_t$]$_4$[L$_t$]$_5$) and **P11** (Phe$_D$-[D$_c$]$_4$-[L$_c$]$_5$) in the concentration range 50-200 μM **A, C, E)** in buffer and **B, D, F)** in TFE

3.10 CD spectra of peptides with solvent dependent conformation: PP-II in (water) to β-structure in (TFE)

Among all the heterochiral alternate and block prolyl polypeptides, only the peptide **P3** (Phe$_L$-L$_t$[D$_t$L$_t$]$_4$) and its fatty (C$_{14}$) chain conjugated peptide **P12** (C$_{14}$-Phe$_L$L$_t$[D$_t$L$_t$]$_4$) undergo solvent dependent conformational change forming two distinct conformations. In water these two peptides form left-handed PP-II conformation, whereas, in solvent TFE they form β-structure.

3.10.1 CD spectra of peptide P3 (Phe$_L$-L$_t$[D$_t$L$_t$]$_4$)

Figures 12 (A-B) are the CD spectra of chirally alternating **P3** (Phe$_L$-L$_t$[D$_t$L$_t$]$_4$) in buffer and in TFE in the concentration range of 50-200 μM. The peptide **P3** (Phe$_L$-L$_t$[D$_t$L$_t$]$_4$) shows weak positive CD band at 225 nm and a strong negative CD band at 207 nm indicative of left-handed PP-II structure in buffer (Figure 12A). In TFE, the peptide **P3** (Phe$_L$-L$_t$[D$_t$L$_t$]$_4$) shows a strong positive CD band at 218 nm and a negative band at 200 nm with cross over at 210 nm suggesting that peptide **P3** adopts D-β-structure (Figure 12B). The handedness of the D-β-structure of the peptide **P3** (Phe$_L$-L$_t$[D$_t$L$_t$]$_4$) is similar to the β-structures generated from (*cis*-(2R,4R)-D-*Amp$_9$*) as explained in Chapter 2. The factors that govern the conformation of D-proline dominate in the case of **P3** in TFE while those that govern the conformation of L-proline dominate in water.
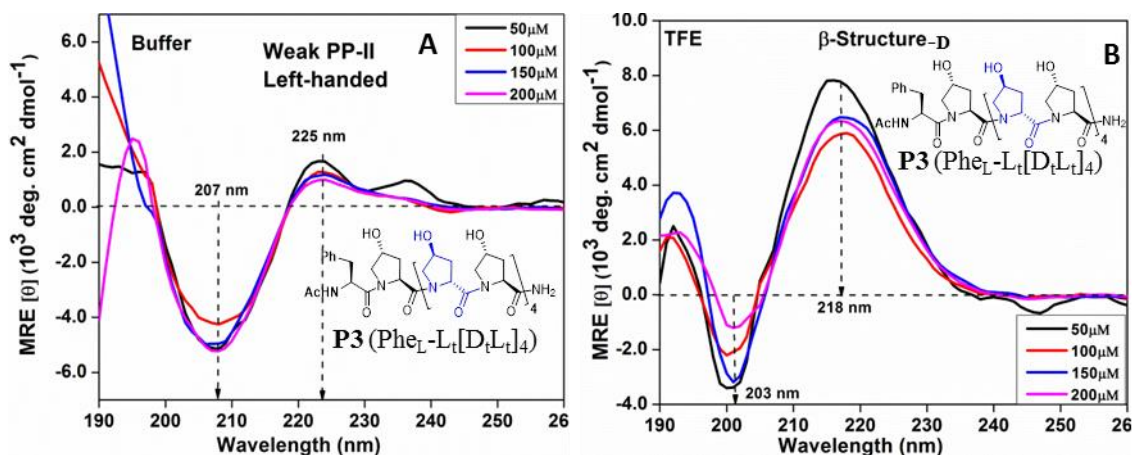
Figure 12: CD spectra of peptide **P3** in the concentration range 50-200 μM **A)** buffer and **B)** in TFE

3.10.2 CD spectra of peptide P12 (C₁₄-Phe_L L_t[D_tL_t]₄)

Figures 13 (A-B) are the CD spectra of lipidated peptide **P12** (C₁₄-Phe_L L_t[D_tL_t]₄) having (C₁₄) fatty chain conjugated at N-terminus. In buffer, CD spectra show a well-defined positive band at 225 nm and less intense negative CD band at 210 nm (Figure 13A). Myristic acid (C₁₄ fatty chain) conjugation to the peptide **P3** (Phe_L L_t[D_tL_t]₄) does not alter the PP-II conformation and stabilizes the same. In TFE, CD spectra of the peptide **P12** shows a strong positive CD band at 217 nm and similar intense negative CD band at 200 nm with crossover at 209 nm clearly representing D-β-structure conformation. Thus conjugation of the peptide with myrstic acid thus does not alter the D-β-structure.
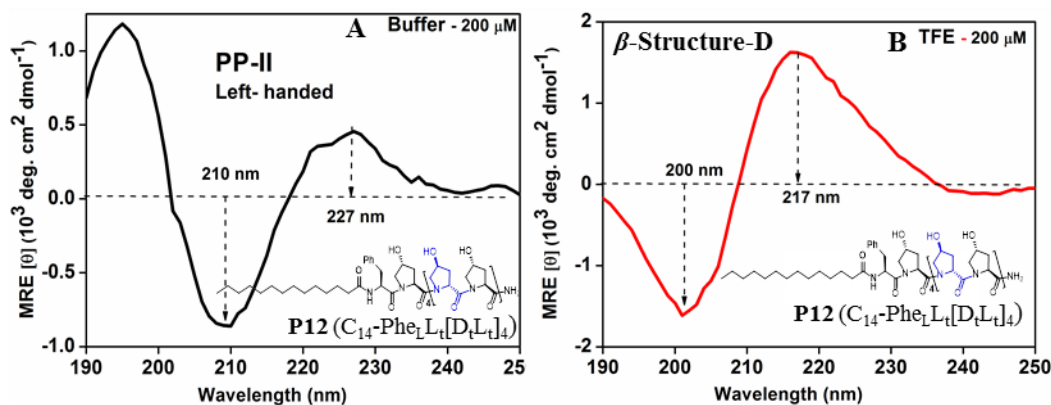
Figure 13: CD spectra of peptide **P12** (C₁₄-Phe_L L_t[D_tL_t]₄) in the concentration range 50-200 μM **A)** in buffer and **B)** in TFE.

3.11 CD spectra of peptides that show β-structure in both water & in TFE

To maintain the hetero chirality over the complete peptide and examine the effect of chirality of terminal residue in the peptide **P3** (Phe_L-L_t[D_tL_t]₄), L-phenylalanine was replaced with D-phenylalanine as in peptide **P6** (Phe_D-L_t[D_tL_t]₄) to abolish the role of chirality at N-terminus with achiral phenyl acetic acid to get the peptide **P8** (PA-[L_tD_t]₄).

3.11.1 CD spectra of peptide P6 (Phe_D-L_t[D_tL_t]₄)

The chirality of N-terminus phenylalanine may have effect on helical handedness and trigger the handedness of the helix. To find out the effect of phenylalanine chirality on

conformation of heterochiral prolyl polypeptides, the peptide **P6** (Phe$_D$-L$_t$[D$_t$L$_t$]$_4$) was studied. Figures 14 (A-B) are the CD spectra of the peptide **P6** (Phe$_D$-L$_t$[D$_t$L$_t$]$_4$) in buffer and TFE in the concentration range 50-200 μM. The CD spectra of peptide **P6** (Phe$_D$-L$_t$[D$_t$L$_t$]$_4$) showed a positive CD band at 218 nm, and a negative CD band at 205 nm with crossover at 210 nm, which suggests a D-β-structure originating from D-configuration (Figure 14A). In TFE, peptide **P6** (Phe$_D$-L$_t$[D$_t$L$_t$]$_4$) shows a strong positive CD band at 218 nm and a negative CD band at 205 nm with cross over at 208 nm depicting that peptide **P6** (Phe$_D$-L$_t$[D$_t$L$_t$]$_4$) adopts a β-structure originating from D-configuration (D-β-structure) (Figure 14B).
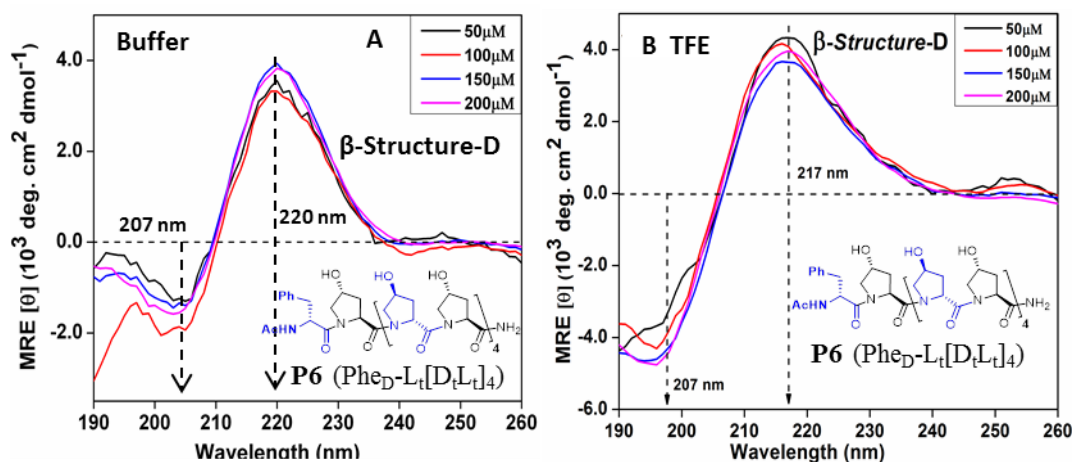
Figure 14: CD spectra of peptide **P6** (Phe$_D$-L$_t$[D$_t$L$_t$]$_4$) in the concentration range 50-200 μM **A)** in buffer and **B)** in TFE

3.11.2 CD spectra of peptide P8 (PA-[L$_t$D$_t$]$_4$)

In order to examine if the chirality of N-terminus phenylalanine is inducing the peptide conformation, peptide **P8** (PA-[L$_t$D$_t$]$_4$) having achiral phenylacetate was studied.
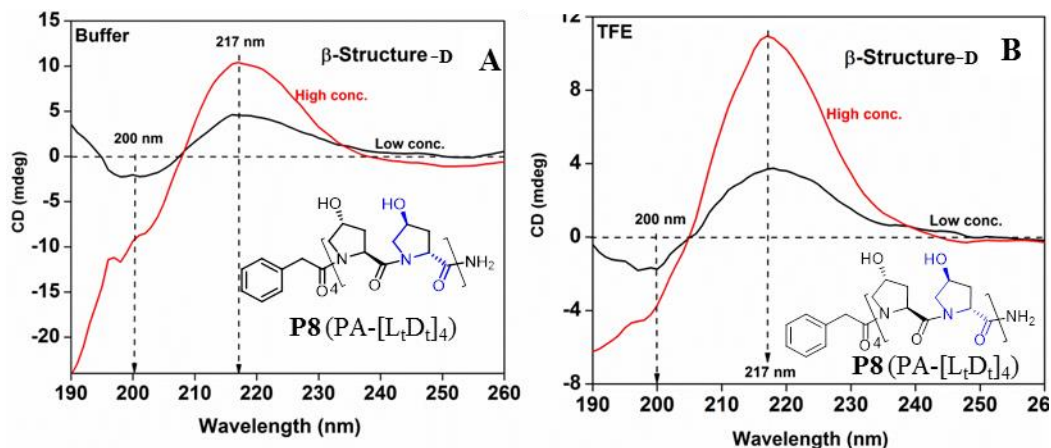
Figure 15: CD spectra of peptide **P8** (PA-[L$_t$D$_t$]$_4$) in the concentration range 50-200 μM **A)** in buffer and **B)** in TFE

The CD spectra of peptide **P8** showed strong positive CD band at 217 nm and relatively weak negative CD band at 200 nm with cross over at 210 nm at low and high concentrations in both water and TFE (Figure 15 A-B). This corresponded to β-structure in D configuration and the result suggested that, even when equal numbers of chirally opposite residues are present, the peptide forms D-β-structure and further suggests that the final conformations seen were not from the effect of terminal phenylalanine.

From various CD studies, one can infer that peptides **P3** (Phe$_L$-L$_t$[D$_t$L$_t$]$_4$) and **P8** (PA-[L$_t$D$_t$]$_4$) which are heterochiral in peptide sequence, adopt β-structure originating from D-configuration. However, the alternate heterochiral peptide **P5** (Phe$_L$-L$_c$[D$_c$L$_c$]$_4$) with (*cis*-(2*S*,4*S*)-L-*hyp* and *cis*-(2*R*,4*R*)-D-*Hyp*) residues present in similar fashion does not adopt any kind of conformation in any of the solvent, although the corresponding homochiral oligomers show β-structure. This clearly suggests that in addition to stereochemistry of 4(*R*/*S*)-hydroxyl group, the sequence also plays an important role in dictating the conformation. Table 2 summarizes the conformations observed by different sets of sequences composed from all diastereomers of 4(*R*/*S*)-L/D-prolyl monomers.

Table 2: Conformations of peptides **P1-P12** in water and in TFE

Pep. No	Peptide Name	Conformation in Water	Conformation in TFE
P1	Phe_L-L[DL]$_4$	**PP-II**	**Undefined**
P2	Phe_L-L$_t$[L$_c$L$_t$]$_4$	**PP-II**	**Random**
P4	Phe_D-D$_t$[L$_t$D$_t$]$_4$	**PP-II**	**Random**
P9	Phe_L-[L$_c$]$_4$[L$_t$]$_5$	**PP-II**	**Random**
P5	Phe_L-L$_c$[D$_c$L$_c$]$_4$	**Random**	**Undefined**
P7	Phe_L-D$_t$[L$_t$D$_t$]$_4$	**Random**	**Undefined**
P10	Phe_D-[D$_t$]$_4$[L$_t$]$_5$	**Random**	**Random**
P11	Phe_D-[D$_c$]$_4$[L$_c$]$_5$	**Random**	**Random**
P3	Phe_L-L$_t$[D$_t$L$_t$]$_4$	**PP-II**	**β-Structure-D**
P12	C_{14}-Phe_L-L$_t$[D$_t$L$_t$]$_4$	**PP-II**	**β-Structure-D**
P6	Phe_D-L$_t$[D$_t$L$_t$]$_4$	**β-Structure-D**	**β-Structure-D**
P8	PA-[L$_t$D$_t$]$_4$	**β-Structure-D**	**β-Structure-D**

3.12 Field Emission-Scanning Electron Microscopy (FE-SEM)

To examine the morphologies of the self-assembled structure of various alternate and block heterochiral peptides **P1-P11**, and with fatty acid conjugation as in case of **P12**, FE-SEM imaging was carried out for each of these peptides at a 200 μM concentration.

3.12.1 Peptides P2, P3 & P5 in water: Spherical nanoparticles

Figures 16(A-C) show self-assembly of peptides **P2** (Phe_L-L$_t$[L$_c$L$_t$]$_4$), **P3** (Phe_L-L$_t$[D$_t$L$_t$]$_4$) and **P5** (Phe_L-L$_C$[D$_c$L$_c$]$_4$) at 200 μM in water. The peptide **P2** (Phe_L-L$_t$[L$_c$L$_t$]$_4$) in which stereochemistry at the C4 position is changed at every residue 4(R/S) keeping C2 position stereochemistry constant [2(S) L-proline] exhibits left-handed PP-II conformation in

water and self-assembled to form disordered particles(Figure 16A). The peptide **P3** (Phe$_L$-L$_t$[D$_t$L$_t$]$_4$), in which stereochemistry at C4 and C2 position is changed at every residue (*R/S*), shows weak PP-II left-handed conformation in CD spectra and self-assembled to form nanospheres of around 200 nm in diameter width (Figure 16B). The peptide **P5** (Phe$_L$-L$_C$[D$_c$L$_c$]$_4$) with alternate D/L-*cis*-prolyl units aggregate to form disordered particles of 200 nm size (Figure 16C).
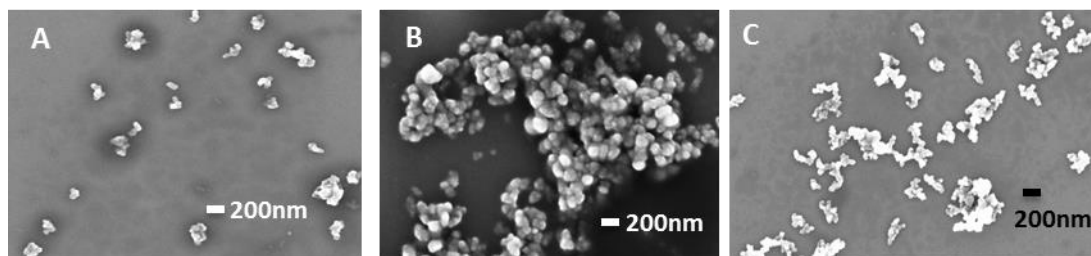
Figure 16: FE-SEM images of peptides **A) P2** (Phe$_L$-L$_t$[L$_c$L$_t$]$_4$), **B) P3** (Phe$_L$-L$_t$[D$_t$L$_t$]$_4$) and **C) P5** (Phe$_L$-L$_C$[D$_c$L$_c$]$_4$), at 200 μM in water.

3.12.2 Peptides P9-P11 in water: Spherical nanoparticles

Figures 17(A-C) show FE-SEM images **P9** (Phe$_L$-[L$_c$]$_4$[L$_t$]$_5$), **P10** (Phe$_D$-[D$_t$]$_4$[L$_t$]$_5$) and **P11** (Phe$_D$-[D$_c$]$_4$-[L$_c$]$_5$) respectively at 200 μM in water. These peptides self-assembled into spherical nanostructures of uniform size 100 nm in diameter (Figure 17 A-B) with peptide **P11** (Phe$_D$-[D$_c$]$_4$-[L$_c$]$_5$) being slightly different showing spherical nanostructures of around 200 nm in diameter size but the particles sticking to each other.
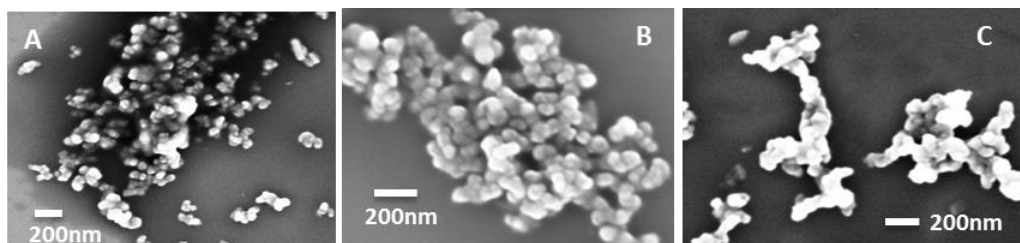
Figure 17: FE-SEM images of peptide **A) P9** (Phe$_L$[L$_c$]$_4$[L$_t$]$_5$), **B) P10** (Phe$_D$[D$_t$]$_4$[L$_t$]$_5$) and **C) P11** (Phe$_D$[D$_c$]$_4$[L$_c$]$_5$), at 200 μM in water.

3.12.3 Peptides P2, P3 & P5 in TFE

Figures 18(A-C) show self-assembly of peptides with all cis **P3** (Phe$_L$-L$_t$[D$_t$L$_t$]$_4$) and all trans **P5** (Phe$_L$-L$_C$[D$_c$L$_c$]$_4$) and alternating cis-trans block L-peptide **P2** (Phe$_L$-L$_t$[L$_c$L$_t$]$_4$) at 200 μM in TFE. As explained in Chapter 2, the chiral homo oligomer Phe$_L$-[L$_c$]$_9$ (*cis-*(2*S*,4*R*)-L-*hyp$_9$*) that shows change in conformation from water to TFE, self-assembles into nanowire in solvent TFE, while Phe$_L$-[L$_t$]$_9$ (*trans-*(2*S*,4*R*)-L-*Hyp$_9$*) that exhibits same conformation in water and TFE did not form nanowires.[31] The peptide **P2** (Phe$_L$-L$_t$[L$_c$L$_t$]$_4$), having alternate C4(*R/S*) stereochemistry in proline show nanospheres of around 100-200 nm in diameter.

The peptide chirally alternating block peptide **P3** (Phe$_L$-L$_t$[D$_t$L$_t$]$_4$) self-assembled to nano rods of length around 200 nm and width 20-30 nm in TFE, wherein it showed D-*β*-structure in CD. This observation suggests that D-*β*-structure seen in solution for peptide **P3** self-assembles to short nanofibers (Figure 18B). The peptide **P5** (Phe$_L$-L$_C$[D$_c$L$_c$]$_4$) also gave nanofibers of similar dimensions (length 200 nm and width 20 nm) (Figure 18C).
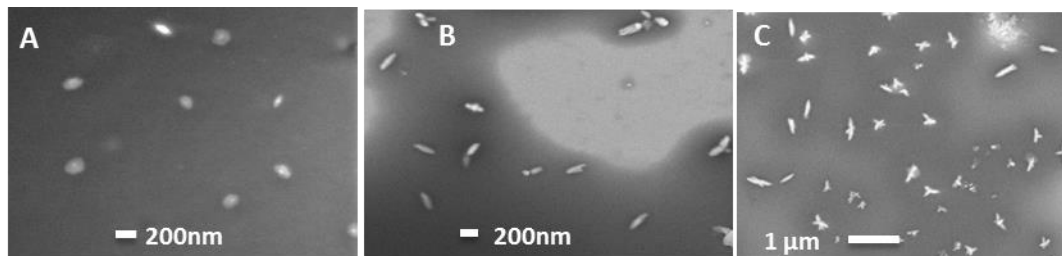
Figure 18: FE-SEM images of peptide **A) P2** (Phe$_L$-L$_t$[L$_c$L$_t$]$_4$), **B) P3** (Phe$_L$-L$_t$[D$_t$L$_t$]$_4$) and **C) P5** (Phe$_L$-L$_C$[D$_c$L$_c$]$_4$), at 200 μM in TFE.

3.12.4 Peptides P9-P11 in TFE

Figures 19(A-C) show FE-SEM images of chiral block peptides **P9** (Phe$_L$[L$_c$]$_4$[L$_t$]$_5$), **P10** (Phe$_D$[D$_t$]$_4$[L$_t$]$_5$) and **P11** (Phe$_D$[D$_c$]$_4$[L$_c$]$_5$) respectively at 200 μM in TFE. The peptide Phe$_L$-[L$_c$]$_4$-[L$_t$]$_5$ **P9,** acquired worm like nanostructure of size around 1μm in length and 100-200 nm width (Figure 23A), the peptide **P9** (Phe$_L$[L$_c$]$_4$[L$_t$]$_5$) showed bundles of needles with

fine edges and sharp points with size of nanostructure 1µm (Figure 23 B) and the peptide **P11** (Phe$_D$[D$_c$]$_4$[L$_c$]$_5$) exhibited random shaped nano structures.
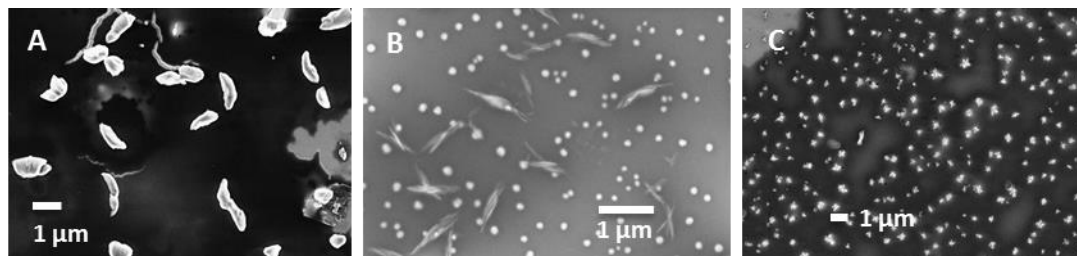
Figure 19: FE-SEM images of peptide **A) P9** (Phe$_L$[L$_c$]$_4$[L$_t$]$_5$), **B) P10** (Phe$_D$[D$_t$]$_4$[L$_t$]$_5$) and **C) P11**
   (Phe$_D$[D$_c$]$_4$[L$_c$]$_5$) at 200 µM in TFE.

3.12.5 Lipidated peptide P12 (C$_{14}$-Phe$_L$L$_t$[D$_t$L$_t$]$_4$) in water

Polyproline peptides synthesized from *trans*-4(*R/S*)-hydroxy-L/D-proline show stereochemistry and solvent dependent change in conformation[31] but fail to self-assemble into well-defined nanostructures. Increasing the *inter*molecular interactions, *via* hydrophilic and hydrophobic forces, by conjugation with different fatty acids, did not alter the conformation n solution, but showed well-defined nanofiber formation. Thus additional fatty acid chain is needed in case of *trans*-4(*R/S*)-hydroxyproline polypeptides to show the self-assembly. The peptide **P3** (Phe$_L$-L$_t$[D$_t$L$_t$]$_4$) with alternating *trans*-(2*S*,4*R*)-L-*Hyp*-*trans*-(2*R*,4*S*)-D-*hyp* units showed conformational change as solvent was switched to TFE. Hence this peptide was conjugated with myristic acid (C$_{14}$) to get peptide **P12** (C$_{14}$-Phe$_L$L$_t$[D$_t$L$_t$]$_4$) and its self-assembly was examined by AFM and FE-SEM techniques (Figure 20A-B). The peptide **P12** self-assembled to nanospheres of around 1µm in diameter, as observed and supported by FE-SEM.
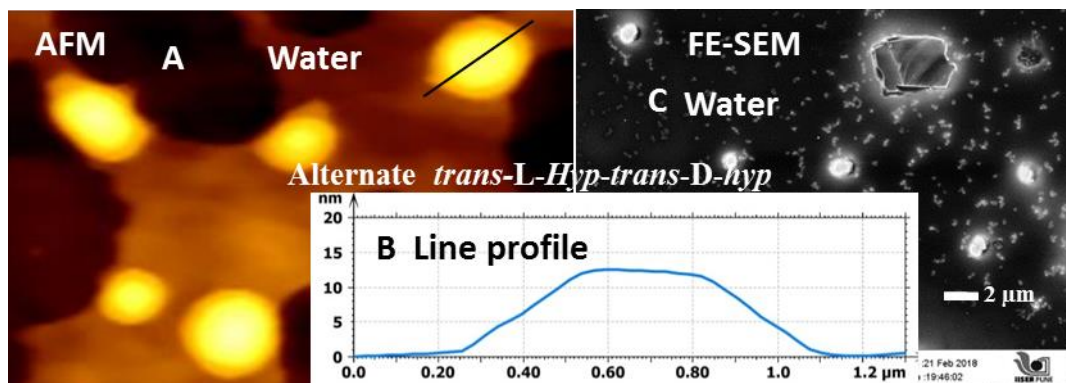
Figure 20: AFM and FE-SEM images of peptide **A) P12** (C_{14}-Phe$_L$L$_t$[D$_t$L$_t$]$_4$) **B)** line profile for figure **A** and **C)** FE-SEM image, at 200 μM in water.

3.12.6 Lipidated peptide P12 (C_{14}-Phe$_L$L$_t$[D$_t$L$_t$]$_4$) in TFE

Figure 21(A-D) are the AFM and FE-SEM images of the peptide **P12** (C_{14}-Phe$_L$L$_t$[D$_t$L$_t$]$_4$) in TFE, wherein formation of long nanofibers of around 2-3 μm in length was observed. The height of the fibers was found to be around 20 nm and interestingly, these wires were twisted in left-handed manner to generate grooves whose depth varied between 4-6 nm on the surface of the nanofibers.
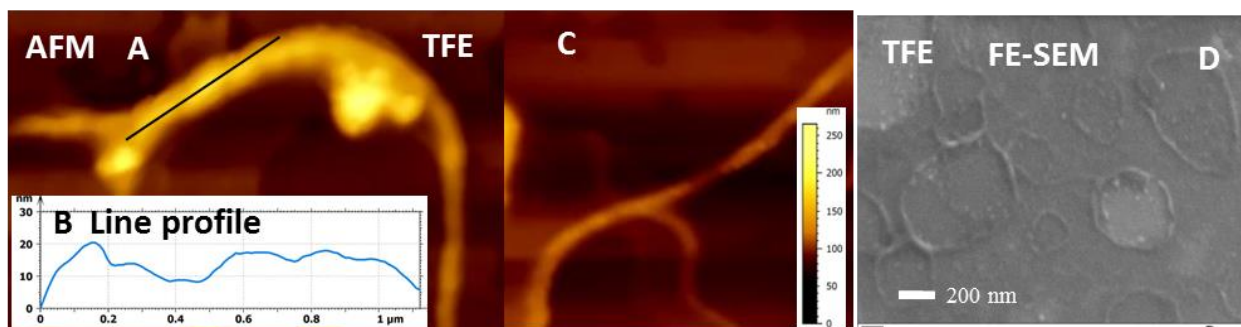
Figure 21: AFM and FE-SEM images of peptide **A,C) P12** (C_{14}-Phe$_L$L$_t$[D$_t$L$_t$]$_4$), **B)** line profile for figure **A** and **D)** FE-SEM image, at 200 μM in TFE.

3.13 Summary

In summary (Figure 22), it is demonstrated here that heterochiral peptide **P3** (Phe$_L$-L$_t$[D$_t$L$_t$]$_4$) shows solvent dependent switch in conformation. In hydrophilic solvent like water,

P3 adopts PP-II conformation where as in hydrophobic solvent such as TFE it shows D-β-structure. On conjugation with fatty (C_{14}) carbon chain to, the lipidated peptide **P12** (C_{14}-Phe$_L$L$_t$[D$_t$L$_t$]$_4$) no change in its conformation was seen water and TFE. However, the peptide **P12** self-assembles into nanospheres in water and long nanowires in solvent TFE. It is demonstrated here that maintaining alternate D/L chirality in the peptide **P6** (Phe$_D$-L$_t$[D$_t$L$_t$]$_4$) but replacing chiral phenylalanine with achiral phenylacyl group as in **P8** (PA[L$_t$D$_t$]$_4$), still results into D-β-structure originating from D-proline in both solvents water as well as in TFE. The two homochiral peptide **P2** (Phe$_L$-L$_t$[L$_c$L$_t$]$_4$) and **P9** (Phe$_L$-[L$_c$]$_4$[L$_t$]$_5$) show solvent dependent conformational change. In water it adopts PP-II conformation but in TFE it changes to random form suggesting that *cis*-(2S,4R)-*hyp* residues in alternate as well as in block polyproline stretch adopt predictable conformation on increasing the molecular interaction (Hydrophilic and hydrophobic) by conjugation with fatty acid chain. Alternate heterochiral peptides **P4**, **P5**, **P7** and block peptides **P10**, **P11** do not adopt any definite conformation in any of the solvent. This study clearly suggests the importance of chirality and stereochemistry at C4 position on proline.

Peptide	Conformation		Morphology	
	water	TFE	water	TFE
P3 Phe$_L$L$_t$[D$_t$L$_t$]$_4$	PP II	β-Structure-D	Nano-sphere	Nano-rods
P12 C$_{14}$-Phe$_L$L$_t$[D$_t$L$_t$]$_4$	PP II	β-Structure-D	Nano-sphere	Nano-wires
P2 Phe$_L$L$_t$[L$_c$L$_t$]$_4$	PP II	Random	Nano-sphere	Nano-rods
P9 Phe$_L$[L$_c$]$_4$[L$_t$]$_5$	PP II	Random	Nano-sphere	Worm like structure
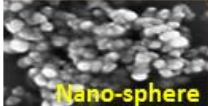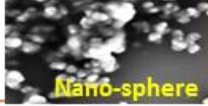
Figure 22: Summary

Future research in experimental as well as theoretical aspects needs to be done in this filed to understand the role of chirality and relative stereochemistry of all possible combinations of heterochiral and block prolylpeptides.

3.14 Experimental section

General methods of peptide synthesis, purification of peptides by HPLC, characterization using MALDI-TOF, conformational analysis by CD spectroscopy and preparation of samples for AFM and FE0SEM are described in Chapter 2.

3.14.1 Synthesis of compounds 14-21

(2*R*,4*S*)-N1-((benzyloxycarbonyl)-*trans*-4-hydroxy-D-proline methyl ester (15)
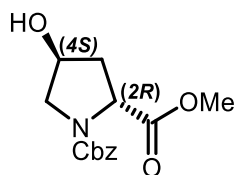
Compound **3** (4.4 g 15.7 mmol), DCC (3.9 g 19 mmol) and CuCl (5 mg) was added in (5 ml) dioxane. The mixture was stirred at 40-50 ^{0}C, for 48 h and dioxane was evaporated on vacuum. To the residue were added toluene (8 ml), formic acid (1.08 g, 23 mmol) and reaction mixture was refluxed for 24h. The insoluble solid was filtered off; the filtrate was successively washed with sat. aq. NaHCO$_3$, brine, and then evaporated in vacuum. The residue was dissolved in THF (20 ml) and treated with aq. 2N NaOH at 10 ^{0}C. The mixture was stirred at 25 ^{0}C for 30 min. and washed with ethyl acetate. After acidifying mixture to (pH 2) with conc. HCl the white suspension was extracted with ethyl acetate. The organic layers were combined and washed with water, dried over anhydrous Na$_2$SO$_4$ and evaporated. To yield compound no **14**: 3g (71%).

The stirred solution of compound **14** (3g, 11 mmol) in anhydrous acetone (35ml) and (6 g, 43 mmol) of anhydrous K$_2$CO$_3$, dimethylsulphate (2 ml, 16 mmol) was refluxed under nitrogen for 4 h. The acetone was removed under vacuum and the resulting residue was dissolved in water then extracted with ethyl acetate three times. The combined organic layer

was washed with water, followed by saturated brine solution, dried over Na_2SO_4 and concentrated under vacuum. The crude material was purified by silica gel chromatography (50% ethyl acetate/hexane) afford compound as colourless thick oil. Yield: 3.1g; 98%. Specific rotation: $[\alpha]^D_{22}$ +35.2 (c 2.0, CH_2Cl_2); HRMS (ESI-MS): Molecular formula ($C_{14}H_{17}NO_5$) Calculated mass (M+Na), 302.1004, observed mass 302.1004; ^{1}H NMR (CDCl_3, 400 MHz) δ: 2.03-2.30 (1H, m), 2.31-2.37 (1H, m), 3.53-3.79 (5H, m), 4.37-4.5(2H, m), 4.98-5.20 (2H, m), 7.25-7.35 (5H, m); ^{13}C NMR δ: 37.8, 38.76, 52.74, 53.04, 57.81, 58.29, 67.59, 70.28, 71.29, 127.96, 128.08, 128.18, 128.53,128.63, 136.33, 154.01, 154.90, 174.59

(2*R*,4*S*)-N1-(benzyloxycarbonyl)- *trans*-4-(*t*-butyl)hydroxy-D-prolinemethyl ester 16

16
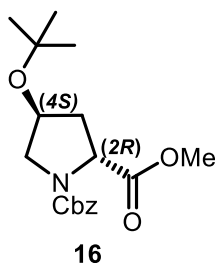
A mixture of compound **15** (1.67 g, 5 mmol), silver oxide (Ag_2O) (3.98 g, 17.2 mmol) and of tertiary butyl bromide(3.2 g, 23.3 mmol) in cyclohexane (50 ml) was stirred for 23 h at room temperature. The resulting suspension was filtered through celite and filtrate was concentrated under reduces pressure, the crude product was purified by column chromatography. Yield: 1.67g (80%); HRMS (ESI-MS): Molecular formula ($C_{18}H_{25}NO_5$) calculated (M+Na), 358.1630, observed 358.1631; ^{1}H NMR (CDCl_3, 400 MHz) δ: 1.14 (9H, s), 2.00-2.07 (1H, m), 2.27-2.37 (1H, m), 3.29-3.35 (1H, m), 3.56-3.80 (5H, m), 4.12-4.20 (1H, m), 4.30-4.40 (1H, m), 5.00-5.19 (2H, m), 7.26-7.37 (5H, m); ^{13}C NMR δ: 28, 38, 39, 51.5, 52, 53.5, 57.8, 58, 67, 68.5, 70, 74, 128, 129, 129.9, 137, 154, 155, 172.5, 173.

(2*R*,4*S*)-N[1]–(benzyloxycarbonyl)-4-(O-tButyl) hydroxy-D-proline 17

17
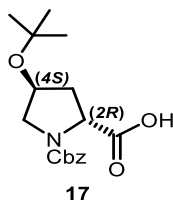
The ester compound **16** was subjected to hydrolysis using aq. 2N LiOH in THF. THF was removed under vacuum and the aq. layer was washed with ethyl acetate to remove organic impurity. The aqueous layer was acidified with 2N HCl up to pH 2 and extracted with ethyl acetate three times; combined organic layer was dried over Na_2SO_4 further purified by column chromatography. Yield: 1.5 g (98%); ^{1}H NMR (CDCl$_3$, 400 MHz) δ: 1.4 (9H, s), 2.00-2.15 (1H, m), 2.30-2.41 (1H, m), 3.31-3.49(1H, m), 3.61-3.70 (1H, m), 4.15-4.25 (1H, m), 4.35-4.41 (1H, m), 5.05-5.20 (2H, m), 7.26-7.37 (5H, m); ^{13}C NMR δ: 28, 30, 37, 38.5, 52.5, 54, 58, 68, 69, 69.9, 74.5, 75.5, 128, 128.9, 129, 136, 154.5, 155.5, 176.

(2*R*, 4*S*)- *trans*-4-(*t*-butyl) hydroxy-D-proline (17)

17
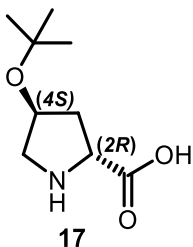
The acid compound **17** (1.5 g, 4.7 mmol) was dissolved in methanol (20 mL) to which 10 % Pd/C (0.3 g) was added and mixture was subjected to hydrogenation under H$_2$ gas, water was added to the reaction mixture which was filtered through Whatman filter paper and filtrate was concentrated under reduced pressure. The product was not purified and used for next step.

(2*R*,4*S*)-N1-(fluorenylmethyloxycarbonyl)-*trans*-4-(*t*-butyl) hydroxy-D-proline (18)

18

Compound **17** (1.2 g, 6.4 mmol) was dissolved in water : dioxane, 1:1 (50 mL) The pH was maintained at 10 by addition of 10 % Na$_2$CO$_3$. The reaction mixture was stirred at 0 ^{0}C for 15 minutes. Fmoc-Cl (2 g, 7.7 mmol) added in portion wise during 45 min. maintained temperature at 0 ^{0}C for first 4 h and then allowed to come room temperature, stirred for

another 18 h. The dioxane was evaporated under vacuum and aqueous layer was extracted with diethyl ether to remove unreacted Fmoc-Cl. The aq. layer was neutralized with KHSO$_4$ to pH 2 followed by extraction with ethyl acetate three times. Concentration of organic layers yield crude product which was purified by column chromatography. Yield: 2.1 g (81%); HRMS (ESI-MS): Molecular formula (C$_{18}$H$_{25}$NO$_5$) calculated mass (M+Na) 432.1786, observed 432.1785; ^{1}H NMR (CDCl$_3$, 400 MHz) δ: 1.16-1.21 (9H, m), 2.11-2.17 (1H, m), 2.32-2.37 (1H, m), 3.39-3.65(2H, m), 4.28-4.43 (3H, m), 5.10-5.20 (2H, m), 7.32-7.76 (8H, m); ^{13}C NMR δ: 28.14, 37.28, 38.25, 52.91, 54.04, 54.65, 58.59, 67.64, 69.06, 69.71,120.10, 125.02, 127.17, 127.87, 128.56, 136.19, 141.47, 174.26.

(2R,4R)-N1-(benzyloxycarbonyl)-cis-4-(t-butyl) hydroxy-D-proline methyl ester (19)


19
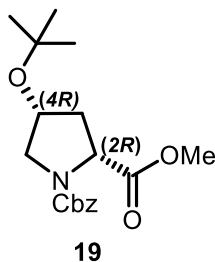
The mixture of ester compound **3** (1.67 g, 5 mmol), silver oxide (Ag$_2$O) (3.98 g, 17.2 mmol) and tertiary butyl bromide(3.2 g, 23.3 mmol) in cyclohexane (50 ml) was stirred for 24 h at room temperature under nitrogen. The resulting suspension was filtered through celite and filtrate was concentrated under reduces pressure, the crude product was purified by column chromatography. Yield: 1.67 g (80 %); HRMS (ESI-MS): Molecular formula (C$_{18}$H$_{25}$NO$_5$) calculated (M+Na), 358.1630, observed 358.1631; ^{1}H NMR (CDCl$_3$, 400 MHz) δ: 1.45 (9H, s), 2.00-2.07 (1H, m), 2.27-2.37 (1H, m), 3.29-3.35 (1H, m), 3.56-3.88 (5H, m), 4.12-4.20 (1H, m), 4.30-4.40 (1H, m), 5.00-5.19 (2H, m), 7.26-7.37 (5H, m); ^{13}C NMR δ: 28, 30, 37, 38.5, 52.5, 54, 58, 68, 69, 69.9, 74.5, 75.5, 128, 128.9, 129, 136, 154.5, 155.5, 176.

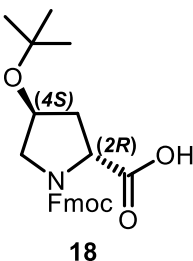**(2*R*, 4*R*)-*cis*-4-(*t*-butyl) hydroxy-D-proline (20)**
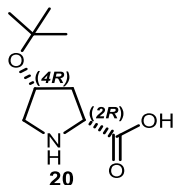
The ester compound **19** was subjected to hydrolysis using aq. 2N LiOH in THF. THF was removed under vacuum and the aq. layer was washed with ethyl acetate to remove organic impurity. The aqueous layer was acidified with 2N HCl up to pH 2 and extracted with ethyl acetate three times; combined organic layer was dried over Na_2SO_4 concentrated under reduced pressure and the above acid compound (1.5 g, 4.7 mmol) was dissolved in methanol (20 mL) to which 10 % Pd/C (0.3 g) was added and mixture was subjected to hydrogenation under H_2 gas, water was added to the reaction mixture which was filtered through Whatman filter paper and filtrate was concentrated under reduced pressure. The product was not purified and used for next step.

(2*R*, 4*R*)-N1-(fluorenylmethyloxycarbonyl)-*cis*-4-(*t*-butyl) hydroxy-D-proline (21)


Compound **20** (1.2 g, 6.4 mmol) was dissolved in water : dioxane, 1:1 (50 mL) The pH was maintained at 10 by addition of 10 % Na_2CO_3. The reaction mixture was stirred at 0 ^{0}C for 15 minutes. Fmoc-Cl (2 g, 7.7 mmol) added in portion wise during 45 min. maintained temperature at 0 ^{0}C for first 4 h and then allowed to come room temperature, stirred for another 18 h. The dioxane was evaporated under vacuum and aqueous layer was extracted with diethyl ether to remove unreacted Fmoc-Cl. The aq. layer was neutralized with $KHSO_4$ to pH 2 followed by extraction with ethyl acetate three times. Concentration of organic layers yield crude product which was purified by column chromatography. Yield: 2.1 g (81%); HRMS (ESI-MS): Molecular formula ($C_{18}H_{25}NO_5$) calculated mass (M+Na) 432.1781,

observed 432.1780; ^{1}H NMR (CDCl$_3$, 400 MHz) δ: 1.21-1.24 (9H, m), 2.13-2.21 (1H, m), 2.33-2.41 (1H, m), 3.37-3.40 (1H, m), 3.58-3.68 (1H, m) 4.23-4.57 (5H, m), 5.10-5.20 (2H, m), 7.24-7.73 (8H, m); ^{13}C NMR δ: 28.09, 28.16, 36.98, 38.18, 47.15, 47.23, 53.94, 54.77, 58.58, 67.89, 68.23, 69.25, 69.62, 120.02, 125.10, 125.40, 127.17, 127.79, 141.39, 143.39, 143.75, 173.7.

3.15 References:

1) Bonner, W., The origin and amplification of biomolecular chirality. *Origin Life Evol Biosphere*, **1991**, *21*, 59-111.

2) Bonner, W.; Grenberg, J.; Rubenstein, E., The extraterrestrial origin of the homochirality of biomolecules-rebuttal to a critique. *Origin Life Evol Biosphere*, **1999**, *29*, 215-219.

3) Milton, R. C.; Milton, S. C.; Kent, S. B.,   Total Chemical Synthesis of a D-Enzyme: The Enantiomers of HIV-1 Protease Show Demonstration of Reciprocal Chiral Substrate Specificity. *Science,* **1992**, *256*, 1445-1448.

4) Taolei, S.; Dong, H.; Kristina, R.; Lifeng, C.; Harald, F., Stereospecific interaction between immune cells and chiral surfaces. *J. Am. Chem. Soc.* **2007**, *129*, 1496.

5) Saghatelian, A.; Yokobayashi, Y.; Soltani, K.; Ghadiri, M. R., A chiroselective peptide replicator. *Nature*, **2001**, *409*, 797-801.

6) Chung, D. M.; Nowick, J. S., Enantioselective molecular recognition between β-sheets. *J. Am. Chem. Soc.,* **2004**, *126*, 3062-3063.

7) Fuhrhop, J. H.; Krull, M.; Buldt, G., Precipitates with β-pleated sheet structure between by mixing aqueous solution of helical poly (D-lysine) and poly (L-lysine). *Angew. Chem., Int. Ed. Engl.*, **1987**, *26*, 699-700.

8) Ramagopal, U. A.; Ramakumar, S.; Mathur, P.; Joshi, R.; Chauhan, V. S., Dehydrophenylalanine zippers: strong helix-helix clamping through a network of weak interactions. *Protein Eng.*, **2002**, *15*, 331-335.

9) Gerber, D.; Shai, Y., Chirality-independent protein-protein recognition between transmembrane domains in *vivo*. *J. Mol. Biol.*, **2002**, *322*, 491-495.

10) (a) Pentelute, B. L.; Gates, Z. P.; Tereshko, V.; Dashnau, J. L.; Vanderkooi, J. M.; Kossiakoff, A. A.; Kent, S. B., X-ray structure of snow-flea antifreeze protein determined by racemic crystallization of synthetic protein enantiomers. *J. Am. Chem. Soc.*, **2008**, *130*, 9695-9701. (b) Patterson, W. R.; Anderson, D. H.; DeGrado, W. F.; Cascio, D.; Eisenberg, D., Centrosymmetric bilayers in the 0.75A resolution structure of a designed alpha-helical peptide, D, L-alpha-1. *Protein Sci*. **1999**, *8*, 1410-1422. (c) Zawadzke, L. E.; Berg, *J. M.,* The structure of centrosymmetric protein crystal. *Proteins*, **1993**, *16*, 301-305.

11) Hirst, A. R.; Smith, D. K.; Feiters, M. G.; Geurts, H. P. M., Two-component dendritic gel: effect of stereochemistry on the supramolecular chiral assembl. *Chem. Eur. J.*, **2004**, *10*, 5901-5910.

12) (a) Luo, X.; Liu, B.; Liang, Y.,Self-assembled organogels formed by mono-chain I-alanine derivatives. *Chem. Commun.*, **2001**, *17*, 1556-1557. (b) Beceril, J.; Escuder, B.; Miravet, J. F.; Gavara, R.; Luis, S. V., Understanding the expression of molecular chirality in the self-assembly of a peptidomimetic organogelator. *Eur. J. Org. Chem.* **2005**, *3*, 481-485. (c) Dzolic, Z.; Wolsperger, K.; Zinic, M., Synergic effect in gelation by two-component mixture of chiral gelators *New J. Chem.*, **2006**, *30*, 1411-1419.

13) Brizard, A.; Oda, R.; Huc, I., *Top. Curr. Chem.*, **2005**, *256*, 814.

14) Marc B. Taraban, Yue Feng, Boualem Hammouda, Laura L. Hyland, and Y. Bruce Yu., *Chem. Mater.* **2012**, *24,* 2299.

15) Hirst, A. R.; Huang, B.; Castelletto, V.; Hamley, I. W.; Smith, D. K., Self-organization in the assembly of gels from mixtures of different dendritic peptide building blocks. *Chem. Eur. J*., **2007**, *13*, 2180-2188.

16) (a) Frkanec, L.; Zinic, M., Chiral bis(amino acid)- and bis(amino alcohol)-oxalamide gelators. Gelation properties, self-assembly motifs and chirality effects. *Chem. Commun.,* **2010**, *46*, 522-537. (b) Makarvic, J.; Jokic, M.; Frkanec, L.; Vujicic, N.; Zinic, M., Oxalyl retro-peptide gelators. Synthesis, gelation properties and stereochemical effects. *Beilstein J. Org. Chem.* **2010**, *6*, 945-959.

17) Peng, W.; Motonaga, M.; Koe, J. R., Chirality control in optically active polysilane aggregates. *J. Am. Chem. Soc*. **2004**, *126*, 13822-13826.

18) Suzuki, N.; Fujiki, M.; Kimpinde-Kalunga, R.; Koe, J. R., Chiroptical inversion in helical Si-Si bond polymer aggregates. *J. Am. Chem. Soc.* **2013**, *135*, 13073-13079.

19) Li, J.; Fan, K.; Guan, X.; Yu, Y.; Song, J., Self-Assembly Mechanism of 1,3:2,4-Di(3,4-dichlorobenzylidene)-D-sorbitol and Control of the Supramolecular Chirality. *Langmuir*, 2014, *30*, 13422-13429.

20) Li, Y.; Li, B.; Fu, Y.; Lin, S.; Yang, Y., Solvent-Induced Handedness Inversion of Dipeptide Sodium Salts Derived from Alanine. *Langmuir*, 2013, *29*, 9721-9726.

21) Duan, P.; Qin, L.; Zhu, X.; Liu, M., Hierarchical Self-Assembly of Amphiphilic Peptide Dendrons: Evolution of Diverse Chiral Nanostructures Through Hydrogel Formation Over a Wide pH Range. *Chem. Eur. J*., **2011**, *17*, 6389-6395.

22) Kumar, J.; Nakashima, T.; Kawai, T., Inversion of supra molecular chirality in bichromophoric perylene bisimide: in fluence of temperature and ultrasound. *Langmuir*, **2014**, *30*, 6030-6037.

23) Jintoku, H.; Dateki, M.; Takafuji, M.; Ihara, H., Supramolecular gel-fuctionalized polymer films with tunable optical activity. *J. Mater. Chem.* C, **2015**, *3*, 1480-1483.

24) Olaf Sparre Anderson, Gramicidinchannels. *Ann. rev. physiol.,* **1984**, *46*, 531-548.

25) Ghadiri, M.R.; Granja, J. R.; Milligan, R.A.; McRee, D.E.; Kgazanovich, N., Self-assembling organic nanotubes based on a cyclic peptide architecture. *Nature,* **1993**, *366*, 324-327.

26) Ghadiri, M.R.; Granja, J. R.; Buehler, L.K., Artificial transmembrane ion channels from self-assembling peptide nanotubes. *Nature,* **1994**, *369*, 301-304.

27) Shuwei L. Jiaming Q. Yi L. Baoong L.Yonggang Yang, Chirality-driven parallel and antiparallel β-sheet secondary structures of Phe-Ala lipodipeptides. *Langmuir*, **2017**, *33*, 8246-8252.

28) Pol Arranz-Gilbert.; Bernat, G. M. M.; Markus, M.; Fanny G.; Meritxell, T. Ernest G., Lipid Bilayer Crossing The Gate of Symmetry. Water-Soluble Phenylproline-Based Blood-Brain Barrier Shuttles. *J. Am. Chem. Soc.*, 2015, *137*, 7357-7364.

29) Mahesh, V. S.; Krishna, N. Ganesh., Water-induced switching of β-structure to polyproline II conformation in the 4*S*-aminoproline polypeptide via H-bond rearrangement. *Org. Lett*, 2010, *12*, 5390-5393.

30) Nitin, D. B.; Madhanagopal, B.; Mahesh, V. S.; Krishna, N. Ganesh., Stereodependent and solvent-specific formation of unusual β -structure through side chain-backbone H-bonding in C4(S)-(NH2/OH/NHCHO)-L-prolyl polypeptides *Peptide Science,* **2017**, *108*, 22981-22991.

31) Nitin, D. B.; Mahesh, V. S.; Krishna, N. Ganesh., A nanofiber assembly directed by the non-classical antiparallel β-structure from 4*S*-(OH) proline polypeptide. *Chem. Commun.,* **2016**, 52, 4884-4887.

32) Linus, Pauling and Robert B. Corey, Two rippled-sheet configuration of polypeptide chains, and a note about the pleated sheets. *PNAS,* **1953**, *39*, 253-255.

33) Ramachandran G. N.; Chandrasekaran, R., Conformation of peptide chains containing both L- and D-residues: Part I-helical structures with alternating L- and D-residues

with special reference to the LD-ribbon and the LD-helices. *Ind.J.biocem. Biophys,* **1972**, *9*, 1-11.

34) Hesselink, F.T. Sceraga, H. A., On the possible existence of α-helical structure of regular sequence D,L-copolymers of amino acid. Conformational energy calculations. *Micromolecules,* **1972**, 5, 455-463.

35) Veatch, W.R. Blout, E.R., Aggregation of gramicidin A in solution. *biochemistry,* **1974**, 13, 5257-5264.

36) Colona-Cesari, F.; Pramilat, S.; Heitz, F.; spach G. Lotz B., Helical structures of poly (D-L-peptides). A conformational energy analysis. *Micromolecules*, **1977**, 10, 1284-1288.

37) (a) Piero, D. C.; Concetta, L. R.; *Tetrahedron: Asymmetry*, **2002**, *13*, 197. (b) Vaclav, V.; Milos, B.; Marketa, R.; Ivan, R. *Tetrahedron*, **2009**, *65*, 862.

38) (a)Alexander, N.D.; Alan, G.; Rohit, V. P., Role of solvent in determining conformational preferences of alanine dipeptide in water. *J. Am. Chem. Soc.*, **2004**, *126*, 2574-2581. (b) Ninad, P.; Kim, S., Protein-solvent interactions. *Chem Rev.* **2006,** *106*, 1616-1623.

39) (a) Goodman, M.; Neider, F.; Toniolo, C., Circular dichroism studies of isoleucine oligopeptides in solution. *Biopolymer.* **1971**, *10,* 1719-1730. (b) Sonnichsen, F. D.; Van Eky, J. C.; Hodges, R. S.; Sykes, B. D., Effect of trifluoroethanol on protein secondary structure: an NMR and CD study using a synthetic actin peptide. *Biochemistry*. **1992,** *31*, 8790-8798.

3.16 Appendix

3.16.1 ^{1}H, ^{13}C NMR spectrum of compounds **14-21**

3.16.2 HPLC and MALDI-TOF of peptides **1-12**

H^1 NMR of compound (2*R*,4*S*)-N1-(benzyloxycarbonyl)-*trans*-4-hydroxy-D-proline methyl ester (15)
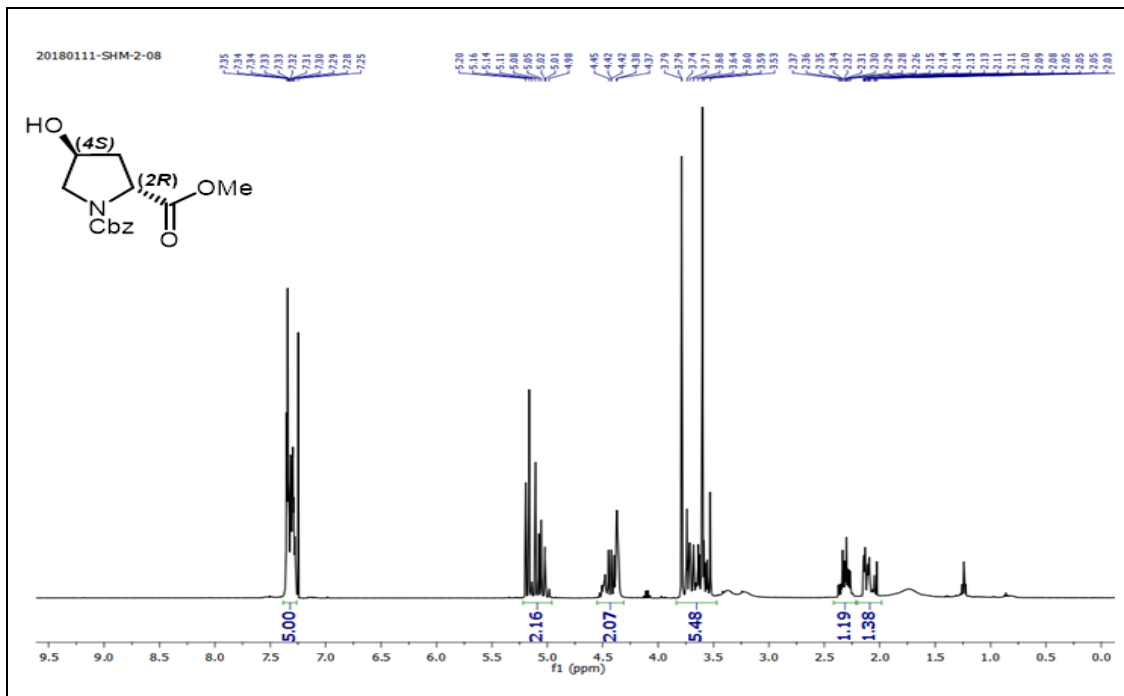
C^{13} NMR of compound (2*R*, 4*S*)-N1-(benzyloxycarbonyl)-*trans*-4-hydroxy-D-proline methyl ester (15)
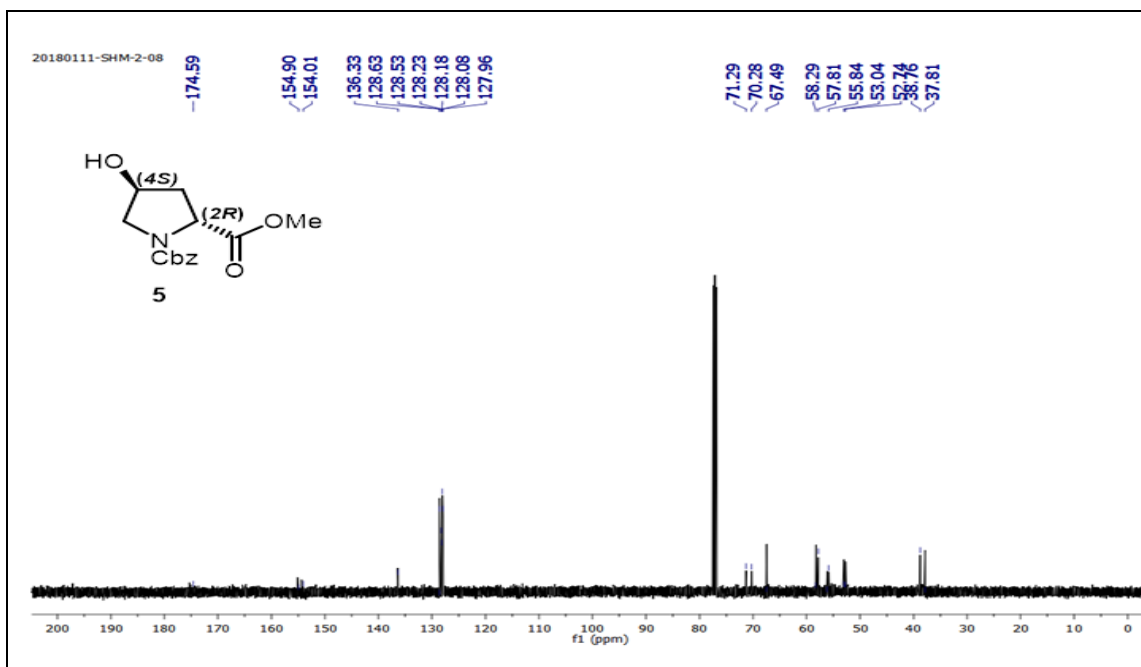
^{1}H NMR of compound (2R,4S)-N1-(benzyloxycarbonyl)-*trans*-4-(*t*-butyl)-hydroxy-D-prolinemethyl ester 16
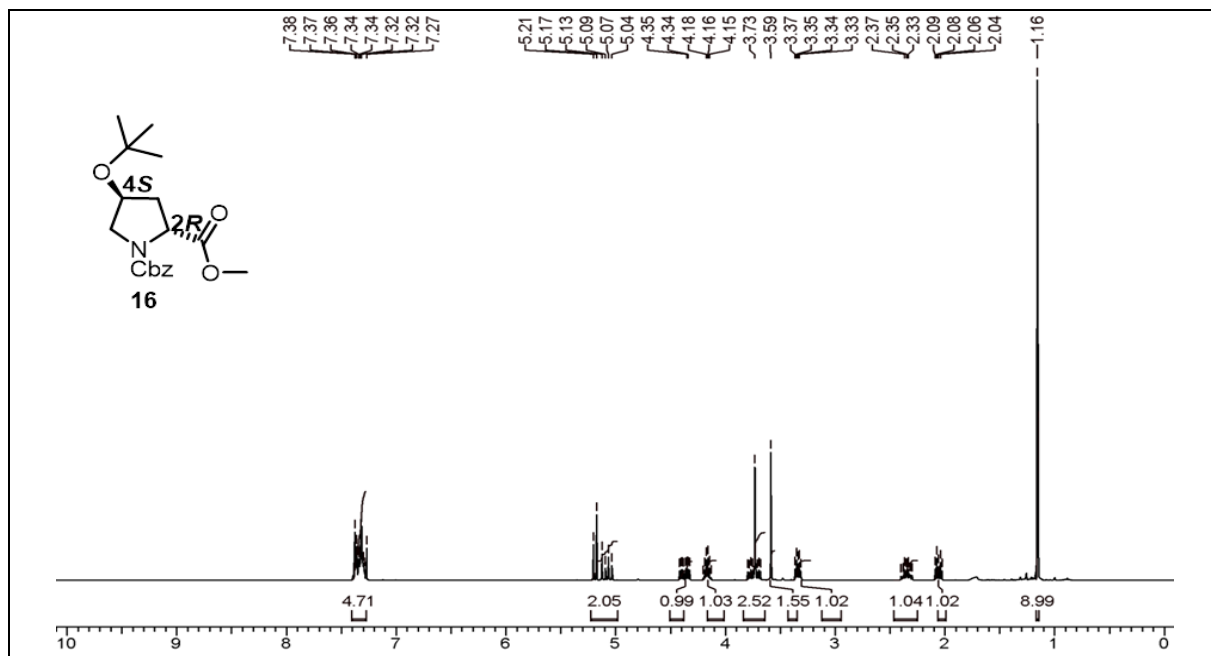
^{13}C NMR of compound (2R,4S)-N1-(benzyloxycarbonyl)- *trans*-4-(*t*-butyl)-hydroxy-D-prolinemethyl ester 16
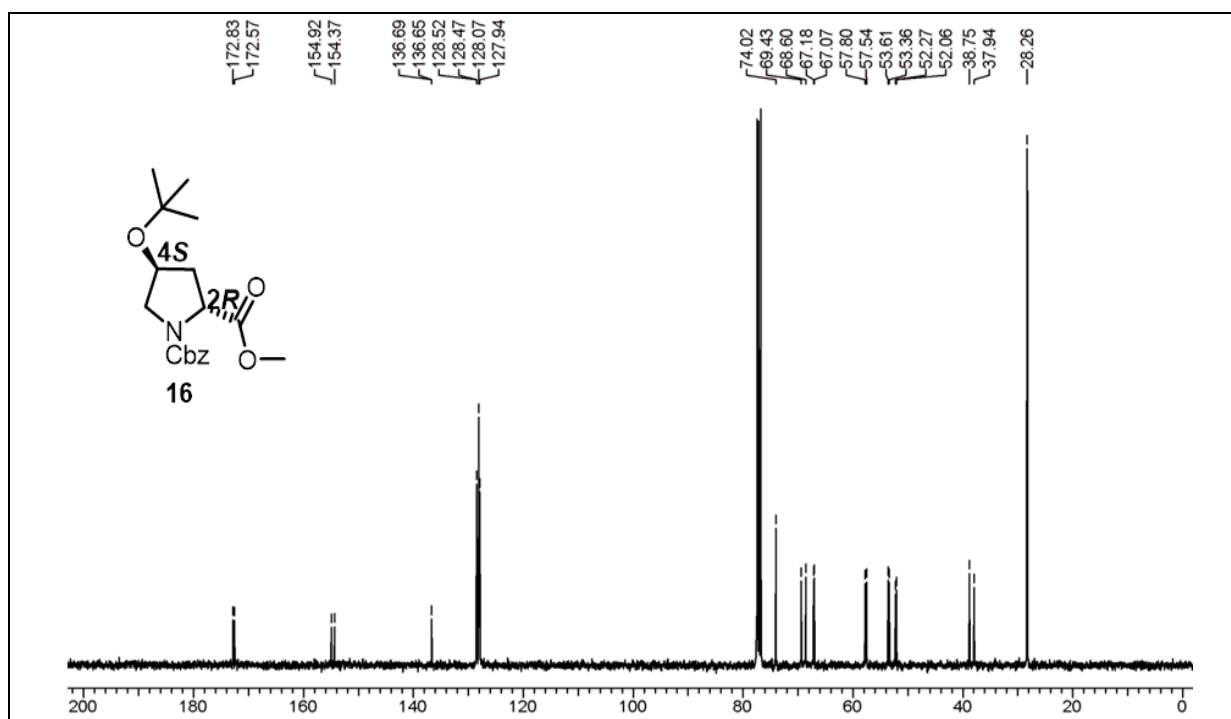
H^1 NMR of compound (2*R*, 4*S*)-N1-(fluorenylmethyloxycarbonyl)-*trans*-4-(*t*-butyl) hydroxy-D-proline (18)
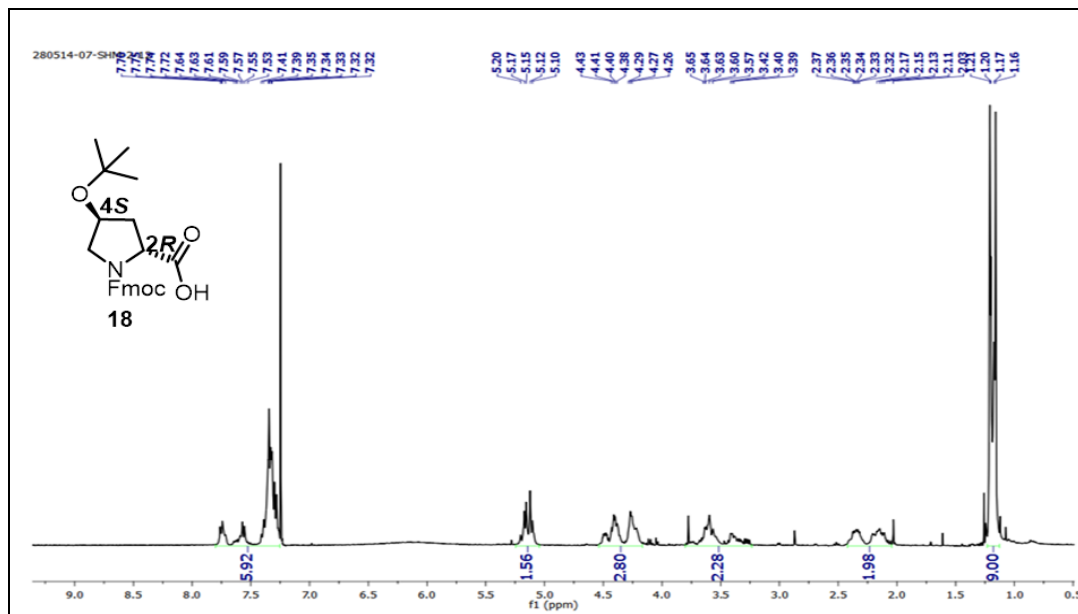
C^{13} NMR of compound (2*R*, 4*S*)-N1-(fluorenylmethyloxycarbonyl)-*trans*-4-(*t*-butyl) hydroxy-D-proline (18)
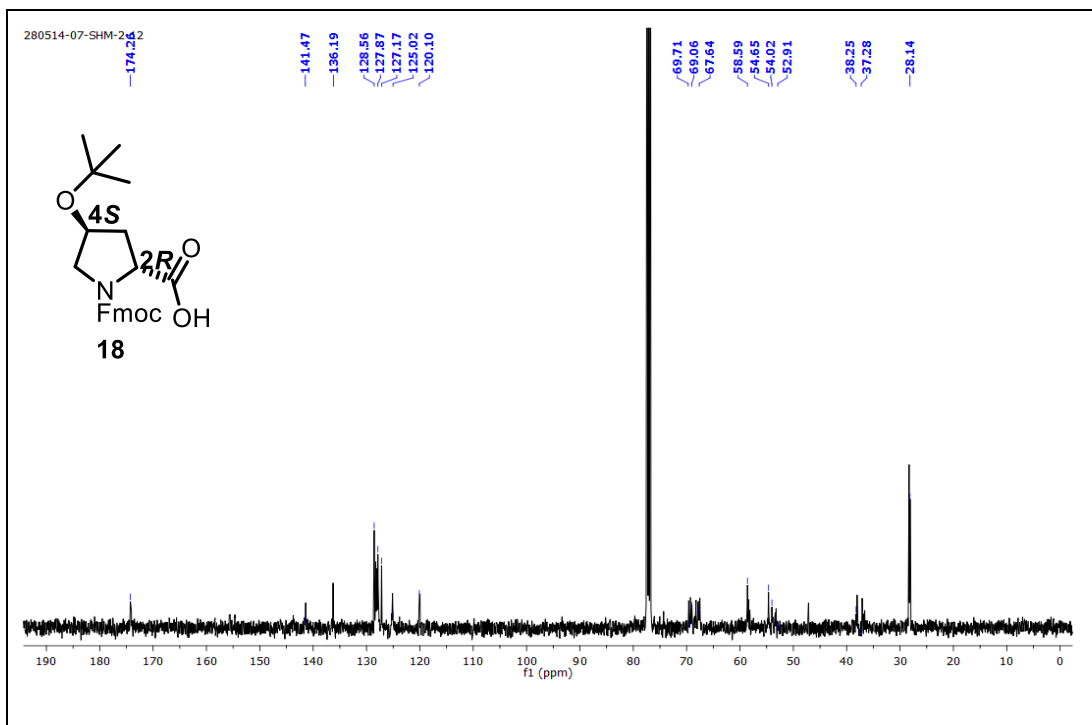
H^1 NMR of compound (2*R*,4*R*)-N1-(benzyloxycarbonyl)-*cis*-4-(*t*-butyl) hydroxy-D-proline methyl ester (19)
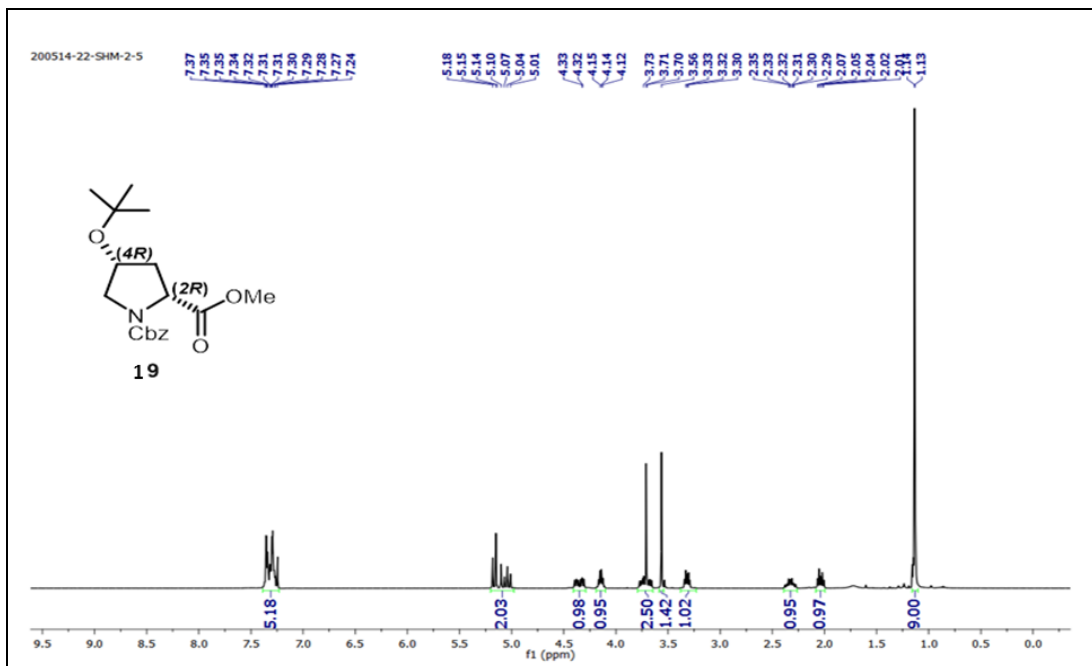
C^{13} NMR of compound (2*R*,4*R*)-N1-(benzyloxycarbonyl)-*cis*-4-(*t*-butyl) hydroxy-D-proline methyl ester (19)
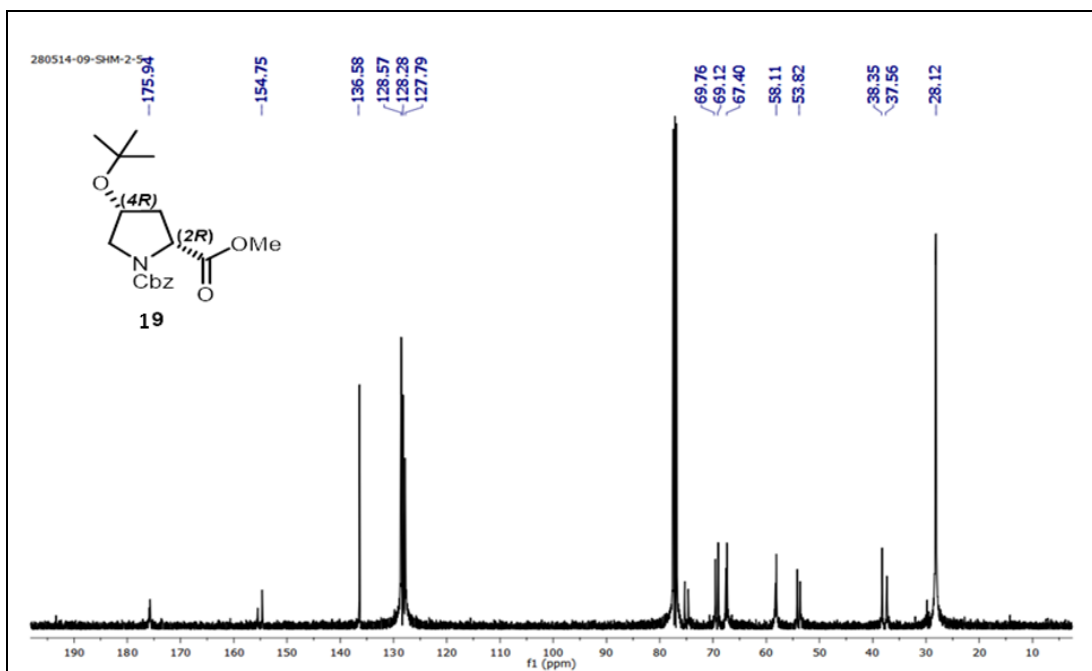
H^1 NMR of compound (2*R*, 4*R*)-N1-(fluorenylmethyloxycarbonyl)-*cis*-4-(*t*-butyl) hydroxy-D-proline (21)
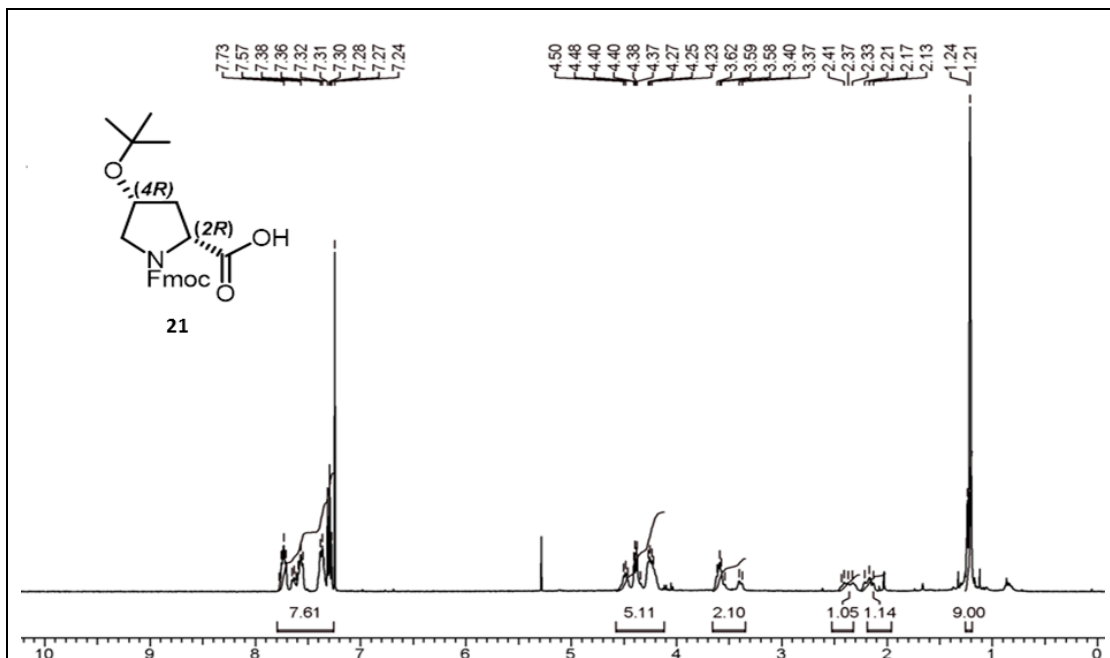
C^{13} NMR of compound (2*R*, 4*R*)-N1-(fluorenylmethyloxycarbonyl)-*cis*-4-(*t*-butyl) hydroxy-D-proline (21)
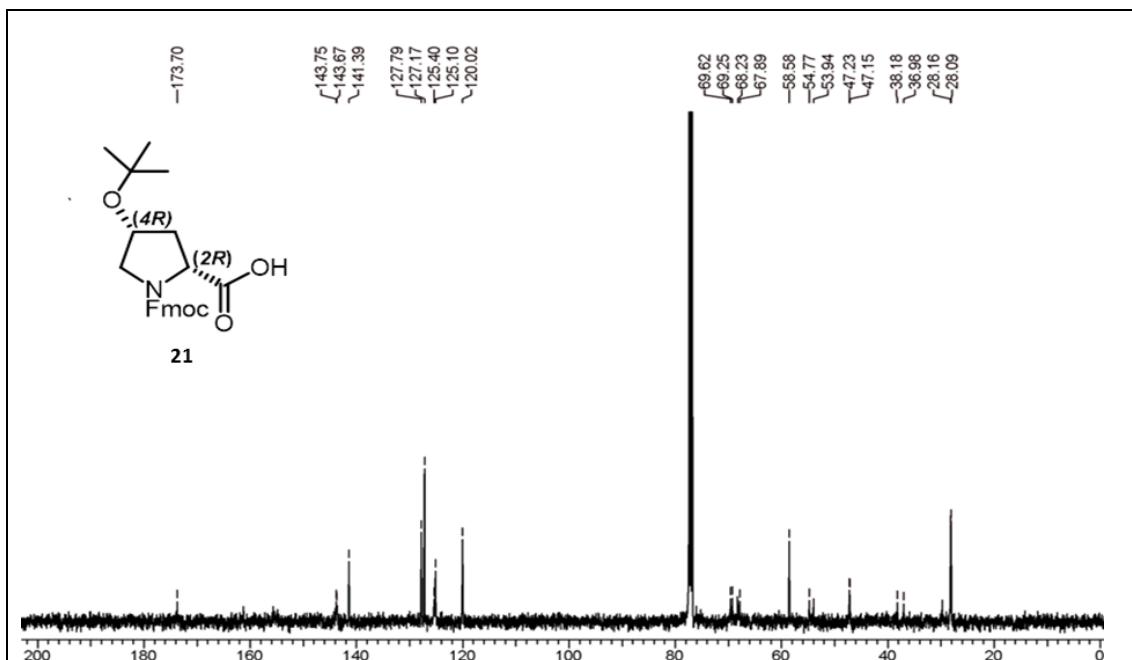
HPLC profile of peptide P1 Phe$_L$-L[DL]$_4$
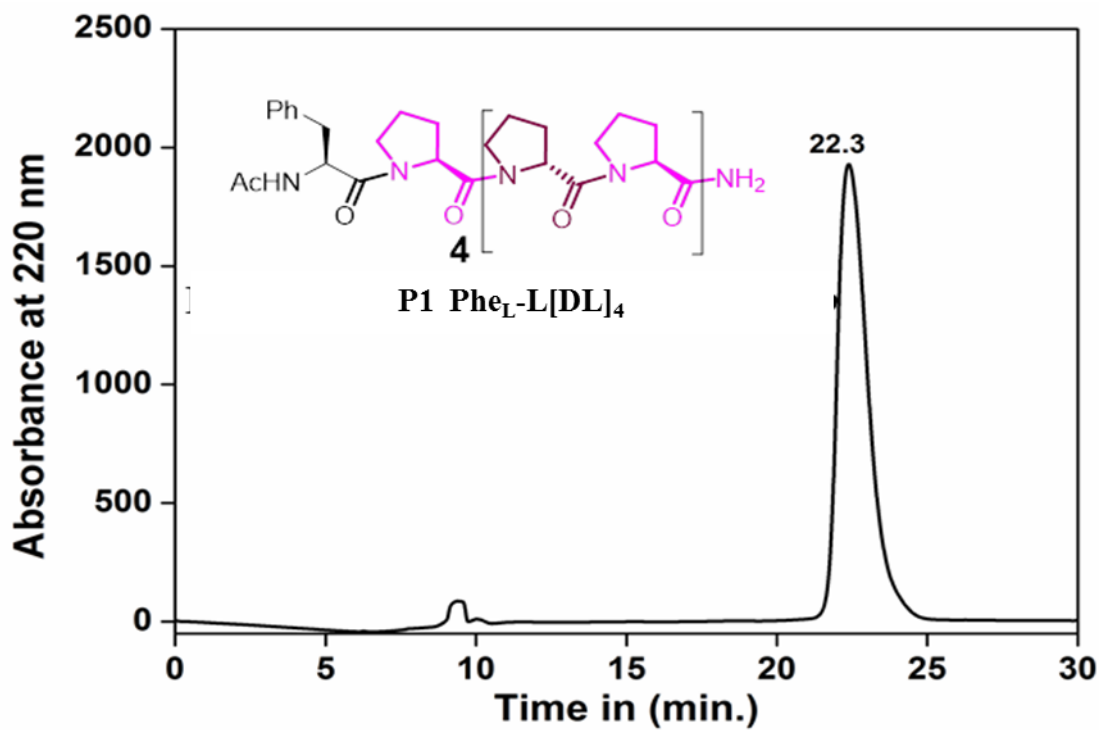
MALDI-TOF of peptide P1 Phe$_L$-L[DL]$_4$
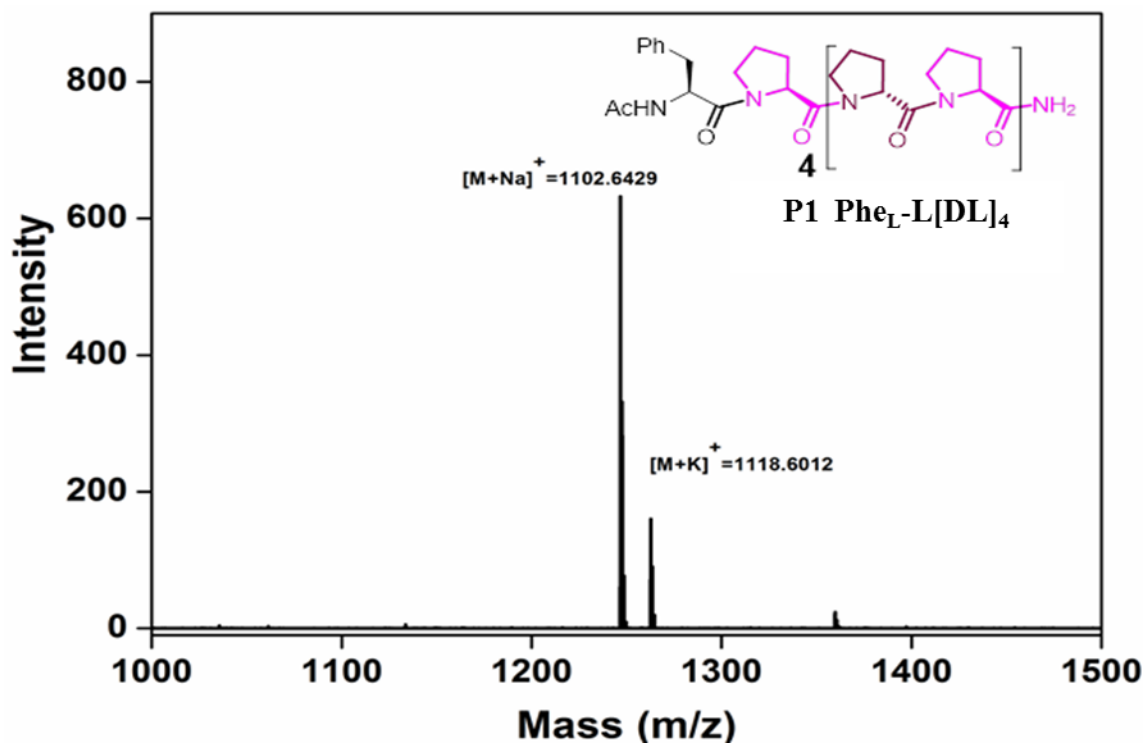
HPLC profile of peptide P2 Phe$_L$-L$_t$[L$_c$L$_t$]$_4$
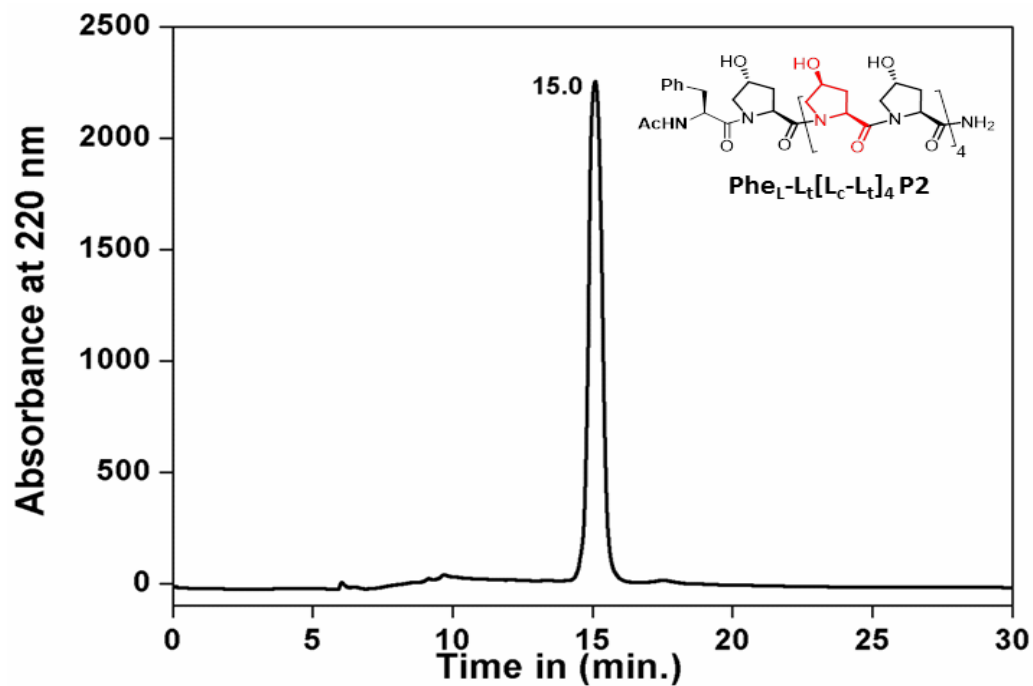
MALDI-TOF Spectra of peptide P2 Phe$_L$-L$_t$[L$_c$L$_t$]$_4$
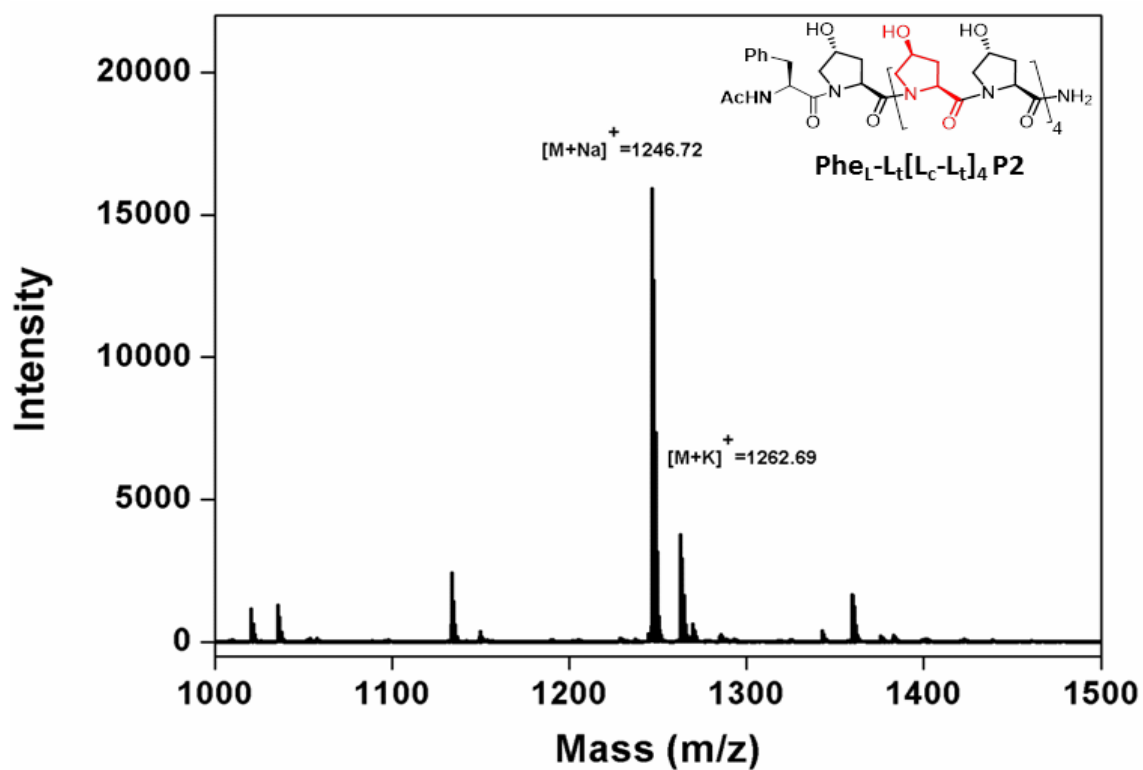
HPLC profile of peptide Phe$_L$-L$_t$[D$_t$L$_t$]$_4$ P3
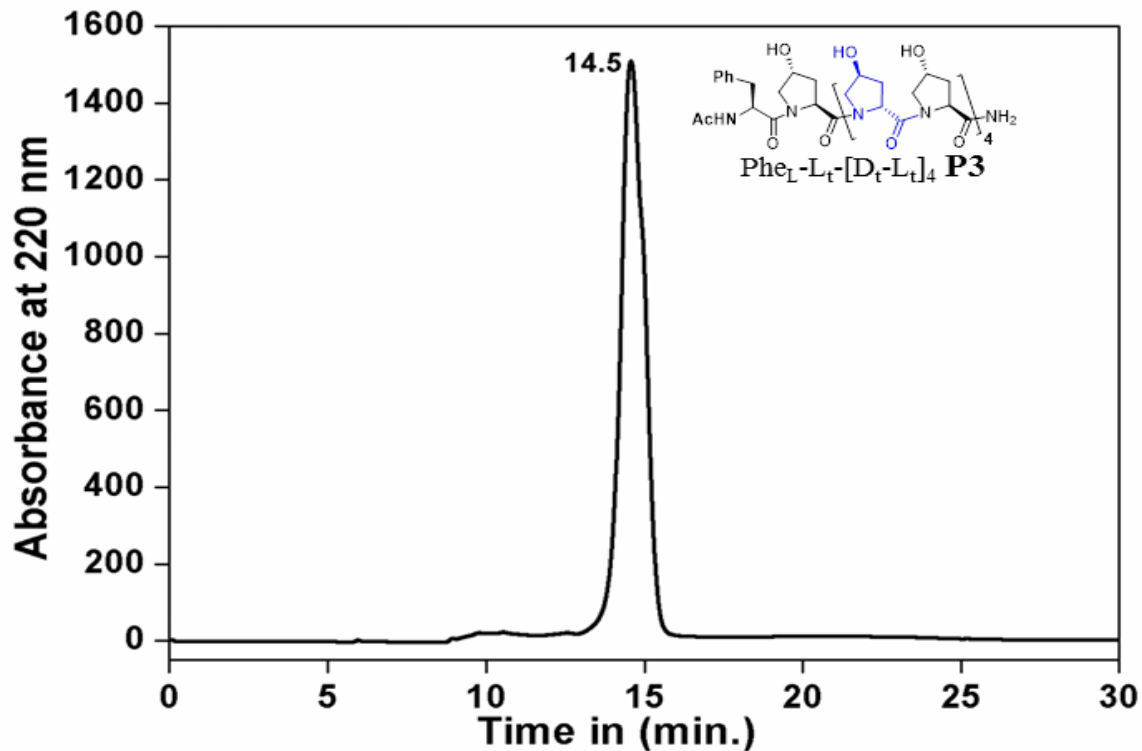
MALDI-TOF spectra of peptide Phe$_L$-L$_t$[D$_t$L$_t$]$_4$ P3
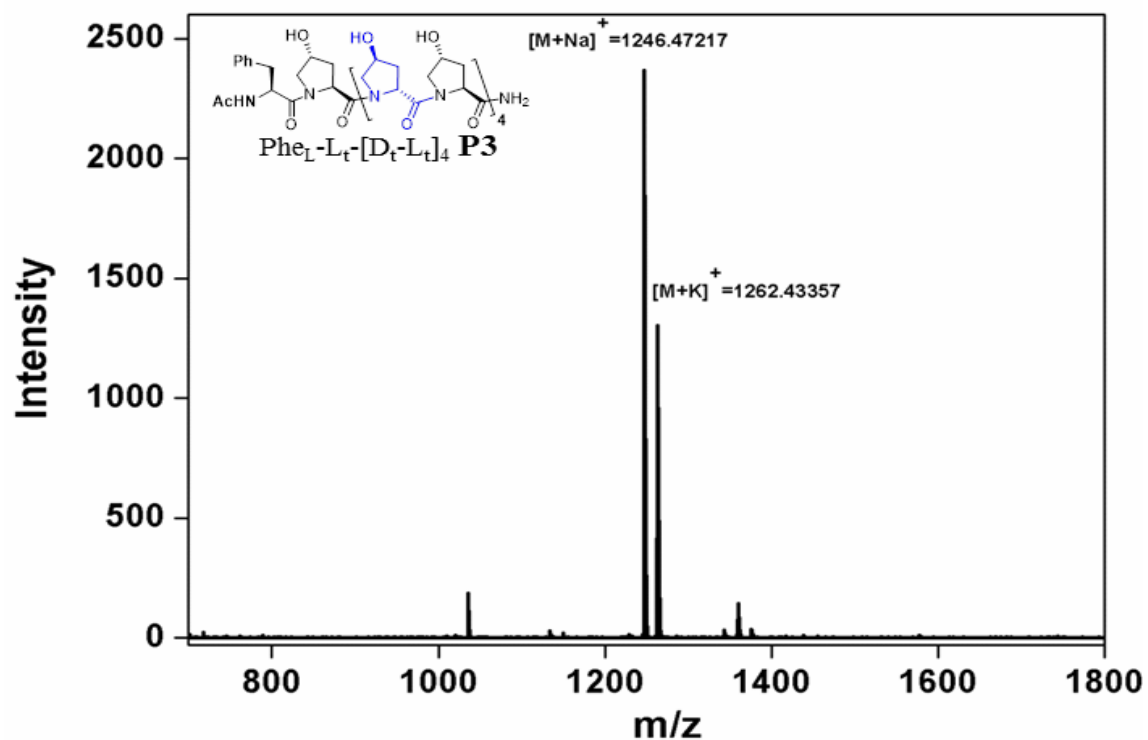
HPLC profile of peptide Phe$_L$L$_c$[D$_c$L$_c$]$_4$ P5
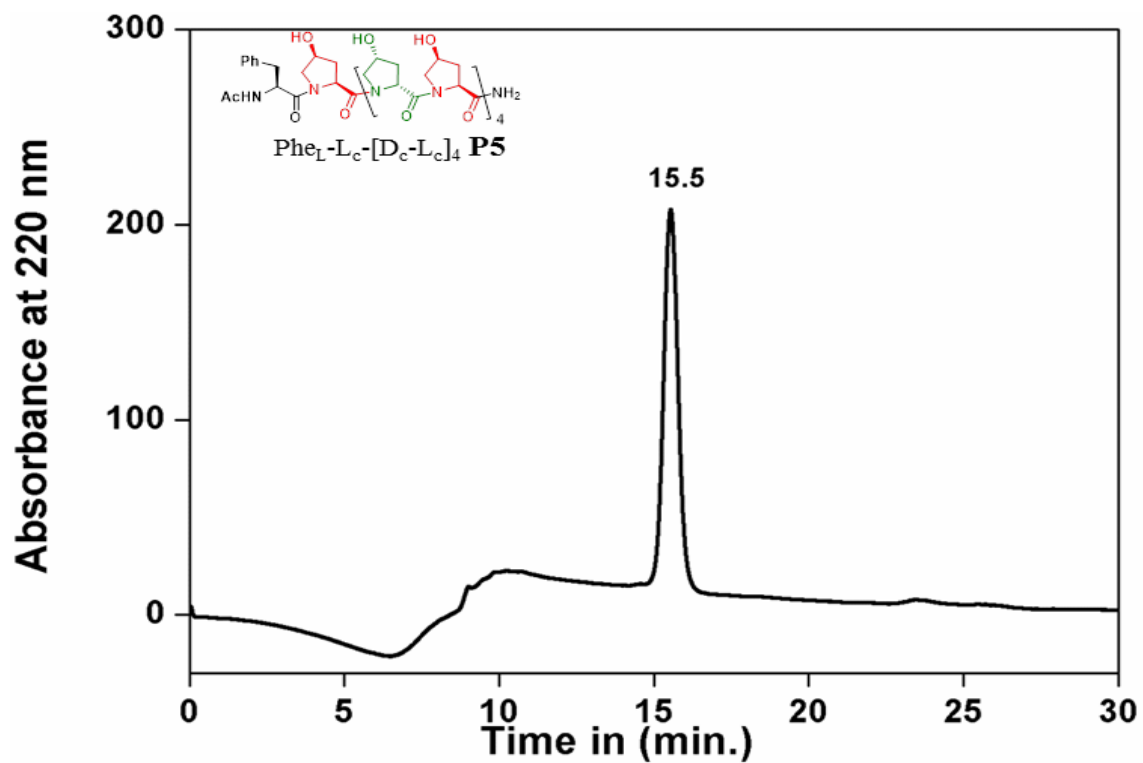
MALDI-TOF Spectra of peptide Phe$_L$-L$_c$[D$_c$L$_c$]$_4$ P5
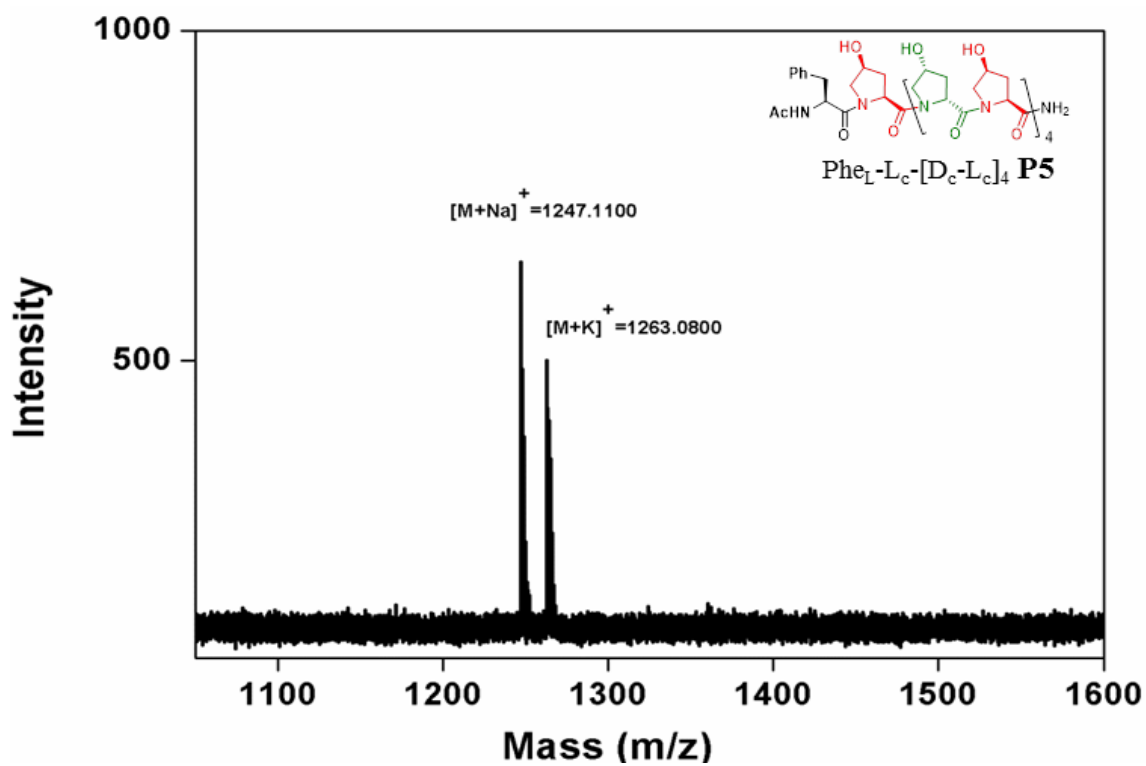
HPLC-Profile of peptide Phe$_D$-L$_t$[D$_t$L$_t$]$_4$ P6
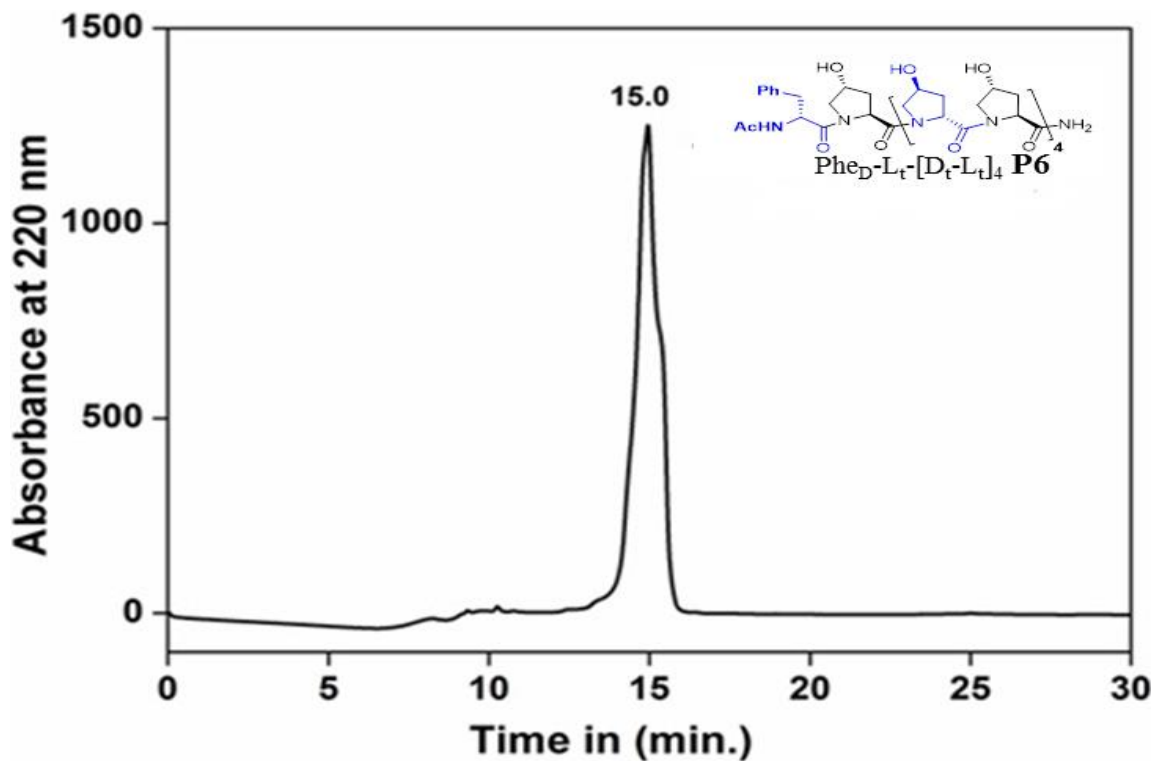
MALDI-TOF of peptide Phe$_D$-L$_t$[D$_t$L$_t$]$_4$ P6
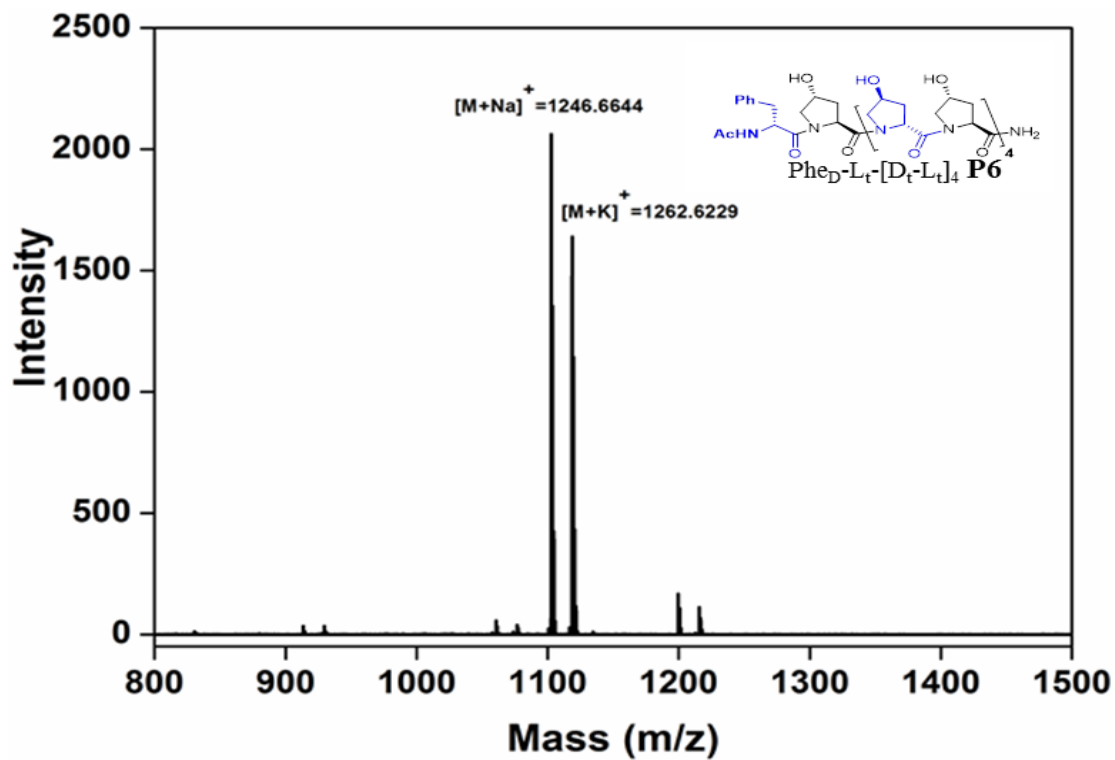
HPLC-Profile of peptide Phe_L-D_t[$L_t D_t$]$_4$ P7
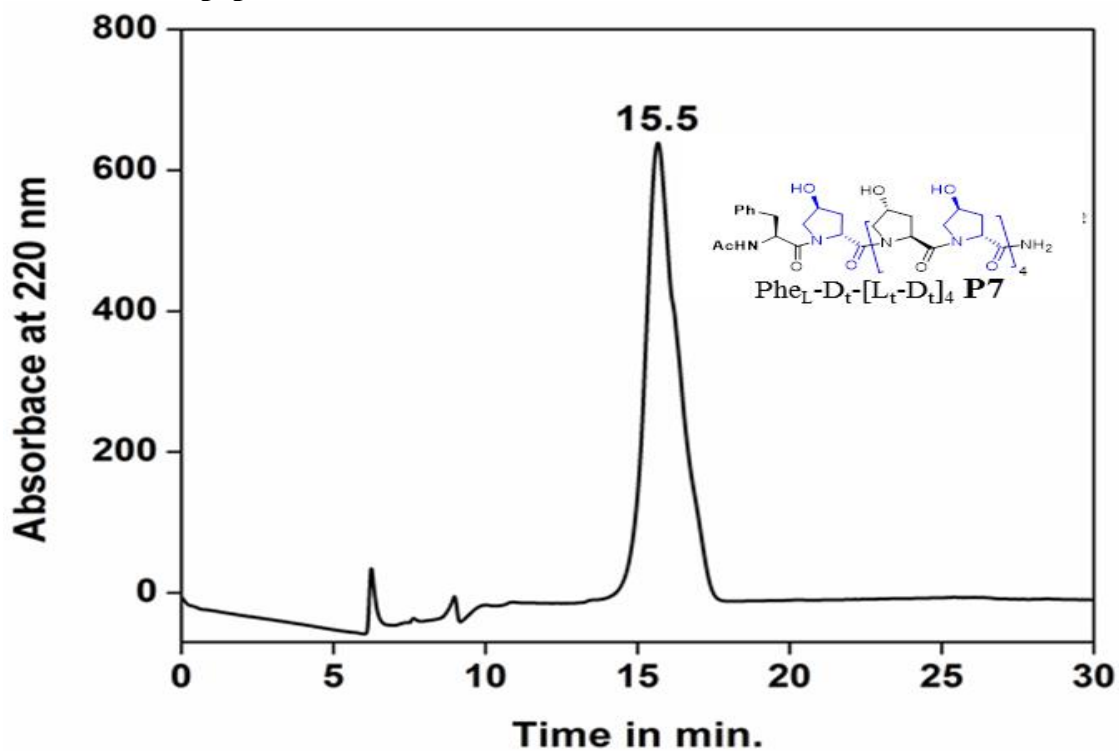
MALDI-TOF of peptide Phe_L-D_t[$L_t D_t$]$_4$ P7
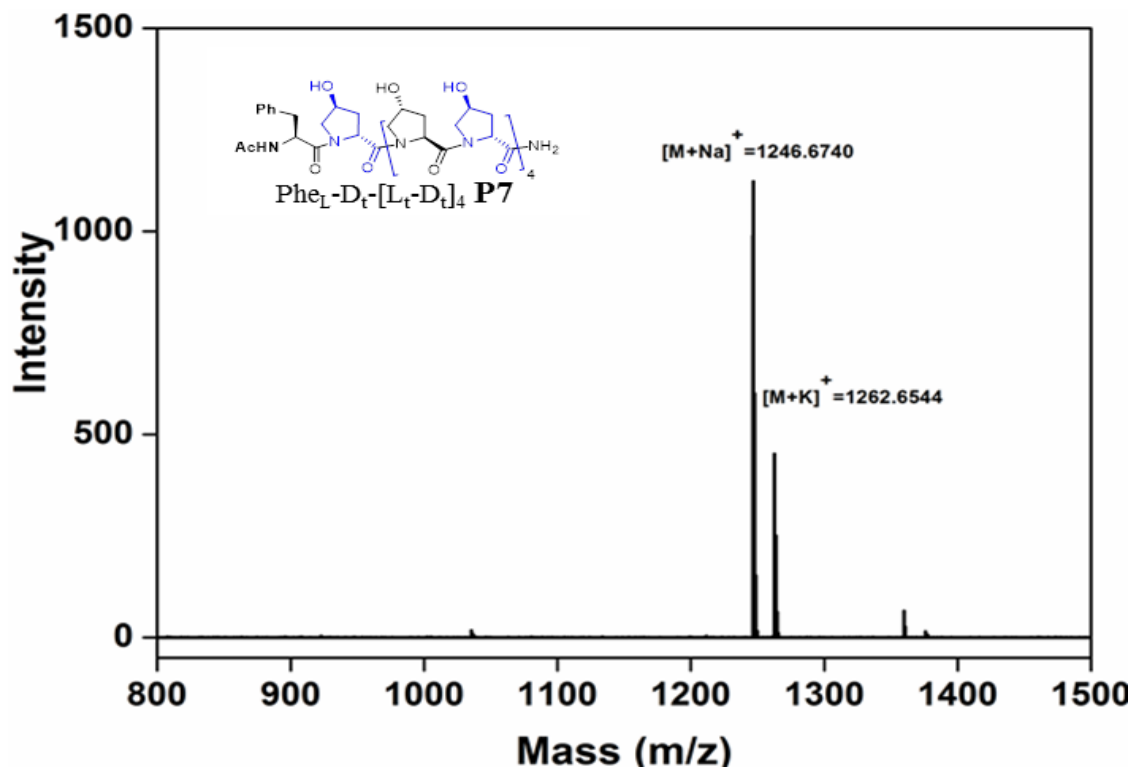
HPLC-Profile of peptide PA-[L$_t$D$_t$]$_4$ P8
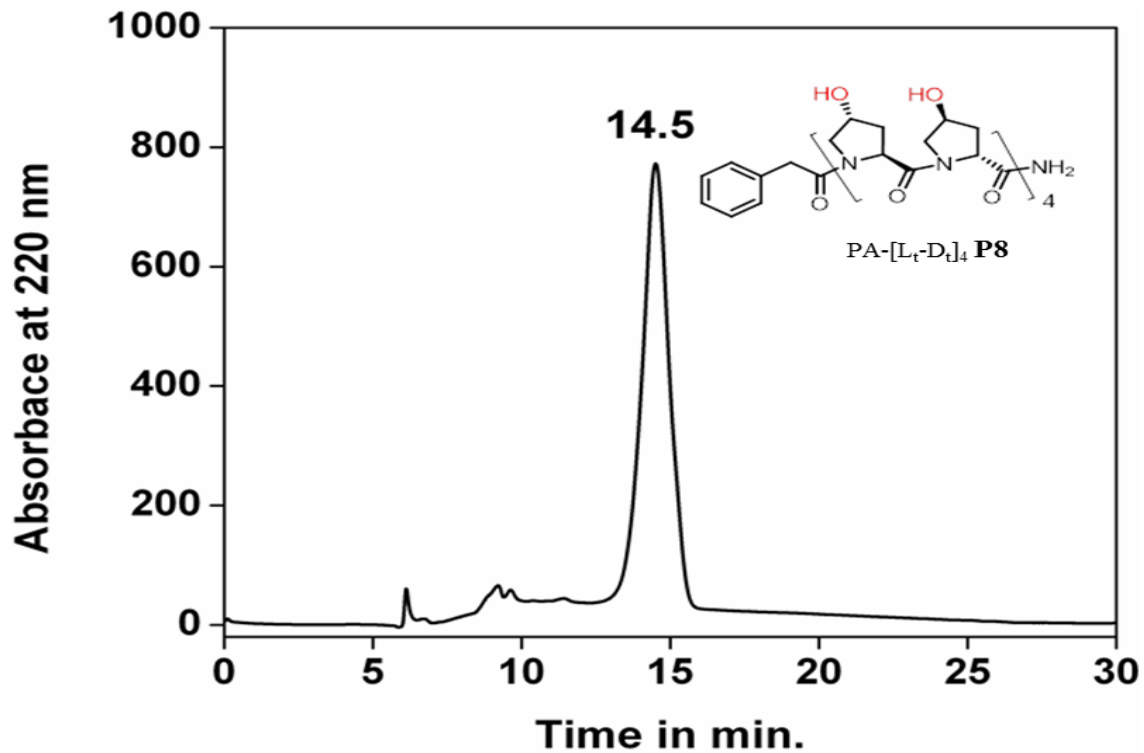
MALDI-TOF of peptide PA-[L$_t$D$_t$]$_4$ P8
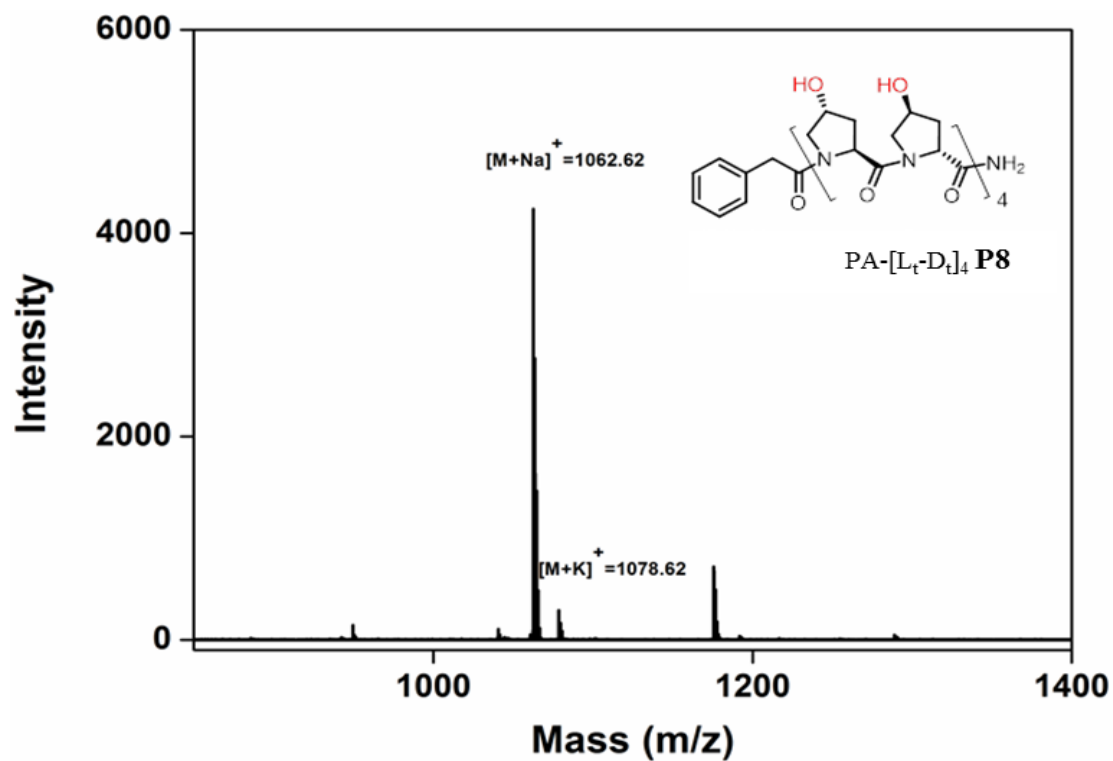
HPLC-Profile of peptide Phe$_L$[L$_c$]$_4$[L$_t$]$_5$ P9
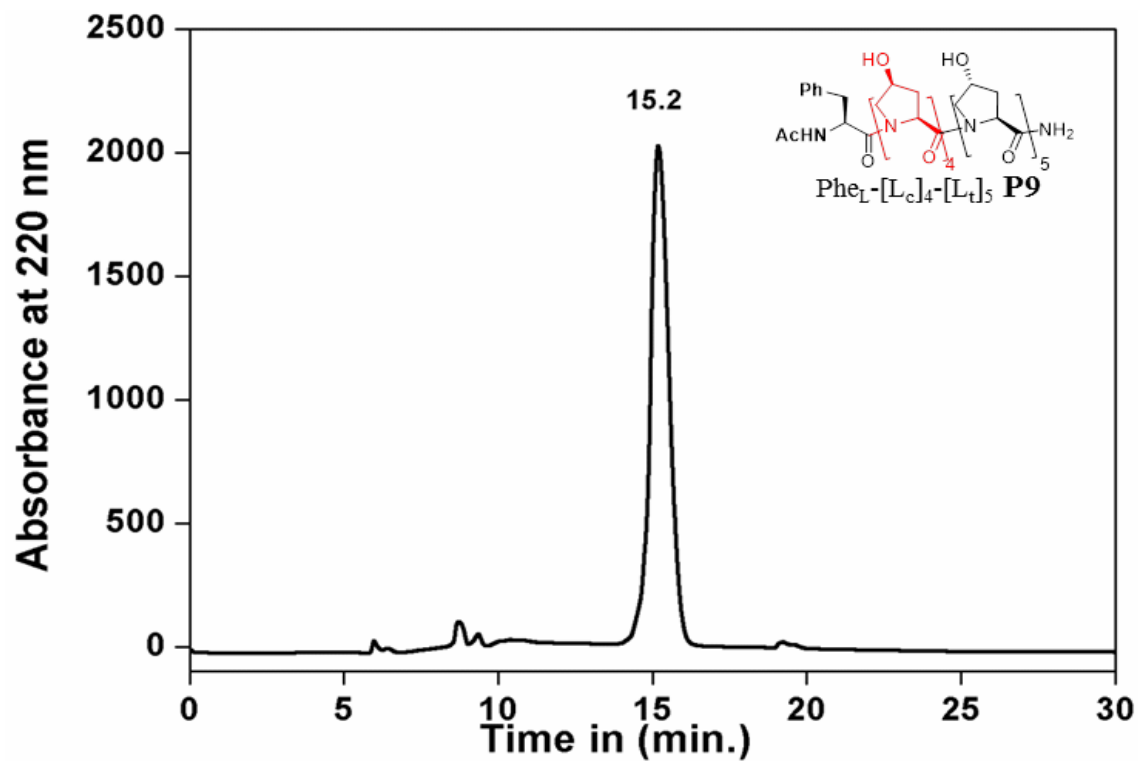
MALDI-TOF Spectra of Phe$_L$[L$_c$]$_4$[L$_t$]$_5$ P9
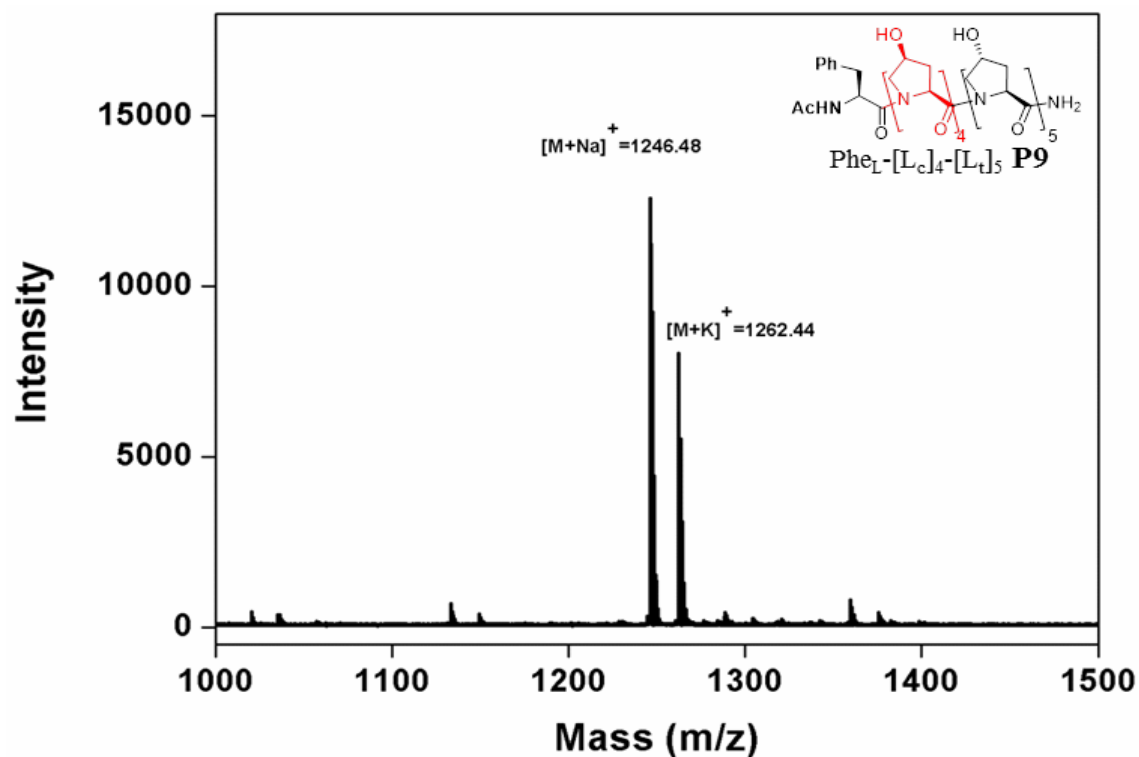
HPLC profile of peptide Phe$_D$[D$_t$]$_4$[L$_t$]$_5$ P10
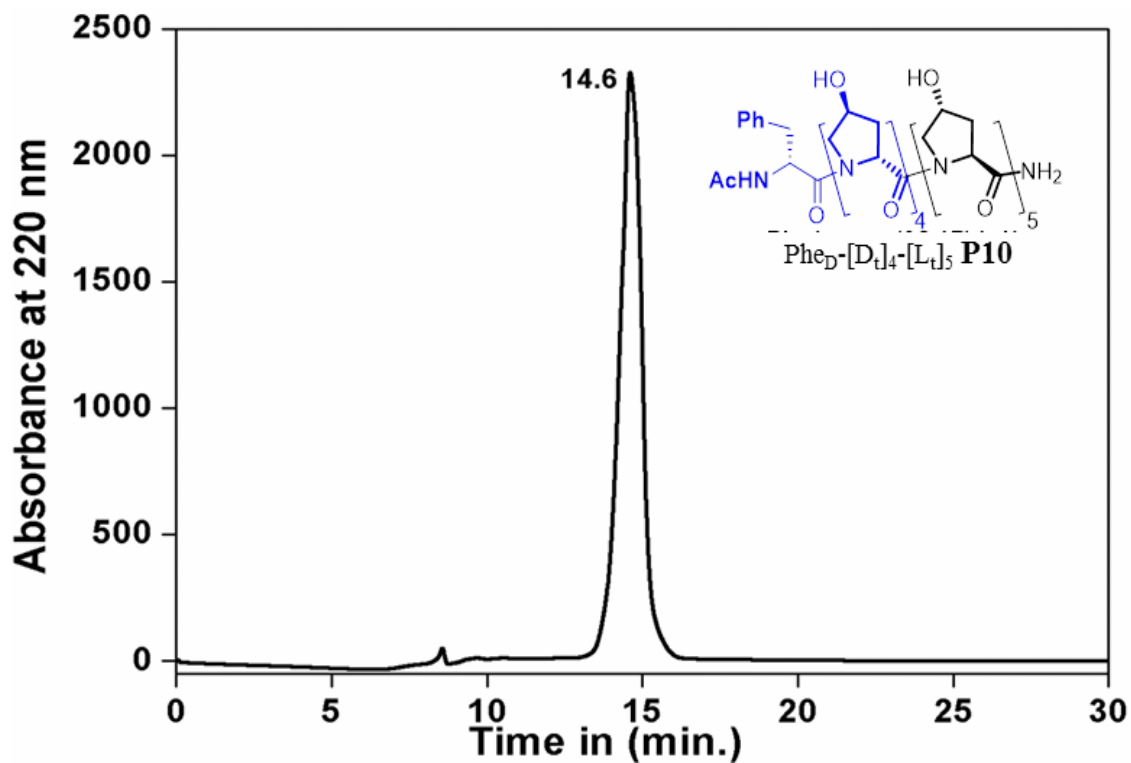
MALDI-TOF spectra of peptide Phe$_D$[D$_t$]$_4$[L$_t$]$_5$ P10
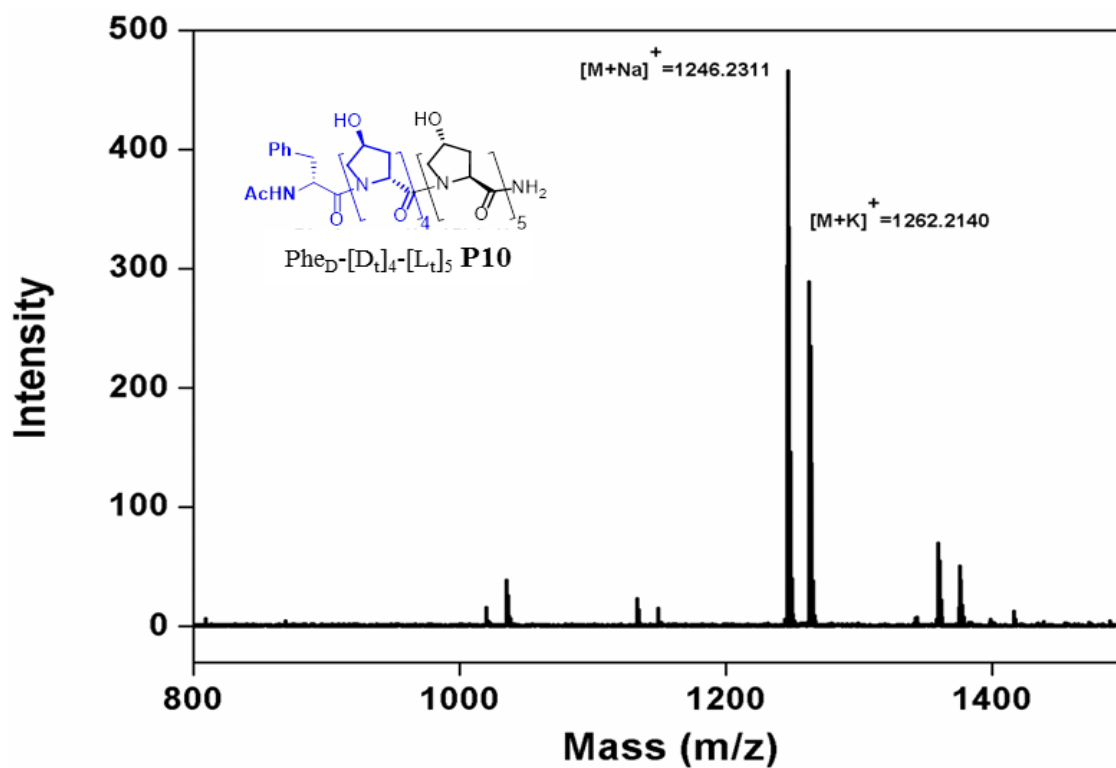
HPLC profile of peptide Phe_D[D_c]_4[L_c]_5 P11
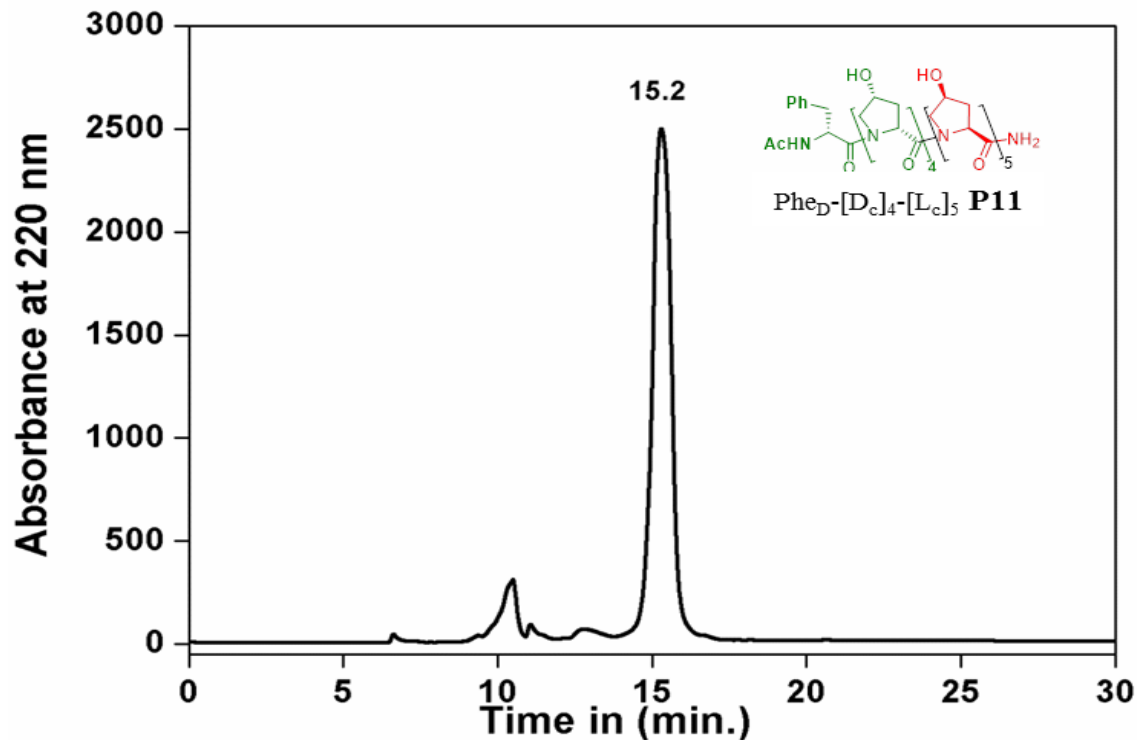
MALDI-TOF Spectra of of peptide Phe_D[D_c]_4[L_c]_5 P11
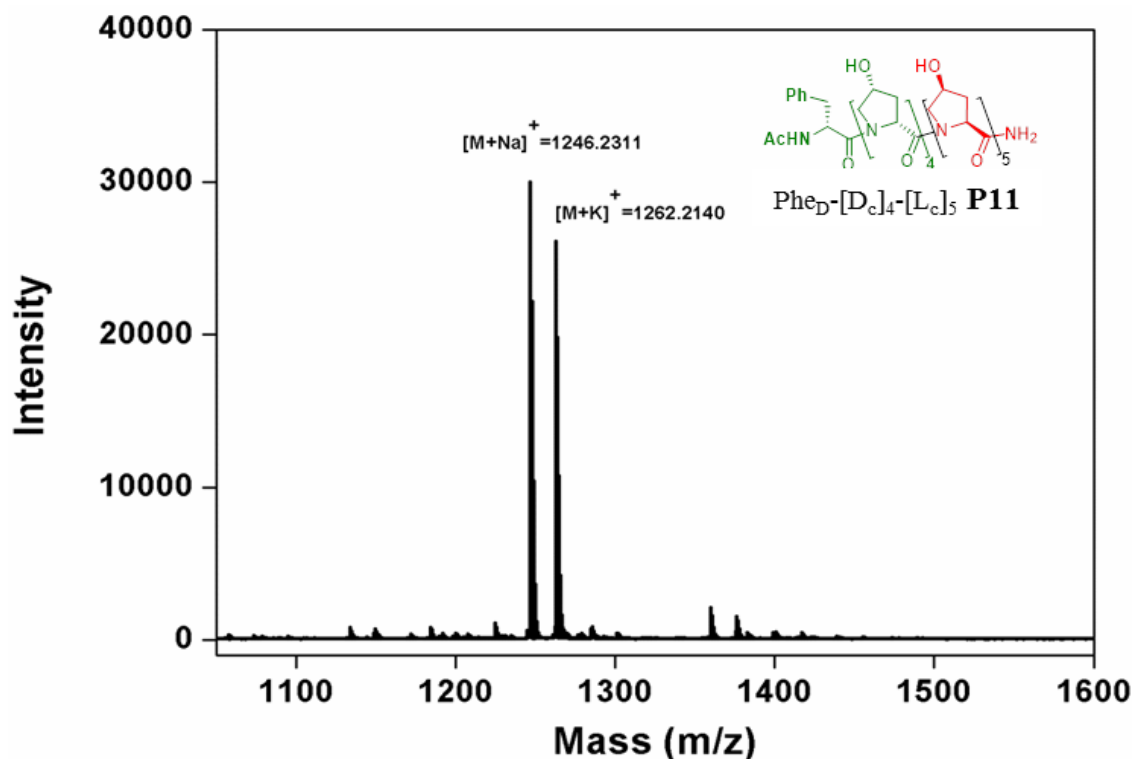
HPLC profile of peptide C$_{14}$-Phe$_L$L$_t$[D$_t$L$_t$]$_4$ P12
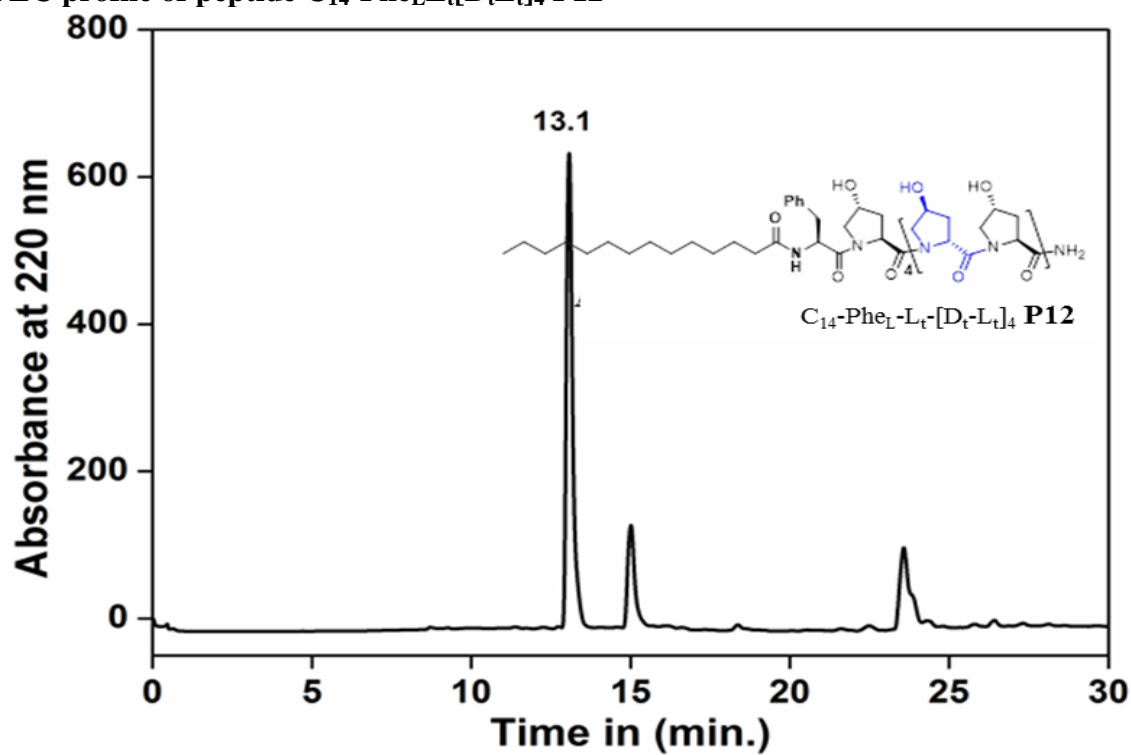
MALDI-TOF of peptide C$_{14}$-Phe$_L$L$_t$[D$_t$L$_t$]$_4$ P12
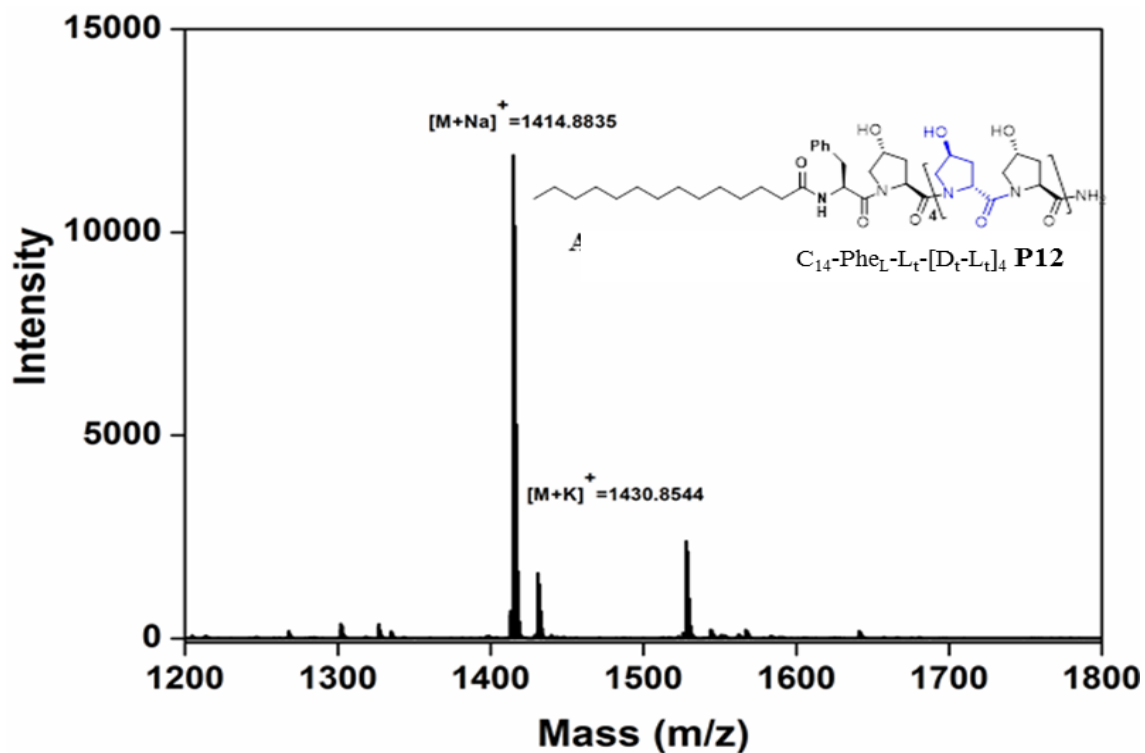
Chapter 4

Self-assembly of 4R/S-Hydroxy/Amino Collagen Peptide Spiegelmers

Section A: Self-assembly of 4R/S-Hydroxy Collagen Peptide Spiegelomers

4.0 Introduction to collagen proteins

The word 'Collagen' is derived from the Greek word meaning glue. Initially it was described as the constituent of connective tissue which gives gelatine on boiling. Collagen is an abundant structural protein found in mammals.[1] In the human body, collagen consists of one-third part of all proteins and is an important component of extracellular matrix (ECM). The collagen belongs to an important family of proteins, which undergo a multi-step hierarchical self-assembly in which individual peptide chains assemble into a canonical triple helix. These triple helices then assemble to form higher order structures which are mostly fibrous in nature. This fibrous protein is present in all connective tissues such as skin, cartilage, tendons, bone, basement membrane, blood vessels and gives stability to perform functions. There are twenty-eight different types of genes conserved in genome for the synthesis of the collagen proteins. The collagen proteins are synthesized in the endoplasmic reticulum (ER) and are then secreted into the extracellular matrix.

The most defining and important structural motif of the collagen proteins is right handed triple helix, where three parallel left-handed polyproline II type (PP II) helices with $\varphi = -75^0$, $\psi = 145^0$, and $\omega 180^0$ are intertwined around one another on a common axis. These three strands are held together by hydrogen bonding, originating from NH (H-bond donor) of glycine and CO (H-bond acceptor) of next proline residue from adjacent strand with one residue staggered, to form right-handed super helix.[2] The primary structure of collagen is composed of X-Y-Gly repeat, the amino acids in the X and Y positions in collagen being predominantly (2*S*)-L-proline (Pro, 28%) and (2*S*, 4*R*)-L-4-hydroxyproline (Hyp 38%) respectively. These amino acids account for 20% of the total amino acids composition of natural collagen. The other commonly found amino acids are Ala, Lys, Arg, Leu, Val, Ser, and Thr.[3] Hydroxyl group in 4-hydroxyproline (Hyp) provides exceptional mechanical strength, broad resistance to the proteolytic enzyme and thermal stability to the triple-helical structure of collagen.

4.1 Literature survey on self-assembly of peptides

The self-assembly process is mediated by non-covalent interaction including van der Waals force, hydrogen bonding, electrostatic and π-π stacking interactions. The

fabrication of new materials using natural building blocks (biomolecules) like oligosaccharides, phospholipids, proteins, peptides, and oligonucleotides has gained special attention.[4] Among them, peptides have become a subject of major interest due to their simple structure, more chemical and thermal stability, diversity in sequences and ease of synthesis in large amount. Due to diversity in sequences and shapes, peptides are known to create self-assembled nano structures of different shapes and size and are used in medical applications because of their intrinsic properties such as biocompatibility and biodegradability.

There are 20 natural L-amino acids from which all proteins and peptides are made. All these naturally occurring amino acids are chiral in nature except glycine. The sequences, types, number of residues and chirality in peptides dictate the surface morphology, nature and dimensions of nano structures.

4.2 Self-Assembly of collagen mimetic peptides and its enantiomers

Self-assembly of collagen mimetic peptides is important because biomaterials made from this biopolymer has several potential applications with advantages over other biopolymers in specific biomedical, cosmetics, drug delivery and various other fields. Materials made from collagen have good properties like biodegradability, super biocompatibility, and weak antigenicity.[5] Along with these properties, it also suffers from some immunological and pathological problems.[6] In this respect, study of the self-assembly of collagen peptides assumes importance. Scientists have achieved self-assembly of collagen peptides in various ways such as electrostatic attraction of opposite charges on N-terminus and C-terminus,[7] hydrophobic force of attraction through (π-π stacking),[8] cation-π interaction,[9] covalent bonding with the help of cysteine knot,[10] chemical ligation[11] to have a three-dimensional structure using metal.[12]

Nanda *et al.*[13] incorporated D-proline, in the repeats of X-Y-Gly, (Pro-Pro-Gly) to form a left-handed triple helix and on mixing of left and right-handed triple helix solutions, they observed nano-sheets, which is derived from hydrophobic groove interactions (Figure 1).
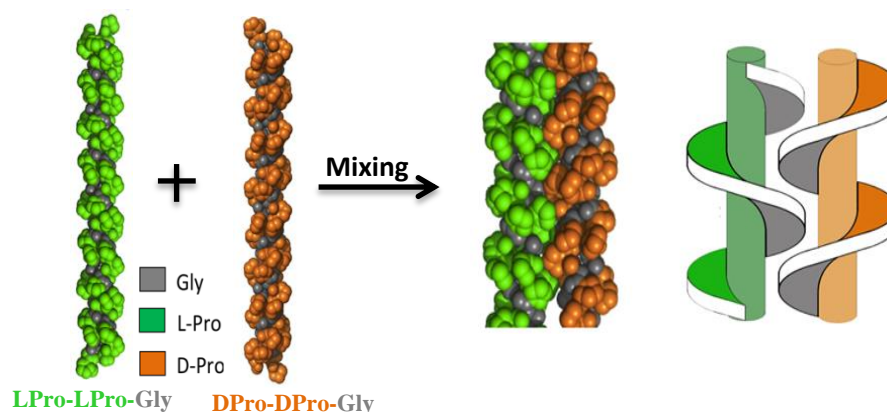
Figure 1. Self-assembly of enantiomeric collagen peptides.[13]

4.3 Self-Assembly of enantiomeric peptides

In 1962, it was shown that the methyl ester of helical homo-polypeptides of L-glutamate and its enantiomer D-glutamate when mixed at room temperature form rigid gel in organic solvents like chloroform:dioxane and precipitation occurred in solvents like DMF.[14] Fuhrhop *et al.*[15] showed that while poly (L-Lysine) forms right-handed α-helix, poly (D-Lysine) forms left handed α-helix and interestingly upon mixing these together in equimolar amounts, they precipitate into *β*-pleated sheet structure, arranged in an anti-parallel orientation (Figure 2).
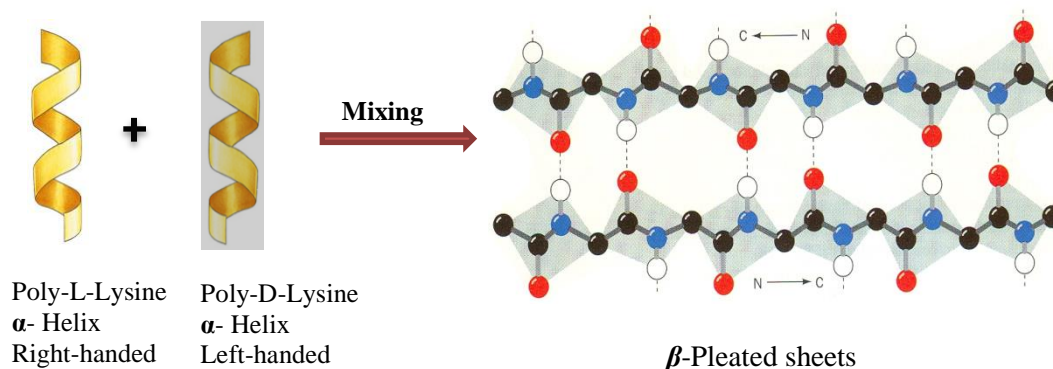
Figure 2. Self-assembly of poly-L-lysine and poly-D-lysine peptides.[15]

Schneider *et al.*[16] synthesized a 20-mer *β*-hairpin forming peptide, each single chain peptide composed of two *β*-strand folding sequence connected with loop which takes type II' *β*-turn and self-assembled into a hydrogel made up of a network of peptide fibrils. Peptides made from L-amino acids and D-amino acids upon mixing in equimolar concentrations, formed hydrogels. These hydrogels from enantiomeric peptides showed

a four fold increase in rigidity than that made from individual peptides of the same concentration (Figure 3).

| MAX1 | VKVKVKVKV^{D}PPTKVKVKVKV$-NH_2$ |
| DMAX1 | VKVKVKVKV^{L}PPTKVKVKVKV$-NH_2$ |
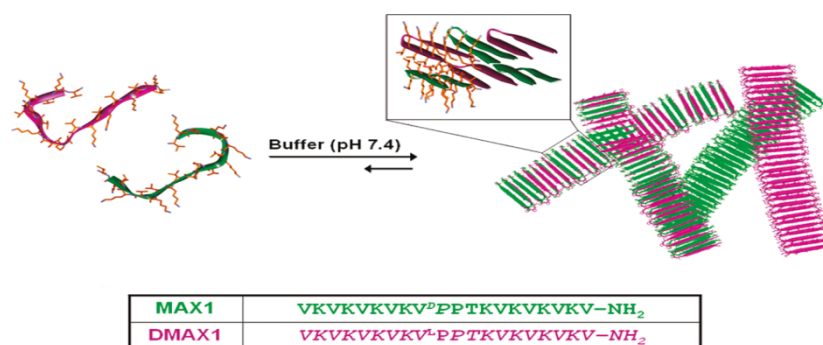
Figure 3. Self-assembly of the β-hairpin folding peptide, mixing results into the hydrogel.[16]

Nilson *et al.*[17] synthesized two octamer amphipathic peptides L-Ac(FKFE)$_2$-NH$_2$ and D-Ac(FKFE)$_2$-NH$_2$ derived from L and D amino acids respectively. Single strand of peptides form β-sheet secondary structure. Mixing of these enantiomeric peptides results in alternate co-assembly of β-sheet fibrils (Figure 4).
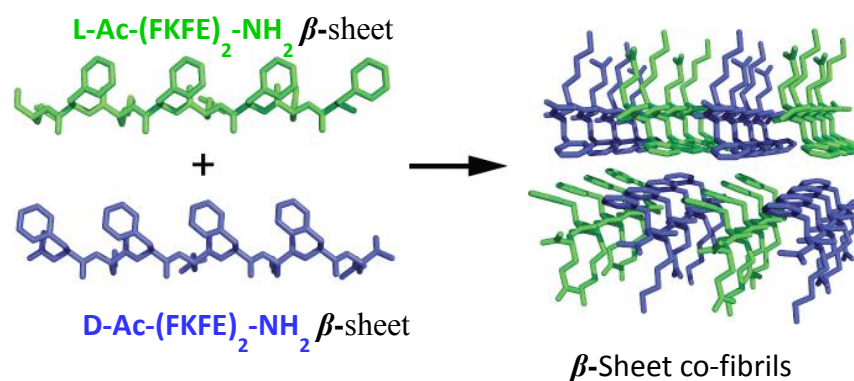
Figure 4. Self-assembly of amphipathic L+D peptides into alternate **β**-sheet fibrils.[17]

4.4 Rationale and objectives of the present work

Nucleation of single chain collagen peptides starts when proly-4-hydroxylase [P4-H] enzyme along with its cofactor, replace C4-H by hydroxyl group (-OH) specifically in 4R-configuration, in post-translational modification at Y site in the peptide triad [-X-Y-Gly-]. The 4R-OH of proline codes for strand association to provide exceptional thermal stability and broad resistance to the proteolytic enzymes. Crystal structure of collagen shows that hydroxyl groups are pointing in one direction on the

periphery of the circle (Figure 5A). By this logic in the enantiomeric peptide chain, the 4-OH groups must point in the opposite direction as in Figure 5B [4*R* vs 4*S*). On this basis, upon mixing, these enantiomeric peptides may come together through complementary association of hydrogen bonds generated by the hydroxyl groups.
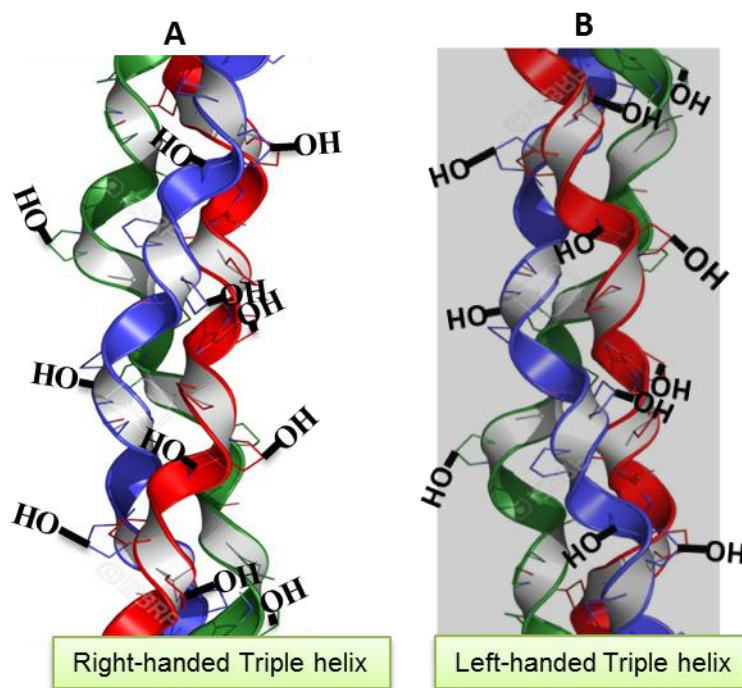
Figure 5. A) L-collagen right-handed[18] **B)** proposed D-collagen left-handed[19]

Literature survey suggests that enantiomeric peptides can self-assemble upon mixing. Poly L-lysine forms right-handed α-helix while poly D-lysine forms left handed α-helix, these peptides alone do not self-assemble into large structures due to charge repulsion. However on mixing the left and right-handed solutions together, a precipitate results with *β*-pleated sheet structure.[15] D-proline was incorporated in the repeats of [-X-Y-Gly-] to form left-handed triple helix and on mixing of left and right-handed triple helix solutions, Nanda *et al*.[13] observed sheet formation based on hydrophobic groove interactions of opposite handed helices.

In the present work, we have synthesized collagen mimetic peptides [-X-Y-Gly]$_n$ where X and Y positions contain (2*S*)-L-proline and (2*S*,4*R*)-4-hydroxy-L-proline, and the corresponding D-enantiomers (2*R*)-D-proline and (2*R*,4*S*)-4-hydroxy-D-proline respectively. Hydroxyproline makes a difference to the model precursor of collagen

peptides (Pro-Pro-Gly), as it provides exceptional thermal stability and broad resistance to the proteolytic enzymes.

The secondary structures of these peptides were investigated by CD spectroscopy, which is also used to determine the thermal stability and that of a mixture of peptides. FE-SEM and AFM techniques were used to diagnose the morphology of self-assembled structures of individual and mixed peptides.

The specific objectives of the present proposed work are as follows

❖ Synthesis of (2*R*,4*S*)-N1-(Fmoc)-4-(O-*t*-Bu) hydroxyproline monomer
❖ Solid phase synthesis, purification & characterization of collagen peptides: L-Collagen peptide **P1** and D-Collagen peptide **P2**
❖ Investigation of the conformation of enantiomeric collagen mimetic peptides and thermal stability of resulting collagen triple helices by CD-spectroscopy.
❖ Self-assembly of peptides studied by imaging techniques AFM, FE-SEM.

L-*Phe*-[-(2*S*)-L-*Pro*-(2*S*, 4*R*)-L-*Hyp*-*Gly*-]₆

L-Collagen peptide P1

D-*Phe*-[-(2*R*)-D-*Pro*-(2*R*, 4*S*)-D-*hyp*-*Gly*-]₆

D-Collagen peptide P2

4.4.1 Synthesis of *trans*-(2*R*,4*S*)-4-hydroxy-D-proline monomer

The *cis*-(2*R*,4*R*)-4-hydroxy-D-proline **1** was synthesized from the commercially available *trans*-(2*S*,4*R*)-4-hydroxy-L-proline by inversion of stereochemistry at C2. This was achieved by reacting *trans*-(2*S*,4*R*)-4-hydroxy-L-proline with acetic anhydride and hydrochloric acid at 140 ^{0}C to obtain *cis*-(2*R*,4*R*)-4-hydroxy-D-proline.[20] This was confirmed by crystal structure and optical activity $[\alpha]^D_{20}$ +59^0 (lit. $[\alpha]^D_{20}$ +59^0) in water. Compound **3** explained in Chapter 2 was used to synthesize the *trans*-D monomer **18**.

To synthesize 4*S*-OH-proline **14**, 4*R*-OH compound **3** was reacted with DCC in presence of catalytic amount of CuCl followed by treatment with formic acid and hydrolysis with aq. 2N NaOH to yield desired *trans*-(2*R*,4*S*)-4-hydroxy-D-proline acid

14. This was esterified to compound **15** and the 4*S*-hydroxyl group was protected with *t*-butylbromide to get compound **16**, followed by hydrolysis of ester with 2N aq. LiOH. The deprotection of Cbz in **16** was done by hydrogenation to yield 4*S*-O-*t*-butyl acid **17.** This was reacted with Fmoc-Cl to obtain monomer **18** [*trans*-(2*R*,4*S*)-4-hydroxy-D-proline]. All compounds were characterized by ^{1}H NMR and mass spectrometry and detailed synthesis of monomer **18** is explained in chapter 3.

Scheme 1: *Synthesis of (2R,4S) hydroxyproline monomer 18*
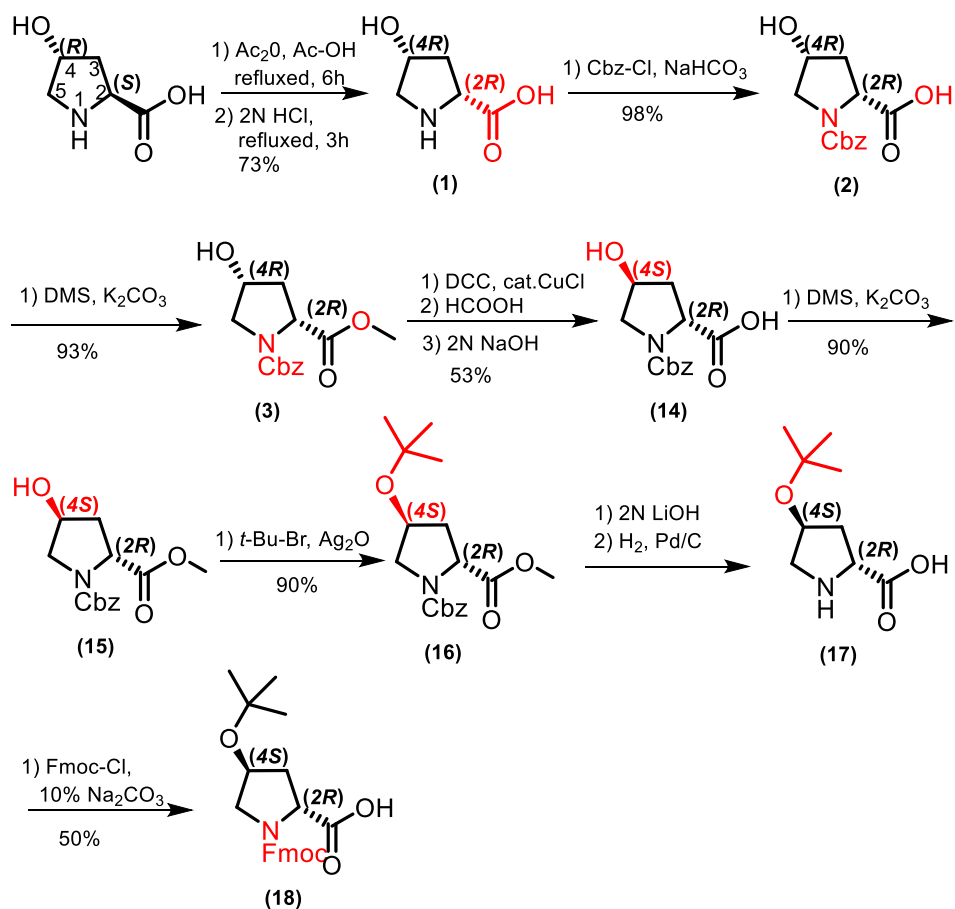
4.4.2 Solid Phase Peptide Synthesis

The desired peptides **P1** and **P2** were synthesized manually on a solid phase by using standard Fmoc protocol on commercial Rink amide resin (Nova biochem 100-200 mesh) with amine substitution of 0.61 mmol/g. The loading on resin was reduced to 0.3 mmol/g by partial capping of resin with acetic anhydride in pyridine.

The Fmoc group was removed by 20% piperidine in DMF, and the acid monomers were sequentially coupled by using HBTU as coupling agent, HOBt as racemisation suppressor and DIPEA as a base in DMF. For quantitative determination of peptides, UV-absorbing aromatic amino acid phenylalanine (L-*Phe*/D-*Phe*) was coupled at the N-terminus end, followed by acetylation using acetic anhydride in pyridine (1:2 v/v) ratio, to obtain the final peptide on solid phase.

4.4.3 Solid Phase Peptide Synthesis Flow Chart
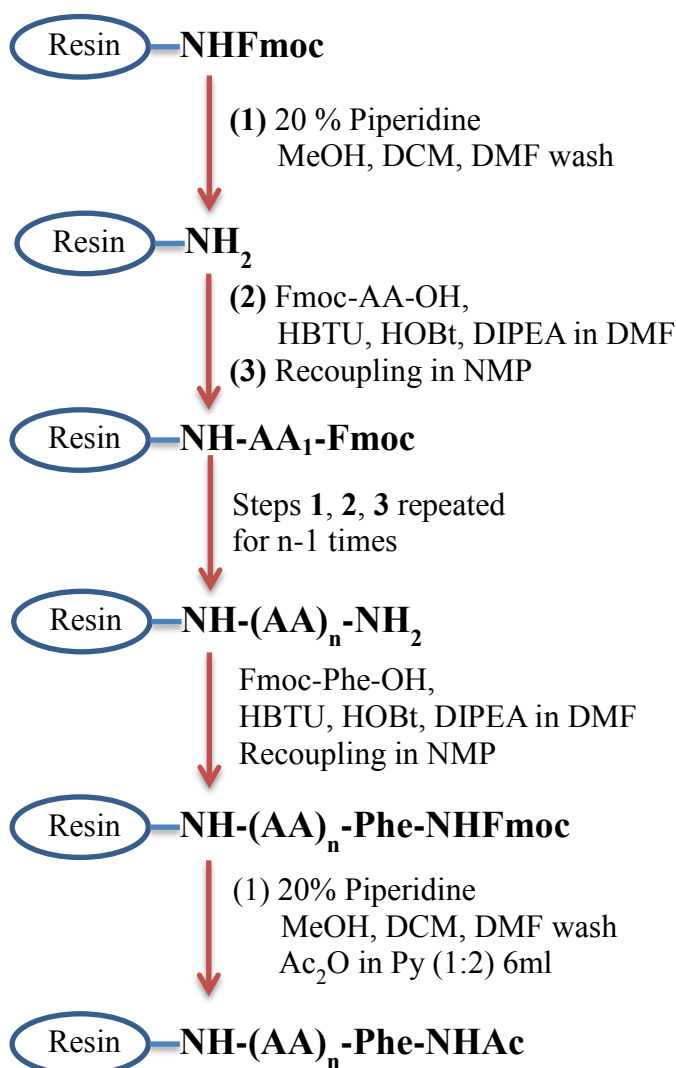
Resin —**NHFmoc**

(1) 20 % Piperidine
MeOH, DCM, DMF wash

Resin —**NH$_2$**

(2) Fmoc-AA-OH,
HBTU, HOBt, DIPEA in DMF
(3) Recoupling in NMP

Resin —**NH-AA$_1$-Fmoc**

Steps **1**, **2**, **3** repeated
for n-1 times

Resin —**NH-(AA)$_n$-NH$_2$**

Fmoc-Phe-OH,
HBTU, HOBt, DIPEA in DMF
Recoupling in NMP

Resin —**NH-(AA)$_n$-Phe-NHFmoc**

(1) 20% Piperidine
MeOH, DCM, DMF wash
Ac$_2$O in Py (1:2) 6ml

Resin —**NH-(AA)$_n$-Phe-NHAc**

The synthesized peptides were cleaved from the solid support by treating them with 90% trifluoroacetic acid (TFA) in DCM containing triisopropylsilane (TIPS) as a scavenger. The peptides were purified by HPLC using RP-C18 column in acetonitrile-water solvent system containing 0.1% TFA. The polypeptides were characterized by MALD-TOF mass spectral data.

Using the above mentioned solid phase protocol, two enantiomeric collagen mimetic peptides were synthesized in which 2(*S/R*)-L/D-proline and 4(*R/S*)-hydroxy-2(*S/R*)-L/D-proline were substituted at X and Y positions respectively in the repeating triad of X-Y-Gly.

Peptide Sequences P1-P2

L-*Phe*-[-(2S)-L-*Pro*-(2S, 4R)-L-*Hyp*-*Gly*-]₆   D-*Phe*-[-(2R)-D-*Pro*-(2R, 4S)-D-*hyp*-*Gly*-]₆

P1 L-Collagen peptide   **P2** D-Collagen peptide

Table 1: HPLC retention time and MALDI-TOF characterization of peptides **P1-P2**.

Sequence	Ret. time	Mol. Formula	Cal. Mass	Obs. mass
AcNH-L-Phe-[-L-Pro-L-Hyp-Gly-]₆-NH₂	16.1	$C_{83}H_{116}N_{20}O_{26}Na$	1832.94	1832.90
		$C_{83}H_{116}N_{20}O_{26}K$	1849.05	1848.92
AcNH-D-Phe-[-D-Pro-D-hyp-Gly-]₆-NH₂	16.2	$C_{83}H_{116}N_{20}O_{26}Na$	1832.94	1833.01
		$C_{83}H_{116}N_{20}O_{26}K$	1849.05	1849.04

4.4.4 Determination of peptide concentrations

To determine the concentrations of the peptides, UV-absorbing aromatic amino acid phenylalanine (*Phe*) was incorporated at the N-terminus, with L-*Phe* for peptide **P1**, and D-*Phe* for peptide **P2**. The concentrations of peptide stock-solutions were determined by phenylalanine absorption maximum at 257 nm and extinction coefficient of 195 $M^{-1}cm^{-1}$.[21] Since all peptides contain phenylalanine at N-terminus, any effect from this residue on collagen self-assembly will be same for all peptides.

4.5 RESULTS AND DISCUSSION

In this chapter CD spectroscopy is used to determine the secondary structure of peptides **P1** and **P2** and its temperature dependence is used to measure the thermal stability of the peptides.

4.5.1 Conformational study of collagen peptides P1 and P2 by CD spectroscopy

L-Collagen mimetic peptide **P1** (AcNH-L-Phe-(-L-Pro-L-Hyp-Gly-)$_6$-NH$_2$) and D-collagen mimetic peptide **P2**, (AcNH-D-Phe-(-D-Pro-D-hyp-Gly-)$_6$-NH$_2$) derived from L and D-prolines respectively are mirror image enantiomeric peptides. In CD spectra a weak positive CD band at 225 nm and a large negative CD band at 205 nm are characteristic peaks for left-handed polyproline-II (PP-II) helix in solution.
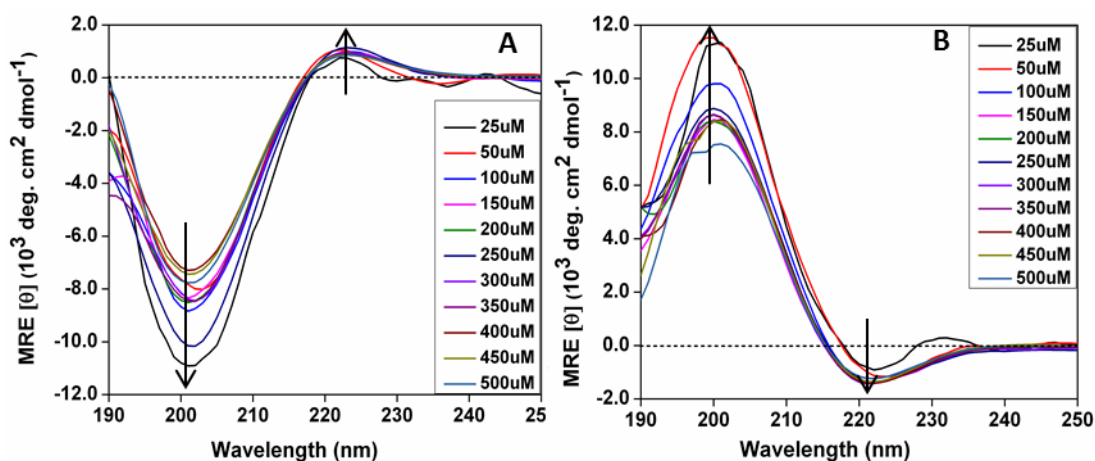
Figure 6. CD spectra of **A)** peptide **P1** and **B)** peptide **P2**, concentration range from 25-500 μM in 10 mM sodium phosphate buffer at pH 7.2, at 25^0 C

Figures 6(A-B) show the CD spectra of L-collagen peptide **P1** and D-collagen peptide **P2** respectively at pH 7.2 in the concentration range from 25-500 μM. In Figure 5A, the large negative CD band at 205 nm and a small intense positive CD band at 225 nm with crossover at 218 nm characterise left handed PP-II helix adopted by L-collagen. The enantiomeric D-collagen peptide **P2** shows CD spectra which is a mirror image of L-collagen peptide **P1** with a large positive CD band at 203 nm and a small negative CD band ~225 nm indicating that it forms right handed PP-II structure. Figure 7 shows the exact mirror images, with inversion of CD bands for these oppositely handed collagen triple helix peptides.
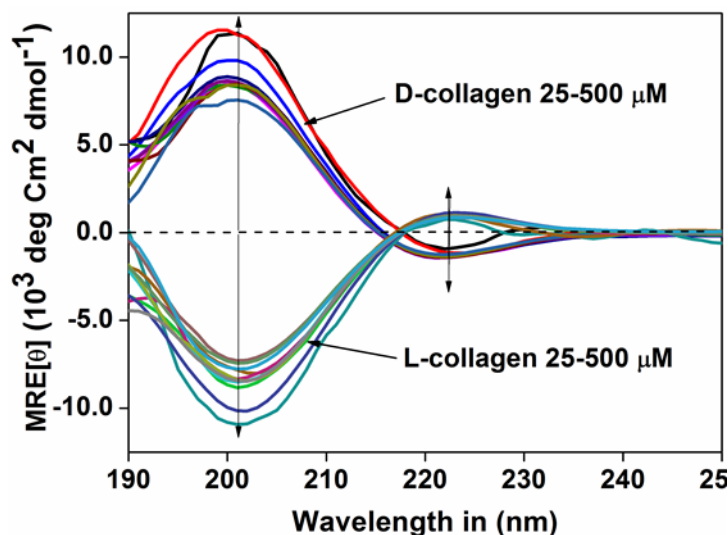
Figure 7. Mirror image CD spectra of peptides L-collagen **P1** and D-collagen **P2** in concentration range from 25-500 µM in 10 mM sodium phosphate buffer at pH 7.2

The association of collagen triple helix from single stranded helices should be a concentration dependent phenomenon, with increase in concentration of single strands driving the formation of triple-helix, reaching saturation at critical triple-helix concentration. The ratio of positive to negative bands ($R_{p/n}$) is used to determine the critical triple-helix concentration (CTC)[22] in L-collagen peptide and in case of D-collagen peptide this ratio is inverse calculated as negative to positive ($R_{n/p}$).
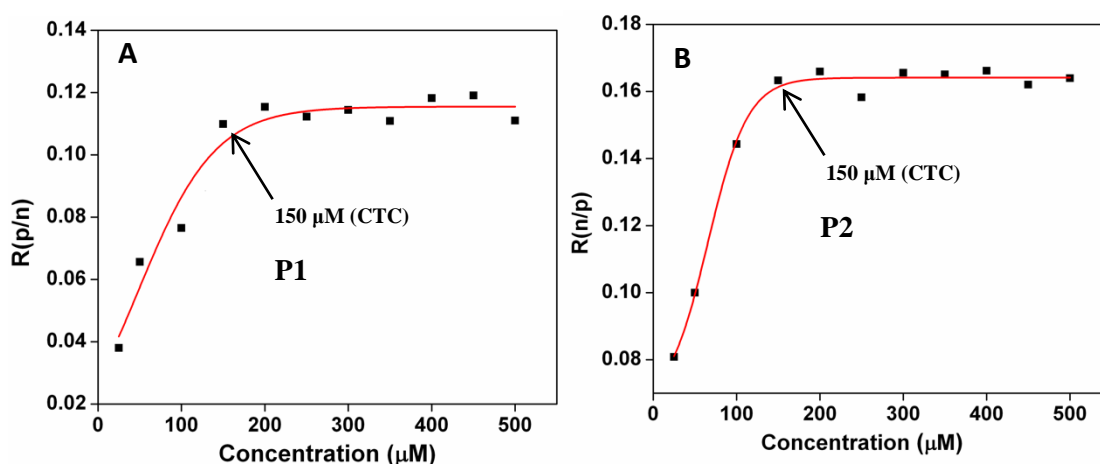
Figure 8 (A-B). Plots of ($R_{p/n}$), ($R_{n/p}$) against concentration **A)** peptide **P1** and **B)** Peptide **P2**

Figures 8(A-B) show the plot of concentration dependent $R_{p/n}$, for peptide **P1** and $R_{n/p}$ for peptide **P2** respectively. This ratio increased up to 150 µM, beyond which it became constant at higher concentrations. Thus the critical triple helix concentration

(CTC) for both peptides is 150 μM above which the peptides remain in triple helix form. It is important to note that, the mirror image peptides show almost identical critical triple helix concentration with similar propensity.

4.5.2 Determination of thermal stability of enantiomeric collagen peptides P1-P2 by CD spectroscopy

To determine the thermal stability of triplex arising from enantiomeric collagen peptides, CD-thermal melting experiments were carried out. Upon heating, the triple-helix structure dissociates into random coils. This change in conformation can be followed by monitoring the change of ellipticity at 225 nm against temperature.
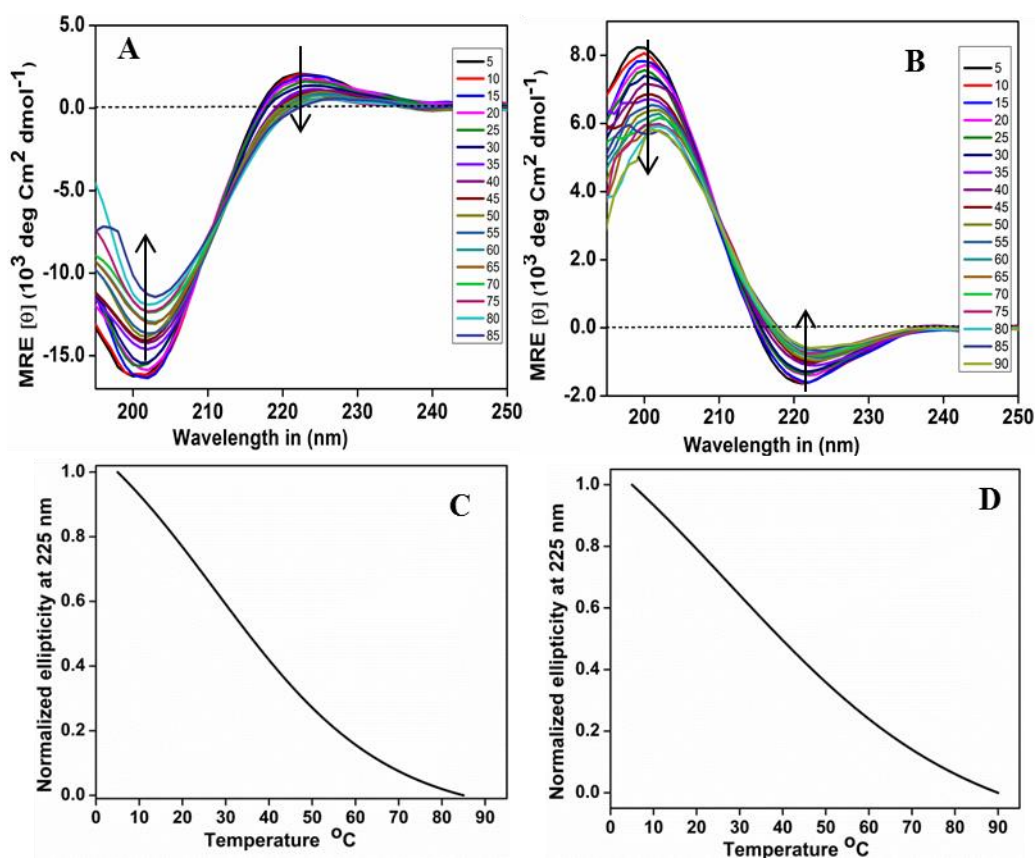
Figure 9 (A-D). CD thermal melting graph **A)** Peptide **P1 B)** Peptide **P2**, conc. 200 μM at pH 7.2 **(C, D)** Normalized thermal denaturation plot of molar ellipticity at 225 nm

Figures 9(A-B) show thermal melting CD spectra of L-collagen peptide **P1** and D-collagen peptide **P2** in the temperature range 5-90 ^{0}C at 200 μM concentration (above CTC). It is seen from CD spectra that positive CD band in L-peptide **P1** at 225 nm decreases with increasing temperature, showing the melting of collagen triple helix. The

intensity of CD bands at 225 nm and 203 nm decreased with increase in temperature. Figures 9(C-D) are the plots of decreasing ellipticity of positive band at 225 nm for L-collagen peptide **P1** and negative band at 225 nm for D-collagen peptide **P2** with increase in temperature. The sigmoidal nature of transition are confirmed for both peptides by observation of a minimum in their first derivative plots (Figure 10A-B). This also confirms two state transition nature of L-collagen (**P1**) and D-collagen (**P2**) peptides and the thermal melting *Tm* values for peptides **P1** and **P2** obtained from minima of the graph are 30 $^{\circ}$C and 29°C respectively. These are almost identical given the experimental error of 0.5 $^{\circ}$C.
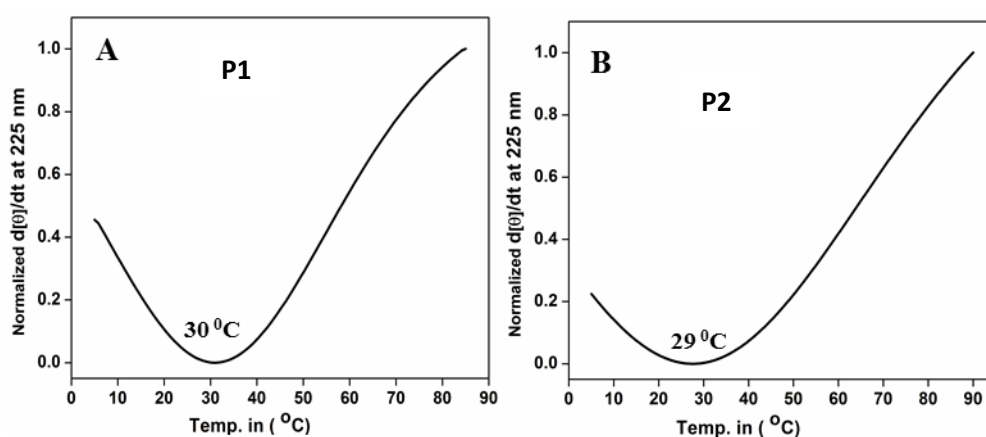
Figure 10 (A-B). First derivative curve of peptide **A)** Peptide **P1**, **B)** Peptide **P2**.

Table 2: CTC, Rp/n and *T*m comparisons of L-collagen **P1** and D-collagen **P2**

Sequence	CTC	Rp/n & Rn/p	*T*m
P1 AcNH-L-Phe-[-L-Pro-L-Hyp-Gly-]$_6$-NH$_2$	150 µM	0.12	30 $^{\circ}$C
P2 AcNH-D-Phe-[-D-Pro-D-hyp-Gly-]$_6$-NH$_2$	150 µM	0.16	29 $^{\circ}$C

4.5.3 CD Spectra of stoichiometric mixing L-collagen P1 and D-collagen P2 peptides

In order to determine the association of oppositely handed triple helices, the CD spectra of mixtures of L and D peptides in different stoichiometry were recorded, keeping the final concentration constant at 400 µM. At equimolar concentration, the CD bands at both 202 and 225 nm cancel out each other, leading to zero net ellipticity.

Figure 11A is the mixing CD spectra of L-collagen peptide **P1** and D-collagen peptide **P2**. It is observed that net helical content changes upon mixing the peptides together. Figure 11B shows a plot of the change in positive CD band at 224 nm and negative CD band at 202 nm, which is linear with stoichiometry and the crossing of the two signals happen at equimolar concentration and zero ellipticity. This suggests the formation of 1:1 complex by enantiomeric peptides **P1** & **P2**.
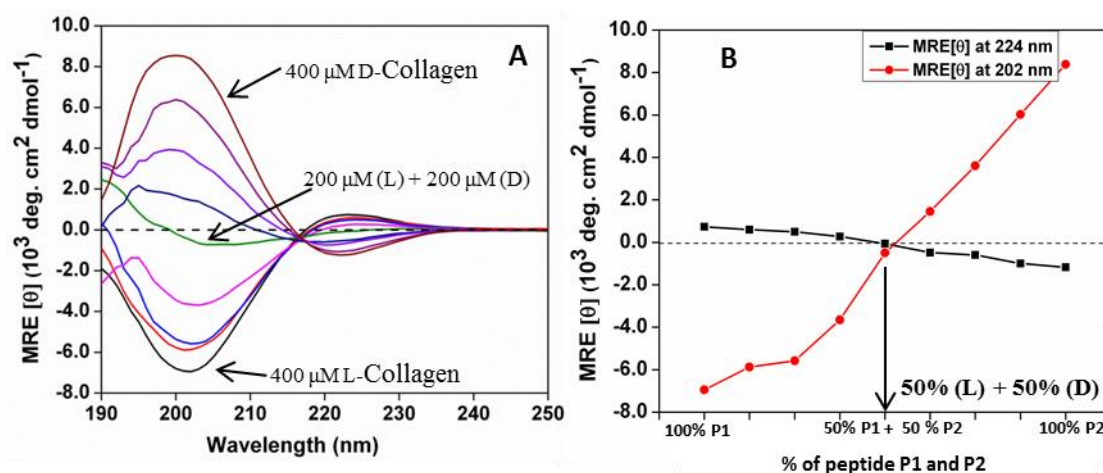
Figure 11. A) Mixing CD-spectra of L-collagen **P1** (400 μM) and D-collagen **P2** (400 μM)

B) The plot of molar ellipticity at 224 and 202 nm.

4.6 Study of morphological behaviour by FE-SEM

FE-SEM technique can be used to characterize the morphology of the self-assembly of the peptides, both individually as well as in the mixture of the enantiomeric peptides. The images were recorded at differernt peptide concentrations from 50 μM to 250 μM with samples prepared in water and the procedural details are in experimental section.

4.6.1 L-collagen peptide P1

Figure 12 shows the concentration dependent self-assembly of L-collagen peptide **P1** in water. At 50 μM concentration, below CTC of 150 μM, FE-SEM of the peptide shows irregular nano spheres of size 60-70 nm, which at CTC (150 μM) increased to 120-200 nm and started taking ellipsoidal rice grain like structure. The increase in size continued at higher concentration (250 μM) to about 300-400 nm. This enhancement in size and adopting particularly rice grain like nanostructure beyond CTC

can be attributed to complete triple helix formation at concentration above CTC, resulting into regular and uniform morphology.
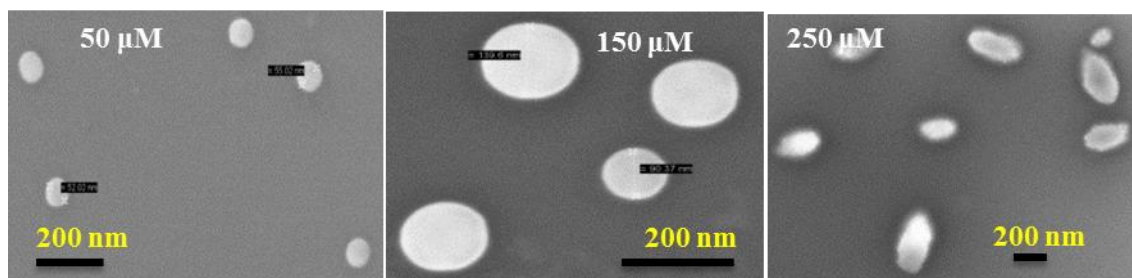
Figure 12. FE-SEM images of peptide L-collagen **P1** in water at 50μM, 150μM and 250 μM concentrations.

4.6.2 D-Collagen peptide P2

Figure 13 shows concentration-dependent self-assembly of D-collagen peptide **P2** in water. This peptide also shows FE-SEM images similar L-collagen peptide **P1** at concentrations, both at below CTC and above CTC.
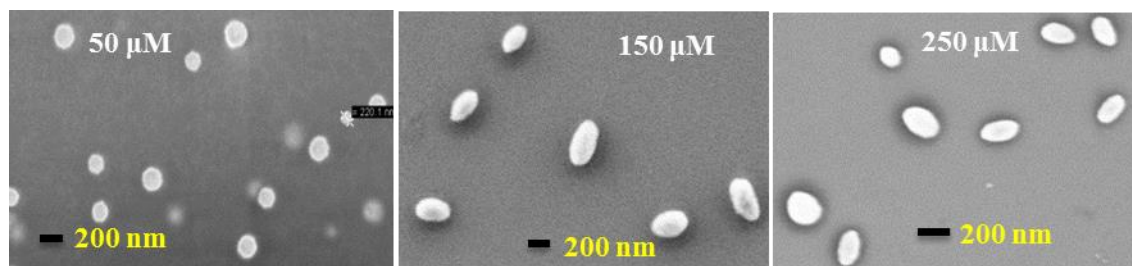
Figure 13. FE-SEM images of peptide D-collagen **P2** in water 50 μM, 150 μM and 250 μM concentrations.

4.6.3 Annealed peptides L-collagen P1 & D-collagen P2 in water

The enantiomeric peptides **P1** and **P2** were mixed in stoichiometric amounts at concentrations below (50 μM), at CTC (150 μM) and above CTC (250 μM) and annealed at 80 ^{0}C, cooled and FE-SEM images were recorded (Figure 14 A-C).

The images show network like structures at all concentrations with the structures being irregular and sticky with no defined self-assembled pattern. The regular shapes of nanoparticles seen in individual peptides were lost upon mixed annealing.
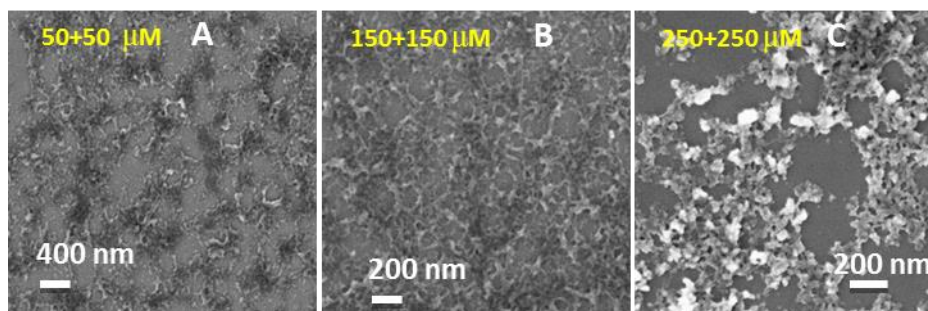
Figure 14 (A-C) Annealed peptide **A)** (50 μM) **P1** and **P2**, **B)** (150 μM) **P1** and **P2** and **C)** (250 μM) **P1** and **P2** in water.

4.6.4 Pre-formed triple helix mixing of peptides P1 & P2

In another experiment, the enantiomeric peptides were mixed stoichiometrically below, and above their CTC at room temperature and FESEM images of the mixtures were recorded, without any annealing step. Unlike in previous annealed experiments at 50 μM concentration, the enantiomeric peptides got assembled in single stranded forms into nanoparticles. At 150 μM and 250 μM where these are in triple helix forms, the inter peptide self-assembly (Figure 15A-C) of the enantiomeric peptides lead to fusion resulting in hollow spherical vesicles of 2-3μm diameter.
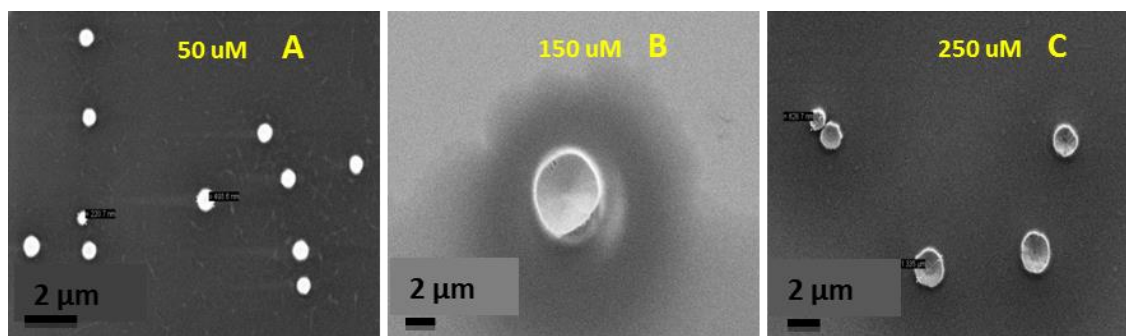
Figure 15 (A-C). Pre-formed triple helix mixing **A)** (50 μM) **P1** and **P2**, **B)** (150 μM) **P1** and **P2** and **C)** (250 μM) **P1** and **P2** in water.

4.7 Atomic Force Microscopy (AFM) of L-collagen peptide P1

Figure 16 shows concentration-dependent self-assembly of L-collagen peptide **P1** imaged by AFM in water at different concentrations in water. Below CTC (50 μM), the peptide shows nano-spheres of size less than 100 nm, and at CTC (150 μM) the size increased to ~200 nm, taking rice grain like structure. At higher concentration (250 μM)

this increased in size to 400-500 nm assuming slightly ellipsoid form. As AFM gives information of 3D shapes, it is observed that all nano spheres are of equal height of 3 nm. Thus at a low concentration, peptide not being in triple helix form lead to small nanospheres, and when the concentration reaches CTC and above, the peptides adopt triple helix form, leading to ellipsoidal and spherical vesicles.
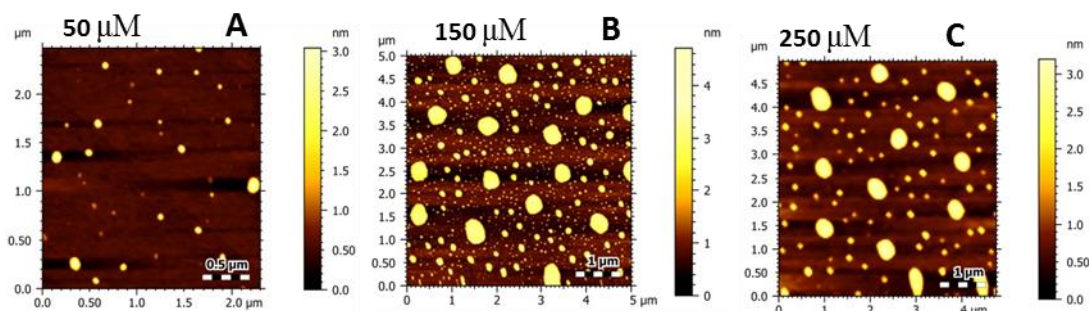
Figure 16. AFM images of peptide **P1 A)** 50 μM, **B)** 150 μM and **C)** 250 μM in water.

4.7.1 Atomic Force Microscopy (AFM) of D-collagen peptide P2

Figure 17 shows AFM images of concentration-dependent self-assembly of D-collagen peptide **P2** in water. This is similar to that seen for L-collagen peptide **P1** with similar shape and size. At low concentrations (50 μM) the peptide shows nano-spheres of less than 100 nm diameter with height 3 nm. At CTC, the diameter increased to ~200 nm and the shape became more ellipsoidal. The size increased at concentrations higher than CTC (250 μM) to about 400-500 nm, with nano structures having similar diameter and height of 3 nm. Thus the enantiomeric peptides **P1** and **P2** showed self-assembled structures similar in size and height as seen in FE-SEM and AFM images. It is important to note that these peptides undergo similar self-assembly process although they are mirror images as seen in CD spectra.
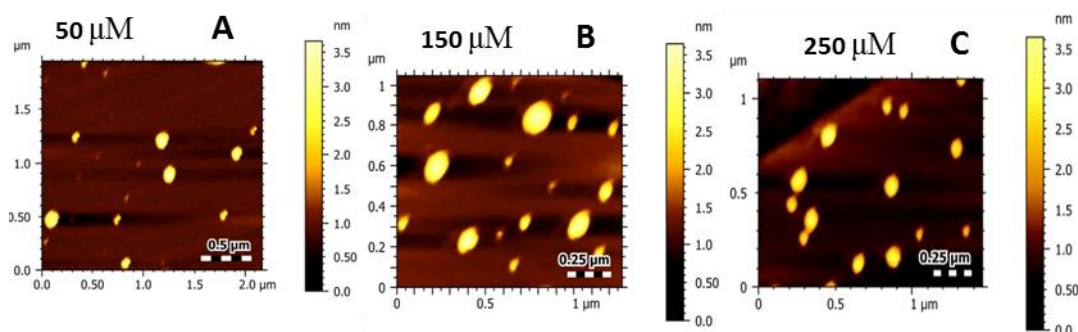

Figure 17. AFM images of peptide **P2 A)** 50μM, **B)** 150μM and **C)** 250 μM in water.

4.7.2 AFM of mixed and annealed enantiomeric peptides P1 and P2 in water

Collagen mimetic peptides provide a good model for study of natural collagen. When two enantiomeric peptides are mixed the interaction of individual left-handed and right-handed peptides may lead to different types of nano structures. Figures 18(A-C) show AFM images of L-collagen peptide **P1** and D-collagen peptide **P2** mixed in stoichiometric amounts in water followed by annealing. At concentration below CTC (50 μM Figure 18A) the enantiomeric peptides formed interconnecting networks which increased in cross linking when its concentration reached to CTC (150 μM Figure 18B) and becoming even more intense at higher concentrations (250 μM Figure 18C). These arise from formation of gel like structures formed through extended fibrils, with height of 3 nm as seen in line profile (Figure 18D) by AFM images.
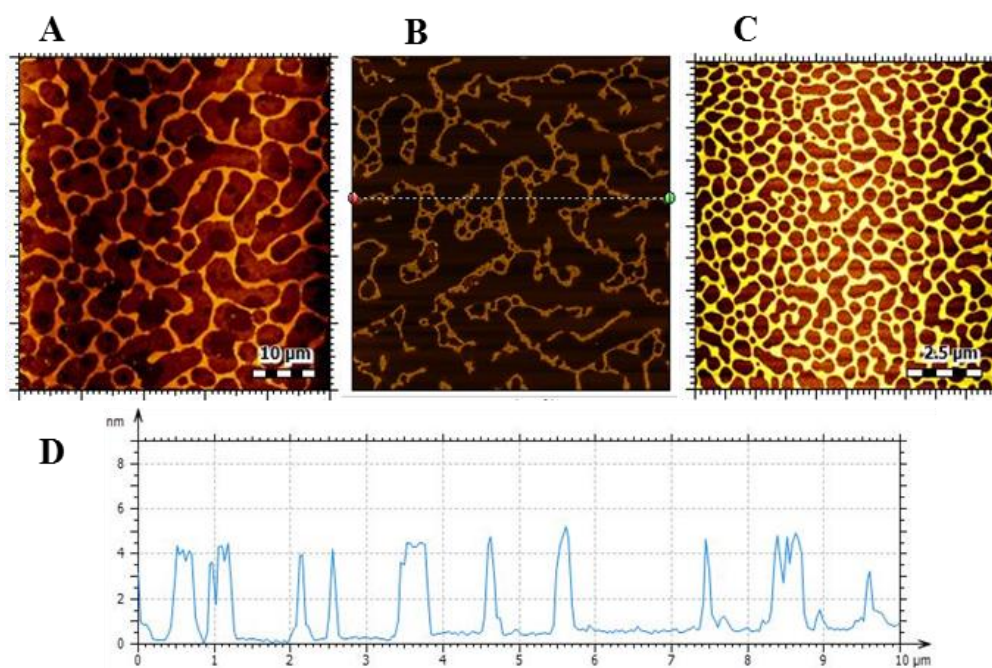
Figure 18 (A-C) AFM images of stoichiometric mixing of L-collagen peptide **P1** and D-collagen peptide **P2** in water **A)** mixing of **P1** and **P2** at (50 μM each) **B)** mixing at (150 μM each) **C)** mixing at (250 μM each) **D)** line profile of image B.

4.7.3 Mixing of enantiomeric peptides P1 & P2 at below CTC

Figures 19(A-C) depict AFM images of mixing peptides **P1** and **P2** in water. Figure 19A shows formation of non-uniform nanosheets of size around 1 μm and height 3 nm. Figure 19B represents the 3D view of the image which shows curved discs

formed at the top, Figure 19C show line profile indicating height of the structure is uniform in between 3-4 nm.
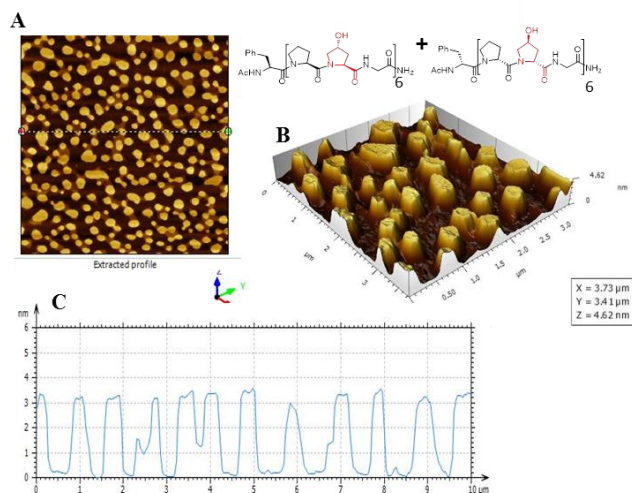
Figure 19 (A-C). AFM images of pre-formed triple helix of L-collagen peptide **P1** and D-collagen peptide **P2** at 50 μM each **B)** 3D view of image, **C)** Line profile.

4.7.4 Mixing of pre-formed triple helices of peptide P1 & P2 at CTC

Figures 20 (A-C) represent AFM images of mixing of pre-formed triple helices peptides **P1** and **P2** in water. Figure 20A shows formation of nanosheets with irregular size around ~1 μm and height 3 nm. It appears that the particles assemble initially into stacked discs that grow into sheets and the results from AFM imaging are consistent with that observed in FE-SEM.
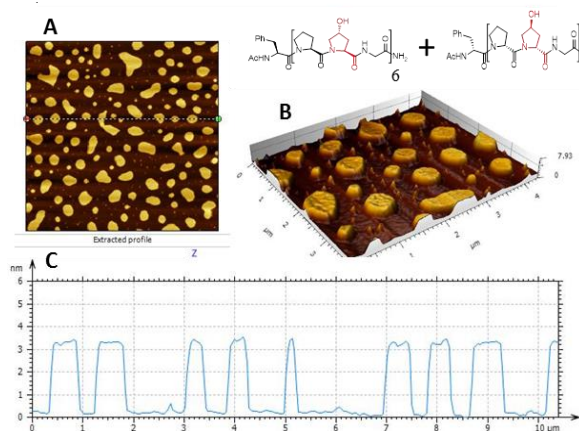
Figure 20 (A-C). AFM images of pre-formed triple helix of peptides **P1** and **P2** at 150 μM each in water **B)** 3D view of image, **C)** line profile.

4.7.5 Mixing of pre-formed triple helices of peptide P1 & P2 above CTC

Figures 21(A-C) show AFM images of pre-formed triple helices at concentration above above CTC (250 µM) after mixing of peptides **P1** and **P2** in water. Figure 21A shows formation of nanoparticles arranged into large homogeneous sized discs of diameter 1-2 µm stacked to height around 3 nm across all discs (Figure 21C). Figure 21B represents the 3D view of the image which shows the particles formed as curved disc.
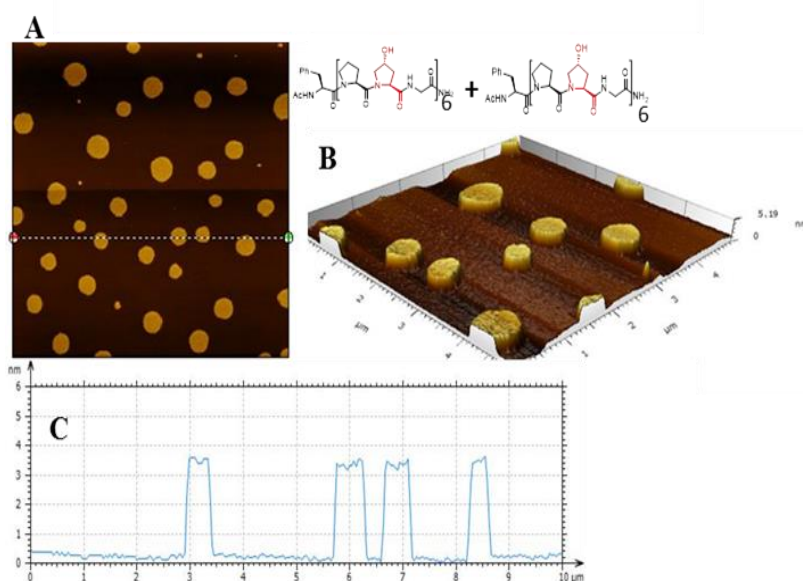
Figure 21 (A-C). AFM images of pre-formed triple helix of peptide **P1** and **P2** at (250 µM) in water **B)** 3D view of image, **C)** line profile.

Section B: Self-assembly of 4R/S-Amino Collagen Peptide Spiegelomers

4.8 INTRODUCTION

As described in section A, the 4(*R*)-hydroxyl group is critically responsible for imparting thermal stability to the collagen triple helix. It was attributed in literature that hydrogen bonding network mediated by 4(*R*)-hydroxyl group and water molecules attributed to the triple helix stability.[23] In order to delineate the role of 4(*R*)-hydroxyl group of proline in directing collagen triplex formation, several modified prolines and unnatural amino acids have been incorporated at X and Y sites of collagen sequence. Raines *et al.*[24] incorporated 4(*R*)-Fluoroproline *Flp* at the place of 4(*R*)-hydroxyl proline (*Hyp)* at Y site in collagen and found stabilization of triple helix in spite of the absence

of H-bonding unlike that with 4(R)-OH group. They invoked a stereo-electronic effect of 4(R)-hydroxyl group in *Hyp* to be responsible for stabilization of collagen triple-helix.

Ganesh *et al.*[25] substituted 4(R)-aminoproline (*Amp*) instead of *Hyp* in collagen triple-helix at Y site with a rationale of (i) increasing H-bond potential (like OH), since amino group is a better hydrogen bond donor with 2 hydrogens and (ii) introducing strong electron withdrawing group effect (like F) since amino group is ionisable and gets protonated to NH_3^+ (even at pH 7.0). It was seen that at all pH conditions, *Amp* incorporated collagen sequences formed stronger triple-helices. In addition to this, 4(S)-NH_2 proline at X site also being ionisable group, collagen triple-helix may switch conformation in a pH-dependent manner.[26]
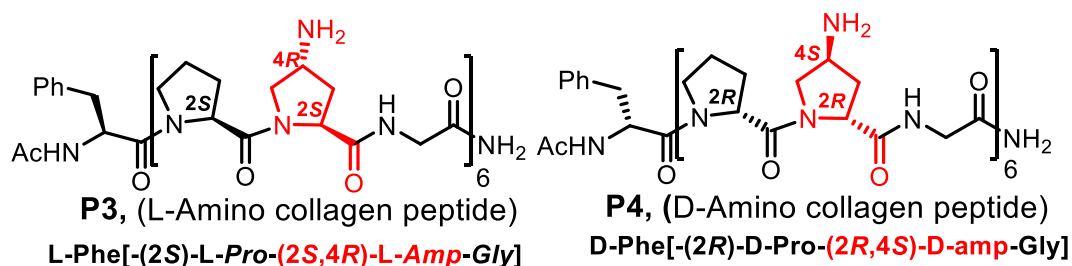
4.9 Rationale and objectives of the work

Collagen mimetic peptides derived from (2S)-L-proline, *trans*-(2S,4R)-4-amino-L-proline, (2R)-D-proline and *trans*-(2R,4S)-4-amino-D-proline were incorporated in different combinations at X and Y positions at the triad of [-X-Y-Gly-]. In Chapter 3 it was shown that polypeptides derived from enantiomeric L and D-proline, being mirror images show interesting self-assembling properties when mixed with each other. In this section, the packing of opposite handed enantiomeric Amp-collagen triplexes to result in hybrid self-assembled structures upon mixing is examined through morphological studies.

4.10 Specific objectives of the work

- ❖ Synthesis of (2R,4S)-N1-(Fmoc)-N⁴-(Boc) aminoproline monomers.
- ❖ Solid phase synthesis of end-capped 4(R/S)-aminoproline-(L/D)-collagen peptides L-Amino collagen **P3** and D-Amino collagen peptide **P4**
- ❖ Purification, and characterization of synthesized 4(R/S)-aminoproline-(L/D)-collagen peptides (**P3** & **P4**).
- ❖ Investigation of the conformation of 4(R/S)-aminoproline-(L/D)-collagen peptides and thermal stability of collagen triple helix by CD-spectroscopy.
- ❖ Study of self-assembled structure of peptides **P3** and **P4** by imaging techniques AFM, FE-SEM.

P3, (L-Amino collagen peptide)

L-Phe[-(2S)-L-*Pro*-(2S,4R)-L-*Amp*-Gly]

P4, (D-Amino collagen peptide)

D-Phe[-(2R)-D-Pro-(2R,4S)-D-amp-Gly]

4.11 Synthesis of (*2R,4S*)-4-aminoproline monomer

Compound **3** [*cis*-(2R,4R)-N1-(benzyloxycarbonyl)-4-hydroxy-D-proline methyl ester] was synthesized as described in previous chapters. To generate 4(S)-amino functionality at C4 position on proline with inversion in stereochemistry, 4*R*-OH compound **3** was reacted with mesyl chloride in the presence of triethylamine in dry DCM to obtain 4*R*-OMs compound **4**. This subsequently reacted with sodium azide to yield the 4*S*-azido compound **5** which was characterized by IR stretching frequency for azide at 2104 cm^{-1}. The 4*S*-azido was reduced by Staudinger reaction to obtain the 4*S*-NH$_2$ compound, which was *in situ* converted to Boc derivative (4*S*-NHBoc) **6**. The hydrolysis of ester with 2N aq. LiOH, and deprotection of Cbz in **6** by hydrogenation yielded 4*S*-NHBoc acid compound **7**. The desired monomer **8** (2R,4S)-N1-(Fmoc)-N^4-(t-Boc)-D-Proline was obtained by reacting amine **7** with Fmoc-Cl. Corresponding L-monomer (2S,4R)-N1-(Fmoc)-N^4-(Boc)-L-Proline was synthesized by earlier reported preocedure.[26]

Scheme 1: *Synthesis of (2R,4S) aminoproline monomer*
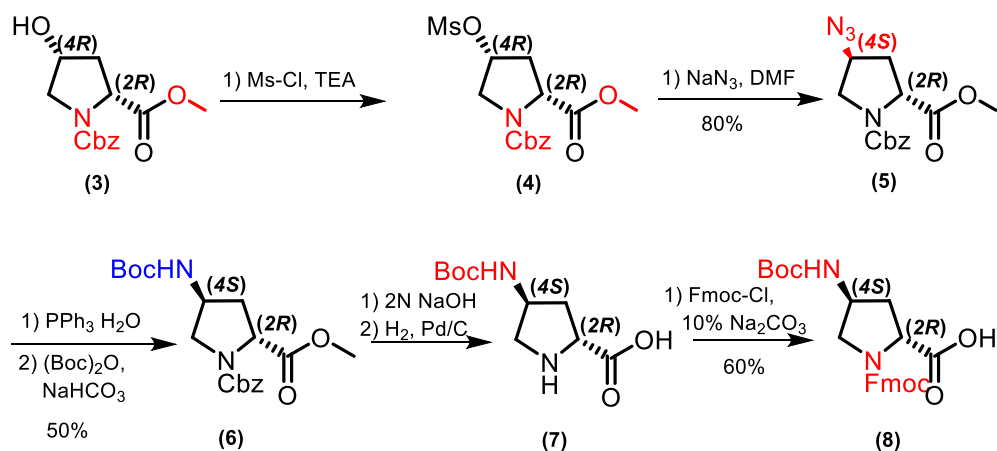
4.11.1 Solid phase peptide synthesis

By following solid phase peptide synthesis protocol described earlier in section A, L-Amino collagen peptide **P3,** (AcNH-(2*S*)-L-Phe-(-(2*S*)-L-Pro-(2*S*,4*R*)-L-Amp-Gly-)**₆**-NH₂ and D-Amino collagen peptide **P4**, (AcNH-(2*R*)-D-Phe-(-(2*R*)-D-Pro-(2*R*, 4*S*)-D-amp-Gly-)**₆**-NH₂ were synthesised. These peptides were purified by HPLC using RP-C18 column in an acetonitrile-water solvent system containing 0.1% TFA.

P3, (L-Amino collagen peptide)
L-Phe[-(2*S*)-L-*Pro*-(2*S*,4*R*)-L-*Amp*-*Gly*]

P4, (D-Amino collagen peptide)
D-Phe[-(2*R*)-D-Pro-(2*R*,4*S*)-D-*amp*-Gly]
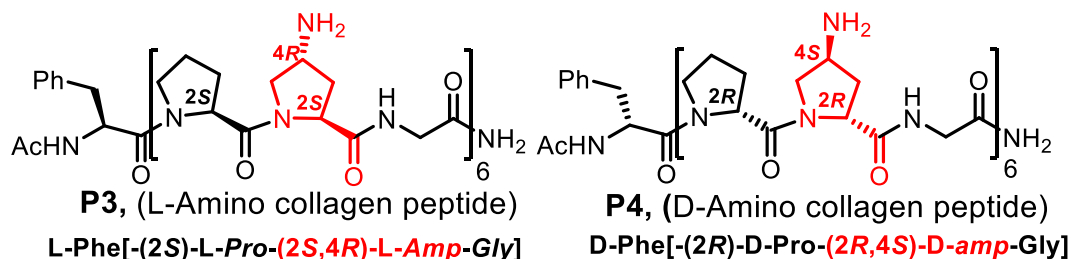
Table 3: HPLC retention time and MALDI-TOF characterization of peptides **P3-P4**.

Sequence	Ret. time	Mol. Formula	Cal. Mass	Obs. mass
AcNH-L-Phe-[-L-Pro-L-Amp-Gly-]₆-NH₂	15.0	$C_{83}H_{122}N_{26}O_{20}Na$	1827.04	1826.55
		$C_{83}H_{122}N_{26}O_{20}K$	1843.14	1842.52
AcNH-D-Phe-[-D-Pro-D-amp-Gly-]₆-NH₂	15.1	$C_{83}H_{122}N_{26}O_{20}Na$	1827.04	1827.91
		$C_{83}H_{122}N_{26}O_{20}K$	1843.14	1842.87

4.12 RESULT AND DISCUSSION

In this chapter CD spectroscopy is used to determine the secondary structures of peptides **P1 and P2** in different solvents and examine the thermal stability of the peptides.

4.12.1 CD studies of L-amino collagen peptide (P3) and D-amino collagen peptide (P4)

Figures 23(A-B) show CD spectra of L-amino collagen peptide (**P3**) and D-amino collagen peptide (**P4**) at pH 7.2 in concentration range from 50-300 µM. A positve CD band at 225 nm, and a negative CD band at 200 nm in L-amino collagen peptide (**P3**) suggest that the synthesized peptide adopts left handed PP-II helix. In case of D-amino

collagen peptide (**P4**) (Figure 23B), a strong positive CD band at 200 nm and a weak negative CD band at 225 nm with crossover at 215 nm suggest that the enantiomeric peptide with all D-proline units has exact mirror image conformation of L-amino collagen peptide **P3**.
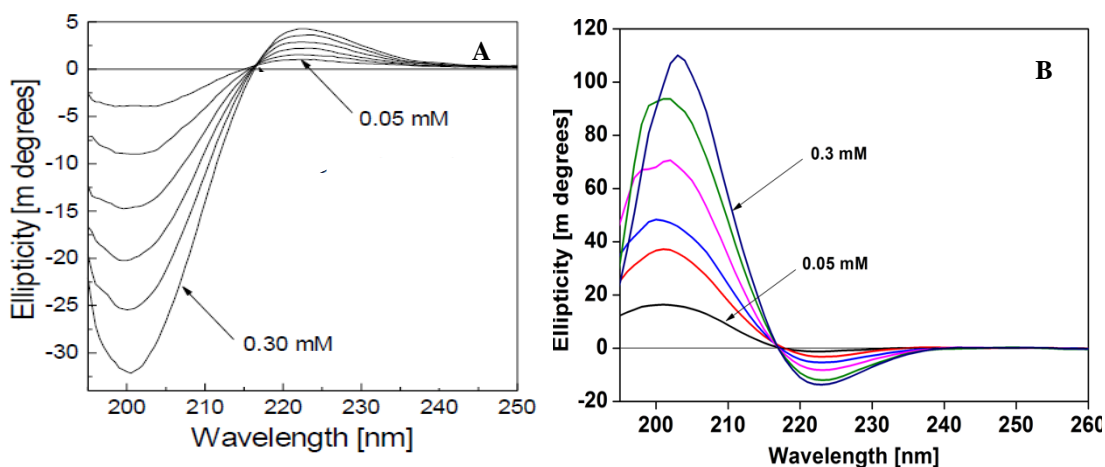
Figure 23 (**A-B**). CD spectra of peptide **A**) Peptide **P3*** and **B**) Peptide **P4** at 25^0 C, concentration range 0.05-0.3 mM in 10 mM sodium phosphate buffer at pH 7.2. *Graph taken from reference 25

Figures 24(A-B) are the plots of $R_{p/n}$ and $R_{n/p}$ (inverse of $R_{p/n}$) against concentrations of L-amino collagen peptide **P3** and D-amino collagen peptide **P4** respectively. This ratio increased upto 150 μM in case of L-amino collagen peptide **P3** and remained constant. In D-amino collagen peptide **P4**, **the** saturation point was at 200 μM followed by no change at higher concentrations. The CTC for the **P3** peptide is 150 μM while for **P4** peptide, it is 200 μM, almost similar within experimental errors.

Figure 24 (**A-B**). Plot of the $R_{p/n}$, $R_{n/p}$ plotted against concentration **A**) L-amino collagen peptide **P3*** **B**) D-amino collagen peptide **P4**.*Graph taken from reference 25

4.12.2 Triple helix melting of L-amino collagen P3 and D-amino collagen P4 at neutral pH 7.2

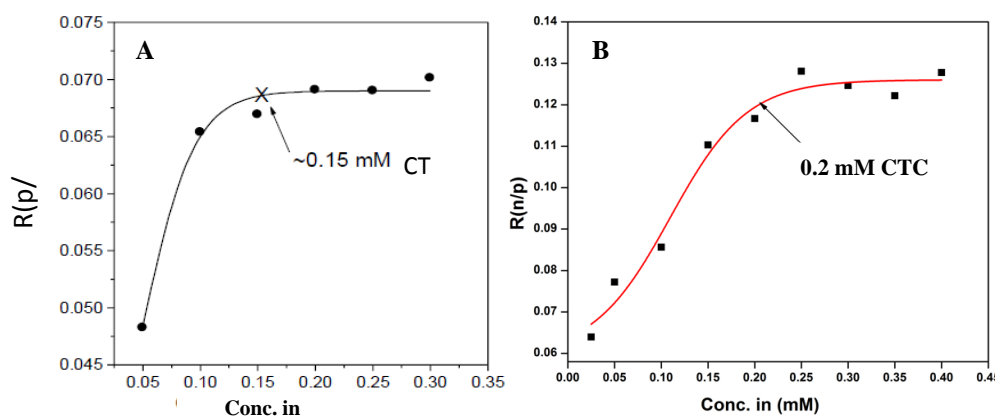Figures 25(A-B) show CD thermal melting graphs of L-amino collagen peptide **P3** and D-amino collagen peptide **P4** in the temperature range from 5-90 ^{0}C. The change in ellipticity at 225 nm was monitored as a function of temperature. It was observed that, the peak intensity at 225 nm decreased with increase in temperature. Like 4-hydroxy collagen peptide, the 4(*R/S*) aminocollagen L and D peptides also showed conformational transition from PP-II to random conformation as temperature was increased. 4(*R*)-Amino proline in collagen sequence enhances the triplex stability as seen in L-amino collagen peptide **P3** as well as in D-amino collagen peptide **P4**. L-amino collagen peptide **P3** melts at 56 ^{0}C, while the D-amino collagen peptide **P4** melts at 54 ^{0}C.
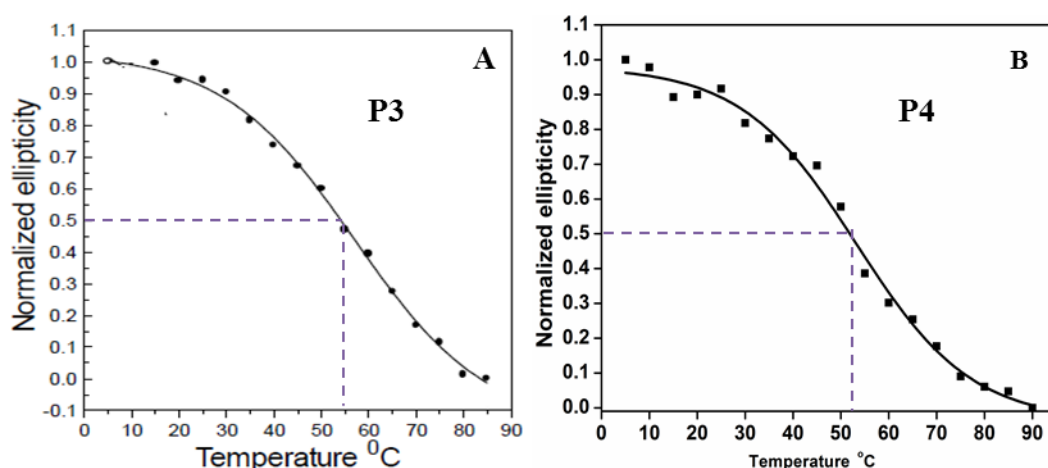
Figure 25 (A-B). Decrease in ellipticity at 223 nm Vs. temperature, range from 5-90^0 C, **A)** L-amino collagen peptide **P3**[*25] (**B)** D-amino collagen peptide **P4** (250 µM at pH 7.2, * Graph and values taken from reference 25.

Table 4: CTC, Rp/n and *T*m comparison of peptides **P3** & **P4** at neutral pH.

Sequence	CTC	Rp/n & Rn/p	*T*m
AcNH-L-Phe-[-L-Pro-L-Amp-Gly-]$_6$NH$_2$*	150 µM	0.07	56.5 ^{0}C
AcNH-D-Phe-[-D-Pro-D-amp-Gly-]$_6$NH$_2$	200 µM	0.12	53.4 ^{0}C

4.12.3 Triple helix melting of L-amino collagen peptide P3 and D-amino collagen peptide P4 at pH 9

Figures 26(A-B) show CD thermal melting graphs of L-amino collagen peptides **P3** and D-amino collagen peptides **P4** at in temperature range from 5-90 ^{0}C. The change in ellipticity at 225 nm was monitored as a function of temperature at pH 9.0 under basic condition. L-amino collagen and D-amino collagen peptides show rapid decrease in ellipticity of CD band at 225 nm and both peptides melt around same temperature. The pKa of 4(R) amino group in *trans*-(4R,2S)-4-amino-L-proline monomer[25] is 9 and 4(S) amino group in *trans*-(4S,2R)-4-amino-D-proline monomer is 8.6. At pH 9.0 (equal to pKa) there is equilibrium between protonated and non-protonated amino groups and since ring pucker depends on protonated/non-protonated states, mixed ring pucker leads to destabilization of proline triplex at pH 9.0 (near pK$_a$) resulting in lower melting temperatures. L-amino collagen peptide **P3** and D-amino collagen peptide **P4** melts at 26 ^{0}C and 27.5 ^{0}C respectively.

Figure 26 (A-B). Decrease in ellipticity at 225 nm Vs. temperature range from 5°-90° C, **A)** Peptide **P3**[25] **B)** Peptide **P4** at pH 9. * Graph and value taken from reference 25

Table 5: Comparison of T_ms of peptides **P3** & **P4** at basic pH-9.

Sequence	pH	Tm
AcNH-L-Phe-[-L-Pro-L-Amp-Gly-]$_6$NH$_2$ *	9	26 ^{0}C
AcNH-D-Phe-[-D-Pro-L-amp-Gly-]$_6$NH$_2$	9	27.5 ^{0}C

4.12.4 Triple helix melting of L-amino collagen peptide P3 and D-amino collagen peptide P4 at pH 12.0

At alkaline pH 12.0, amino group is in free non-protonated form. Figures 27(A-B) show CD thermal melting graphs of L-amino collagen peptide **P3** and D-amino collagen peptide **P4** in temperature range from 5-90 $^\circ$C. The change in ellipticity at 225 nm was monitored and plotted as a function of temperature at basic pH 12. It is observed that, when amino groups in L-amino collagen peptide **P3** are in deprotonated form, it stabilizes the triple helix and gives melting temperature 49 $^\circ$C. Similar results are observed for D-amino collagen peptide **P4** which melts at 48.5 $^\circ$C at pH 12.0, and not much stability difference was seen between these two enantiomeric peptides.
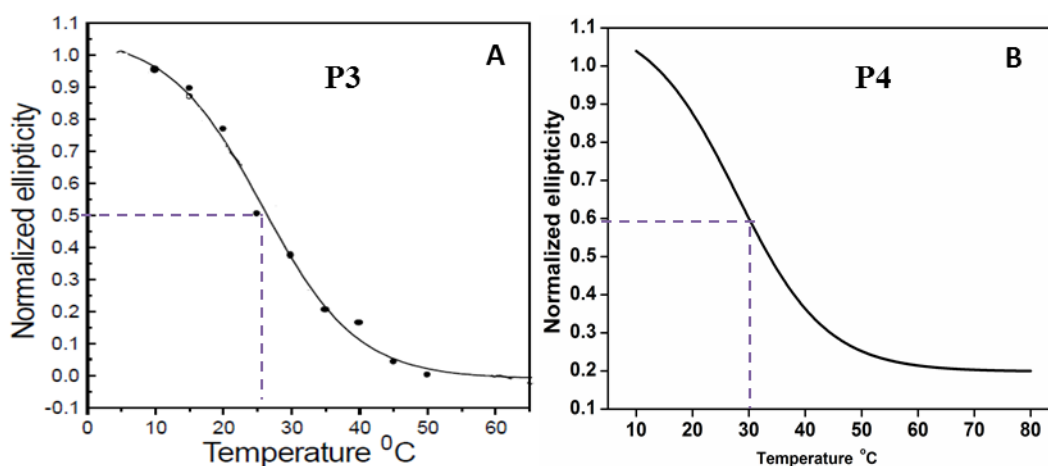

Figure 27 (A-B). Decrease in ellipticity at 225 nm Vs. temperature range from 5-90° C, **A)** peptide **P3**[25] **B)** peptide **P4**, at pH 12. ∗ Graph and values taken from reference 25

Table 6: Comparison of T_ms of peptides **P3** & **P4** at basic pH 12.0

Sequence	pH	T_m
AcNH-L-Phe-[-L-Pro-L-Amp-Gly-]$_6$-NH$_2$ ∗	12	49 $^\circ$C
AcNH-D-Phe-[-D-Pro-L-amp-Gly-]$_6$-NH$_2$	12	48.5 $^\circ$C

4.12.5 Triple helix melting of L-amino collagen peptide P3 and D-amino collagen peptide P4 at pH 3.0

At acidic pH 3.0, the amino group is in fully protonated form. Figure 28(A-B) show CD thermal melting graphs of L-amino collagen peptide **P3** and D-amino collagen peptides **P4** at in temperature range from 5-90 $^{\circ}$C. The change in ellipticity at 225 was monitored as a function of temperature at pH 3.0 where amino groups are totally protonated. In this form, it acts as strong electron withdrawing group such as fluorine and due to favourable stereoelectronic factors, it should stabilize at pH 3.0 to the triplex. 4(R) amino L-proline substituted collagen peptide **P3** melts at 60 $^{\circ}$C while the enantiomer 4(S) amino D-proline substituted collagen peptide **P4**, melts at 58.5 $^{\circ}$C.
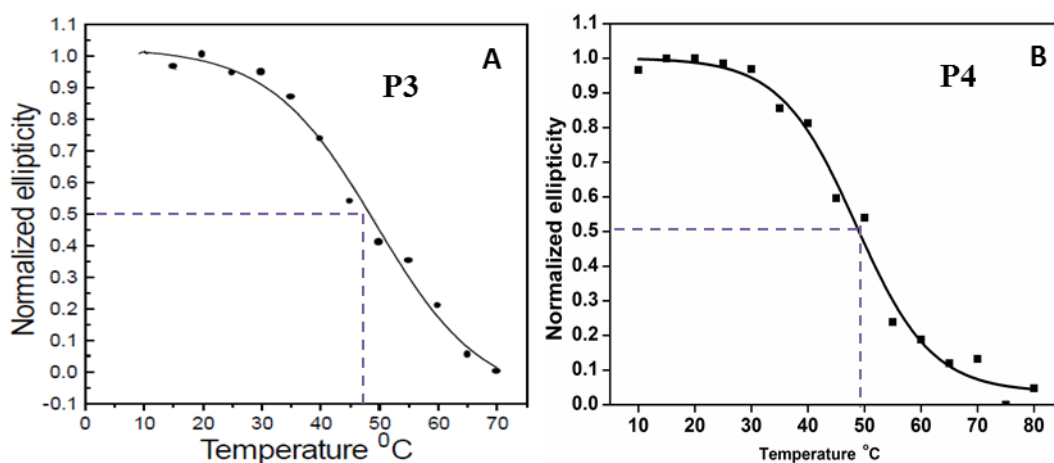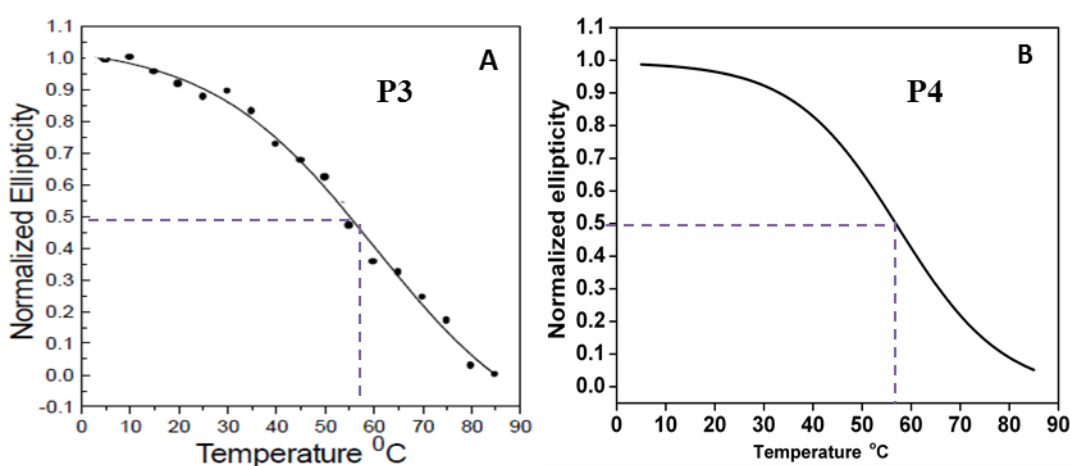

Figure 28 (A-B). Decrease in ellipticity at 225 nm Vs. temperature range from 5-90^{0} C, **A)** Peptide **P3**[25] **B)** Peptide **P4**, at pH 12 * Graph and value taken from reference 25

Table 7: Comparison of T_ms of peptides **P3** and **P4** at acidic pH-3.

Sequence	pH	T_m
AcNH-L-Phe-[-L-Pro-L-Amp-Gly-]$_6$NH$_2$*	3	60^{0}C
AcNH-D-Phe-[-D-Pro-L-amp-Gly-]-NH$_2$$_6$	3	58.5^{0}C

4.12.6 Comparison of T_ms of L-amino collagen peptide P3 and D-amino collagen peptide P4 in pH range from 3.0 to 12.0

Figure 29 shows comparative T_ms of L-amino collagen peptide **P3** and D-amino collagen peptide **P4** in pH range from 3.0 to 12.0. It is seen that there are no significant stability differences seen between the two enantiomeric peptides at acidic, neutral and basic conditions. However 4(R) amino L-proline substitution in L-collagen as well as 4(S) amino D-proline in D-collagen sequence enhance the triplex stability at all pH range from 3.0 to 12.0, compared to the corresponding hydroxy collagen peptides. The triplex stability of both enantiomers was least at pH 9.0 and increased at both acidic and basic pH.
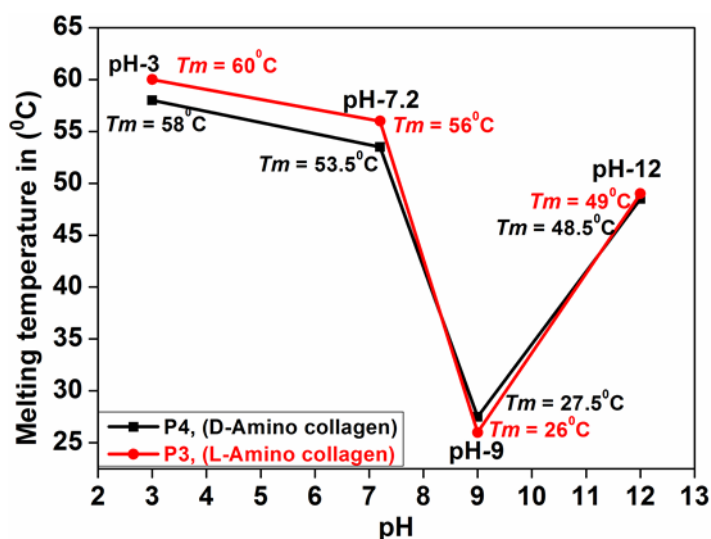
Figure 29. Melting temperatures of (red) L-amino collagen **P3**[25] and (block) D-amino collagen **P4** at pH range, from 3.0 to 12.0, * Values taken from reference 25

Table 8: Comparison of T_ms of peptides **P3** & **P4** at different pHs.

Sequence	pH-3	pH-7.2	pH-9	pH-12
AcNH-L-Phe-[-L-Pro-L-Amp-Gly-]$_6$NH$_2$ *	60 ^{0}C	56 ^{0}C	26 ^{0}C	49 ^{0}C
AcNH-D-Phe-[-D-Pro-L-amp-Gly-]$_6$NH$_2$	58.5 ^{0}C	53.5 ^{0}C	27.5 ^{0}C	48.5 ^{0}C

4.13 Morphological studies of L-Amino collagen peptide P3 and D-amino collagen peptide P4 at pH range, from 3.0 to 12.0

Figure 30 shows FE-SEM images of self-assembly of peptide **P3** and **P4** in various buffers at 1 mM concentration. At pH 3.0, the peptides do not show any regular self-assembled structures and are completely disordered. At pH 5.0 and pH 7.0 both

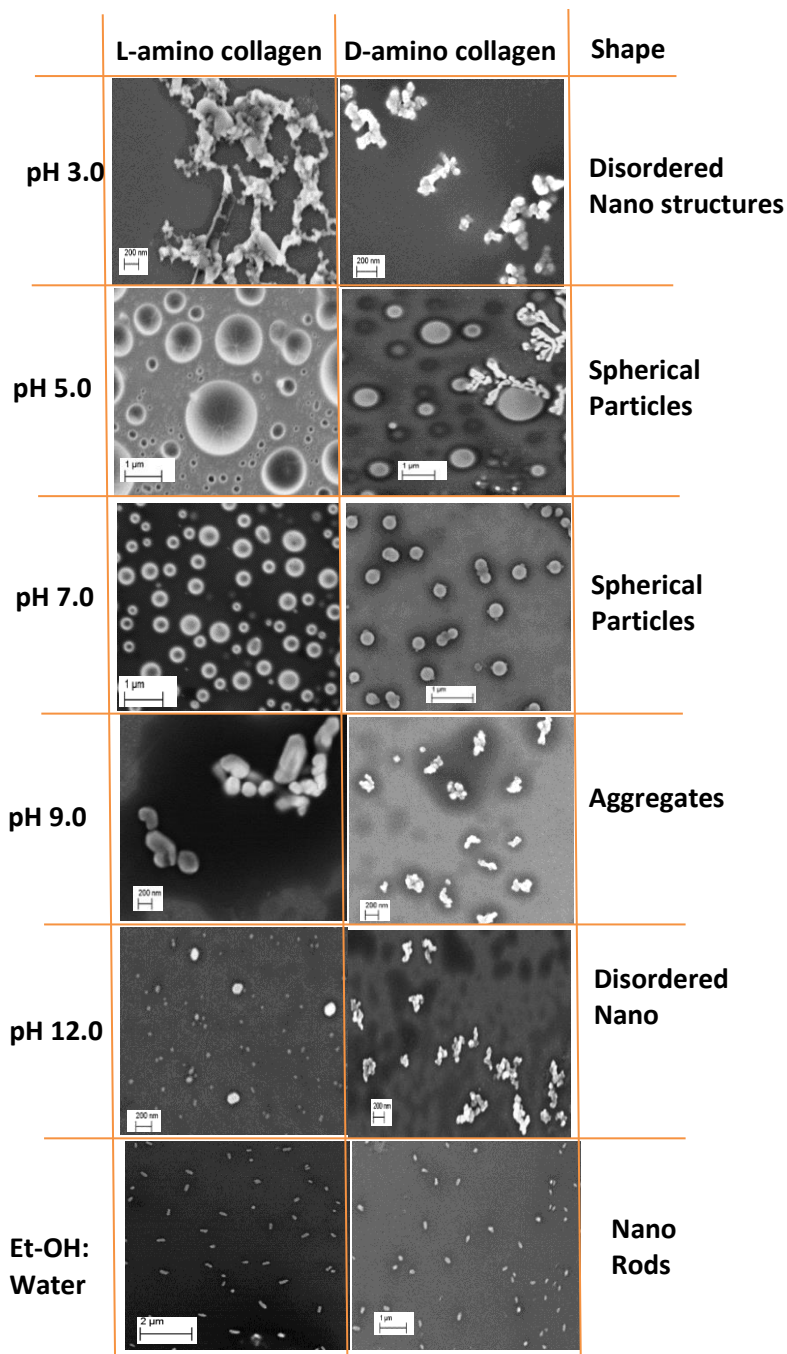|	L-amino collagen	D-amino collagen	Shape
pH 3.0			Disordered Nano structures
pH 5.0			Spherical Particles
pH 7.0			Spherical Particles
pH 9.0			Aggregates
pH 12.0			Disordered Nano
Et-OH: Water			Nano Rods

Figure 30. FE-SEM images (left column) L-amino collagen peptide **P3** and (right column) D-amino collagen peptide **P4** at pH range, from 3.0 to 12.0 and in ethanol water (1:1)

peptides **P3** and **P4** form regular nano spherical particles of diameter width ~1 μm. In basic conditions at pH 9.0 and pH 12.0, peptides **P3** and **P4** form small nanospheres of diameter 200 nm. The lower thermal stability observed at pH 9.0 in CD melting did not manifest in different morphology at pH 9.0. At extremes of pHs of 3.0 and 12.0, both peptides exhibited disordered nanostructures, but reasonably well defined structures at intermediates pHs of 5.0, 7.0 and 9.0.

The self-assembly of L-amino collagen peptide **P3** and D-amino collagen peptide **P4** in ethanol:water (1:1) resulted in short nanorods of length 0.5 μm the size and the dimensions of the nano rods remained same for both peptides **P3** and **P4**. Peptides at all pH showed similar nanostructures.

4.13.1 Mixing of pre-formed triple helix of L-amino collagen peptide P3 and D-amino collagen peptide P4 at various pHs: FESEM

L-4-amino collagen peptide **P3** is known to stabilize the triple helix throughout the pH range from pH 3.0 to pH 12.0 better than that from L-4-hydroxy collagen peptide. Similarly D-4-amino collagen peptide **P4** also stabilized triple helix to a similar extent at all pHs. It was thought to mix two enantiomeric peptides to see the resultant morphology. Triple helix enantiomeric peptides **P3** and **P4** were mixed to associate with one another in triple helix form. It was observed that at pH 3.0, 5.0 and pH 7.0, the racemic mixture of self-assembled peptides form nanofibrous sheets of size around 1-2 μm in diameter with sharp edges and flat surface. The racemic mixture of peptides at pH 9.0 and pH 12.0 self-assembled to form large disordered aggregates.

As compared to individual peptides, the racemic mixture of peptides **P3** and **P4** exhibited very distinct morphology. As described in previous section, under similar experimental conditions, the enantiomeric pepties L-hydroxy collagen peptide **P1** and D-hydroxy collagen peptide **P2** on mixing resulted in nano-discs of 1-2 μm size diameter with 4-6 nm in height. Compared to 4-hydroxy collagen peptides, 4-amino prolyl collagen peptides make not only a difference in terms of thermal stability, but also induce distinct morphological features.

In a different experiment the two enantiomeric peptides were first mixed and then annealed to interact with one another in a single stranded form. It was observed that at pH 3.0, 5.0 and pH 7.0 the racemic mixtures of enantiomeric collagen peptides

self-assembled into curved nano fibrous sheets (Figure 31, second column) of size around 1-2 μm in length with sharp edges and flat surface.
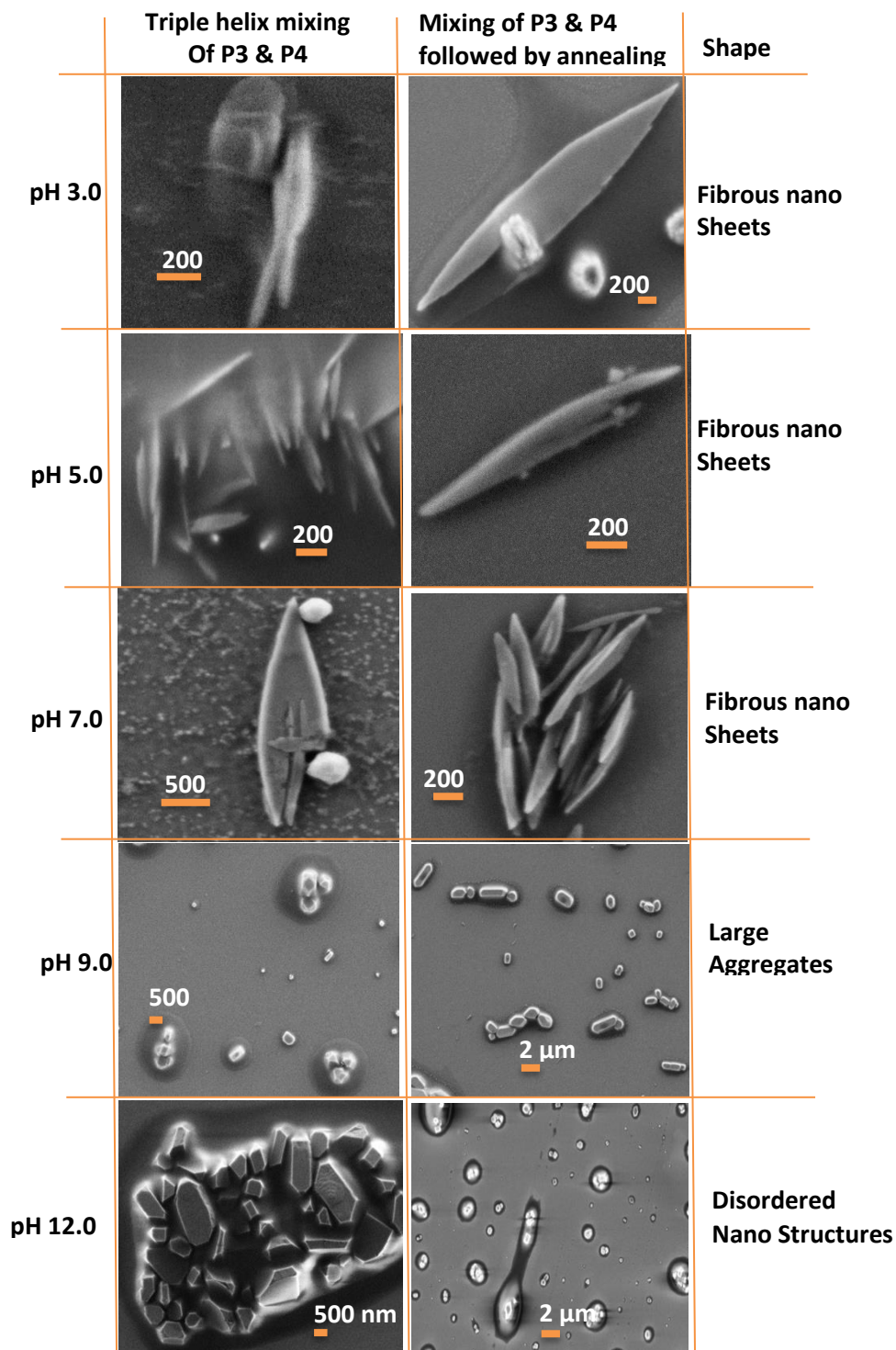

Figure 31. FE-SEM images of mixing of pre-formed triple helix of peptide **P3** and **P4** (first column), cold mixing of **P3** and **P4** (second column) in pH range, from 3.0 to 12.0

The racemic mixture of peptides, **P3** and **P4** (equimolar concentration) upon annealing showed very similar morphology like the mixing of pre-formed triple helix. As explained in Chapter 2, under similar experimental conditions the enantiomeric peptides L-hydroxy collagen peptide **P1** and D-hydroxy collagen peptide **P2** resulted in nanofiber network like structures with height of fibers of 4-6 nm in height.

4.14 AFM images of mixing of preformed triple helix of L-amino collagen peptide P3 and D-amino collagen peptide P4 at pH range from 3.0 to 12.0

AFM images provide 3D information of nanostructures in terms of height and surface morphology. The enantiomeric peptides **P3** and **P4** were recorded in triple helix form in both mixed and in annealed state. It was observed that the nanostructures corresponded to those seen by FE-SEM images. As compared to individual peptides, the racemic mixture of peptides **P3** and **P4** exhibited very distinct morphology.

Figure 32 (first and second column) indicates that from pH 3.0, 5.0 and pH 7.0 the racemic mixture of self-assembled peptides **P3** and **P4** form nanofibrous sheets of size around 1-3 μm in length with sharp edges and flat surface, with height of the sheets in the range 30 to 40 nm. Under similar experimental conditions, peptide **P3** and **P4** on mixing in equimolar concentrations and upon annealing in triple helix state showed very same morphology.
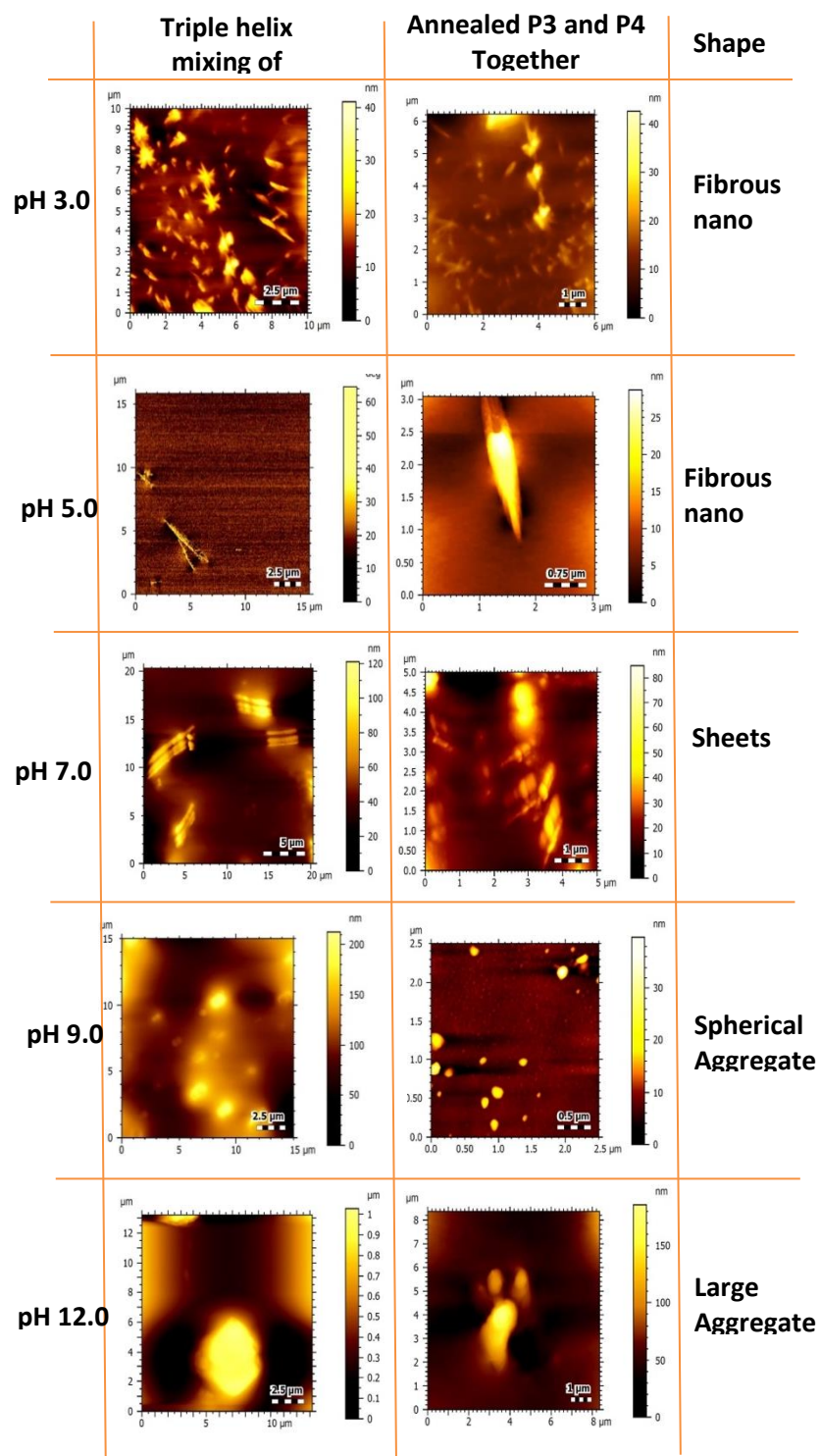
Figure 32. AFM images of mixture of pre-formed triple helix of peptides **P3** and **P4** (first column), annealed peptides **P3** and **P4** (second column) in pH range, from 3.0 to 12.0

4.15 Summary

Section A of chapter described the comparative studies of enantiomeric 4-hydroxy substituted prolyl collagen peptides **P1** and **P2** derived from L-proline and D-proline respectively. The studies comprised of design, synthesis, conformational behaviour and thermal stability of peptides **P1-P2** by CD spectroscopy and examination of their morphology in individual as well as in mixed state.

In the concentration dependent triple helix formation study, it is observed that both the enantiomeric peptides **P1** and **P2** form triple helices of opposite handedness, (Figure 33 A). The T_m values for enantiomeric peptides **P1** and **P2** are found nearly the same, with melting around 30 ^{o}C showing similar thermal stability (Figure 33B).
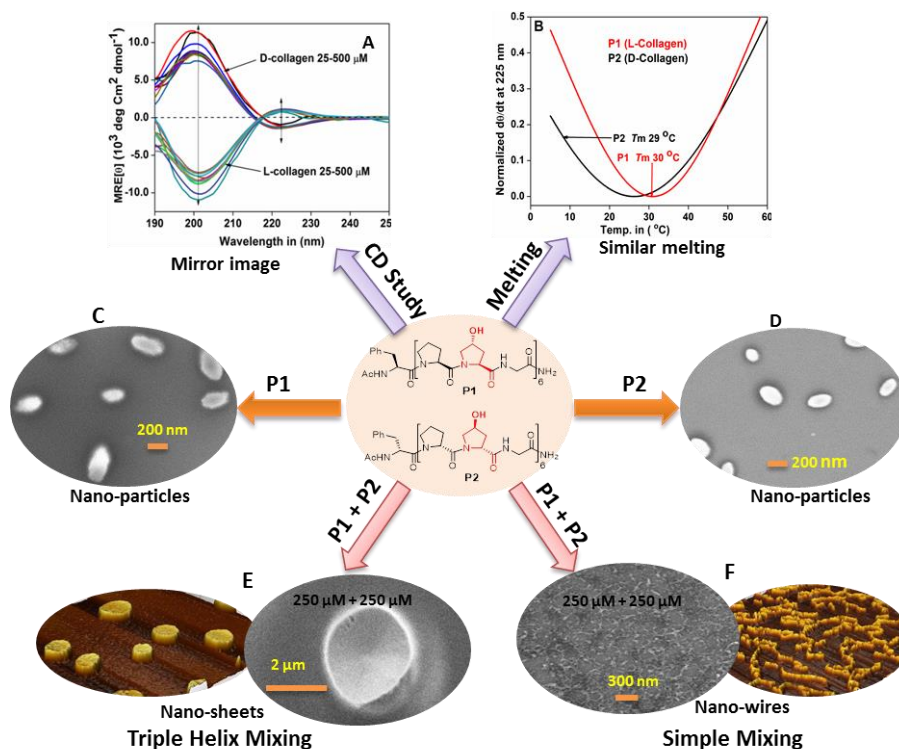

Figure 33. A) CD study of peptides **P1** and **P2**; **B)** CD Thermal stability of **P1** and **P2**; **C-D)** FE-SEM of **P1** and **P2** respectively; **E)** FE-SEM and AFM of **P1** and **P2** in triple-helix mixing; **F)** FE-SEM and AFM of **P1** and **P2** in simple mixing.

The collagen peptides **P1** and **P2** have very distinct self-assembling properties and their morphological behaviour depends upon the mixing preference. The peptides **P1** and **P2** individually showed uniform ellipsoid rice like nanostructures of size around 300 nm (Figure 33 C-D). Upon stoichiometric mixing of preformed triple helix, inter self-assembly occurs leading to nanofibrous discs (Figure 33E). In another experiment

when the peptides were mixed at identical concentrations followed by annealing, the resultant product self-assembled into nanowires (Figure 33F).

Section B of Chapter 4 investigated the enantiomeric 4-amino collagen peptides **P3** and **P4**. These peptides were synthesized, purified and characterized successfully. The enantiomeric peptides **P3** and **P4** exhibited CD spectra (Figure 34A-B) characteristic of triple helices and which are mirror images of each other. The T_m values for peptides **P3** and **P4** at various pHs were nearly the same, showing similar thermal stability (Figure 34C).

As seen by FESEM and AFM, the 4-amino collagen peptides **P3** and **P4** self-assembled into nanospheres of size around 500 nm in diameter at physiological pH 7.0 (Figure 34 D-E). Upon stoichiometric mixing of peptides **P3** and **P4** in triple-helix form, inter self-assembly lead to formation of nano fibrous sheets with sharp edges (Figure 33F). When peptides **P3** and **P4** were mixed together and annealed, the product was morphological nano structures (Figure 33G), similar to that of independent peptides.
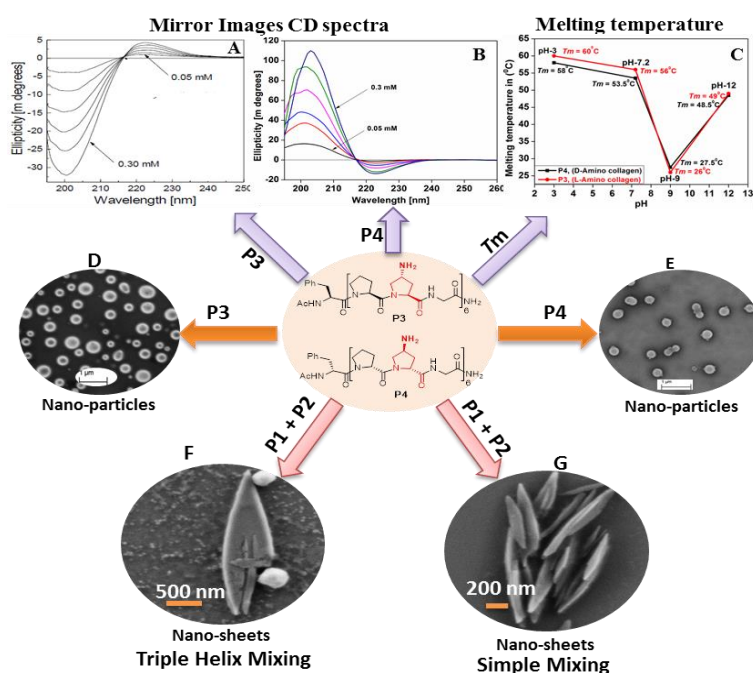

Figure 34. A) and **B)** CD study of peptides **P3** and **P4**; **C)** Thermal stability of **P3** and **P4**; **D)** and **E)** FE-SEM of **P3** and **P4** respectively; **F)** FE-SEM image of **P3** and **P4** in triple-helix mixing; **G)** FE-SEM image of **P3** and **P4** in simple mixing.

The results reinforce the important role of 4-substitution (hydroxy vs amino) on proline, chirality at C2 and C4 positions and their effects on triplex forming ability of derived collagen peptides. The total inversion of stereochemistry at both C2 and C4 throughout collagen peptide sequence results into exact mirror image triple helices which possess identical physical properties such as thermal stability and secondary structure. When mixed together, these form hybrid structures different from that of individual peptides. The unnatural D-collagen peptide triple helices (4-hydroxy and 4-amino) hitherto unknown are likely to be stable to degradative enzymes. Future potential of this work involves rationally combining enantiomeric collagen peptides for biomedical applications.

4.16 Experimental section

4.16.1 General methods for peptide synthesis

The desired peptides were synthesized manually on solid phase using standard Fmoc strategy, on a readily available Novabiochem rink amide resin (100-200 mesh) having 0.61 mmol/g loading. The resin bound Fmoc group was first deprotected with 20% piperidine in dry DMF, and coupling reactions were carried out using *in situ* generation of an active ester, using HBTU, in presence of DIPEA as a base and HOBt as a recemization suppresser.

4.16.2 High-performance liquid chromatography

All peptides were purified by reverse phase-HPLC using semi-preparative RP-C18 columns. The solvent system for elution comprised of acetonitrile:water, with following compositions. **Solvent A:** Acetonitrile:water (5:95, v/v) with 0.1% TFA. **Solvent B:** Acetonitrile:water (50:50, v/v) with 0.1% TFA, with gradient from 0-100% and a flow rate of 2 mL/min. The elutants were monitored at 220 nm (peptide bond) and at 254 nm for phenylalanine.

4.16.3 MALDI-TOF characterization

MALDI-TOF mass spectra were obtained on either Voyager-Elite instrument (PerSeptive Biosystems Inc., Farmingham, MA) equipped with delayed extraction or on Voyager-De-STR (Applied Biosystems) instrument. Sinapinic acid or α-cyano-4-

hydroxycinnamic acid (CHCA) were used as matrices for peptides of which CHCA was found to give satisfactory results. A solution of matrix was spotted on the metal plate along with the oligomers and allowed to co-crystallize. The metal plate was loaded into the instrument and then accelerated by an applying high voltage (15-25 kV) in reflector mode, separated in a field-free flight tube and detected as an electrical signal at the end of the flight tube. HPLC purified peptides were characterized through this method.

4.16.4 Circular dichroism spectroscopy

CD spectra were recorded on JASCO J-715 spectropolarimeter using quartz cell (1 mm path length), with sample holder connected to Julabo water cooling circulator, using spectral bandwidth of 1.0 nm at 25 °C with a time constant of 1 s and a step resolution of 1 nm. All spectra were corrected for respective buffer signals and recorded as the average of 3-5 scans and each spectra is the result of 3-5 accumulations. A quartz cell with a path length of 1 mm was used with solutions containing approximately 0.2 mL (50-300 μM) peptide solutions. For the blank spectrum, buffer was recorded and subtracted from the subsequent samples. CD thermal melting was done in the temperature range 5-90 °C with heating rate is 0.3 °C /min. All samples were equilibrated for at least 24 h before measurement. Bandwidth, 1.0 nm; Sensitivity, (standard); Response, 1 sec; Speed, 50 nm/min; Accumulation, 3-5 scans.

4.16.5 Field Emission Scanning Electron Microscopy (FE-SEM)

FE-SEM imaging was performed using ZEISS *ULTRA PLUS* electron microscope operating at 30 kV. Collagen peptides were taken in Eppendorf tube from the stock solution, and water was evaporated by using speed vac (concentrator *plus*) machine. The desired solvent was added and the solution was vortexed for 1 min and centrifuged. The supernatant solution (5 μL) was then drop cast on silicon wafer. The samples were allowed to dry at room temperature and then kept under ordinary light for 4 h for complete drying and before imaging coated with gold.

4.16.6 Atomic Force Microscopy (AFM)

Atomic force microscopy imaging was carried out on AFM instrument using tapping mode cantilever which was auto-tuned for frequency. The samples (5 μL) were

spotted on fresh mica allowed to dry at room temperature followed by complete drying under an ordinary lamp for 4 h.

4.17 References

1) Prockop, Kivirikko, K. I. *Annu. Rev. Biochem.* **1995**, *64*, 403- 434.

2) (a) Ramachandran, G. N.; Kartha, G. *Nature* **1955**, *176*, 593-595. (b) Rich, A.; Crick, F. H. C. *J. Mol. Biol.* **1961**, *3*, 483-506. (c) Bella, J.; Eaton, M.; Brodsky, B.; Berman, H. M. *Science* **1994**, *266*, 75-81.

3) Woodhead-Galloway, J. *Collagen*: *The Anatomy of a Protein*; Edward Arnold Limited: London, **1980**, 10-19.

4) (a) Shuguang Zhang. *Materialstoday*, **2003**, 20-27. (b) Shuguang Zhang. *Naturebiotechnology*, **2003**, *21*, 1171-1178.

5) Maeda, M., Tani, S., Sano, A., Fujioka, K., *J. Controlled. Rel.***1999,** *62*, 313.

6) (a) Lee, C. H.; Singla, A.; Lee, Y. *Int. J. Pharm.***2001**, *221*, 1-10. (b) O'Grady, J. E.; Bordon, D. M. Adv. *Drug Delivery Rev*. **2003,** *55*, 1699.

7) (a) O'Leary, L. E. R.; Fallas, J. A.; Bakota, E. L.; Kang, M. K.; Hartergrink, J. D. *Nat. Chem*. **2011,** *3*, 821. (b) Rele, S.; Song, Y.; Apkarian, R. P.; Qu, Z.; Conticello, V. P.; Chaikof, E. L. *J. Am. Chem. Soc.* **2007**, *129*, 14780.

8) Mabel A. C.; William A. K.; Cailin C.; Jeremy G. V.; Harold R. A.; Karin M. B.; Cynthia A.M.; Ute S.; Michael B.; Andrew M.; Eilyn L.; Bruce E. Maryanoff, *PNAS, **2008***, *105*, 8513.

9) Chen, C. C.; Hsu, W.; Kao, T. C.; Horng, J. C. *Biochemistry,* **2011**, *50*, 2381.

10) (a) Kotch, F. W.; Raines, R. T. *Proc. Natl. Acad. Sci. U.S.A*. **2006**, *103*, 3028. (b) Koide, T.; Homma, D. L.; Asada, S.; Kitagawa, K. *Bioorg. Med. Chem. Lett.* **2005**, *15*, 5230. (c) Krishna, O. D.; Kiick, K. L. *Biomacromolecules,* **2009**, *10*, 2626.

11) Sergey, E. P.; Varun, G.; Jeffrey D. Hartgerink. *Macromolecules.* **2005**, 38, 7555.

12) (a)Pires, M. M.; Chmielewski, J. *J. Am. Chem. Soc*. **2009**, *131*, 2706. (b) Pires, M. M.; Przybyla, D. E.; Chmielewski, J. *Angew. Chem., Int. Ed*. **2009**, *48*, 7813. (c) David, E. P.; Charles, M. R. P.; Jermey, G.; Vikas, N.; Jean Chemielevski.*J. Am. Chem. Soc.***2013**, *135*, 3418.

13) Fei, X.; Khan, I. J.; Kenneth, M.; Avanish, S. P.; Teresita, S.; Sanjeeva, M.; Vikas Nanda. *J. Am. Chem. Soc.***2013**, *135*, 18762.

14) Yoshida, T.; Sakurai, S.; Okuda, T.; Takagi, Y. *J. Am. Chem. Soc.* **1962**, *84*, 3590.

15) Fuhrhop, J. H.; Krull, M.; Büldt, G., *Angew. Chem. Int. Ed. Eng.* **1987**, *26*, 699.

16) Katelyn, J. N.; Michael, C. G.; Albert, J.; Darrin, J. P.; Schneider, J. P. *J. Am. Chem. Soc.* **2011**, *133*, 14975.

17) Rai, J. S.; T. M. DiMaio.; Charles, J. B.; Bradley L. Nilsson. *J. Am. Chem. Soc.* **2012**, *134*, 5556.

18) Image taken from internet source link given below and modified to show hydroxyl groups pointing outside of the helix https://www.google.co.in/search?q=collagen+images&source=lnms.

19) Image in ref no 18 was vertically rotated twice to get mirror image using Microsoft program.

20) Piero, D. C.; Concetta, L. R. *Tetrahedron: Asymmetry*, **2002**, *13*, 197-201.

21) Molar extinction coefficient value of F, Phe, (Phenylalanine) taken from link http://www.biosyn.com/tew/How-is-Extinction-Coefficient-Determined-for-Proteins.aspx

22) Feng, Y.; Melacini, G.; Taulane, J. P.; Goodman, M. *J. Am. Chem. Soc.* **1996**, *118*, 10351.

23) (a)Nimni, M. E. (ed.) *Collagen* 1–4 (CRC, Boca Raton, Florida, **1988**).(B) Bella, J., Brodsky, B. & Berman, H. M. *Structure.* **1995,** *3***,** 893. (C) Bella, J., Eaton, M., Brodsky, B., Berman, H. M. *Science* **1994,** *266***,** 75.

24) Steven, K. H., Kimberly, M. T., Lynn, E. B., Ronald, T R. *Nature* **1998**, *392*, 666.

25) Babu, R. I., Ganesh, K. N.*J. Am. Chem. Soc.* **2001,** *123,* 2079.

26) (a) Umashankar, M., Babu, R. I., Ganesh, K. N.*Chem.Commun*. **2003**, 2606. (b) Umashankar, M., Sonar, M. V., Bansode, N. D., Ganesh, K. N. *J. Org. Chem.* **2015,** *80*, 8552.
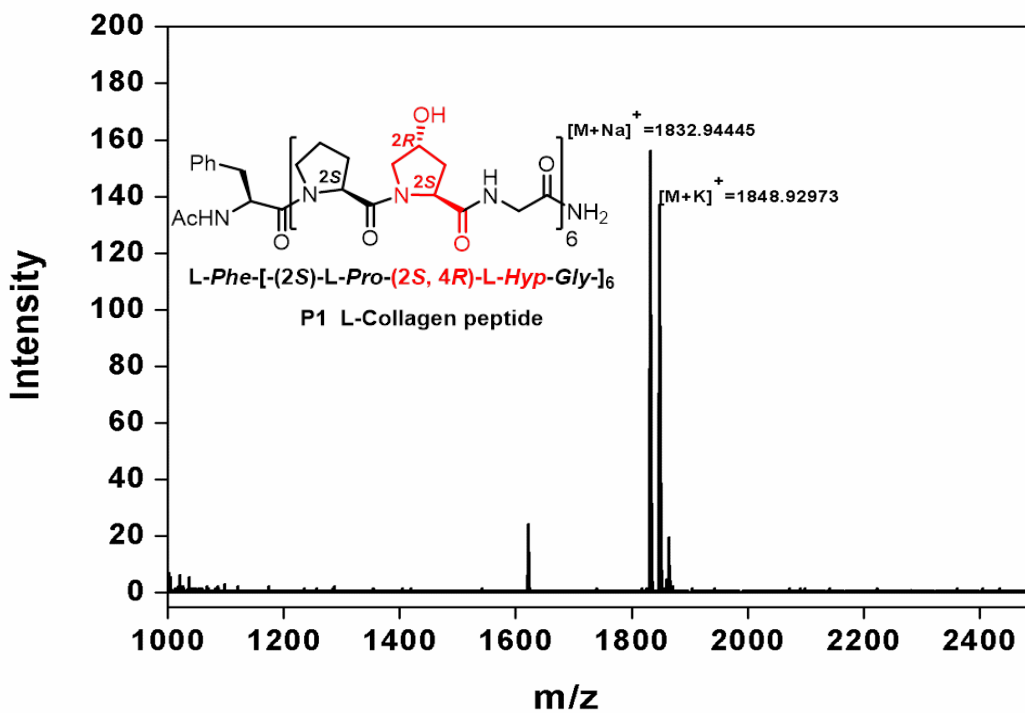
4.19 Appendix 1: Purification and characterization of peptides 1-4
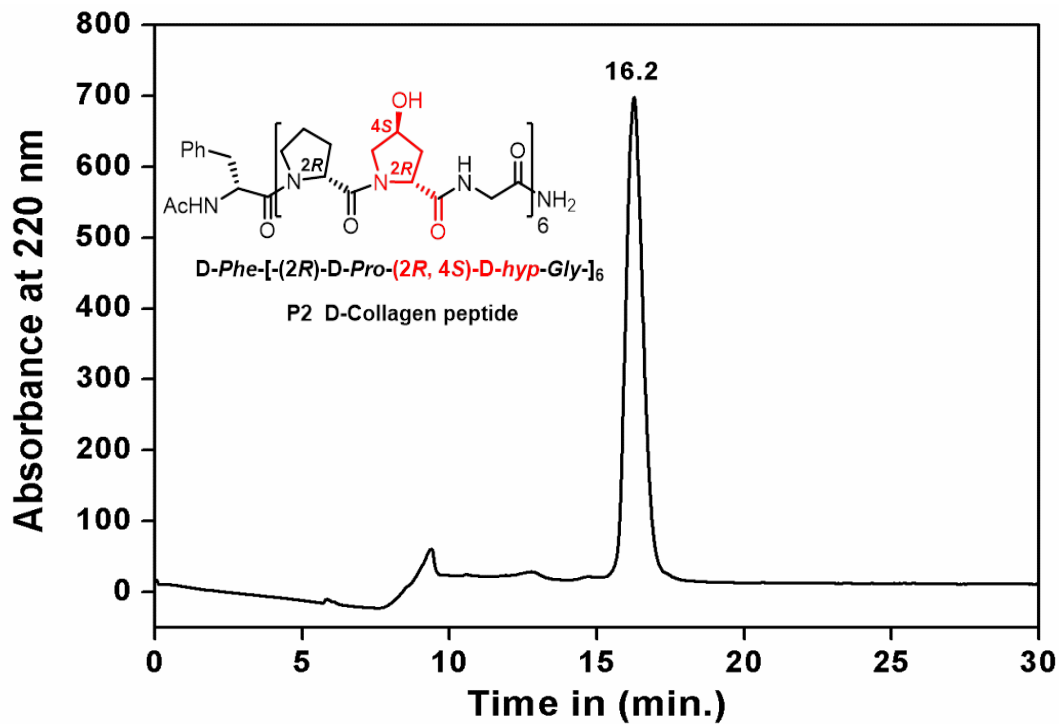
A) HPLC and MALDI-TOF of peptides (1-4)
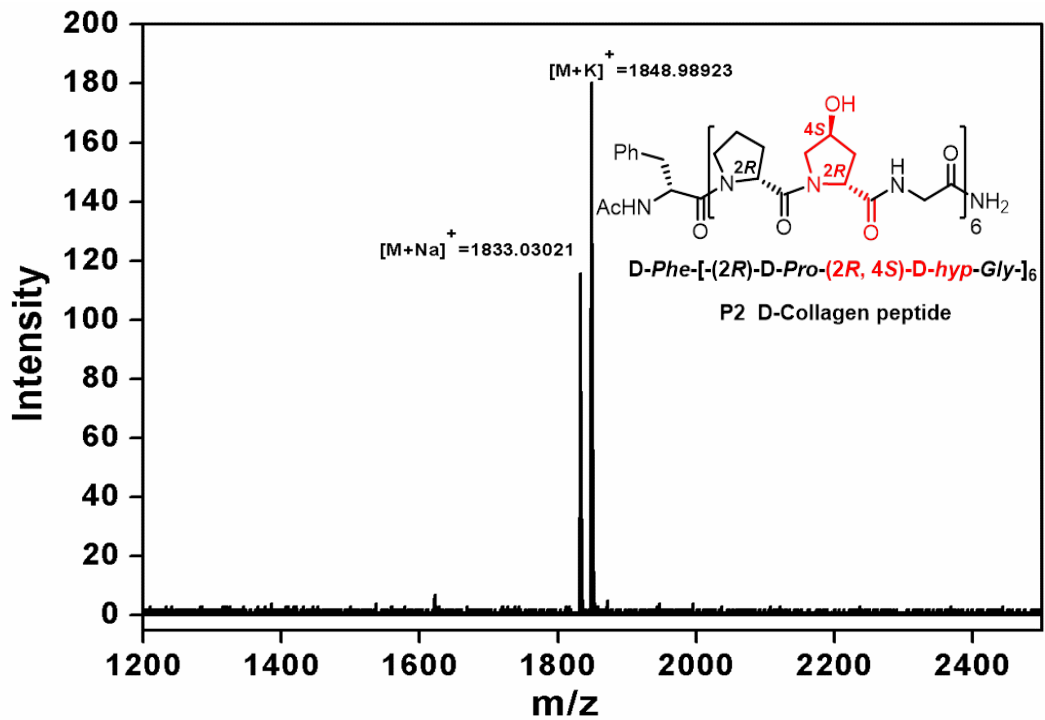
HPLC Profile of L-Collagen Peptide P1
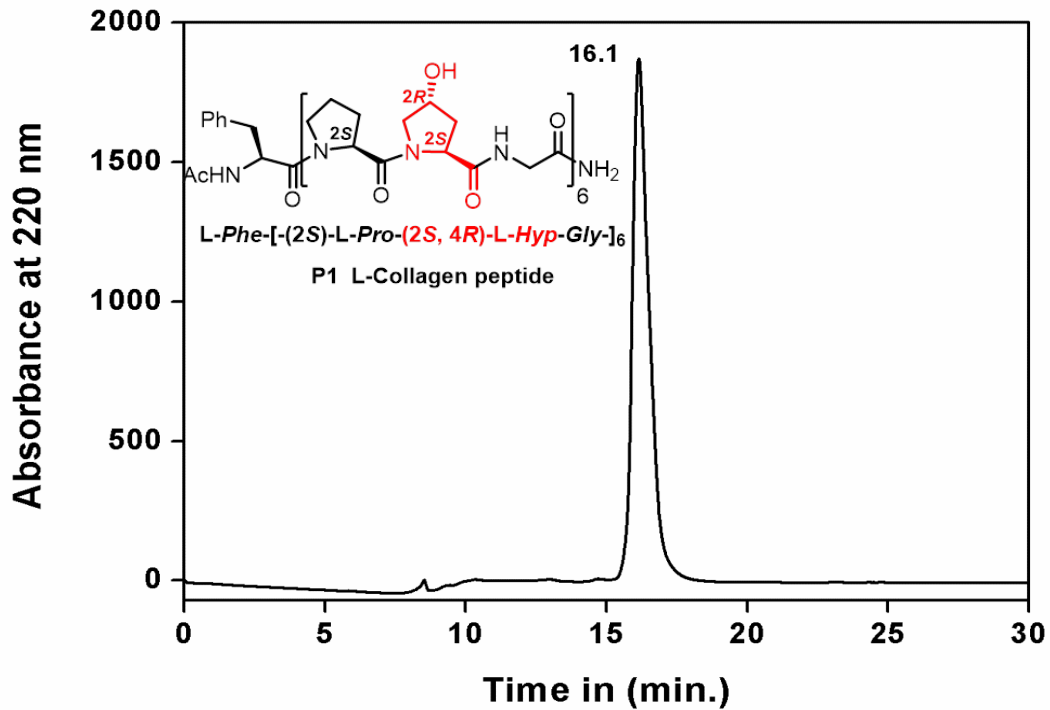
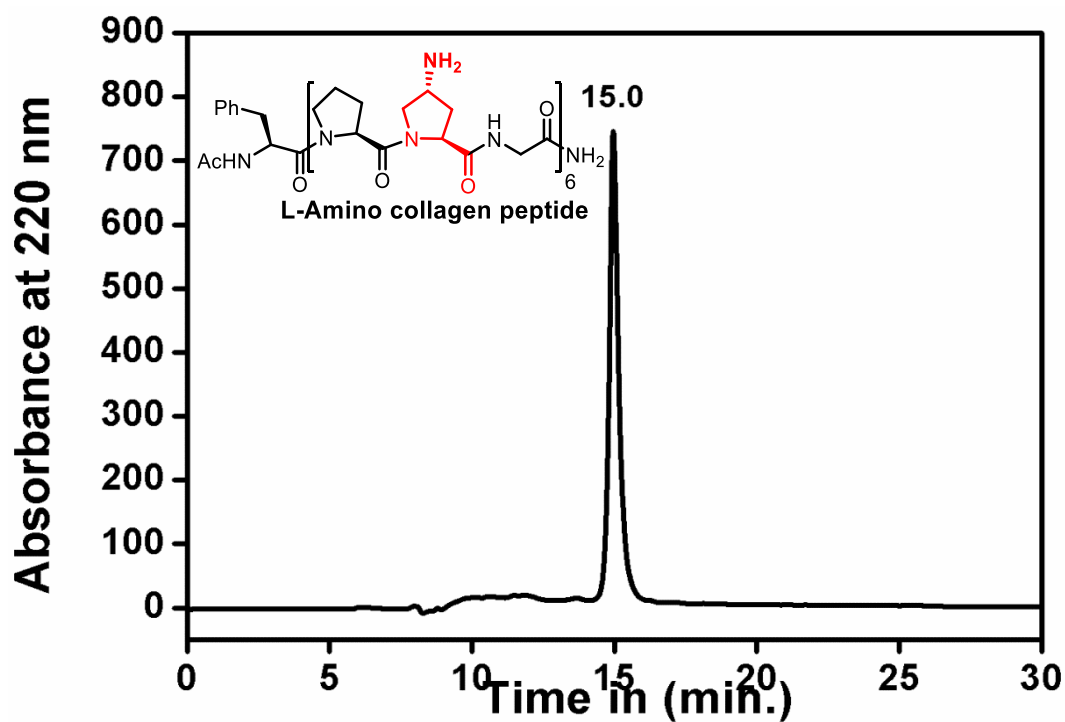## MALDI-TOF: Characterization of L-Collagen Peptide P1

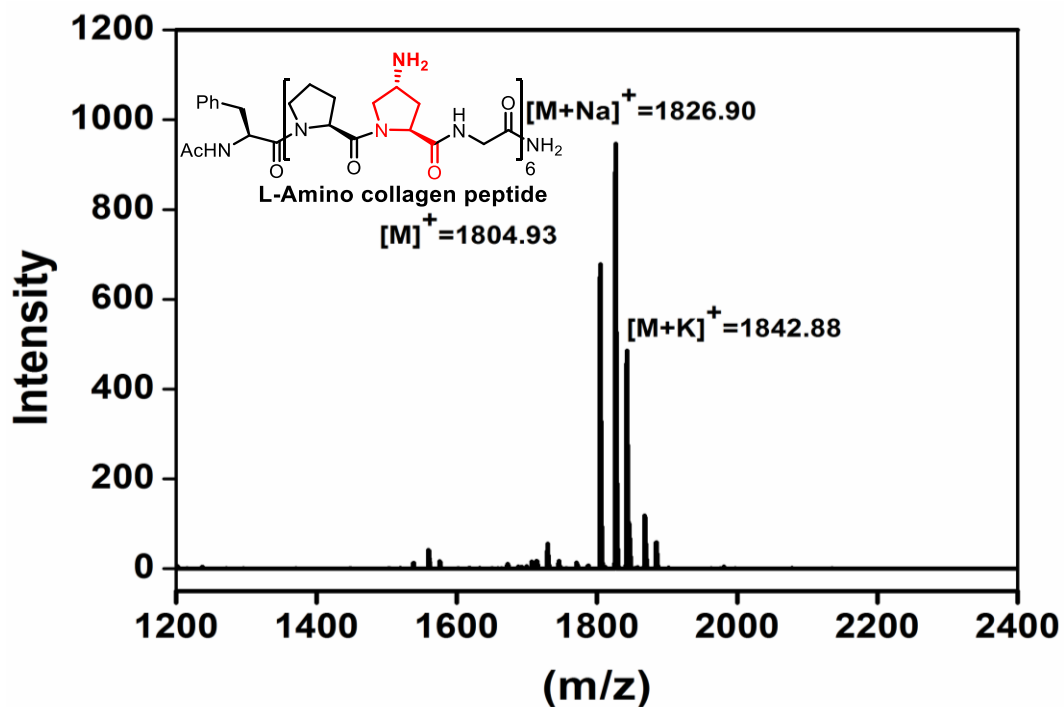**HPLC Profile of D-Collagen Peptide P2**

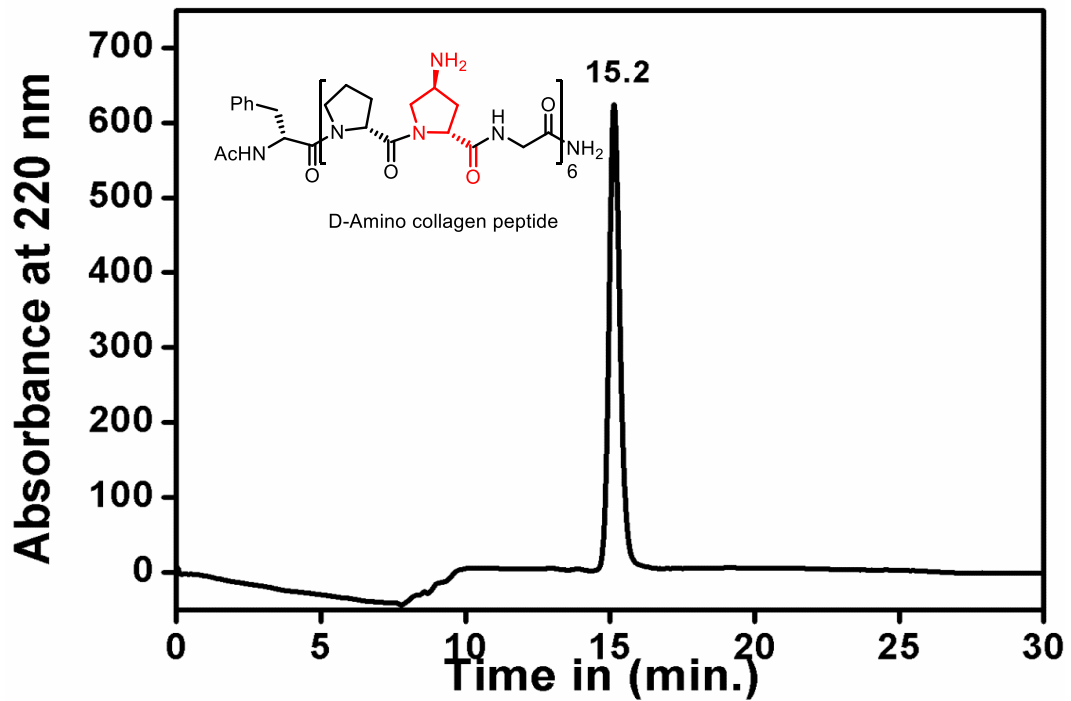**MALDI-TOF: Characterization of D-Collagen Peptide P2**

HPLC profile: L-Amino collagen peptide P3

MALDI-TOF: Characterization of L-Amino collagen peptide (P3)

HPLC profile: D-Amino collagen peptide P4

MALDI-TOF: of D-Amino collagen peptide P4